

**SYNTHETIC AND NATURAL N, S, O DONOR
SYSTEMS AS CORROSION INHIBITORS FOR
MILD STEEL IN ACID ENVIRONMENTS**

*Thesis Submitted
to the University of Calicut for the
award of*

DOCTOR OF PHILOSOPHY IN CHEMISTRY

Sr. ASHA THOMAS

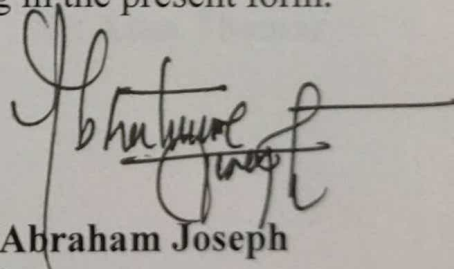


**DEPARTMENT OF CHEMISTRY
UNIVERSITY OF CALICUT
KERALA- 673635
DECEMBER 2020**

Certificate

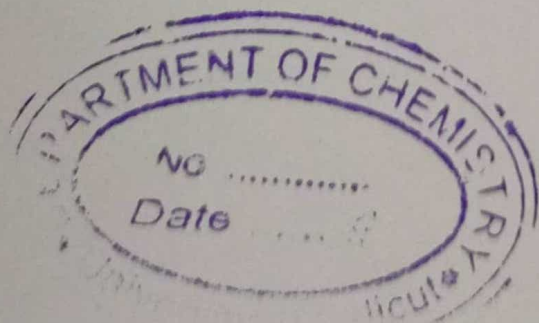
This is to certify that the thesis entitled "Synthetic and Natural N, S, O Donor Systems as Corrosion Inhibitors for Mild Steel in Acid Environments" submitted to the University of Calicut, is a record of precise research work carried out by Sr.Asha Thomas at the Department of Chemistry, the University of Calicut under my guidance and supervision. The contents of the thesis have been checked for plagiarism using the software 'Urkund' and the similarity index falls under the permissible limit, and I further certify that the thesis or part has not previously formed the basis for the award of any degree, diploma or associateship of any other University or Institute.

I also certify that the adjudicators have not suggested any change / corrections in the thesis and recommend accepting in the present form.



Dr. Abraham Joseph
Professor

University of Calicut



Declaration

I, **Sr. Asha Thomas** hereby declare that thesis entitled as "Synthetic and Natural N, S, O Donor Systems as Corrosion Inhibitors for Mild Steel in Acid Environments" submitted to the University of Calicut is a bonafide record of project work done by me under the supervision and guidance of **Dr. Abraham Joseph**, Professor, Department of Chemistry, University of Calicut-and it has not formed the basis for the award of any Degree/Diploma/Associateship/Fellowship or other similar titles of any other University or Institution.



University of Calicut

Sr. Asha Thomas

Acknowledgement

“Ask and it will be given to you; seek and you will find; knock and the door will be opened to you. For everyone who asks receives; the one who seeks finds; and to the one who knocks, the door will be opened.” (Bible).

*My profound thanks to “**The Lord Almighty**” for His blessings and graces which enabled me to complete this research work*

*I am deeply indebted to **Prof. Abraham Joseph**, my guide who was ready to accept me as a part-time research scholar knowing well, the limitations of a part - time researcher. Thank you sir for the freedom you have given in modifying the research work, understanding my personal responsibilities and difficulties, and the confidence you have in me. I am privileged to be your student. I wish to learn much more from you especially Inorganic Chemistry*

*My sincere thanks to the Head of the Department, **Dr. A. I. Yahya**, and former Heads of the Department, Dr. P. Raveendran and Dr. K. Muraleedharan for providing me all the facilities to carry out my research work.*

My special thanks to Prof. K.K Aravindakshan for his support and encouragement.

I express my gratitude to all the faculty members and non-teaching staff in the Department of Chemistry of the University of Calicut.

My loving thanks to the senior members of the research group Dr. Sam John, Dr. Ramya K, Dr. Anupama K K, Dr. Rugmini Ammal, Dr. Prajila M, Dr. Shainy K M, Dr. Sabeel M Basheer and Dr. Jaseela P K for their guidance in the initial stages of my research. I thank each of you my friends, Anupama R Prasad, Shamsheera k O, Julia Garvasis, Jeeja Rani A T, Sowmya P, Linda Williams, Muhammed Arshad, and Sumitha Tom, for your love, laughter and timely help that smoothed the hardships of research and made this place beautiful for me.

I thank all the other research scholars of the dept. for sharing their valuable time and knowledge whenever needed.

Words are not enough to thank the former Manager Dr.(Sr.) M Ancilla and the present manager of Providence Women's College, Calicut, Sr. Maria Karuna. I am grateful to Dr. (Sr.) M Neetha the former Principal and Dr. (Sr.) Ashmitha, Principal, Providence Women's College, Calicut, for their love and constant encouragement.

My sincere thanks to faculty members of Dept. of Chemistry, Providence Women's College, Calicut, for imparting their knowledge in computational calculations, organic synthesis, and sharing my responsibilities. Thank you Ms. B. Lakshmidevi, Dr. Gigy Abraham, Dr. Anjana George, Dr. Deepthi Jose, Dr. Anu Jose, Dr. A Sareena, Sr. Alphonsa Joseph, and Ms Shahla.

With grateful hearts, I remember Sr. Nirmalini, the Superior General of Apostolic Carmel Congregation and Sr. M Susheela, former Superior General for their concern in completing the research. I acknowledge my gratitude to Sr. Marian, Superior of Carmel Hill Convent the former superior Sr. Lalitha, and the members of the community for supporting me all through these years with their prayers and love. My special thanks to Sr. M Rosarita for the inspiration to research fruit rinds. Thanks to Sr. Jeevitha and Sr. Mable Rose for collecting the samples for the studies

Words truly cannot express my gratitude to my dear parents, for being with me in spirit at each moment sharing my struggles and encouraging me to complete the work. I thank my brothers, sister and their family members, well wishers, students and friends for their love

I hereby acknowledge the help rendered by the Central Sophisticated Instrument Facility (CSIF) of University of Calicut, PSG College of Technology, Coimbatore. Gandhigram Rural Institute, Dindigul, Tamil Nadu and CArE KERALAM, Koretty, Trissur Kerala

Sr. Asha Thomas

“Time heals everything apart from Corrosion”

21st century brought forth unimaginable changes in the standards of human life, bringing the whole globe as a village; yet corrosion remains as a challenge to mankind. Being a spontaneous process corrosion needs a lot of attention to control, manage and to maintain material safety and reliability. Corrosion engineers and chemists are preoccupied with designing new materials that can resist corrosion and the development of better strategies that could reduce corrosion to an acceptable limit. One of the efficient and established methods used for the control of corrosion is the use inhibitors. The selection of eco-friendly, sustainable, and cost-effective inhibitors is an art and a science. Wide varieties of organic molecules have been tested as corrosion inhibitors and are branded as commercially available inhibitors. The unfolding of newer efficient inhibitors remains a hot topic of research. Nature has hidden a large number of organic molecules in the plant kingdom which could be effectively used as corrosion inhibitors. The thesis entitled *“Synthetic and Natural N, S, O donor systems as corrosion inhibitors for mild steel in acid environments”* is a conscious effort in the unveiling of the inhibition capacity of some of the pyrazole derivatives and fruit rind extract as corrosion inhibitors for mild steel in acidic media.

Chapter1 provides a brief and general introduction to corrosion, cost of corrosion, chemistry of corrosion, thermodynamics, and kinetics of

corrosion, corrosion control techniques, and corrosion testing methods. A brief review of the literature of pyrazoles as corrosion inhibitors and a detailed review of the literature of fruit, fruit rind, seed as corrosion inhibitors are also included in this chapter.

Chapter 2 deals with the materials and methods used in this work. The synthesis strategies of the pyrazolones and fruit rind extracts of *Garcinia Indica* and *Myristica Fragrans* is mentioned in this chapter. A brief description of various instrumental methods and theoretical calculations used for the study is included in the chapter. The mathematical equations and expressions used in this thesis are also given in this section.

Chapter 3 describes the characterisation of the inhibitor 5-Chloro-3-methyl-1-phenyl-1H-pyrazole-4-carbaldehyde (**CMPPC**) and its capacity to offer corrosion protection to mild steel in HCl media. The effect of acid concentration, inhibitor concentration, and temperature on the inhibition capacity are evaluated by weight loss, EIS (Electrochemical Impedance Spectroscopy), PDP (Potentiodynamic Polarisation) techniques. The most probable mode adsorption of the inhibitor on the metal surface is obtained from the best fitting isotherm and the kinetic parameters calculated are discussed in this chapter. The global descriptors calculated by the Gaussian 09 package and the adsorption pattern of CMPPC on Fe(100), Fe(110), and Fe(111) plane done using Biovia Material studio simulations are also discussed in this chapter.

Chapter 4 provides the summary of the inhibition efficacy of two pyrazolone chalcones (4Z)-4-(4-(dimethylamino) benzylidene)-3-methyl-1-phenyl-1H-pyrazole-(4H)-one- **PD** and (4Z)-4-(4-(dimethylamino) benzylidene)-1-phenyl-3-propyl-1H-pyrazole-(4H)-one-**PD1** and the details of the difference in their activity. Corrosion testing is done using nonelectrochemical and electrochemical methods in HCl at different concentrations and temperatures. A comparison of the global parameters obtained by Gaussian calculations and binding energy obtained by Material studio simulations are given in this chapter. Fukui indices of the inhibitors calculated with UCA_FUKUI software is also included here.

Chapter 5 begins with the characterisation of the inhibitor and further explains the synergistic interaction of **PY1** (3-propyl -1-phenyl-1H-pyrazolyl-5(4H)-one and Thiourea (**TU**) for corrosion inhibition in 1M HCl especially at elevated temperatures. The adsorption, kinetic, and synergism parameters calculated for the PY1/TU pair are also included in this chapter. Gaussian calculations and material studio simulations of the individual and combined systems are also given in this chapter.

Chapter 6 deals with corrosion inhibition properties of CMPPC, PY1, PD, and PD1 in 0.5M H₂SO₄ towards mild steel at different temperatures. The adsorption isotherms, Arrhenius, and transition state approaches in the context of metal corrosion are discussed in this chapter.

Chapter 7 includes the study of the corrosion inhibition property of various concentrations of Garcinia Indica fruit rind extract (GIW) in

HCl up to 333K. Characterisation and identification of the constituent molecules of the extract are carried out with UV Visible, and IR spectroscopy. The influence of iodide ions on the inhibition capacity of GIW is also discussed in this chapter. The geometry optimisation, calculation of global parameters, Fukui indices, and Monte Carlo simulations of the constituent molecules are briefly discussed in this chapter.

Chapter 8 provides a comparative study of the inhibition efficacy of *Myristica Fragrans* fruit rind aqueous extract (MFW) and ethanolic extract (MFE) towards mild steel in 1M HCl. The UV Visible and IR spectra of the extract and the GCMS of the ethanolic extract are discussed in this chapter. Inhibition performance of the extract is done using weight loss, EIS, and PDP analysis. The optimised geometry of the most abundant constituent molecules, their global descriptors, adsorption characteristics and kinetic behaviour are also discussed in this chapter. The thesis ends up with **Summary and Future Outlook**.

CONTENTS

	<i>Page No.</i>
Preface	
Chapter 1	1-45
Introduction	
1.1 Corrosion	1
1.2 Cost of corrosion	1
1.3 Chemistry of corrosion	6
1.4 Types of corrosion	8
1.5 Thermodynamics of corrosion	10
1.6 Kinetics of corrosion	11
1.7 Corrosion control measures	14
1.8 Mechanism of inhibition by mixed inhibitors	17
1.9 Adsorption isotherms	18
1.10 The concept of synergism	19
1.11 Corrosion detection and monitoring techniques	20
1.12 Pyrazole derivatives as corrosion inhibitors- A review	29
1.13 Review – Fruit rind/peel/seeds as corrosion inhibitors	31
Chapter 2	47-65
Materials and Methods	
2.1 Introduction	47
2.2 Electrodes and Electrolytes	47
2.3 Inhibitors	48
2.4 Characterisation Techniques	54
2.5 Corrosion Tests	55
2.6 Thermodynamic and kinetic parameters	59
2.7 Surface morphological studies	60
2.8 Quantum chemical calculations	61
2.9 Material studio simulations	63

Chapter 3	67-90
<i>Control of mild steel corrosion in HCl using CMPPC as mixed type inhibitor</i>	
3.1 Introduction	67
3.2 Results and discussion	67
3.2.1 Characterisation of CMPPC	67
3.2.2 Corrosion studies	68
3.2.2.1 Effect of acid and inhibitor concentration	68
3.2.2.2 EIS Analysis	70
3.2.2.3 Effect of Acid concentration	71
3.2.2.4 Effect of inhibitor concentrations	73
3.2.2.5 Potentiodynamic studies	75
3.2.2.6 Effect of temperature	77
3.2.3 Adsorption Isotherms	78
3.2.4 Kinetic parameters	81
3.2.5 Quantum chemical calculations	82
3.2.6 Material studio simulations	84
3.2.7 Surface Analysis	85
3.2.8 Proposed inhibition mechanism	86
3.3 Conclusions	87
Chapter 4	91-125
<i>Inhibition of Mild Steel Corrosion in HCl using Substituted Pyrazole derivatives</i>	
4.1 Introduction	91
4.2 Results and Discussion	91
4.2.1 Synthesis and characterisation of the inhibitors	91
4.2.2 Corrosion Studies	93
4.2.2.1 Weight loss Analysis	93
4.2.2.2 Electrochemical Analysis	95
4.2.2.3 Potentiodynamic polarisation studies	101

4.2.2.4 Effect of temperature	106
4.2.2.5 Bode and phase angle plots	107
4.2.2.6 Effect of side chain length on corrosion inhibition	109
4.2.3 Adsorption Isotherms	111
4.2.4 Kinetic parameters	113
4.2.5 Theoretical Calculations	115
4.2.5.1 Fukui Indices	118
4.2.6 Material studio calculations	119
4.2.7 AFM analysis	121
4.3 Conclusions	122
Chapter 5	127-149
<i>Extended protection of mild steel in HCl at elevated temperatures using the synergistic interaction of Pyrazolone and Thiourea</i>	
5.1 Introduction	129
5.2 Results and Discussions	129
5.2.1 Synthesis and characterisation of the inhibitor	129
5.2.2 Corrosion Analysis	129
5.2.2.1 Weight loss studies	129
5.2.2.2 EIS analysis	130
5.2.2.3 Potentiodynamic polarisation studies	133
5.2.3 Effect of Temperature	137
5.2.4 Synergistic interaction of TU and PY1	139
5.2.5 Adsorption Study	140
5.2.6 Quantum mechanical calculations	141
5.2.7 Material studio Treatment	143
5.2.8 AFM Analysis	144
5.3 Conclusions	145

Chapter 6	151-172
<i>Protection of Mild steel in H₂SO₄ using CMPPC, PY1, PD and PDI-A comparative study</i>	
6.1 Introduction	151
6.2 Results and Discussion	151
6.2.1 Weight loss Studies	151
6.2.2 Electroanalytical studies	153
6.2.2.1 EIS Measurements	153
6.2.2.2 PDP Analysis	158
6.2.3 Adsorption Studies	163
6.2.4 Effect of temperature on the rate reaction	164
6.2.5 Surface Analysis	168
6.2.6 Mechanism of Inhibition	169
6.3 Conclusions	170
Chapter 7	173-217
<i>Corrosion Inhibition of mild steel in HCl using fruit rind extract of Garcinia Indica (Binda)</i>	
7.1 Introduction	173
7.2 Results and Discussion	173
7.2.1 Chemical composition of the extract	173
7.2.2 Corrosion studies	176
7.2.2.1 Gravimetric Studies	176
7.2.2.1.1 Effect of immersion time	176
7.2.2.2 Analysis of EIS data	178
7.2.2.2.1 Effect of Acid concentration	179
7.2.2.2.2 Effect of GIW concentration	180
7.2.2.2.3 Effect of temperature	182
7.2.2.2.4 Bode Plots	183
7.2.2.3. Polarisation studies	184
7.2.3 Influence of KI on the inhibition property of GIW extract	187

7.2.3.1 Gravimetric analysis	187
7.2.3.2 EIS Analysis	188
7.2.3.3 Potentiodynamic polarisation studies	191
7.2.3.4 Synergism between GIW and KI	193
7.2.4 Adsorption Studies	195
7.2.5 Kinetics of corrosion inhibition	197
7.2.6 Calculation of global descriptors	199
7.2.7 Condensed Fukui functions	201
7.2.8 Monte Carlo simulations	203
7.2.9 Surface Analysis	207
7.2.9.1 AFM studies	207
7.2.9.2 SEM Analysis	208
7.2.10 Mechanism of inhibition	209
7.3 Conclusions	211
Chapter 8	219-242
<i>Inhibition of mild steel corrosion in HCl using Myristica fruit rind extract</i>	
8.1 Introduction	219
8.2 Results and Discussion	219
8.2.1 Chemical composition of the extract	219
8.2.2 Corrosion Analysis	223
8.2.2.1 Weight loss Analysis	223
8.2.2.2 EIS studies	225
8.2.2.3 Potentiodynamic polarisation (PDP) studies	231
8.2.3 Adsorption studies	233
8.2.4 Effect of temperature and Kinetics of the reaction	234
8.2.5 Surface Analysis	236
8.2.6 Mechanism of inhibition	237
8.3 Conclusions	239
Summary and Future out look	243-245

Chapter 1

Introduction

A brief outline of the mechanism of corrosion, control measures, different types of corrosion monitoring techniques, and the review of literature on pyrazoles and fruit parts as inhibitors are discussed in this chapter.



Contents

1.1 Corrosion	01
1.2 Cost of corrosion	01
1.3 Chemistry of corrosion	06
1.4 Types of corrosion.....	08
1.5 Thermodynamics of corrosion	10
1.6 Kinetics of corrosion	11
1.7 Corrosion control measures.....	14
1.8 Mechanism of inhibition by mixed inhibitors.....	17
1.9 Adsorption isotherms	18
1.10 The concept of synergism	19
1.11 Corrosion detection and monitoring techniques.....	20
1.12 Pyrazole derivatives as corrosion inhibitors- A review	29
1.13 Review – Fruit rind/peel/seeds as corrosion inhibitors.....	31

1.1 Corrosion

Corrosion is a natural environmental problem, a billion-dollar business, and an age-old process which affects people of all walks. Therefore, it is a hot topic of research and discussion to corrosion engineers and chemists. The term includes all processes of deterioration of materials such as rotting of wood, weathering of concrete, damage to metals etc[1]. More specifically it is the deterioration of a metal by a chemical (dry corrosion) or electrochemical (wet corrosion) process by its interaction with the surroundings. The ISO (International standard organisation) and IUPAC define corrosion as a physicochemical interactive process between the metal and its surroundings that impair the functioning of a system[2]. Tarnishing of silver, development of green patina over copper and grey patina over zinc, rusting of iron are typical examples of corrosion. Corrosion is a spontaneous process through which the system coming to a low energy state by transforming into its naturally existing form as oxides, hydroxides, sulphides, etc. Corrosion changes the specific and superior properties of metals such as malleability, ductility, electrical conductivity, and mechanical strength.

1.2 Cost of corrosion

Corrosion is the major loss producing process in many areas of the nation's industry due to loss of material, energy, and labour. Corrosion critically affects the economy of a nation but the social cost of corrosion is about 2-10% greater than the direct effects. Corrosion affects all types of the industry by premature failure of components, operates at the suboptimal level, affects productivity, and safety of the environment and consume non-renewable natural resources. Though

Introduction

the other mechanisms fail, corrosion remains the single major reason for damage to industrial components. Corrosion plays a key role in the oil and gas industry which has a giant network of metallic framework starting from extraction to separation of hydrocarbons to use them as fuels[3]. Potential accidents are portrayed in the history of mankind due to corrosion destroying human life and worthy constructions such as bridges, buildings, etc[4].

The cost of corrosion is divided into direct cost and indirect cost by Revie and Uhlig in 2002.

The direct cost includes

- The replacement cost of corroded /failed equipment and accessories
- Painting of corrosion susceptible structures
- Expenses for other corrosion control measures such as coating, inhibitor, galvanic protection, electroplating etc.
- Cost for developing and using corrosion-resistant alloys instead of carbon steel
- Storing expenses for metallic components by dehumidification of the storerooms

Indirect costs add very heavily to the direct cost and which includes

- Production loss due to shut down of the industry and this is much higher in magnitude than direct loss.

Introduction

- Product loss due to leakage or failure of the equipment and the loss is huge when the pressure of the vessel and pipe carrying a large amount of finished products
- Contamination of carefully produced finished products
- Protection measures are taken by increasing the thickness-overdesign

Also, unquantifiable losses such as loss of life due to leakage of gases, explosions due to corrosion, and other corrosion-related accidents demand huge compensation losses[4].

1.2.1 The world and the Indian scenario

The earlier studies on corrosion costs by Herbert H.Uhlig of USA followed by studies by Hadfield from UK and many other evaluations on corrosion process end up with the same idea that corrosion is a major challenge faced by most of the developed and developing countries[5][6]. They calculated the direct cost of corrosion whereas the actual cost of corrosion is much greater than this. A realistic study on money loss due to corrosion related issues is conducted by the American government in 1998-2001 and published in 2002 estimated the corrosion cost as 3.1% (276 US\$ billion) of GDP. The highlights on actualisation of corrosion savings by appropriate engineering practices and corrosion control technologies is mentioned by Thompson et al[6] and emphasis on the corrosion control methods by selection of materials, operating environments, and sustainment systems are described by Keith Legg in their papers. In India calculation of

Introduction

corrosion cost is done by Rajagopalan et al and updated by Bhaskaran et al[7]. The demand for steel because of its mechanical competency and availability is increasing each year. The crude steel production of different countries in 2019-2020 is shown in the Fig1.1

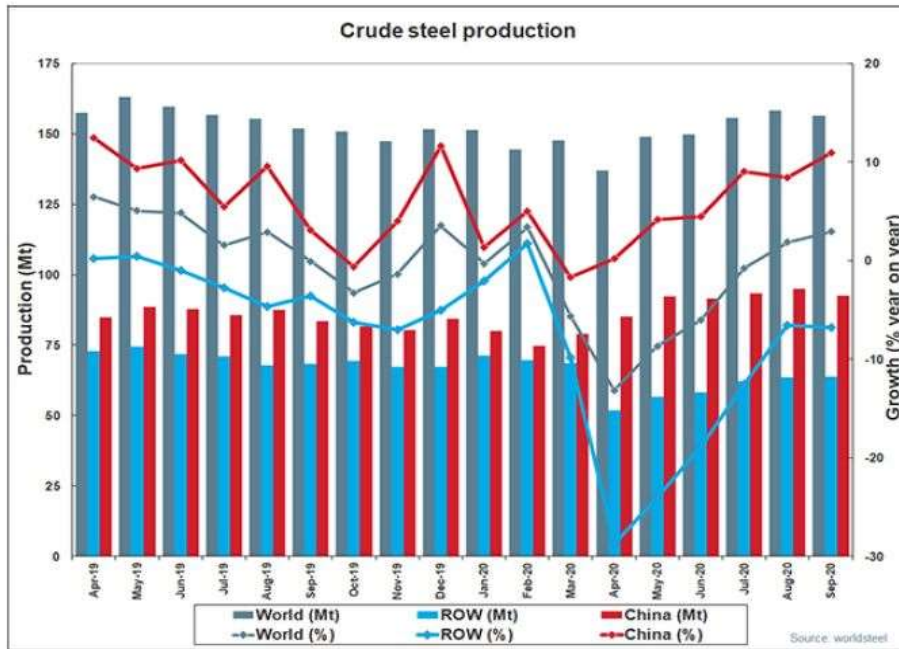


Fig1.1 Global crude steel production 2020 (Source World steel Association Sept.2020 press release)

Increasing steel consumption and depletion of natural resources also contribute to the cost of corrosion. IMPACT 2016 (International Measures of Prevention, Application, and economics of Corrosion Technologies) an initiative of NACE international (The National Association of Corrosion Engineers) reports the global cost of corrosion as 3.4% (US\$ 2.5 trillion) whereas in India 4.2% and in the United States 2.7% of GDP. The variation in the cost of corrosion in different

Introduction

countries reveals their capabilities to manage corrosion. Better strategies in selecting the material, designing, control measures could save 15-35% of the expenditure. Moreover, accidents and critical loss can be avoided if there is a well-defined corrosion management system. The IMPACT divides the world into nine economic regions and calculated the cost of corrosion in terms of GDP is shown below (Fig1.2). It gives a clear idea that the cost of corrosion is minimum in Japan whereas the maximum cost of corrosion is shouldered by Arab world. India's corrosion loss is comparably large and also it is observed that the agricultural sector too contributes to corrosion costs. This conclusion leads to the fact that the corrosion mitigation is a challenge to be taken care of.

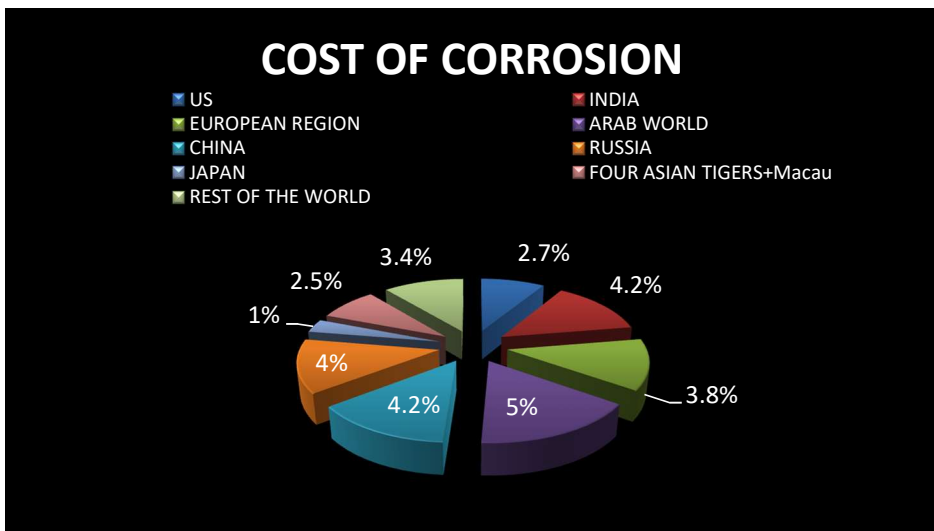


Fig1.2 Cost of corrosion 2016-NACE IMPACT report (Source NACE international 2016 report)

1.3 Chemistry of corrosion

Corrosion mechanisms are so vast that it cannot be defined by a simple route. Dry/chemical theory of corrosion and galvanic/wet/electrochemical theory of corrosion are the two major theories regarding corrosion.

1.3.1 Electrochemical (wet) corrosion

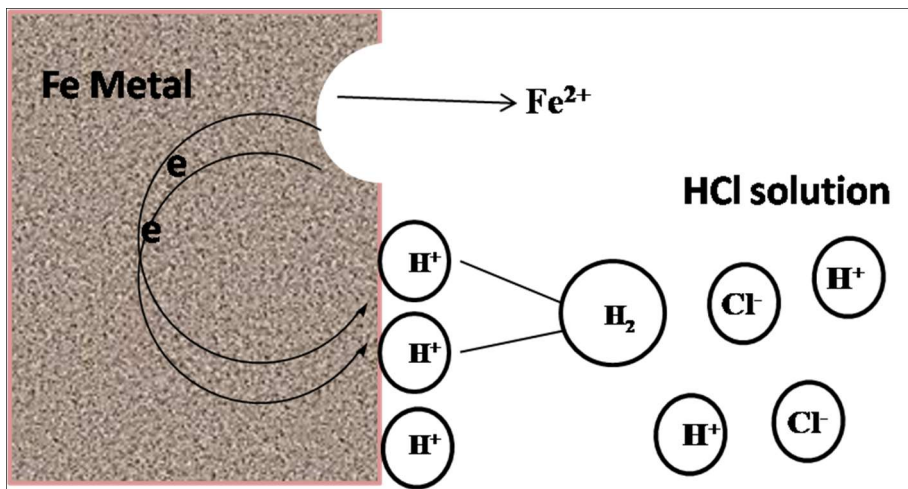


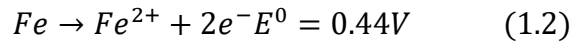
Fig1.3 Electrochemical corrosion of Iron in HCl

This type of corrosion occurs in a corrosive aqueous environment. The environment known as electrolytes can be liquids like acids, NaCl solution, water, etc, or gases such as air, CO_2 or it can be a combination of solid and liquid or liquid and gas. The metal and the electrolyte form an electrochemical cell comprised of two reactions. Anodic oxidation, and a cathodic reduction reaction (Fig 1.3). For a reaction to proceed electrochemically there should be a potential difference between the anodic and cathodic regions. A continuous conduction path and a mechanism for charge transfer between

electronic and electrolytic conductors are also essential for the electrochemical process. The anodic oxidation reaction is given as



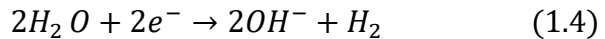
For steel anodic reaction can be shown as



Depending on the pH of the electrolyte, presence of moisture, oxygen etc the cathodic reactions vary. The different reactions are given as follows

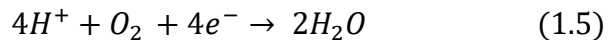
In acidic medium $2H^{+} + 2e^{-} \rightarrow H_2$ (1.3)

In a neutral and basic medium

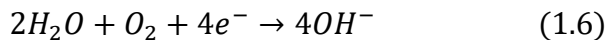


or oxygen absorption-type reaction such as

In acidic medium



In a neutral or basic medium



or even the metal ion can be reduced into the metal which does not happen usually.

1.3.2 Chemical (dry) corrosion

This type of corrosion arises due to the direct reaction of metals with gases such as O₂, SO₂, H₂S, oxides of nitrogen, halogens, anhydrous inorganic liquids, etc. The extent of corrosion depends on the affinity

of metals to these substances. Among the gases, O₂ is the main cause of dry corrosion on the metal surface. It is again classified as

- a) Oxidation corrosion: Alkali metals and alkaline earth metals in the absence of moisture directly react with O₂ is an example of oxidation corrosion. The noble metals such as Au, Pt, Ag do not undergo this reaction. The metal oxides formed on the metal surface act as a protective covering and this oxide barrier play an important role in preventing corrosion. The mechanism can be written as



- b) Corrosion by other gases: Other gases such as CO₂, H₂S, etc reacts with metal surface forms protective or nonprotective layers. The reaction of Ag with Cl₂ forms AgCl is an example of this type of corrosion. At high temperatures, H₂S reacts with Fe forms an unprotective coating of FeS.
- c) Liquid metal corrosion. This arises due to the dissolution of molten metal when it passes through metallic pipes. The formation of mercuric amalgam is an example of such a process.

1.4 Types of Corrosion

Corrosion can be classified differently based on the environment, the physical effect caused by corrosion, temperature, the region of corrosion, etc. One such classification is given below(Fig 1.4).

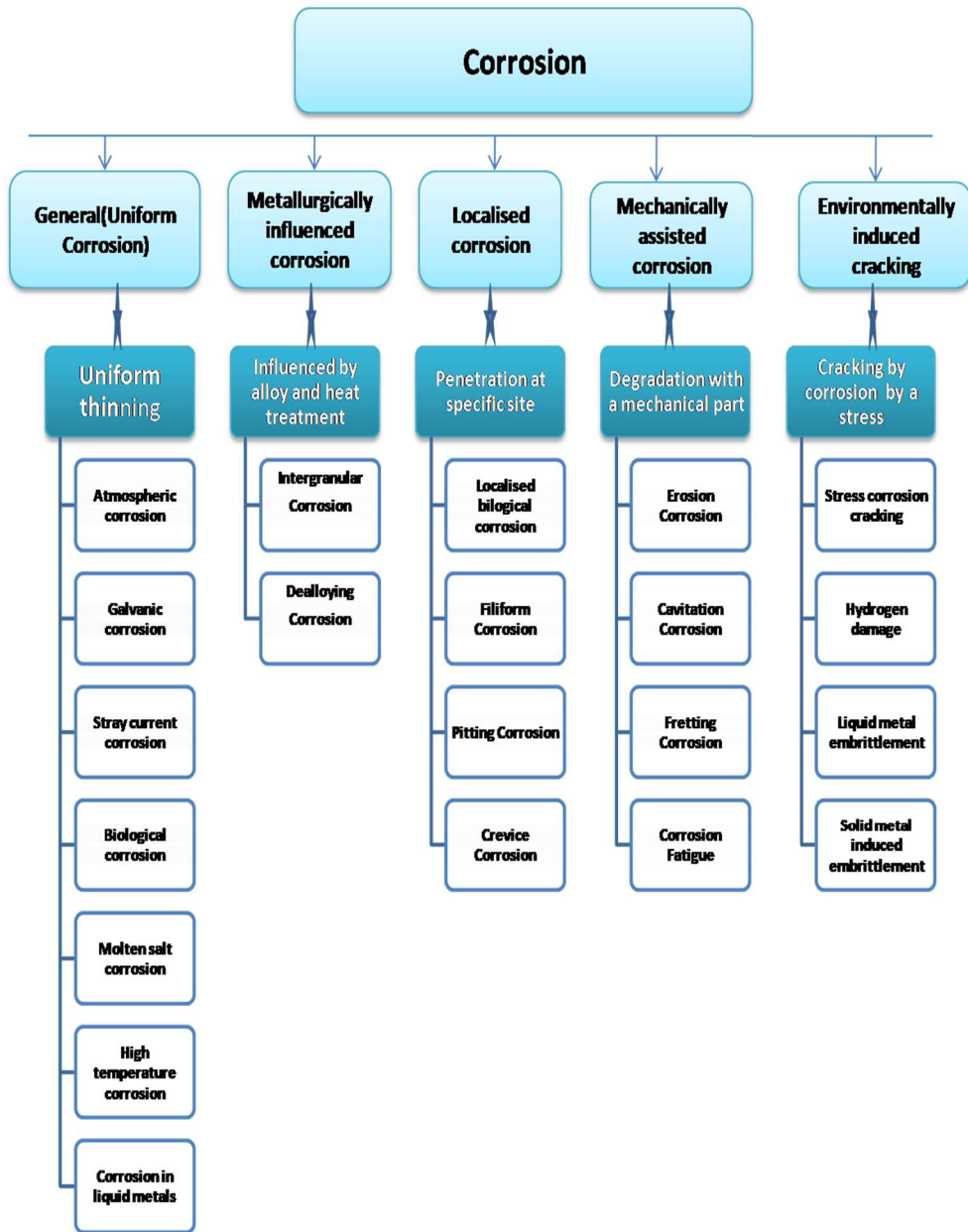


Fig1.4 Classification of different types of corrosion

1.5 Thermodynamics of corrosion

Electrochemistry and thermodynamics play a key role in understanding the spontaneity and driving force of corrosion[1]. The free energy change (ΔG) is negative for a spontaneous reaction. In an electrochemical cell there exist an equilibrium between the electrode and the electrolyte and the feasibility of corrosion of a metal in a corrosive medium can be monitored by thermodynamic principles. ΔG of corrosion is related to emf (ΔE) of the cell by the equation

$$\Delta G = -nF\Delta E \quad (1.9)$$

where n is the number of electrons transferred, F is Faraday constant and ΔE is the potential difference between the two half cells. Pure metals are in a high energy state than their compounds. Therefore the oxidation process of metal (corrosion) is a spontaneous process except for certain noble metals such as gold, platinum, etc[8]. In principle, a metal undergoes corrosion when there is a potential difference exist between the electrode and the electrolyte at a given pH and temperature[9]. A summary of the thermodynamic aspect of corrosion of a metal in a given pH condition is given by the Pourbiax diagram. This diagram is useful in identifying the potential-pH domain where the metal is immune to corrosion and also to regulate the potential and the pH to control corrosion (Fig1.5)[10]

Simplified Pourbaix diagram for iron-water system at 298K

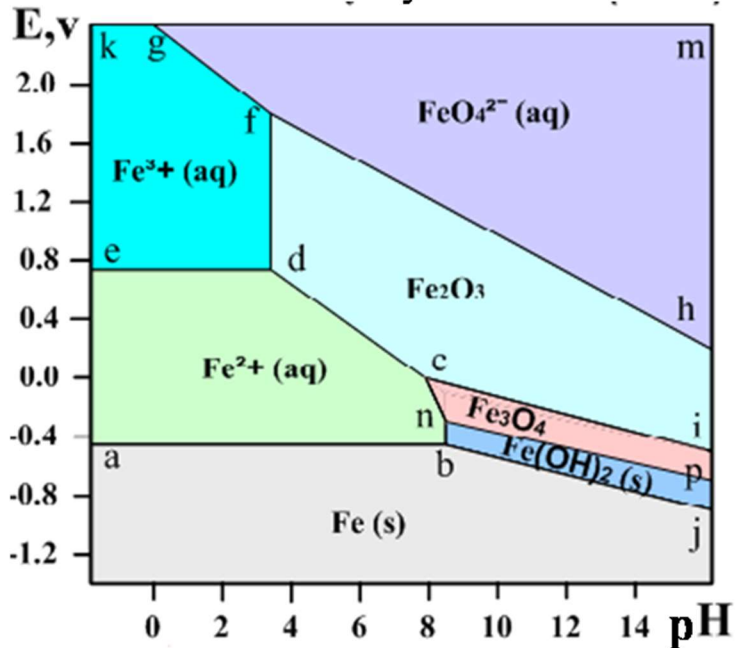


Fig1.5 Pourbiax diagram of Fe in a water system

(source www.substech.com)

1.6 Kinetics of corrosion

Though the tendency of corrosion is evaluated using thermodynamic data, the rate of corrosion is studied using electrochemical kinetic data. Kinetics explains how various factors account for the electrode potential and corrosion rate. The rate of corrosion depends strongly on electron (current) flow to or from the metal-electrolyte interface or between the cathode and the anode. Electrode kinetics is the study of reaction rates at the interface between an electrode and an electrolyte.

Polarisation, overvoltage, and mixed potential theory play an important role in the rate of corrosion.

1.6.1 Polarisation

When a metal corrodes it is no longer in its equilibrium potential. This shift in equilibrium potential to a positive or negative value is termed as polarisation. The three different types of polarisation are activation polarisation, concentration polarisation, and ohmic polarisation.

Activation polarisation is caused by a slow electrode reaction that requires activation energy. For a cathodic or anodic reaction, the activation polarisation dominates is called activation control.

Concentration polarisation occurs when there is a diffusion of a specific species from bulk to the electrode-electrolyte interface. Concentration polarisation predominates when the concentration of the active species is low. For corrosion, only a cathodic reaction will be under concentration polarisation.

Ohmic polarisation is shown when the electrolyte has poor conductivity compared to metals or electrolyte surrounding the electrode has high resistance or metal surface is covered with insulating systems such as paints, films, etc. This gives rise to a potential drop and is known as resistance (IR) drop.

1.6.2 Overvoltage

The magnitude of deviation from the equilibrium potential is termed as overvoltage. In anodic polarisation the electrons are removed from the

Introduction

metal surface and the equilibrium potential shifts to a positive value and in cathodic polarisation electrons are supplied hence the equilibrium potential is shifted to a more negative value. At corrosion potential (E_{corr}) the rate of both the reaction becomes equal and the overvoltage becomes zero.

1.6.3 Mixed Potential Theory

The theory proposed by Wagner and Traud is used to describe the behaviour of metals in various corrosive environments. The electrochemical reaction according to this theory consists of one or more anodic and cathodic reactions. The theory emphasises that the anodic current in an electrochemical cell should be equal to the cathodic current and the number of electrons produced by the oxidation reactions must be equal to the number of electrons consumed in the reduction reactions. The mixed potential is E_{corr} where the rate of cathodic reaction and anodic reaction becomes equal. The current density at E_{corr} is i_{corr} which is a measure of corrosion rate.

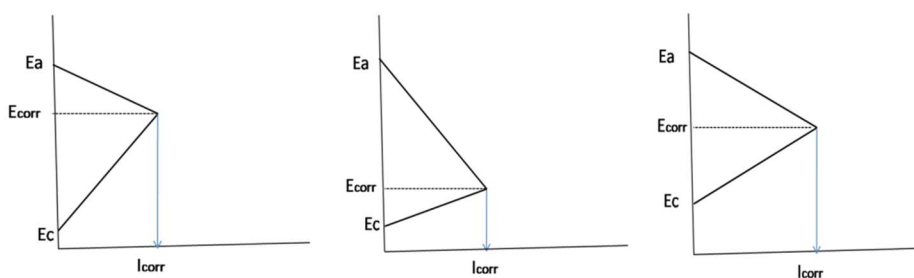


Fig1.6 Evans cathodic, anodic and mixed polarisation diagrams

1.7 Corrosion control measures

The primary control measures of corrosion are

1. Material selection and modification of the environment
2. Proper design
3. Protective coating
4. Cathodic protection
5. Use of inhibitors

1.7.1 Material selection and modification of environment

Each metal has an inherent capacity for corrosion resistance which varies from inert noble metals such as gold and silver to highly reactive metals such as sodium and magnesium. The environment plays a major role in the corrosion resistance of a metal. The rate of corrosive attack is determined by the ratio of corrosivity of the environment to the corrosion resistance of the metal. Factors such as temperature, velocity, pH, etc can critically affect the rate of corrosion. The corrosion due to moisture can be reduced by dehumidification using silica gel, alumina, etc, or corrosion due to oxygen can be reduced by deaeration.

1.7.2 Proper design

Rational design principles can reduce corrosion to a considerable extent especially at the crevices where the accumulation of the corrosive medium is aggressive. Avoiding contact of dissimilar metals in a corrosive medium and by increasing the surface area of anode

compared to cathode if dissimilar metals are in contact can reduce corrosion.

1.7.3 Protective coating

Coatings are a physical barrier between the metal and the environment. The materials used for coating should be inert and must be able to prevent penetration of the environment. In metallic coating metals which are nobler or less noble can be used. Iron can be coated with copper provided there should not be any cracking to avoid the formation of the dissimilar metal corrosion cell. In the case of coating with less noble metals, they act as a sacrificial electrode and protect the metal. Examples are electroplating, galvanisation etc. The inorganic coating includes enamel coating, cement coating etc, and organic coating include paint, coal tar, etc [11].

1.7.4 Corrosion inhibitors

The modification of the environment is an acceptable practice for the mitigation of corrosion and one of the established and efficient practices is the use of inhibitors. Corrosion inhibitors are chemicals which are added in small quantities enormously reduces the rate of corrosion. They reduce the corrosion rate by

- Inhibiting anodic dissolution of metal or cathodic reduction reaction or inhibiting both reactions.
- Controlling the diffusion of ions from the solution to the metallic surface
- Increasing the resistance of the metallic surface

The action of a corrosion inhibitor depends on the nature of the metal and the aggressiveness of the environment. Depending upon the functionality the inhibitors are classified as inorganic and organic by Jones et al. With regard to specific functioning the corrosion inhibitors are classified as follows (Fig 1.7).

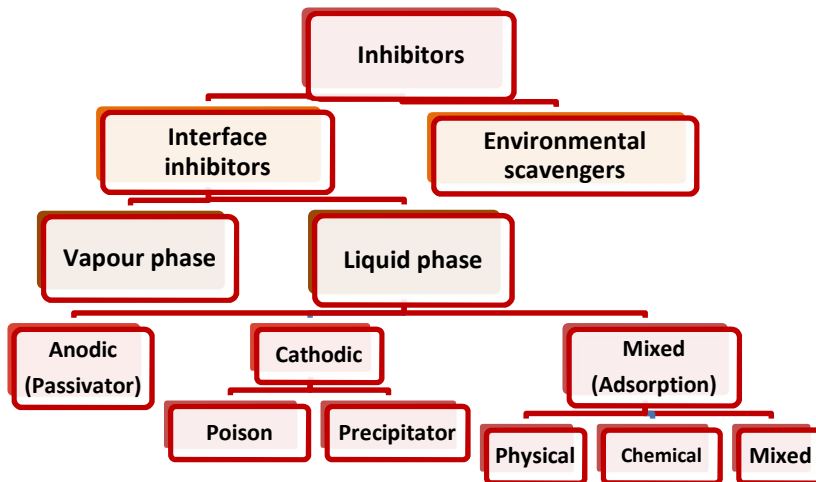


Fig1.7 Classification of corrosion inhibitors

Anodic inhibitors affect the anodic reaction. Anodic inhibitors are used in neutral solutions and they facilitate the formation of a passivating film and prevent anodic process of metal dissolution.

Cathodic inhibitors reduce the corrosion rate either by reducing the cathodic reduction process or by precipitating on the cathodic region. Compounds such as selenides and sulfides are adsorbed on the metal surface whereas arsenic, bismuth, etc reduced on the metal surface to form a metallic layer. Anions such as phosphates, borates, etc limit the diffusion of oxygen to the metal surface forming a protective film.

Introduction

Mixed inhibitors/adsorption inhibitors are in general organic in nature which adsorbs on the metal surface and retard both oxidation and reduction reaction. The organic compounds with N, S, O hetero atoms and aromatic rings are found to be efficient inhibitors. The effectiveness of these inhibitors depends on their capacity to be adsorbed on the metal surface and adsorption capacity depends on the structure of the inhibitor, the surface charge of the metal, and the electrolyte. They protect the metal surface through physisorption, chemisorption, or by film formation. When the metal surface is positively charged the adsorption of a negatively charged compound is facilitated and vice versa. An increase in temperature cause desorption of physisorbed molecules whereas an increase in temperature improves the efficiency and adsorption of chemisorbed molecules. Adsorbed inhibitor molecule may undergo surface reactions to form polymeric films of several angstrom thicknesses and can reduce the corrosion. They are both non conducting ohmic inhibitors increasing the resistance of the circuit and protecting the metal or self-healing conducting inhibitors[12].

Vapour phase inhibitors (VPI) are used against atmospheric corrosion especially in closed vessels.

Scavengers /Environmental conditioners remove oxygen by a chemical reaction and thus reduce the rate of reaction.

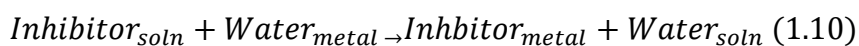
1.8 Mechanism of inhibition by mixed inhibitors

The process of adsorption depends on the charge on the metal surface and the electron density of the inhibitor molecule. The charge on the

Introduction

metal is given as the difference between the corrosion potential and zero charge potential (E_{corr} -ZCP). The charge of the inhibitor depends on lone pair of electrons, loosely bound electrons, presence of pi electrons, benzene rings, functional groups having N, O, S, etc. Most of the organic compounds have an anchoring group which determines the strength of adsorption and the other framework of the molecule influence the charge density of the anchoring group.

In general, adsorption can be explained in two ways. One such is that of HSAB principle based and which describes as hard acid combines with hard bases and soft acids combine with soft bases. Metal in acidic solution is considered as soft and form a strong bond with soft elements such as sulfur. Another idea of adsorption is such as a quasi-substitution of water molecules adsorbed on the metal surface by organic molecules.



The number of water molecules displaced from the metal surface depends on the size, structure, and orientation of the inhibitor molecule. This molecule which is physisorbed on the metallic surface under favourable conditions could be chemisorbed on the metallic surface. The nature and strength of the adsorption are studied by deducing adsorption isotherms.[12]

1.9 Adsorption Isotherms

Adsorption isotherms relate surface coverage (θ) and the concentration of the inhibitor at a particular temperature. The isotherms distinguish the type of preferable adsorption (physisorption/chemisorption) of the inhibitor, accounts for monolayer, multilayer adsorption, the

spontaneity of adsorption process, etc. The different types of adsorption isotherms and their expressions are given below. The basic equation to denote adsorption phenomenon is given as

$$f(\theta, x)e^{-\alpha\theta} = kC \quad (1.11)$$

where $f(\theta, x)$ is the configuration factor representing the physical model and assumptions made in deriving the isotherm. The quantity x represents the number of water molecules replaced by the inhibitor and α is the interaction parameter, C is the concentration of the inhibitor and k is the equilibrium constant[13].

Table 1.1. Different adsorption isotherm models

Isotherm	Equation	Plotting data
Langmuir	$\frac{C}{\theta} = \frac{1}{k} + C$	$\frac{C}{\theta}$ vs C
Frumkin	$\left[\frac{\theta}{1-\theta} \right] e^{-2\alpha\theta} = kC$	$\log C \left(\frac{\theta}{1-\theta} \right)$ vs θ
Temkin	$\alpha\theta = \ln k \cdot C$	θ vs $\log c$
Flory Huggins	$\log \frac{\theta}{C} = \log k + x \log(1 - \theta)$	$\log \frac{\theta}{C}$ vs $\log(1 - \theta)$
Freundlich	$\beta C^{1/n} = \theta$	$\log \theta$ vs $\log C$

For a particular inhibitor at a given temperature isotherms are drawn and the best fit isotherm describes the mechanism of adsorption.

1.10 The concept of synergism

The word synergism means acting together. The total efficiency of the synergistic pair is greater than the efficiency of individual components.

Introduction

The synergism mechanism usually differs from solo action, and the combined effect is neither linear nor additive. The synergism can take advantage of making a less effective yet environmentally benign compound more efficient. The synergism parameter, S is given as

$$S = \frac{1 - I_{1+2}}{1 - I^*_{1+2}} \quad (1.12)$$

where I_{1+2} is the sum of efficiencies of individual components and I^*_{1+2} the efficiency of the mixture[14]. When S, is greater than one indicates a synergistic effect where a bulk chemical reaction between the component molecules occurs or co-operative adsorption takes place by the interaction of component molecules with each other. 'S' less than one represents an antagonistic effect, competitive adsorption, where there is no interaction between the individual components.

1.11 Corrosion Detection and Monitoring Techniques

The understanding of electrochemical aspects of corrosion forms the basis of corrosion testing, gives simple and accurate values of corrosion rate. The proper detection of corrosion implies huge savings of money, time, energy, fewer accidents, and improved quality of products. The testing methods include electrochemical, non-electrochemical methods such as the oldest weight loss method to nondestructive methods such as ultrasonic acoustic and spectroscopic methods (Fig.1.8). The electrochemical methods take the advantage of modern instrumentation, measure very small currents, work on control measures, and less time -consuming.

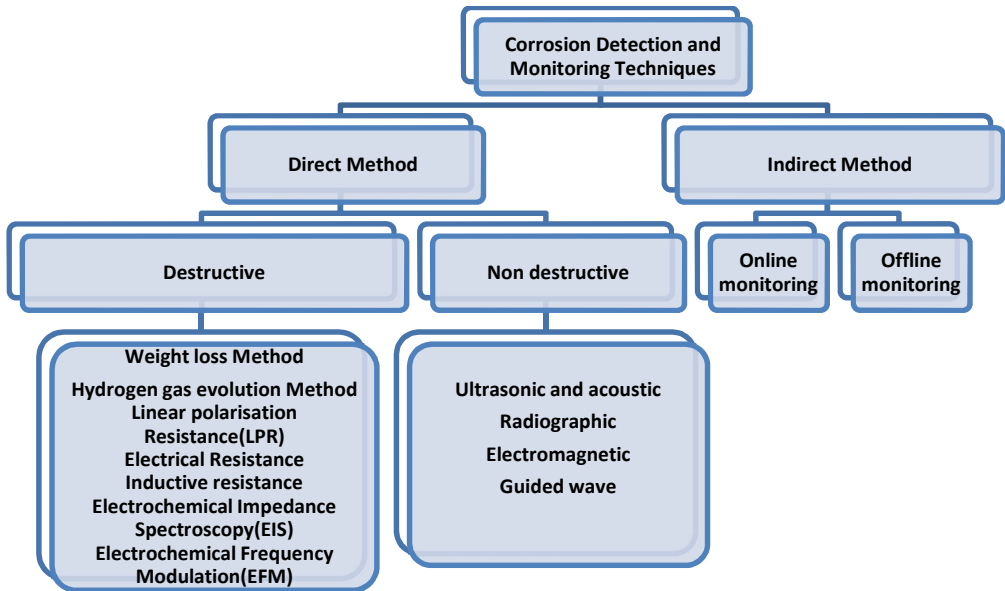


Fig1.8 Classification of corrosion detecting and monitoring techniques

1.11.1 Nonelectrochemical Methods

Because of the simplicity, accuracy, and reliability of non electrochemical methods such as weight loss, is widely used in the industry. The disadvantage of this method is that they are time-consuming and imply minimum information on the mechanism of corrosion.

1.11.1.1 Weight loss (Gravimetric) Method

This is a very simple and accurate method known as the “Gold standard” in corrosion testing. A precleaned weighed metal sample is exposed to a corrosive environment for a certain time duration. The basic measurement is weight loss of the sample and the rate calculated using the time of exposure. The technique is very versatile because the

Introduction

corrosion of any commercially fabricated metals or alloys can be studied. Variety of corrosion processes such as stress corrosion, galvanic corrosion, differential aeration, temperature effect, and different environments such as gases, liquids could be analyzed is the advantage of this method.

1.11.1.2 Hydrogen gas Evolution Method

This method is used for determining the corrosion rate of metals in acidic solutions. The basic measurement is the volume of hydrogen gas evolved due to cathodic reduction process. The volume of the electrolyte replaced by hydrogen gas is noted at various time intervals and it is directly proportional to the rate of corrosion[15].

1.11.2 Electrochemical Methods

1.11.2.1 Electrical Resistance Method(ER)

ER probe method basically measures the weight loss. The advantage over the gravimetric method is that we can measure the weight as frequently as we need since the probe is in situ and is permanently exposed to the corrosion process. The process of corrosion on the metal surface decreases the cross-sectional area and the corresponding increase in electrical resistance is directly related to weight loss.

1.11.2.2 Linear Polarization Resistance method (LPR)

In this method, polarization is done by applying a small overvoltage of 20-25mV. For small overvoltage, there is a linear relationship between

the potential and the current density. The slope of this linear portion is termed as R_p (polarization resistance) and is given as

$$R_p = \frac{\Delta E}{\Delta i} = \frac{\beta_a \beta_c}{2.303(\beta_a + \beta_c) i_{corr}} \quad (1.13)$$

where β_a and β_c are Tafel anodic and cathodic slopes and from corrosion current density (i_{corr}) the corrosion rate is determined. The advantage of this technique is that even a very small corrosion rate (CR) can be determined and can be used for the determination of CR in various process streams. The disadvantage of the method is that it requires Tafel constants to calculate the corrosion rate and when the solution resistance is very high the corrosion rate calculated is inaccurate.

1.11.2.3 Electrochemical Impedance Spectroscopy (EIS)

In the EIS technique, a small amplitude AC signal ($\pm 10\text{mV}$) is applied over a wide range of frequencies (10^5 to 10^{-2}Hz) at 5 to 10 discrete frequencies per decade. Since the applied voltage is of low magnitude it is like LPR, does not polarize the system far from the E_{corr} and therefore it is considered as a non-destructive method. For a linear system, the current response will be a sine wave of the same frequency as the excitation signal but shifted in phase (θ). The impedance is the ratio of these two sine waves and is a complex number and can be represented as a sum of amplitude and a phase shift or sum of real and imaginary components [16].

$$Z_{\omega} = \frac{E_0 \sin \omega t}{I_0 \sin(\omega t + \theta)} = Z_0 \frac{\sin \omega t}{\sin(\omega t + \theta)} = Z_{real}(\omega) + Z_{img}(\omega) \quad (1.14)$$

where Z_{ω} is the impedance, ω is angular frequency- $2\pi f$, f - signal frequency, $Z_{real}(\omega)$ -real part of the impedance, $Z_{img}(\omega)$ - imaginary part of the impedance and

$$\theta = \tan^{-1} \left[\frac{Z_{real}(\omega)}{Z_{img}(\omega)} \right]$$

Discontinuity created in the electrolyte by the introduction of electrode results in separation of charges and the electrode-electrolyte interface act as a capacitor. It is a differential capacitor and the circuit comprises of a capacitor and a resistor (R_p) in parallel. In electrochemical reaction, the polarization is activation controlled and the polarization resistance (R_p) is termed as charge transfer resistance (R_{ct}) and the capacitance is shown as double -layer capacitance (C_{dl}). The impedance of such systems can be described as

$$Z_{\omega} = \left[R_s + \frac{R_{ct}}{1 - \omega^2 C_{dl}^2 R_{ct}^2} \right] - j \left[\frac{\omega C_{dl} R_{ct}^2}{1 - \omega^2 C_{dl}^2 R_{ct}^2} \right] \quad (1.15)$$

The circuit diagram shown below accounts also for the ohmic resistance in solution (solution resistance) between the sample and the reference electrode which is shown as a serially connected resistor (R_s) and the simplest equivalent circuit is termed as Randles circuit(Fig. 1.9). For a diffusion-controlled process, diffusion impedance is also incorporated. At very low frequencies the measured response is a series combination of two resistors (R_s and R_{ct}). At intermediate frequencies,

the capacitor controls the overall circuit. These situations can be given as

When $\omega=0$, $Z\omega =R_s+R_{ct}$ and when $\omega = \infty$, $Z\omega=R_s$

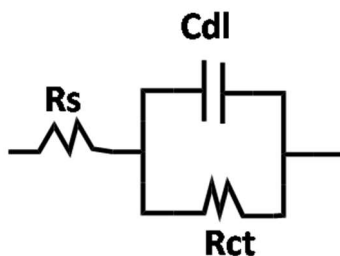


Fig1.9 Randles circuit

The impedance data is reported in three ways; Bode phase angle plot, Bode magnitude plot and Nyquist plot

1.11.2.3.1 Bode Phase Angle and Bode Magnitude Plot

In Bode magnitude plot, the log of the impedance magnitude and log of the frequency of the excitation signal is plotted. In Bode phase angle plot phase angle and log of the frequency is plotted (Fig1.10). From the slope and the phase angle, various processes can be analysed. For the capacitive process, the plot will be linear with a slope of -1 and phase angle shift for a pure capacitor approaches 90° . At high frequencies, the impedance is given by the ohmic resistance and at low frequencies, the impedance is the sum of ohmic resistance and polarisation resistance. Therefore, the polarisation resistance (R_p) will be the difference between impedance at high frequency and low frequency. In the phase angle plot, the phase shift at low and high frequency reaches zero indicating the resistive behaviour. The capacitance can be

measured by extrapolating the linear portions at intermediate frequencies.

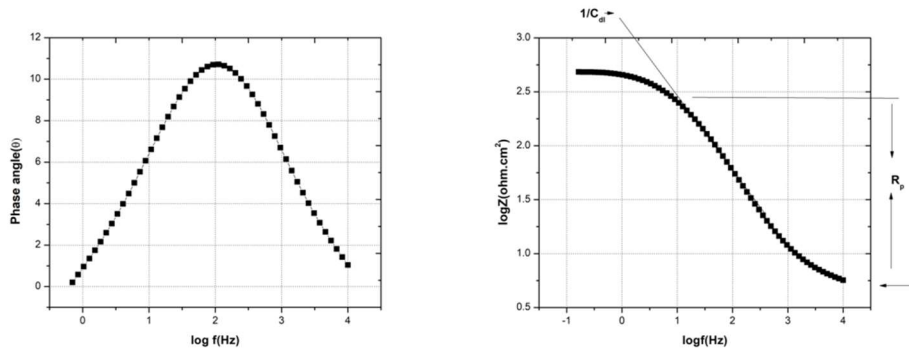


Fig1.10 Bode phase angle and magnitude plot

1.11.2.3.2 Nyquist Plot

In Nyquist plot the imaginary component of the impedance is plotted as a function of the real component. For a perfect RC circuit, Nyquist plot is a perfect semicircle that intercepts the real axis twice. The high-frequency intercept is ohmic resistance and the low-frequency resistance is the sum of ohmic resistance and the charge transfer resistance. Usually, the electrochemical system is not a collection of perfect electrical components. Therefore, the Nyquist plots will be imperfect semicircles (maximum imaginary component is less than double of the R_{ct}) (Fig1.11). These imperfections arise due to impurities, surface in homogeneities, and the roughness of the metal surface, known as frequency dispersion.

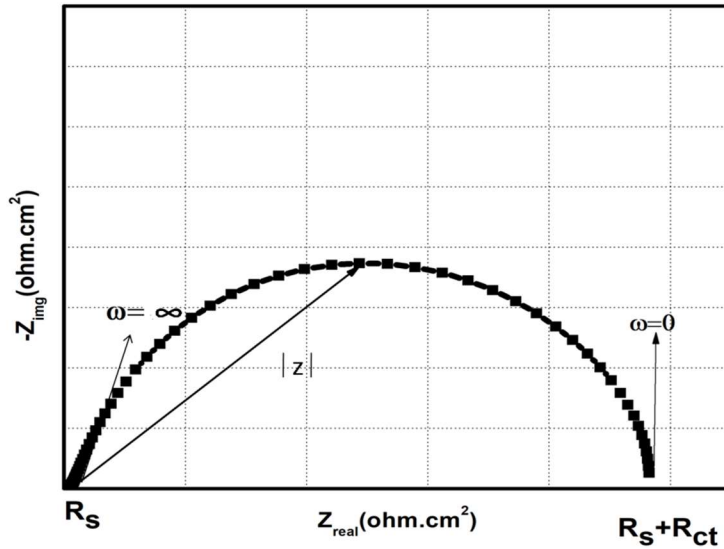


Fig1.11 Nyquist plot

1.11.3 Potentiodynamic Polarisation technique (PDP)

In linear polarisation a small overvoltage is applied to the system whereas in potentiodynamic polarisation studies the E_{corr} is shifted $>\pm 150\text{mV}$ and polarisation curves are obtained. Most often the current response as a function of applied potential is studied in PDP. For many of the metals and alloys, the polarisation curve at high overvoltage is linear to $\log i$ and the representation of this is known as the Stern diagram. The calculations of the rate of corrosion using PDP data is done by extrapolation of the linear part (Tafel extrapolation) of anodic and cathodic polarisation to meet a single point, at E_{corr} and the current density at the point is taken as i_{corr} (Fig1.12). The Tafel equations representing the relationship between the $\log i$ and linear part of polarisation curve is derived from Butler-Volmer equation

$$\log i = \log i_{corr} + \frac{\alpha Z F}{2.303 R T} \eta \quad (1.16)$$

where α is symmetry coefficient, Z is the oxidation state of the metal ion and F is Faraday constant, η is the applied overvoltage

For anodic polarisation Tafel equation is written as

$$\eta_a = \frac{2.303 R T}{\alpha Z F} \log \frac{i_a}{i_{corr}} = \beta_a \log \frac{i_a}{i_{corr}} \quad (1.17)$$

and for cathodic polarisation

$$\eta_c = \frac{2.303 R T}{(1 - \alpha) Z F} \log \frac{i_c}{i_{corr}} = \beta_c \log \frac{i_c}{i_{corr}} \quad (1.18)$$

where β_a and β_c are termed as anodic and cathodic Tafel constants.

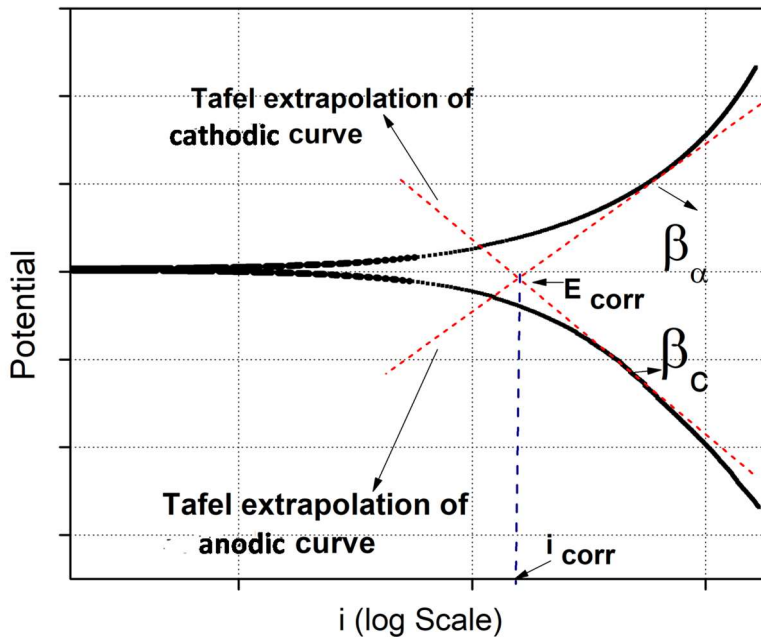


Fig1.12 Tafel extrapolation of polarisation curve

1.11.4 Electrochemical Frequency Modulation (EFM)

The advantage of the EFM method is that it can give corrosion current densities without the prior knowledge of Tafel constants. Similar to EIS, this technique makes use of a small amplitude AC signal. Since the current response is a nonlinear function of the applied voltage two signals are simultaneously applied to the system and the system responds nonlinearly to the applied potential. The current response contains the frequency components of sum, difference, and multiples of input frequencies[17].

1.12. Pyrazole derivatives as corrosion inhibitors- A Review

Pyrazole is a five membered heterocyclic ring with two nitrogen atoms in the adjacent positions. A partially reduced form of pyrazole is named pyrazolines and a completely reduced form is named pyrazolidine [18]. Pyrazoles and their derivatives are having interesting biological, medicinal and corrosion inhibition properties[18].Kun Cao et al have studied the inhibition property of 1-phenyl-3-methyl-5-pyrazolone in 1M HCl at 298K for mild steel and obtained an efficiency of 97.2% for 1mM(200ppm)[19]. Corrosion inhibition behaviour of 3-phenyl-1H-pyrazole-4-carboxaldehyde on corrosion of mild steel in 1.0 M HCl has been studied by EL Aoufir Yet al[20].It has remarkable inhibition efficiency of 96.33% for 5×10^{-3} M concentration.5-chloro-1-phenyl-3-methylpyrazolo-4-methinethiosemicarbazide, synthesised by reaction between pyrazole carbaldehyde and thiosemicarbazide was investigated as corrosion inhibitor for carbon steel in HCl by the chemical and electrochemical method by R.S. Abdel Hameed et al observed an inhibition efficiency

Introduction

of 95.5% for 200ppm of the inhibitor[21]. Chandrabhan Verma et al have synthesised four pyrazole derivatives and maximum inhibition efficiency of 94.03% is given by 4, 4'-((2-hydroxy-4-methoxy phenyl)methylene)bis(3-methyl-1-phenyl-1H-pyrazol-5-ol) for 4.58M concentration by EIS analysis[22]. Corrosion inhibition capacity of 4, 4'-(1, 4phenylene)bis(6-amino-3-methyl-2, 4 dihydropyrano[2, 3-c]pyrazole-5-carbonitrile was determined by Priyanka Singh et al and obtained an efficiency of 98% for 150ppm in 0.5M H₂SO₄[23].The inhibition efficiency of 4-substituted pyrazole-5-ones in 0.5M H₂SO₄ for 304stainless steel is analysed using electrochemical methods and found that methoxy substituted derivative has a maximum efficiency of 70.87%[24]. The inhibitive capacity of 1-phenyl pyrazolidine-3, 5-dione(PPD), d4-(4-benzylidene)-1-phenylpyrazolidine-3, 5-dione(BPP) is investigated in 1M H₂SO₄ by weight loss, EIS and PDP techniques and a maximum efficiency of 90.94% is reported for BPP. An efficiency of 61.79% is given by 1-methyl pyrazole in 1M HCl. The analysis is carried out by PDP and EIS method[25]. Five Pyrazolo[3, 4-b]pyridines corrosion inhibition strength is measured in 1M HCl for mild steel and AP-5 is found to be the best inhibitor[26], N1-bis (2-(bis ((3, 5-dimethyl-1H-pyrazol-1-yl) methyl) amino)ethyl)-N2, N2-bis ((3, 5-dimethyl-1H-pyrazol-1-yl) methyl) ethane-1, 2-diamine: PAP and diethyl 1, 1'-(((4-acetylphenyl) azanediyl) bis (methylene)) bis (5-methyl-1H-pyrazole-3-carboxylate): PAC are found to be efficient inhibitors for mild steel in 1M HCl solution[27].Considerable corrosion inhibition capacities are reported for four pyrazoline derivatives giving a maximum efficiency of 84.31% for PCT[28]. (E)-5-(4- (dimethylamino)phenyl)-3-(4-(dimethylamino)styryl)-2, 3-dihydro-1H-pyrazole-1-carbothioamide (DDP) is found to be efficient

Introduction

inhibitors for carbon steel in 2M HCl[29]. Synergism studies of phenylazo-3-methyl-2-pyrazolon-5-one and derivatives with KBr, KCN, KI are done and observed that inhibition efficiency increased to 74.7% for the synergistic pair from 60.1%. 1-{{[benzyl-(2-cyano-ethyl)-amino]-methyl}}-5-methyl-1H-pyrazole-3-carboxylic acid methyl ester (P1) and 1-{{[benzyl-(2-cyano-ethyl)-amino]-methyl}}-5-methyl-1H-pyrazole-3-carboxylic acid ethyl ester (P2) in 1M HCl gives an efficiency of 92.3%[30]. Nine pyrazolone chalcones inhibition efficiency is determined by Zahraa Talib et al and obtained an inhibition efficiency of 85% in 1M H₂SO₄[31]. The anticorrosive properties of three biologically active pyrazole chalcones, namely AA-1, AA-2 and AA-3 for mild steel in hydrochloric acid at temperature range 303–333 K was analysed by Chaouiki A. et al and are found as effective inhibitors[32].

1.13. Review-Fruits/fruit rind/peel/seeds as corrosion inhibitors

In recent years many of the natural products because of their availability, non-toxicity, and biodegradability have been used as corrosion inhibitors. Various parts of the plants such as flowers, leaves, fruits, etc are proved to be efficient and eco-friendly corrosion inhibitors [33-37]. Most often fruits, fruit rinds, peels, some fruits, and seeds are considered as wastes and face disposal problems. The fruit wastes are rich in a variety of complex yet nontoxic organic compounds that could be used as efficient inhibitors. A review of the fruit/fruit rind/pericarp/peel/seed/juice is summarised in the following table discussing specifically mentioning the corrosion inhibition properties.

Inhibitor	Medium / Material	Temperature	Methods	C _{inh}	Highest Efficiency	Reference
Banana peel (Musa paradisiac)	HCl MS	299K	WL, EIS, PDP	Raw 300mg/L	90%	[38]
Pomegranate husk (Punica granatum)	1M HCl Q235 steel	333K	WL, PDP	Aqueous 1000mg/L	95%	[39]
Longan seed and peel (Aristolochic indica)	0.5M HCl MS	298K - 328K	WL, EIS, PDP	600mg/L	92.93% (298K)	[40]
Lychee's peel and seed (Litchi chinensis)	0.5M HCl MS	298K	WL, EIS, PDP	66mg/L	97.95%	[41]
(Rice hull) OryzaSativa L	1M HCl MS	300K	EIS, PDP	1000ppm	88%	[42]
Orange Peel	0.1M HCl CS	-	EIS, PDP	10%	95%	[43]
Watermelon rind	1M HCl, MS	298K & 333K	WL, EIS, PDP	1000ppm	92%(298K)	[44]
Pisum sativa peel (green pea)	1M-4M HCl MS	303K-333K	WL, PDP, EIS	400mg/L	91%(1M HCl)	[45]
Cucumber peel (Cucumis sativus)	1M HCl CS	298K, 313K, 323K and 333K	EIS, PDP	50%	82.7%(298K)	[46]
Watermelon rind, seed and peel	1M HCl MS	298K	EIS, PDP	2g/L	83.35(R) 85.96(S) 79.52(P)	[47]
Pistacia Atlantic Gals(pistachio)	1M HCl X 52 steel	298K	WL, EIS, PDP	10ppm	97.1%	[48]
Brown onion peel	1M HCl, CS	298K	WL, EIS, PDP	300mg/L	94%	[49]
Strychnicnix-vomica (poison nut)	4% and 8% HCl, CS	298K	WL, EIS, PDP	2 g/L	89% (4%) 88.6% (8%)	[49]

Introduction

Inhibitor	Medium / Material	Temperature	Methods	C _{inh}	Highest Efficiency	Reference
Akee Apple (Blighia sapida)	2M HCl, MS	303K-333K	WL, Thermometric	0.5g/L	86.9(303K)	[50]
Sunflower (seed hull)	1M HCl, MS	298k-333K	EIS, PDP	400ppm	98%(298K)	[34]
Kola Nitida (kola nut)	0.1M HCl, Al alloy	303K	WL, EIS, PDP	1200mg/L	85%	[51]
Vietnam orange peel essential oil	1M HCl, MS	289K-338K	WL, EIS, PDP	4g/L	93%	[52]
Date palm (Phoenix dactylifera)/seed	1M HCl, MS	298K-333K	WL, PDP, EIS	2.5g/L	86.8%	[53]
Psidium Guajava(guava) seed	0.5M HCl Aluminium alloy	303K-353K	WL	1.206g/L	81%	[54]
Retama monosperma (L.) Boiss. seed	1M HCl, CS	303K	EIS, PDP	400mg/L	94.4%	[55]
Mango, orange, passion fruit and cashew peel	1M HCl, CS	298K	WL, EIS, PDP	600mg/L 400mg/L 500mg/L 800mg/L	91%(M) 95%(O) 90%(P) 80%(C)	[56]
Theobroma cacao peels(coco)	1.5M HCl, MS	298K	WL, PDP	2.5%	95.6%	[57]
Opuntia ficus-indica (Prickly pear) seed	1M HCl, MS	298K-328K	WL, PDP, EIS	5g/L	90%(298K)	[58]
Jamun (syzygium cumini)seed	1M HCl, MS	308K	WL, LPR, PDP, EIS	600ppm	94.28%	[59]

Introduction

Inhibitor	Medium / Material	Temperature	Methods	C_{inh}	Highest Efficiency	Reference
Trigonella foenum-graecum L seeds (Fenugreek)	1M HCl, MS	298K	EIS, PDP	1400ppm	86.66	[60]
Tamarindus indica	1M HCl, MS	298K-328K	EIS, PDP	800ppm	85%	[61]
Cashew nut testa tannin	0.1M, 0.5M, 2M HCl, Aluminium	303K	WL, Thermometric	0.5g/L	63%	[62]
Avocado seed powder (persea americana) butter fruit	0.5M HCl, SAE 1008 CS	-	WL, EIS, PDP	-	-	[63]
Arak tree (Salvadora persica) fruits	1M HCl, Low Alloy steel	303K-333K	WL, EIS, PDP	500ppm	94.35%	[64]
Terminalia chebula fruit (Kadukka)	1M HCl, MS	303K	WL, EIS, PDP	800mg/L	88.9%	[65]
Tender arecanut seed	1M HCl, Aluminium	303K-333K	WL, EIS, PDP	4.5g/L	96.15%	[66]
Mango and orange peels	1M HCl, CS	298K	WL, PDP, EIS	600mg/L	96%(M) 91%(O)	[67]
Orange peel	1M HCl, MS	-	WL, EIS, PDP	0.25%	99.19%	[68]
Fruits of cashew (Anacardium occidentale L.)	0.1M HCl, MS	303K	WL	80%	80.5%	[69]
Chinese gooseberry fruit shell	1M HCl, CS	298K	WL, EIS, PDP	1000ppm	94%	[70]

Introduction

Inhibitor	Medium / Material	Temperature	Methods	C _{inh}	Highest Efficiency	Reference
Musa paradisiaca peels(banana)	1M HCl 0.5M H ₂ SO ₄ MS	299K	EIS, PDP	400mg/L	90% 83%	[71]
Prunus dulcis(Almond) peel	0.1M HCl MS	299K	EIS, PDP	240mg/L	83%	[72]
grape pomace	1M HCl, CS	298-300K	WL, EIS, PDP	3%	93%	[73]
Peganum harmala seed	1M HCl, MS	-	EIS, PDP	800ppm	94%	[74]
Citrullus lanatus fruit(watermelon)	1M HCl, MS	-	EIS, PDP	800ppm	91%	[75]
Cucumis sativus (cucumber) peel and seed oil	2M HCl AISI1007steel	Ambient temp.	WL, EIS, PDP	1g/L	86.63%(peel) 39.23%(seed)	[76]
Lemon peel	1M HCl, MS	-	WL, PDP	10%	74.08	[77]
Lemon seed Chloroform extract(CLS)	1M HCl, MS	298K	EIS, PDP	CLSD (2layer coating)	95%	[78]
Carrot (Daucus Carota L.) Peels	1M HCl, MS	298K, 308K, 323K	WL, PDP	0.5g/L	88.08%	[79]
Bablos Naranga(Pomelo) Peel	0.1M HCl, MS	303K	WL, PDP, EIS	10000ppm	70.75%	[80]
Iraqi orange peel (Citrus sinensis)	0.5M HCl SAE AISI 1018 steel	298K	WL, PDP	500ppm	56.83%	[81]
Orange juice	MS-	-	WL	-	-	[82]
Garcinia kola seed	2M HCl MS	303K & 333K	Gasometric	50%	93.08(303K) 76.82(333K)	[83]

Inhibitor	Medium / Material	Temperature	Methods	C_{inh}	Highest Efficiency	Reference
Garcinia Mangostana fruit pericarp	5%HCl MS	303K-318K	WL, EIS, PDP	25%	97.45%(303K) 96.34%(318K)	[84]
garcinia cola seed	1M HCl, MS	-	WL, EIS, PDP	100ppm	96%	[85]
Papaya peel	1M HCl Aluminium alloy	303K	EIS, PDP	2g/L	98.1%	[86]
Citrus Paradisi (Grapefruit)	0.5M HCl, MS	303K-323K	WL	2.5%	46%	[87]
Punica Granatum and Citrus Sinesis peel	0.5M HCl MS	303K-333K	WL	15%	92.54%	[88]
Red apple (Malus domestica)	0.5M HCl, MS	303K-333K	WL, EIS, PDP	5g/L	87.9%	[89]
Myristica fragrans(Nutmeg) fruit	0.5M H ₂ SO ₄ MS	298K	WL, EIS, PDP	500mg/L	87.81%	[90]
Garcinia Indica seed	0.5M H ₃ PO ₄ Aluminium	303K-323K	EIS, PDP	500ppm	85.59%	[91]

MS- Mild steel, CS-Carbon steel, WL- Weight loss, EIS-Electrochemical impedance spectroscopy PDP-Potentiodynamic polarisation.

1.14 The present work

The present work focuses on the corrosion inhibition properties of a few synthesised pyrazolone derivatives and selected fruit rind extracts in acidic environments such as HCl and H₂SO₄. The synergistic interaction of pyrazolones and fruit rind extracts are also studied using selected inorganic and organic molecules.

References

1. Fontana, M.G. and N.D. Greene, *Corrosion engineering*. 2018: McGraw-hill.
2. Pedferri, P., *Corrosion science and engineering*. 2018: Springer.
3. Prasad, A.R., A. Kunyankandy, and A. Joseph, *Corrosion Inhibition in Oil and Gas Industry: Economic Considerations*. *Corrosion Inhibitors in the Oil and Gas Industry*, 2020: p. 135-150.
4. Elayaperumal, K. and V.S. Raja, *Corrosion Failures: Theory, Case Studies, and Solutions*. 2015: John Wiley & Sons.
5. Uhlig, H.H., *The cost of corrosion to the United States*. *Corrosion*, 1950. **6**(1): p. 29-33.
6. Thompson, N.G., M. Yunovich, and D. Dunmire, *Cost of corrosion and corrosion maintenance strategies*. *Corrosion Reviews*, 2007. **25**(3-4): p. 247-262.
7. Bhaskaran, R., N. Palaniswamy, and N. Rengaswamy, *Cost of corrosion and corrosion auditing in indian industries*. *Corrosion Reviews*, 2009. **27**(Supplement): p. 1-35.
8. Davies, M., *Corrosion: understanding the basics*. *Corrosion*, 2000. **56**(11): p. 1192.
9. Perez, N., *Electrochemistry and corrosion science*. Vol. 412. 2004: Springer.
10. McCafferty, E., *Introduction to corrosion science*. 2010: Springer Science & Business Media.
11. Davis, J.R., *Corrosion: Understanding the basics*. 2000: Asm International.
12. Papavinasam, S., *5> J Corrosion Inhibitors*. 1999.
13. Shibli, S. and V. Saji, *Co-inhibition characteristics of sodium tungstate with potassium iodate on mild steel corrosion*. *Corrosion Science*, 2005. **47**(9): p. 2213-2224.
14. Umoren, S., Y. Li, and F. Wang, *Synergistic effect of iodide ion and polyacrylic acid on corrosion inhibition of iron in H2SO4 investigated by electrochemical techniques*. *Corrosion Science*, 2010. **52**(7): p. 2422-2429.

15. Song, G., A. Atrens, and D. StJohn, *An hydrogen evolution method for the estimation of the corrosion rate of magnesium alloys*, in *Essential readings in magnesium technology*. 2016, Springer. p. 565-572.
16. Frankel, G.S., *Electrochemical techniques in corrosion: status, limitations, and needs*. Journal of ASTM International, 2008. **5**(2): p. 1-27.
17. Obot, I. and I.B. Onyeachu, *Electrochemical frequency modulation (EFM) technique: Theory and recent practical applications in corrosion research*. Journal of Molecular Liquids, 2018. **249**: p. 83-96.
18. Kumar, K.A. and P. Jayaroopa, *Pyrazoles: synthetic strategies and their pharmaceutical applications-an overview*. Int J PharmTech Res, 2013. **5**(4): p. 1473-1486.
19. Cao, K., W. Li, and L. Yu, *Investigation of 1-Phenyl-3-Methyl-5-Pyrazolone as a corrosion inhibitor for mild steel in 1M hydrochloric acid*. Int. J. Electrochem. Sci, 2012. **7**: p. 806-818.
20. Aoufir, E.Y., et al., *Pyrazole Derivative as Corrosion Inhibitor for Mild Steel in Hydrochloric Acid Medium: Electrochemical and Theoretical Studies*. Research journal of pharmaceutical biological and chemical sciences, 2016. **7**(5): p. 1219-1227.
21. Hameed, R.A., et al., *Pyrazole derivatives as corrosion inhibitor for C-steel in hydrochloric acid medium*. J. Mater. Environ. Sci, 2012. **3**(2): p. 294.
22. Verma, C., et al., *Pyrazole derivatives as environmental benign acid corrosion inhibitors for mild steel: Experimental and computational studies*. Journal of Molecular Liquids, 2020. **298**: p. 111943.
23. Singh, P., et al., *Corrosion Inhibition by Green Synthesized Inhibitor: 4, 4'-(1, 4Phenylene) bis (6-amino-3-methyl-2, 4dihydropyrano [2, 3-c] pyrazole-5 carbonitrile) for Mild Steel in 0.5 MH 2 SO 4 Solution*. Journal of Bio-and Tribo-Corrosion, 2019. **5**(1): p. 11.
24. Abdallah, M., *Corrosion behaviour of 304 stainless steel in sulphuric acid solutions and its inhibition by some substituted pyrazolones*. Materials Chemistry and Physics, 2003. **82**(3): p. 786-792.
25. Khaled, K. and S. Abdel-Rehim, *Electrochemical investigation of corrosion and corrosion inhibition of iron in hydrochloric acid solutions*. Arabian Journal of Chemistry, 2011. **4**(4): p. 397-402.

26. Dandia, A., et al., *Ultrasound-assisted synthesis of pyrazolo [3, 4-b] pyridines as potential corrosion inhibitors for mild steel in 1.0 M HCl*. ACS Sustainable Chemistry & Engineering, 2013. 1(10): p. 1303-1310.
27. El Arrouji, S., et al., *The influence of some pyrazole derivatives on the corrosion behaviour of mild steel in 1M HCl solution*. Journal of Materials and Environmental Science, 2016. 7(1): p. 299-309.
28. Anusuya, N., et al., *Corrosion inhibition effect of hydroxy pyrazoline derivatives on mild steel in sulphuric acid solution together with Quantum chemical studies*. J. Mater. Environ. Sci, 2015. 6(6): p. 1606-1623.
29. Boudjellal, F., et al., *Experimental and theoretical approach to the corrosion inhibition of mild steel in acid medium by a newly synthesized pyrazole carbothioamide heterocycle*. Journal of Molecular Structure, 2020. 1199: p. 127051.
30. Herrag, L., et al., *1-{[Benzyl-(2-cyano-ethyl)-amino]-methyl}-5-methyl-1H-pyrazole-3-carboxylic acid methyl ester*. Molbank, 2006. 2006(5): p. M493.
31. Khudhair, Z.T. and M.S. Shihab, *Preparation and Investigation of Some New Pyrazole Derivatives as Corrosion Inhibitors for Mild Steel in Acidic Media*. Al-Nahrain Journal of Science, 2016. 19(2): p. 33-42.
32. Chaouiki, A., et al., *Assessing the impact of electron-donating-substituted chalcones on inhibition of mild steel corrosion in HCl solution: Experimental results and molecular-level insights*. Colloids and Surfaces A: Physicochemical and Engineering Aspects, 2020. 588: p. 124366.
33. Khan, M., et al., *Evaluation of Matricaria aurea Extracts as Effective Anti-Corrosive Agent for Mild Steel in 1.0 M HCl and Isolation of Their Active Ingredients*. Sustainability, 2019. 11(24): p. 7174.
34. Hassannejad, H. and A. Nouri, *Sunflower seed hull extract as a novel green corrosion inhibitor for mild steel in HCl solution*. Journal of Molecular Liquids, 2018. 254: p. 377-382.
35. Molina-Ocampo, L., M. Valladares-Cisneros, and J. Gonzalez-Rodriguez, *Using hibiscus sabdariffa as corrosin inhibitor for Al in 0.5 M H2SO4*. Int. J. Electrochem. Sci, 2015. 10: p. 388-403.

36. Yetri, Y. and N. Jamarun, *Inhibitory action of Theobroma Cacao peels extract on corrosion of mild steel in different media*. rjc, 2016.**9**(4): p. 716-727.
37. Manikandan, C.B., et al., *Corrosion Inhibition of Mild Steel by using Banana Peel Extract*. 2018.
38. Ji, G., et al., *Musa paradisiaca peel extract as green corrosion inhibitor for mild steel in HCl solution*. Corrosion Science, 2015. **90**: p. 107-117.
39. Chen, G., et al., *Extracts of Punica granatum Linne husk as green and eco-friendly corrosion inhibitors for mild steel in oil fields*. Research on Chemical Intermediates, 2013. **39**(8): p. 3545-3552.
40. Liao, L.L., et al., *Longan seed and peel as environmentally friendly corrosion inhibitor for mild steel in acid solution: experimental and theoretical studies*. Journal of colloid and interface science, 2017. **499**: p. 110-119.
41. Liao, L.L., et al., *Corrosion protection for mild steel by extract from the waste of lychee fruit in HCl solution: Experimental and theoretical studies*. Journal of colloid and interface science, 2018. **520**: p. 41-49.
42. Prabakaran, M., et al., *Anticorrosion properties of momilactone A isolated from rice hulls*. Journal of Industrial and Engineering Chemistry, 2017. **45**: p. 380-386.
43. M'hiri, N., et al., *Corrosion inhibition of carbon steel in acidic medium by orange peel extract and its main antioxidant compounds*. Corrosion Science, 2016. **102**: p. 55-62.
44. Odewunmi, N.A., et al., *L-citrulline: An active corrosion inhibitor component of watermelon rind extract for mild steel in HCl medium*. Journal of the Taiwan Institute of Chemical Engineers, 2015. **51**: p. 177-185.
45. Srivastava, M., et al., *Low cost aqueous extract of Pisum sativum peels for inhibition of mild steel corrosion*. Journal of Molecular Liquids, 2018. **254**: p. 357-368.
46. Al-Senani, G.M., *Corrosion inhibition of carbon steel in acidic chloride medium by Cucumis sativus (cucumber) peel extract*. Int. J. Electrochem. Sci, 2016. **11**: p. 291-302.
47. Odewunmi, N., S. Umoren, and Z. Gasem, *Watermelon waste products as green corrosion inhibitors for mild steel in HCl solution*.

- Journal of Environmental Chemical Engineering, 2015. **3**(1): p. 286-296.
48. Dekmouche, M., et al., *Green approach to corrosion inhibition by ethyl acetate extract from Pistacia atlantica gals in hydrochloric acid solution*. Int. J. Electrochem. Sci, 2014. **9**: p. 3969-3978.
 49. Ferreira, K., et al., *Corrosion inhibition of carbon steel in HCl solution by aqueous brown onion peel extract*. Int. J. Electrochem. Sci, 2016. **11**: p. 406-418.
 50. Stephen, J. and A. Adebayo, *Inhibition of corrosion of mild steel in hydrochloric acid solution using akee apple seed extract*. Journal of Failure Analysis and Prevention, 2018. **18**(2): p. 350-355.
 51. Njoku, D.I., et al., *Natural products for materials protection: corrosion protection of aluminium in hydrochloric acid by Kola nitida extract*. Journal of Molecular Liquids, 2016. **219**: p. 417-424.
 52. Bui, H.T., et al., *Comparative study on Corrosion Inhibition of Vietnam Orange Peel Essential Oil with Urotropine and Insight of Corrosion Inhibition Mechanism for Mild Steel in Hydrochloric Solution*. Journal of Electrochemical Science and Technology, 2019. **10**(1): p. 69-81.
 53. Umoren, S.A., Z.M. Gasem, and I.B. Obot, *Natural products for material protection: inhibition of mild steel corrosion by date palm seed extracts in acidic media*. Industrial & Engineering Chemistry Research, 2013. **52**(42): p. 14855-14865.
 54. Sharma, Y. and S. Sharma, *Corrosion Inhibition of Aluminum by Psidium Guajava Seeds in HCl Solution*. Portugaliae Electrochimica Acta, 2016. **34**(6): p. 365-382.
 55. El Hamdani, N., et al., *Alkaloids extract of Retama monosperma (L.) Boiss. seeds used as novel eco-friendly inhibitor for carbon steel corrosion in 1 M HCl solution: Electrochemical and surface studies*. Applied Surface Science, 2015. **357**: p. 1294-1305.
 56. Da Rocha, J.C., J.A.d.C.P. Gomes, and E. D'Elia, *Corrosion inhibition of carbon steel in hydrochloric acid solution by fruit peel aqueous extracts*. Corrosion Science, 2010. **52**(7): p. 2341-2348.
 57. Yetri, Y. and N. Jamarun, *Corrosion inhibitor of mild steel by polar extract of theobroma cacao peels in hydrochloric acid solution*. Asian Journal of Chemistry, 2015. **27**(3): p. 875-881.

58. Hmamou, D.B., et al., *Prickly pear seed oil extract: a novel green inhibitor for mild steel corrosion in 1 M HCl solution*. International Journal of Electrochemical Science, 2012. **7**(2): p. 1303-1318.
59. Singh, A. and M. Quraishi, *The extract of Jamun (Syzygiumcumini) seed as green corrosion inhibitor for acid media*. Research on Chemical Intermediates, 2015. **41**(5): p. 2901-2914.
60. Ennouri, A., A. Lamiri, and M. Essahli, *Corrosion Inhibition of Aluminium in Acidic Media by Different Extracts of Trigonellafoenum-graecum L Seeds*. Portugaliae Electrochimica Acta, 2017. **35**(5): p. 279-295.
61. Dehghani, A., et al., *Electronic/atomic level fundamental theoretical evaluations combined with electrochemical/surface examinations of Tamarindus indiaca aqueous extract as a new green inhibitor for mild steel in acidic solution (HCl 1 M)*. Journal of the Taiwan Institute of Chemical Engineers, 2019. **102**: p. 349-377.
62. Nnaji, N.J., N.O. Obi-Egbedi, and C.O. Okoye, *Cashew nut testa tannin: assessing its effects on the corrosion of aluminium in HCl*. Portugaliae Electrochimica Acta, 2014. **32**(2): p. 157-182.
63. de Jesus, M.E.S., et al., *Evaluation of Efficiency of avocado seed powder (Persea Americana) as a corrosion inhibitor in SAE 1008 carbon steel in acidic medium*. Brazilian Journal of Development, 2020. **6**(10): p. 77197-77215.
64. Hassan, A.A. and H.T. Abdel-Fatah, *Aqueous Extract of Salvadora Persica as a Novel Green Corrosion Inhibitor for Low-Alloy Steel in Acidic Media-Part I*. Int. J. Electrochem. Sci, 2016. **11**: p. 6959-6975.
65. Oguzie, E., et al., *Biomass extracts for materials protection: corrosion inhibition of mild steel in acidic media by Terminalia chebula extracts*. Chemical engineering communications, 2014. **201**(6): p. 790-803.
66. Raghavendra, N. and J.I. Bhat, *Green approach to inhibition of corrosion of aluminum in 0.5 M HCl medium by tender arecanut seed extract: insight from gravimetric and electrochemical studies*. Research on Chemical Intermediates, 2016. **42**(7): p. 6351-6372.
67. Rocha, J.C.d., J.A.d.C.P. Gomes, and E. D'Elia, *Aqueous extracts of mango and orange peel as green inhibitors for carbon steel in hydrochloric acid solution*. Materials Research, 2014. **17**(6): p. 1581-1587.

68. Xavier Stango, S.A. and U. Vijayalakshmi, *Studies on corrosion inhibitory effect and adsorption behavior of waste materials on mild steel in acidic medium*. Journal of Asian Ceramic Societies, 2018. **6**(1): p. 20-29.
69. Olawale, O., J. Bello, and P. Akinbami, *A study on corrosion inhibitor of mild-steel in hydrochloric acid using cashew waste*. International Journal of Modern Engineering Research, 2015. **5**(8): p. 25-30.
70. Dehghani, A., G. Bahlakeh, and B. Ramezanzadeh, *A detailed electrochemical/theoretical exploration of the aqueous Chinese gooseberry fruit shell extract as a green and cheap corrosion inhibitor for mild steel in acidic solution*. Journal of Molecular Liquids, 2019. **282**: p. 366-384.
71. Tiwari, P., et al., *Economic use of waste Musa paradisiaca peels for effective control of mild steel loss in aggressive acid solutions*. Journal of environmental chemical engineering, 2018. **6**(4): p. 4773-4783.
72. Pal, S., et al., *Experimental and theoretical investigation of aqueous and methanolic extracts of Prunus dulcis peels as green corrosion inhibitors of mild steel in aggressive chloride media*. Journal of Molecular Liquids, 2019. **276**: p. 347-361.
73. Da Rocha, J., et al., *Grape pomace extracts as green corrosion inhibitors for carbon steel in hydrochloric acid solutions*. Embrapa Agroindústria de Alimentos-Artigo em periódico indexado (ALICE), 2012.
74. Bahlakeh, G., et al., *Novel cost-effective and high-performance green inhibitor based on aqueous Peganum harmala seed extract for mild steel corrosion in HCl solution: Detailed experimental and electronic/atomic level computational explorations*. Journal of Molecular Liquids, 2019. **283**: p. 174-195.
75. Dehghani, A., et al., *A combined experimental and theoretical study of green corrosion inhibition of mild steel in HCl solution by aqueous Citrullus lanatus fruit (CLF) extract*. Journal of Molecular Liquids, 2019. **279**: p. 603-624.
76. Shuaib-Babata, Y., et al., *Corrosion Inhibition of AISI 1007 Steel in Hydrochloric Acid using Cucumis Sativus (Cucumber) Extracts as Green Inhibitor*. Acta Technica Corviniensis-Bulletin of Engineering, 2018. **11**(4): p. 153-161.

77. Agarwal, K., *Fenugreek leaves and lemon peel as green corrosion inhibitor for mild steel in 1M HCl medium*. Journal of Materials Science & Surface Engineering, 2014. **1**(2): p. 44-48.
78. Pal, S., et al., *Lemon seeds as green coating material for mitigation of mild steel corrosion in acid media: Molecular dynamics simulations, quantum chemical calculations and electrochemical studies*. Journal of Molecular Liquids, 2020. **316**: p. 113797.
79. Saeed, M.T., et al., *Carrot (Daucus Carota L.) Peels Extract as an Herbal Corrosion Inhibitor for Mild Steel in 1M HCl Solution*. Modern Applied Science, 2020. **14**(2).
80. Yee, Y.P., S.N. Saud, and E. Hamzah, *Pomelo Peel Extract as Corrosion Inhibitor for Steel in Simulated Seawater and Acidic Mediums*. Journal of Materials Engineering and Performance, 2020: p. 1-14.
81. Hammood, a.s., *Iraqi orange peel extract inhibits corrosion of metallic alloys in hydrochloric acid solution*. Journal of Engineering Science and Technology, 2020. **15**(5): p. 3433-3448.
82. Oladel, S. and H.K. Okoro, *Investigation of corrosion effect of mild steel on orange juice*. African Journal of Biotechnology, 2011. **10**(16): p. 3152-3156.
83. Oguzie, E., K. Iyeh, and A. Onuchukwu, *Inhibition of mild steel corrosion in acidic media by aqueous extracts from Garcinia kola seed*. Bulletin of Electrochemistry, 2006. **22**(2): p. 63-68.
84. Kumar, K., M. Pillai, and G.R. Thusnavis, *Pericarp of the fruit of garcinia mangostana as corrosion inhibitor for mild steel in hydrochloric acid medium*. Portugaliae Electrochimica Acta, 2010. **28**(6): p. 373-383.
85. Boujakhrou, A., et al., *Antioxidant activity and corrosion inhibitive behavior of Garcinia cola seeds on mild steel in hydrochloric medium*. Journal of Materials Environmental Science, 2015. **6**: p. 3655-66.
86. Chaubey, N., V.K. Singh, and M. Quraishi, *Papaya peel extract as potential corrosion inhibitor for Aluminium alloy in 1 M HCl: Electrochemical and quantum chemical study*. Ain Shams Engineering Journal, 2018. **9**(4): p. 1131-1140.

Introduction

87. Olusegun, A., N. Oforka, and E. Ebenso, *The inhibition of mild steel corrosion in an acidic medium by the juice of Citrus paradisi (Grapefruit)*. J Corros Sci Eng, 2004. **8**: p. 1-5.
88. Anitha, R., et al., *Comparitive Study And Effect Of Fruit Peel Extracts Of Punica Granatum And Citrus Sinensis To Inhibit Corrosion On Mild Steel By Using In Hcl-A Review*. International Journal of Innovations in Scientific and Engineering Research (IJISER), 2015. **3(9)**: p. 68-72.
89. Umoren, S., et al., *Experimental and theoretical studies of red apple fruit extract as green corrosion inhibitor for mild steel in HCl solution*. Journal of Dispersion Science and Technology, 2015. **36(6)**: p. 789-802.
90. Haldhar, R., D. Prasad, and A. Saxena, *Myristica fragrans extract as an eco-friendly corrosion inhibitor for mild steel in 0.5 M H2SO4 solution*. Journal of Environmental Chemical Engineering, 2018. **6(2)**: p. 2290-2301.
91. Prabhu, D. and P. Rao, *Garcinia indica as an environmentally safe corrosion inhibitor for aluminium in 0.5 M phosphoric acid*. International Journal of Corrosion, 2013. **2013**.

Chapter 2

Materials and Methods

This chapter describes the materials and methods used for study. The synthesis route, the principles of characterisation techniques and corrosion monitoring techniques are given in this chapter.



Contents

2.1 Introduction.....	47
2.2 Electrodes and Electrolytes.....	47
2.3 Inhibitors	48
2.4 Characterisation Techniques.....	54
2.5 Corrosion Tests.....	55
2.6 Thermodynamic and kinetic parameters.....	59
2.7 Surface morphological studies	60
2.8 Quantum chemical calculations	61
2.9 Material studio simulations.....	63

2.1 Introduction

Appropriate selection of material, the inhibitor systems, and the analysis methods are of great importance in corrosion studies. Screening of cost-effective, environmentally benign inhibitors matters a lot in the struggle against managing and controlling corrosion. This chapter discusses the materials and methods used for the current study.

2.2 Electrodes and electrolytes

The material selected for corrosion tests is mild steel coupons from Tata steel Limited provided by Plasto Mek, Koyilandi Calcut. Mild steel coupons made by cold rod process and are having a composition of Fe (98.75%), C (0.20%), Mn (1.0%), P (0.030%), S (0.020%) is taken as the working electrode for all the measurements. Mechanically cut specimens of $2 \times 1.8 \text{ cm}^2$ area are used in weight loss studies and discs of 1 cm^2 are used for electrochemical corrosion testing. Mild steel specimens are cleaned according to the ASTM G1-03, (Standard practice for preparing, cleaning, and evaluating corrosion test specimens) method before each experiment [1].

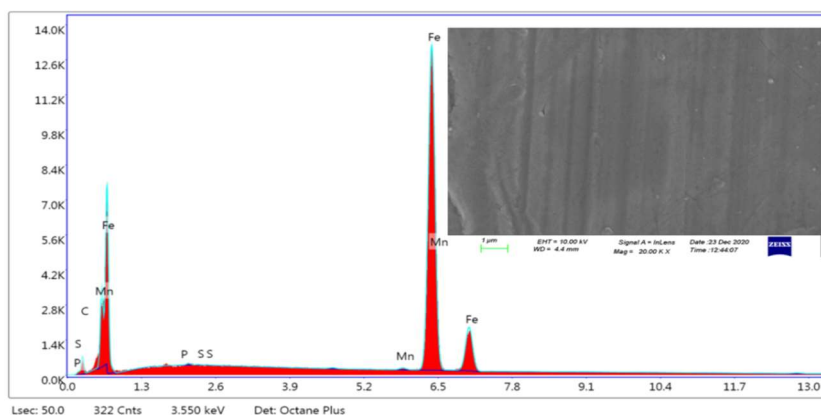


Fig2.1 SEM image and EDAX of polished mild steel sample

Different concentrations of HCl and H₂SO₄ (E. Merck) are prepared by diluting with distilled water. Test solutions are prepared by dissolving particular amounts of inhibitor in ethanol/water and the tests are conducted at various temperatures using a constant temperature bath.

2.3 Inhibitors

2.3.1 Pyrazole Derivatives

The inhibitors used for corrosion testing are mainly pyrazole derivatives. The pyrazole system consists of a doubly unsaturated five-membered ring with two adjacent nitrogen atoms and its derivatives are a class of heterocyclic compounds. They exhibit interesting biological and medicinal properties. The following pyrazoles are used as corrosion inhibitors in this study.

- 1) 3-methyl-1-phenyl-1H-pyrazolyl-5(4H)-one–**PY**: The structure is given as Fig.2.2.

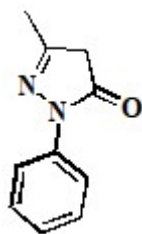
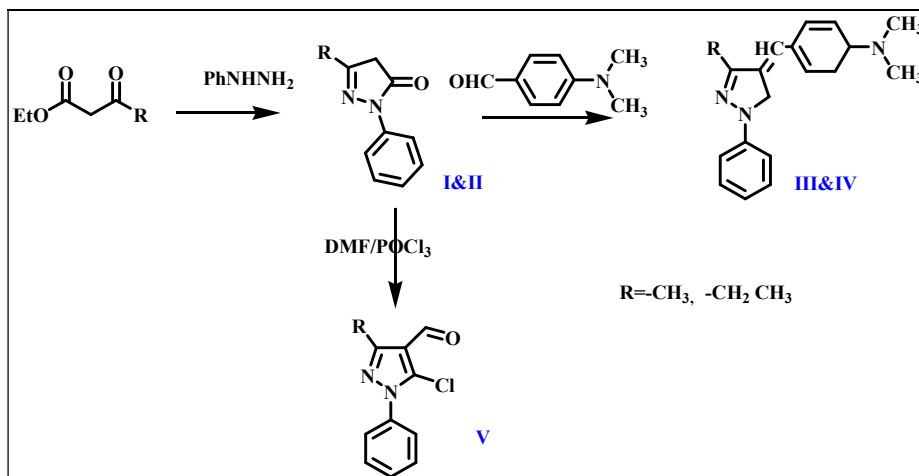


Fig.2.2 PY

- 2) 3-propyl -1-phenyl-1H-pyrazolyl-5(4H)-one –**PY1**: It is prepared by mixing 22mL phenyl hydrazine (Merck) and 22mL of ethyl butyryl acetate (Alfa Aesar) in a large china dish and heated the

mixture in a boiling water bath for two hours with intermittent stirring.



The solution is allowed to cool and to the heavy reddish syrup 100 mL of ether was added and part of it is not soluble in ether got solidified within 15 minutes. Filtered and washed with ether to remove the coloured impurities. It is recrystallised from ethanol [2]. The route of synthesis is given in Scheme 2.1 (Fig 2.3)

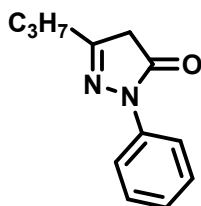


Fig 2.3 PY1

3) 5-Chloro-3-methyl-1-phenyl-1H-pyrazole-4-carbaldehyde-**CMPPC**

To an ice-cold solution of dimethyl formamide (0.3mol) phosphoryl chloride (0.7mol) is added drop wise. To this mixture 3-methyl-1-phenyl-5-pyrazolone (0.1mol) is added and the reaction mixture is heated under reflux for an hour. Then it is poured into ice-cold water. The product is filtered and recrystallised from ethanol(Scheme.2.1) (Fig 2.4) [3].

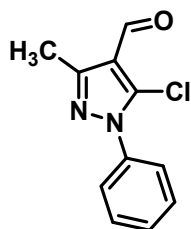


Fig 2.4. **CMPPC**

4) (4Z)-4-(4-(dimethylamino)benzylidene)-3-methyl-1-phenyl-1H-pyrazol-(4H)-one-**PD** (Fig 2.5)

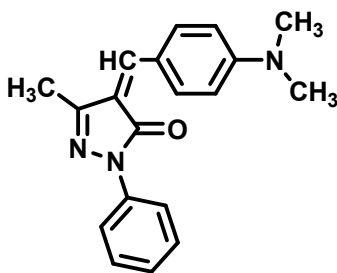


Fig 2.5. **PD**

- 5) (4Z)-4-(4-(dimethylamino) benzylidene)-1-phenyl-3-propyl-1H-pyrazol-(4H)-one-**PD1** (Fig 2.6)

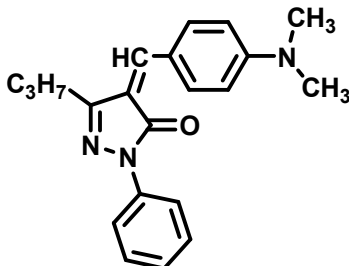


Fig 2.6. PD1

About 0.02M of PY is dissolved in 60 mL of freshly prepared 20% ethanolic NaOH and stirred for half an hour in an R B flask. To the resulting solution, 0.02M 4-dimethyl amino benzaldehyde is added and the reaction mixture is stirred further for 10h. It is then transferred into crushed ice and neutralised with dil. HCl to form the precipitate. It is then kept in freeze overnight and then filtered, washed, dried, and recrystallised from ethanol. The general scheme of synthesis is given below(Scheme2.1)[4].

Table 2.1 The abbreviation and molecular formula of inhibitor molecules

	Abbreviation	'R'	Molecular formula	Formula Weight	Colour	Remark
I	PY	Methyl	C ₁₀ H ₁₀ N ₂ O	174.08	Off white	Alfa Aesar
II	PY1	Propyl	C ₁₂ H ₁₄ N ₂ O	202.11	Off white	Synthesised
III	PD	Methyl	C ₁₉ H ₁₉ N ₃ O	305.15	Brick red	Synthesised
IV	PD1	Propyl	C ₂₁ H ₂₃ N ₃ O	333.18	Brick red	synthesised
V	CMPPC	Methyl	C ₁₁ H ₉ ON ₂ Cl	220.12	Pale yellow	synthesised

2.3.2 Fruit rind extracts

2.3.2(a) Garcinia Indica (Binda) fruit rind extract(GIW): The fruits are collected in April and May from Providence Women's college campus, near Calicut city, Kerala, India(Fig2.7).The seeds are separated and the rind is washed and dried under sunlight. A 10% aqueous extract is prepared from the dried and powdered fruit rind by refluxing with water for 3h at 90⁰C. It is kept overnight and filtered to obtain the stock solution. The solution is acidic.



Fig 2.7 Photograph of Garcinia Indica fruit(Binda)

2.3.2(b) Myristica Fragrans (Nutmeg) fruit rind extract (MFW and MFE):The samples are collected in the month of July-August from Providence Women’s College campus, near Calicut city, Kerala, India (Fig. 2.8). After separating the seed and the mace, the pericarp is washed with water to remove mud, sliced and dried in an air oven at

Materials and Methods

60⁰C. The drying reduced the weight to 80%. A 10% aqueous (MFW) and ethanolic (MFE) extract is prepared by refluxing the dried powdered fruit rind for three hours at 90⁰C. It is kept overnight and filtered. The filtered solution is used as the stock solution for corrosion studies. The stock solution is acidic.



Fig 2.8 Photograph of *Myristica fragrans* fruit (Nutmeg)

2.3.3 Synergism studies

Synergism studies of PY1 with thiourea (Sigma Aldrich), and GIW with KI (Alfa Aisear) are carried out at different temperatures and inhibitor concentrations.

2.4 Characterisation Techniques

The characterisation of the inhibitors is done using UV-Visible, IR, and NMR (^1H and ^{13}C) and GC-MS spectral studies.

2.4.1 UV-Visible spectroscopy

UV-Visible spectroscopy works on the principle of Beer- Lambert's law. The peaks corresponding to $n-\pi^*$ and $\pi-\pi^*$ transitions gives an idea about the structure of the compound. The spectrum is taken with JASCO- UV Visible spectrometer within the range of 200-800nm.

2.4.2 IR Spectroscopy

The group frequencies obtained from the IR spectrum is a source of information about the different functional groups present in the molecules. The identification of the compound could be done with the help of the fingerprint region. KBr pellets of the compounds/powdered fruit rind are analysed using a JASCO FTIR spectrometer at a range of 200-4000 cm^{-1} .

2.4.3 ^1H and ^{13}C NMR spectroscopy

The shielding and the deshielding of the magnetic nucleus by the surrounding electrons create a difference in the absorption position of the protons in an external magnetic field forms the basis of NMR. In ^1H NMR the chemical shift of protons is observed. Using ^{13}C NMR the different types of carbon atoms of a compound could be identified. The samples are analysed in CDCl_3 with Bruker Avance 400 MHz FT-

NMR spectrometer from Gandhigram rural institute, Dindigul, Tamilnadu.

2.4.4 Gas chromatography mass spectroscopy (GC- MS)

The basic principle of gas chromatography is the distribution of vaporised components between a mobile phase and a stationary phase. The retention time helps in identification of the compounds and the peak area conveys the abundance of the components present in the sample. The analysis begins with the gas chromatography where the components are vapourised in to gaseous state and separated by passing through a capillary column coated with a stationary phase. The carrier gases pass the separated components to a mass spectrometer and the molecular ion peaks obtained helps in identification of the components. The GC- MS analysis is done from CARE Keralam, Ltd, Koretty, Trissur, Kerla using 7890 A GC with 5975 C triple axis detector.

2.5 Corrosion Tests

2.5.1 Weight loss Method

Weight loss studies are carried out by immersing the mild steel coupons of $2 \times 1.8 \text{cm}^2$ area in 80 mL of blank and the electrolyte containing various concentrations of inhibitors. In acidic solution the weight loss of the metal is due to oxidation of Fe to Fe^{2+} in the anode and reduction of hydrogen ions to hydrogen gas at the cathode. Before the experiment, the metal coupons are cleaned as per the ASTM standards[1].The weight loss of the metal specimens is calculated as

the difference between the initial weight and the weight of the metal after immersing for a particular time period. These experiments are carried out at room temperature (303K) for 24, 48, 72, 96, 120 h in acids of various concentrations. The data is used for the determination of efficiency and corrosion rate. The efficiency is calculated using the following equation

$$\%IE = \frac{W_a - W_b}{W_a} \times 100 \quad (2.1)$$

where W_a and W_b are the weight loss in the blank and the weight loss in the electrolyte containing a particular concentration of the inhibitor. The rate of corrosion (CR) can be expressed in different ways as given below

$$CR = \frac{W}{A \times t} \text{ mgcm}^{-2}\text{h}^{-1} \quad (2.2)$$

$$CR = \frac{87.6\Delta W}{DA t} \text{ mmy} \quad (2.3)$$

ΔW is weight loss in mg, D is the density in g/cm^3 , A is the area in cm^2 , and t is the exposure time in hours.

2.5.2 Electrochemical Tests

A computer-controlled electrochemical work station Gill AC (U K Model No.1475) is used for both EIS and PDP studies (Fig.2.5). A conventional three-electrode system consisting of a saturated calomel electrode attached to luggin capillary filled with saturated KCl solution to minimise IR drop as the reference electrode, a platinum electrode as

the auxillary electrode and mild steel coupons of 1cm² as the working electrode is used. A constant temperature water bath is used for corrosion testing at different temperatures. Before each experiment, the metal samples are dipped in test solutions for an hour to attain steady-state potential and the OCP (open circuit potential) is plotted for three minutes.



Fig2.5 experimental set up for electrochemical measurements

2.5.2.1 Electrochemical impedance spectroscopy

The EIS studies are done by altering the E_{corr} by 10mV at a frequency range of 0.1Hz to 10KHz. Inbuilt software is used for fitting the data. Various parameters such as R_{ct} (charge transfer resistance), I_{corr} (corrosion current), CR (corrosion rate), R_{s} (solution resistance), C_{dl} (double layer capacitance), depression angle, CPE(constant phase element) 'n' is obtained by Gill AC software. The equations used to calculate these parameters are as follows

$$CR = \frac{\beta A}{R_{\text{ct}} \times Z \times F \times \rho} \quad (2.4)$$

$$I_{corr} = \frac{\beta}{R_{ct}} \quad (2.5)$$

$$\beta = \frac{\beta_a \beta_c}{2.303(\beta_a + \beta_c)} \quad (2.6)$$

$$C_{dl} = \frac{1}{\omega(R_{ct})} \quad (2.7)$$

The efficiency of the inhibitor is calculated with the following equation.

$$IE\% = \frac{R_{ct}^* - R_{ct}}{R_{ct}^*} \times 100 \quad (2.8)$$

where R_{ct}^* and R_{ct} are the charge transfer resistance of the inhibited and the uninhibited solution. CR is corrosion rate, A is the area exposed, Z is the charge on the metal F is Faraday constant and ρ is the density in g/cm^3 β_a and β_c is the anodic and cathodic Tafel constants and ω is the angular frequency given as $2\pi f$ where f is the frequency at which the imaginary part of the impedance has maximum value.

2.5.2.2 Potentiodynamic polarisation studies (PDP)

In PDP measurements the working electrode (mild steel coupons) is polarised +250mV anodically and -250mV cathodically at a scan rate of 1mV/s. Tafel extrapolation of the linear portions of the polarisation curve is done using Tafel rulers. The parameters such as E_{corr} , LPR (linear polarisation resistance), β_a and β_c , I_{corr} , CR are obtained from the analysis. The inhibition efficiency is calculated as follows

$$IE\% = \frac{i_{corr} - i_{corr}^*}{i_{corr}} \times 100 \quad (2.9)$$

where i_{corr}^* and i_{corr} are the corrosion current density in the inhibited and the uninhibited solution.

2.6 Thermodynamic and kinetic parameters

The thermodynamic and the kinetic parameters are calculated using the surface coverage ($\theta = \text{IE}\%/100$) and the corrosion rate (CR) obtained from the weight loss, EIS and, the PDP studies. The equilibrium constant of adsorption (K_{ads}) is obtained by plotting the fitting adsorption isotherm and the free energy change (ΔG) is related to K_{ads} by the following equation

$$\Delta G_{\text{ads}}^0 = -RT \ln 55.5 K_{\text{ads}} \quad (2.10)$$

where 55.5 is the concentration of water in mol/L. The entropy of adsorption and the enthalpy of adsorption are calculated using Van't Hoff equation as follows

$$-\ln K_{\text{ads}} = \frac{\Delta H_{\text{ads}}^0}{RT} - \frac{\Delta S_{\text{ads}}^0}{R} \quad (2.11)$$

The activation parameters are calculated using the Arrhenius equation and Transition state equations given as

$$CR = A e^{-E_a/RT} \quad (2.12)$$

$$CR = \frac{RT}{Nh} e^{\frac{\Delta S_a}{R}} e^{\frac{\Delta H_a}{RT}} \quad (2.13)$$

where CR is the corrosion rate in mm/year, E_a is the activation energy for metal dissolution or corrosion, A is the pre-exponential factor, N is

Avogadro's number, h is Planck's constant, ΔH_a and ΔS_a are enthalpy of activation and, the entropy of activation.

2.7 Surface Morphological studies

Surface morphology is monitored by FESEM (Field emission scanning electron microscope) and AFM (Atomic force microscope)

2.7.1 FESEM and EDAX (Energy-dispersive X-ray analysis)

A high-energy electron beam interacts with the atoms of the sample producing signals that contain information of the characteristic properties of the samples such as surface topology, conductivity, the composition of the material, etc. Qualitative information about the sample is obtained from the high-resolution SEM images whereas a quantitative idea about the elemental composition of the metal, the composition of the adsorbed or coated inhibitor is obtained from EDAX. SEM/EDAX analysis is done from PSG College, Coimbatore and, CSIF Calicut university using EVOL18 Carl Zeiss scanning electron microscope.

2.7.2 AFM (Atomic force microscopy)

The basic principle of AFM is explained as the difference in the interaction between two molecules separated by a few angstroms. When they are very close to each other there is a repulsive interaction and when they are at a larger distance the attractive interactions dominate. The summing of these attractive and repulsive interactions forms the basis of AFM. The AFM probe interacts with the substrate

through a raster scanning motion. The up/down and side to side motion of the AFM tip as it scans along the surface is monitored through a laser beam reflected off the cantilever. The increase and decrease in the surface roughness under various conditions of the metal is detected by AFM. Analysis of the metal samples is done using NTEGRA PRIMA atomic force microscope of CSIF of Calicut university.

2.8 Quantum chemical calculations

The theoretical calculation is a powerful tool in determining the molecular structure, electron density, and reactivity of the inhibitor. So it is a common practice to carry out theoretical calculations of the inhibitor molecules. The molecules with desired properties can be chosen with the help of quantum chemical calculations. The quantum mechanical calculations are based on solving the time-independent Schrödinger equations. The quantum mechanical calculations of the inhibitor molecules are carried out using DFT (density functional theory). In DFT calculations, the energy of a poly-electronic system can be presented as a sum of the total electronic density rather than the use of electronic wave function, and this constitutes the fundamental of this theory[5]. The DFT (Density functional theory) calculations are done using B3LYP functional with double zeta plus polarisation 6-311G (d, p) basis set implemented in Gaussian 09 package. The images of optimised geometry, FMO (HOMO and LUMO), and ESP(electrostatic potential) map are taken for the validation of the data. The global descriptors such as total energy, E_{HOMO} , E_{LUMO} , hardness, electronegativity, electron affinity, electrophilicity index,

ΔN , the fraction of electron transferred and dipole moment give an idea about the inhibition property of the molecule. Following relationships are used for the calculations.

$$\text{Ionisation enthalpy (IE)} = -E_{\text{HOMO}} \quad (2.14)$$

$$\text{Electron affinity (EA)} = -E_{\text{LUMO}} \quad (2.15)$$

$$\text{Electronegativity, } \chi = \frac{\text{IE} + \text{EA}}{2} \quad (2.16)$$

$$\text{Hardness, } \eta = \frac{E_{\text{LUMO}} - E_{\text{HOMO}}}{2} \quad (2.17)$$

$$\Delta N = \frac{\chi_{\text{Fe}} - \chi_{\text{inh}}}{2(\eta_{\text{Fe}} + \eta_{\text{inh}})} \quad (2.18)$$

where $\chi_{\text{Fe}} \approx 7\text{eV}$ and $\eta_{\text{Fe}}=0$ is the electronegativity and hardness of iron obtained from Pearson's electronegativity scale, χ_{inh} , and η_{inh} are the electronegativity and hardness of the inhibitor.

The calculation of the Fukui indices gives an idea about the centres of reactivity. $f(r)$, the Fukui indices are defined as the first derivative of total electron density $\rho(r)$ with respect to the total number electrons at constant external potential $v(r)$

$$f(r) = \left(\frac{\delta \rho(r)}{\delta N} \right)_{v(r)} \quad (2.19)$$

$$\rho^+(r) = \rho_{\text{LUMO}}(r) \quad (2.20)$$

$$\rho^-(r) = \rho_{\text{HOMO}}(r) \quad (2.21)$$

where $\rho_{LUMO}(r)$ is the electron density of LUMO and $\rho_{HOMO}(r)$ is the electron density of the HOMO and here the relaxation due to addition and removal of electronic charges are not considered. Condensed Fukui functions are obtained from the NBO analysis by taking finite difference approximation by removing and adding charges to the neutral molecule.

$$f_k^+ = q_k(N + 1) - q_k(N) \quad (2.22)$$

$$f_k^- = q_k(N) - q_k(N - 1) \quad (2.23)$$

where $q_k(N + 1)$, $q_k(N - 1)$, $q_k(N)$ is the charge on anionic, cationic, and neutral species. Though the concept of charge on the atom has no absolute meaning it helps in explaining the properties of molecules[6]. The anionic and cationic species are determined by adding an electron to the LUMO of the molecule and removing an electron from the HOMO of the molecule. The atoms with the highest f_k^- will be the best nucleophilic centre and f_k^+ will be the electrophilic centre[7]. The Fukui indices are calculated using UCA_FUKUI free software.

2.9 Material studio simulations

Molecular simulations are a recent development of molecular mechanics yet complex than molecular mechanics. There are two ways to perform molecular simulations; the stochastic and deterministic approaches. The stochastic approach is known as Monte Carlo simulation is based on exploring the energy surface by randomly probing the geometry of the molecular system. The deterministic approach, called Molecular Dynamics (MD), actually simulates the

time evolution of the molecular system and provides us with the actual trajectory of the system. Material studio is a simulation and modeling software distributed by BIOVIA. Using Material studio/Biovia 2017, the geometry optimisation of the inhibitors is performed by the FORCITE module and adsorption of the inhibitor on the Fe surface is performed by the ADSORPTION LOCATOR module. The parameters such as total energy, adsorption energy, deformation energy is obtained from the calculations, and using these data interaction energy and binding energy are calculated

$$E_i = E_{Total} - (E_{surface} + E_{inhibitor}) \quad (2.24)$$

$$E_b = -E_i \quad (2.25)$$

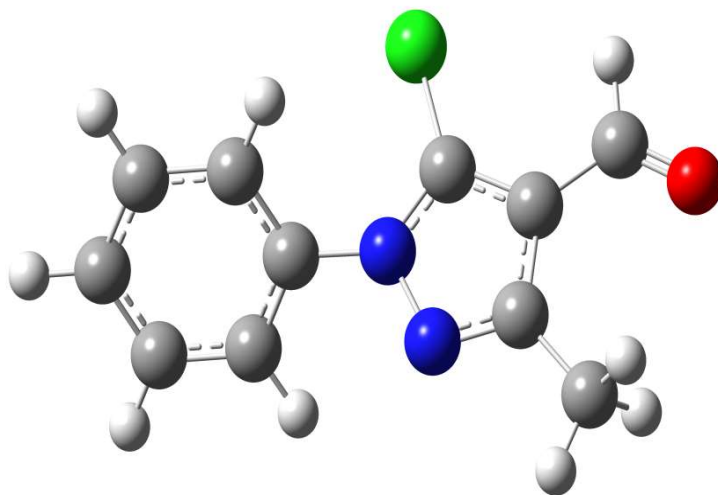
References

1. Gl, A., *Standard practice for preparing, cleaning, and evaluation corrosion test specimens*. ASTM international. Iggg, 2003.
2. Bule, S.S., M. Kumbhare, and P. Dighe, *Synthesis and in-vitro biological evaluation of a novel series of 4-(substituted)-5-methyl-2-phenyl-1, 2-dihydro-3H-pyrazol-3-one as antioxidant*. Journal of Chemical, Biological and Physical Sciences (JCBPS), 2013. **3**(3): p. 1996.
3. Xu, C.-J. and Y.-Q. Shi, *Synthesis and crystal structure of 5-chloro-3-methyl-1-phenyl-1H-pyrazole-4-carbaldehyde*. Journal of Chemical Crystallography, 2011. **41**(12): p. 1816-1819.
4. Prajuli, R., J. Banerjee, and H. Khanal, *Synthesis of some pyrazolone derivatives and evaluation of its antibacterial and cytotoxic activity*. Oriental Journal of Chemistry, 2015. **31**(4): p. 2099-2106.
5. Rodríguez-Valdez, L.M., A. Martínez-Villafañe, and D. Glossman-Mitnik, *Computational simulation of the molecular structure and properties of heterocyclic organic compounds with possible corrosion inhibition properties*. Journal of Molecular Structure: Theochem, 2005. **713**(1-3): p. 65-70.
6. Guo, L., et al., *Theoretical evaluation of the corrosion inhibition performance of 1, 3-thiazole and its amino derivatives*. Arabian Journal of Chemistry, 2017. **10**(1): p. 121-130.
7. Olasunkanmi, L.O., et al., *Some quinoxalin-6-yl derivatives as corrosion inhibitors for mild steel in hydrochloric acid: experimental and theoretical studies*. The Journal of Physical Chemistry C, 2015. **119**(28): p. 16004-16019.

Chapter 3

Control of mild steel corrosion in HCl using CMPPC as mixed type inhibitor

This chapter discusses the corrosion inhibition property of CMPPC (5-Chloro-3-methyl-1-phenyl-1H-pyrazole-4-carbaldehyde) for mild steel in HCl at different temperatures. Quantum chemical calculations and material studio simulations are given in this chapter.



Contents

3.1 Introduction	67
3.2 Results and discussion	67
3.3 Conclusions	87

3.1 Introduction

Mild steel is low carbon steel, widely used for machining, for making components like nuts, bolts, etc. HCl is commonly used in the acid pickling process of metal cleaning and finishing. For the pickling process, 0.5M to 2M HCl is usually used and most of these processes take place around 30°C make them more appealing for pickling than other mineral acids [1]. Therefore corrosion prevention is an essential requirement in such situations. This chapter discusses the synthesis of 5-chloro-3-methyl-1-phenyl-1H-pyrazole -4- carbaldehyde (CMPPC) and its inhibition property against mild steel corrosion in hydrochloric acid by electrochemical, physicochemical, and quantum chemical methods.

3.2 Results and discussion

3.2.1 Characterisation of CMPPC

The synthesised inhibitor CMPPC is characterised by IR and NMR and the data is given below. Yield 80%, light yellow flakes, m.p is 140°C, IR (KBr, ν cm^{-1} ; 3059 (Ar C-H), 2936 (Alkyl C-H), 2830 and 2759 (aldehydic doublet C-H), 1680(C=O), 1592(C=N cyclic), 740(C-Cl); ^1H NMR (CDCl_3 , δ (ppm); 9.982 (1H, CHO), 2.548(3H, CH_3) and 7.8-7.5(5H, aromatic protons). IR, UV, and NMR spectrum of CMPPC is displayed in Fig 3.1 and Fig 3.2.

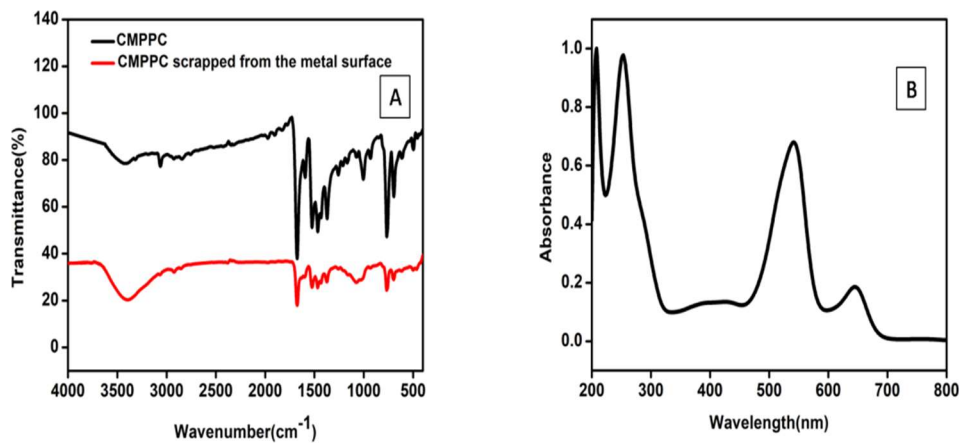


Fig 3.1(A) IR Spectrum of CMPPC and that of the film obtained from the metal surface **(B)** UV-visible spectrum of CMPPC

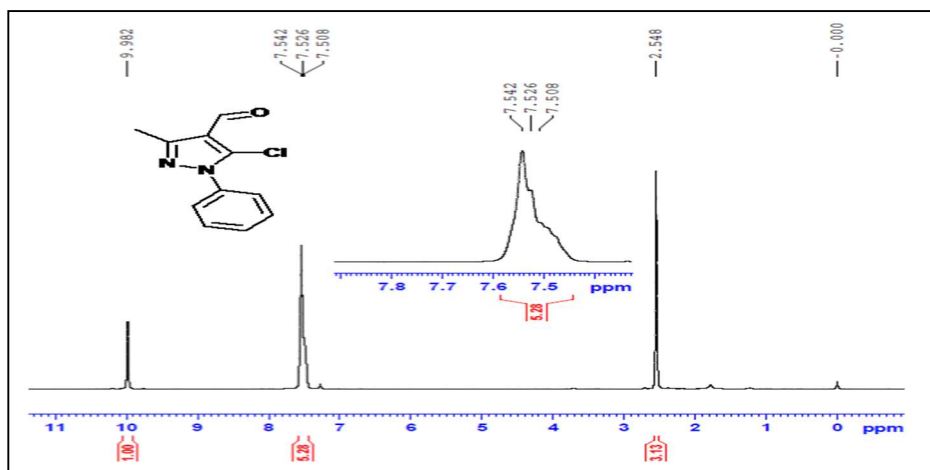


Fig 3.2 ^1H NMR spectrum of CMPPC

3.2.2 Corrosion studies

3.2.2.1 Weight Loss studies

3.2.2.1.1 Effect of acid and inhibitor concentration

The weight loss of mild steel coupons is calculated after dipping them for 24 hours in various concentrations of HCl at room temperature. The

data is used for the calculation of efficiency (%IE) and corrosion rate (Table 3.1). The rate of corrosion is inversely proportional to inhibitor concentration and directly proportional to acid concentration. The inverse relationship between corrosion rate and inhibitor concentration is due to the adsorption of a greater number of molecules on the active sites of the metal.

Table 3.1 Variation of CR and IE% for mild steel in different concentrations of CMPPC and HCl by weight loss analysis

Con. of Acid	Parameters	Blank	25	50	75	100
0.5	ΔW (mg)	627	71	46	33	22
	CR(mgcm ⁻² h ⁻¹)	7.26	0.82	0.53	0.38	0.26
	%IE	-----	89	93	95	96
1	ΔW (mg)	942	99	70	52	50
	CR(mgcm ⁻² h ⁻¹)	10.9	1.11	0.81	0.60	0.58
	%IE	---	88	92	94	95
1.5	ΔW (mg)	1049	139	101	73	82
	CR(mgcm ⁻² h ⁻¹)	12.1	1.61	1.12	0.84	0.94
	%IE	----	87	90	93	92
2	ΔW (mg)	1203	345	251	191	126
	CR(mgcm ⁻² h ⁻¹)	13.9	4.00	2.90	2.20	2.03
	%IE	-----	71	83	84	89
2.5	ΔW (mg)	1324	491	355	293	211
	CR(mgcm ⁻² h ⁻¹)	15.3	5.68	4.11	3.40	2.45
	%IE		70	73	78	84

A plot of log CR Vs HCl concentration gives straight lines (Fig.3.3) with unit correlation coefficient describes the linearity between them and which agrees Mathur's empirical equation(3.1)[2, 3].

$$\log CR = \log k + BC \quad (3.1)$$

where CR is the corrosion rate, k is the concentration pre-exponential factor, B is the acid concentration constant, and C is the acid

concentration. This is because of the excessive metal dissolution with an increase in the number of H^+ ions [3, 4].

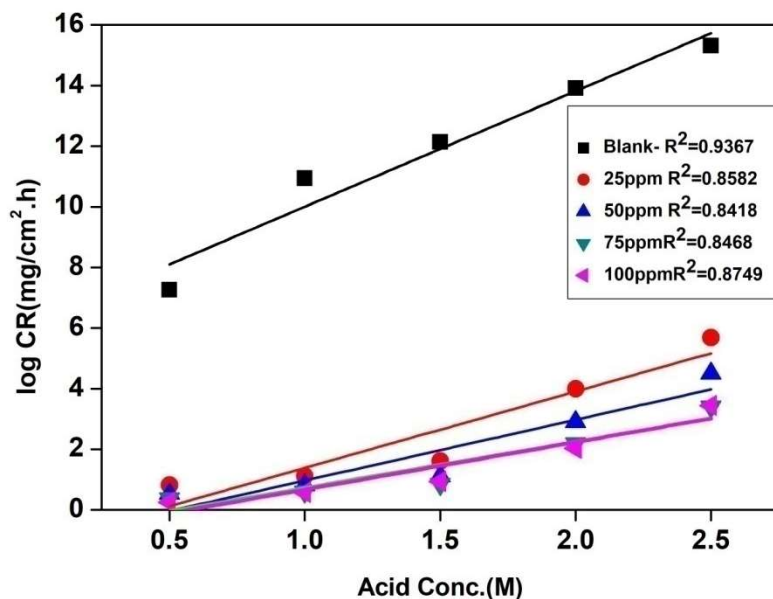


Fig 3.3 Linear relationship between HCl concentration and CR

3.2.2.2 EIS Analysis

Impedance analysis is done in 0.5M, 1M, and 1.5M HCl with and without the inhibitor concentration varying between 25ppm and 100ppm at different temperatures, and the data is given in Table 3.2 and Table 3.3. The %IE is calculated using equation 2.8. Nyquist plots obtained are given as Fig 3.4 and Fig 3.6. For the blank and the inhibited solution, the Nyquist plot consists of single imperfect semicircles. Surface inhomogeneities, roughness, presence of impurities, etc. generally known as frequency dispersion contributes to the imperfectness of the semicircle [5, 6]. EIS parameters are obtained

with the help of Randle's electrical circuit given in Fig 1.9 consisting of solution resistance (R_s) in series with the parallel double-layer capacitance (C_{dl}) and charge transfer resistance (R_{ct}).

3.2.2.3 Effect of Acid concentration

The variation of efficiency in different acid concentrations is given in Fig 3.5. The decrease in inhibition efficiency with an increase in acid concentration is attributed to the increase in the number of active species such as H^+ ions whereas the similar shape of the Nyquist plot (Fig3.4 and Fig3.6) ascertain the similar mechanism for corrosion inhibition

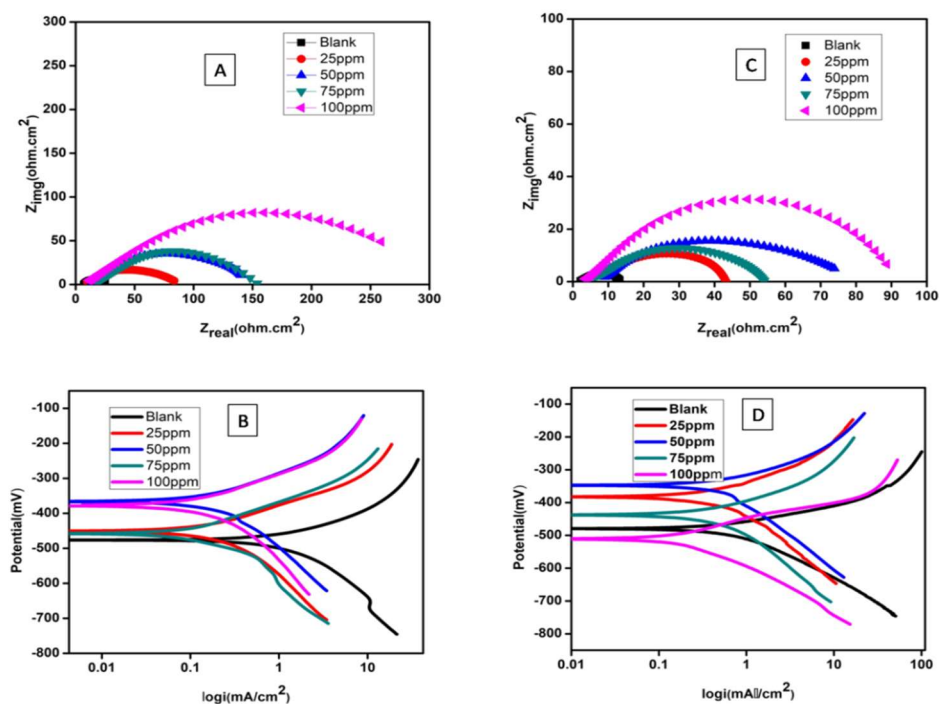


Fig 3.4 (A&B) The Nyquist and the PDP curves corresponding to the corrosion inhibition of mild steel by CMPPC in 0.5M and (C&D) 1.5M HCl at room temperature

Table 3.2 EIS and PDP data for CMPPC in 0.5M and 1.5M HCl

C _{Acid.} (mol/L)	C _{inh.} (ppm)	EIS Data			PDP Data		
		R _{ct} (ΩCm^2)	C _{dl} ($\mu\text{F}/\text{cm}^2$)	%IE	-E _{corr} (mV)	I _{corr} (mA/cm ²)	IE%
0.5M	Blank	15.56	2422	----	475	2.0787	----
	25	108.8	1025	85.69	457	0.5961	71.32
	50	138.2	558.7	88.74	367	0.2749	86.77
	75	158.0	259.6	90.15	451	0.2306	88.90
	100	269.0	168.2	94.74	380	0.2000	90.01
1.5M	Blank	11.75	1633	-----	479	1.3635	-----
	25	40.96	1113	71.31	383	0.5301	61.12
	50	50.50	814.4	76.32	346	0.4094	69.74
	75	75.58	1246	84.24	437	0.3708	72.80
	100	88.29	215.2	86.69	509	0.2054	84.95

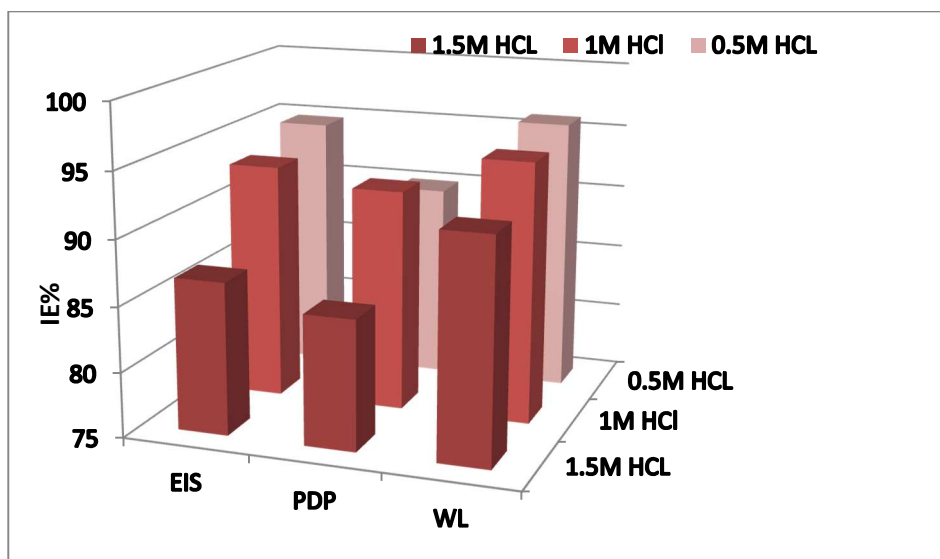


Fig 3.5 Variation of inhibition efficiency (IE%) with respect to HCl concentrations by EIS, PDP, and weight loss (WL) studies

3.2.2.2.4 Effect of inhibitor concentration.

As the concentration of the inhibitor increases, the diameter of the Nyquist plot (charge transfer resistance) increases (Fig3.6), and %inhibition efficiency increases. The increase in CMPPC concentration causes difficulty in charge transfer processes. It is observed that with the increase of the inhibitor concentration double-layer capacitance (C_{dl}) decreases (Table3.3). This is because with an increase in inhibitor concentration, the thickness of the double layer increases due to the adsorption of CMPPC on the metal surface. An increase in the thickness of the double layer is determined by the equation

$$C_{dl} = \frac{\epsilon_0 \epsilon_s}{d} \quad (3.2)$$

where d is the thickness of the double layer, ϵ_0 is the dielectric constant of vacuum ϵ_s is the relative dielectric constant of the inhibitor[7, 8]. The formation of a differential capacitance at the metal solution interface is because of the larger volume occupied by ions on the solution side than the volume occupied by electrons on the metal side[9]

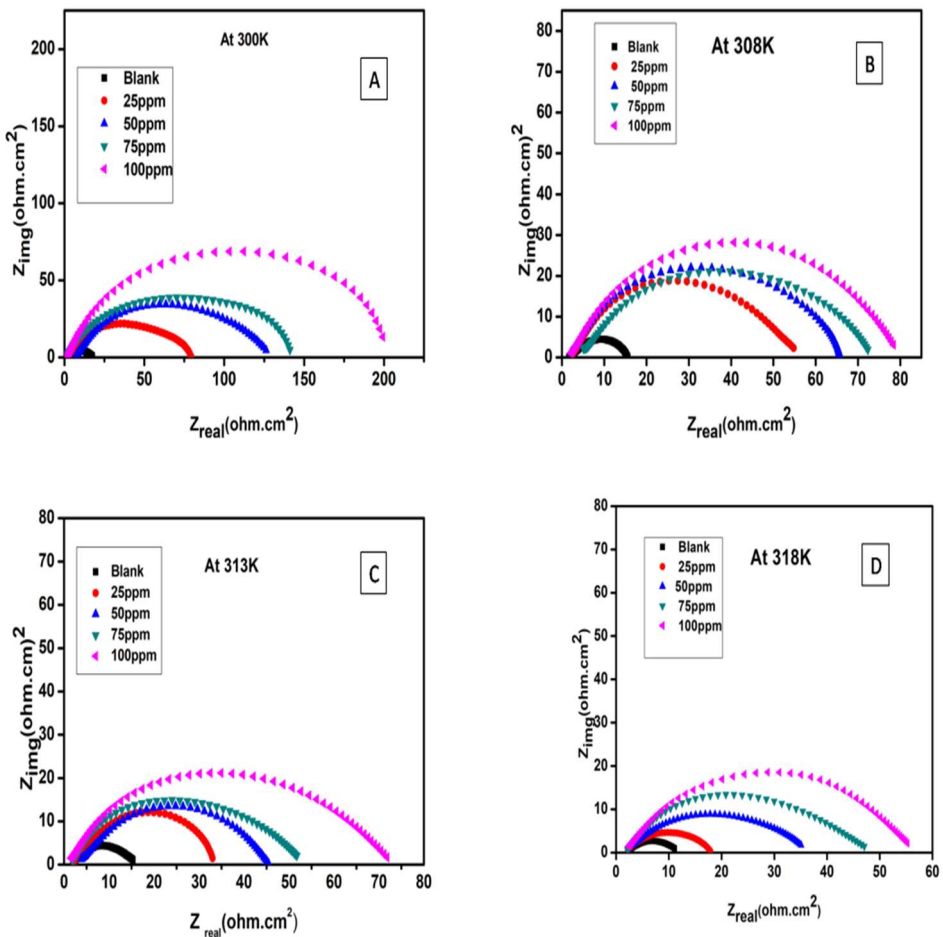


Fig 3.6. Nyquist plots for corrosion inhibition in 1 M HCl at (A) 300 K, (B) 308 K, (C) 313 K and (D) 318 K

Table 3.3 EIS parameters for the corrosion of mild steel in the presence and absence of CMPPC at different temperatures in 1M HCl

Temp (K)	C _{inh.} (ppm)	R _{ct} (Ωcm^2)	C _{dl} ($\mu\text{F}/\text{cm}^2$)	I _{corr} (mA/Cm ²)	CR (mm/y)	IE%
300	Blank	14.60	716.9	1.787	20.71	-----
	25	76.65	302.9	0.3403	3.950	80.95
	50	119.6	272.0	0.2181	2.528	87.29
	75	124.2	265	0.2100	2.434	88.24
	100	213.8	104.7	0.1220	1.951	93.17
308	Blank	12.93	1017	2.013	23.33	----
	25	53.30	255.7	0.5079	5.887	75.74
	50	63.47	156.6	0.4110	4.764	79.62
	75	69.12	359	0.3770	4.374	81.29
	100	75.84	172.4	0.3440	3.987	82.95
313	Blank	11.90	977.4	2.192	25.22	-----
	25	42.45	518.2	0.6174	7.156	71.96
	50	51.86	393.5	0.5030	5.830	77.05
	75	53.59	289.0	0.4868	5.642	77.79
	100	71.96	218.4	0.3625	4.202	83.46
318	Blank	10.11	2298	2.580	29.91	-----
	25	16.94	893	1.540	17.85	40.31
	50	35.00	745	0.7453	8.633	71.11
	75	40.41	658	0.6456	7.48	75.31
	100	45.73	605	0.5705	6.61	78.16

3.2.2.5 Potentiodynamic Studies

The polarization studies of both blank and inhibited solutions are conducted and the polarization curves are depicted in Fig 3.4 and Fig 3.7. The parameters obtained are given in Table 3.2 and Table 3.4. The inhibition efficiency (IE %) is calculated using eqn. 2.9. It is observed that the shift in corrosion potential of all the inhibited solution is around $\pm 30\text{mV}$ with respect to that of the blank solution infers that

CMPPC act as a mixed inhibitor[10], by acting on both anodic metal dissolution and cathodic hydrogen evolution. The results show that the corrosion current and the corrosion rate are brought to a controlled level by the addition of CMPPC and hereafter the inhibition efficiency is increased with an increase in the concentration of CMPPC.

Table 3.4 PDP parameters for mild steel corrosion in the presence of various concentrations of CMPPC at different temperatures in 1M HCl

Temp (K)	C _{inh} ppm	-E _{corr} (mV)	β_a (mV)	$-\beta_c$ (mV)	I _{corr} (mA/cm ²)	CR (mm/y)	IE (%)
300K	Blank	461	117	186	1.2971	40	----
	25	458	99	125	0.2194	3	83.08
	50	467	95	136	0.2065	2.5	84.07
	75	463	112	150	0.1625	2	87.47
	100	473	86	112	0.1035	1	92.03
308	Blank	483	137	157	1.9754	49	---
	25	450	88	191	0.4729	6	76.06
	50	461	96	230	0.3746	5	81.03
	75	457	102	161	0.3448	4	82.54
	100	458	120	171	0.3420	4	82.68
313	Blank	476	201	195	1.4652	51	---
	25	458	113	160	0.5156	6	64.81
	50	451	81	163	0.3943	5	73.08
	75	444	94	183	0.3717	5	74.31
	100	464	89	109	0.2612	2	82.17
318	Blank	463	165	183	1.4871	57	----
	25	442	94	149	0.5748	7	61.34
	50	454	102	162	0.4966	6	66.60
	75	456	87	154	0.3602	4	75.77
	100	479	93	119	0.2703	3	81.82

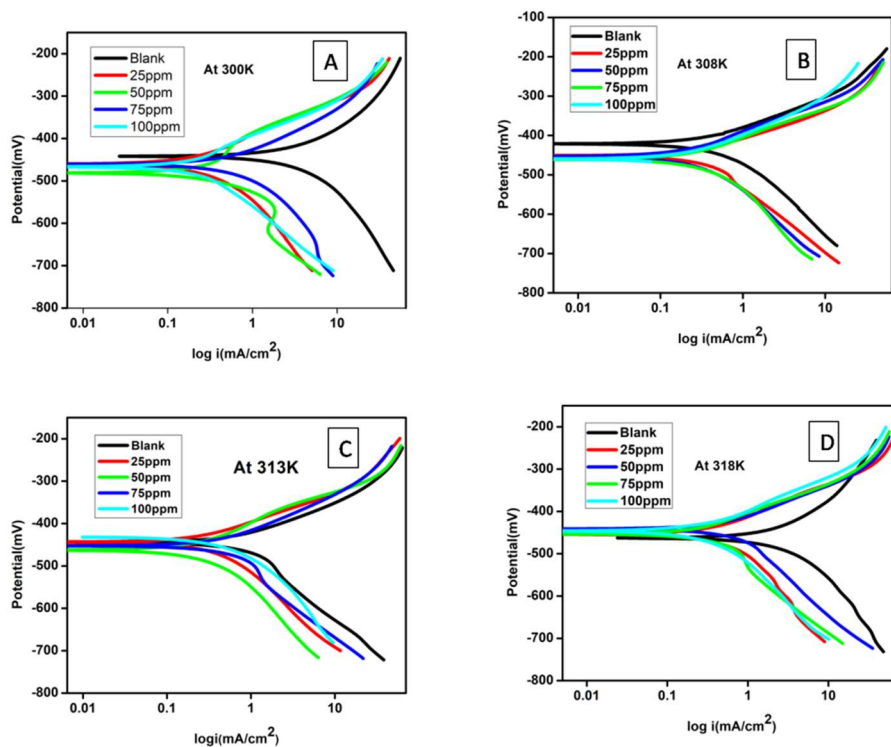


Fig 3.7 PDP plots for corrosion of mild steel in 1 M HCl in the absence and presence of CMPPC at (A) 300K(B) 308 K (C) 313 K (D) 318K.

3.2.2.6 Effect of Temperature

It is found that with the increase in temperature, the efficiency decreases for a particular inhibitor concentration (Fig3.8). This can be explained in three different ways;

(1) Increase in temperature increases the kinetic energy of the molecules and that leads to lesser interaction of the inhibitor to the metal surface[5, 11]. (2) As the temperature increases the rate of desorption is greater than the rate of adsorption leading to more

corrosion[12] and (3) An increase in temperature can cause molecular rearrangements or fragmentation of the inhibitor and that causes the declining trend of efficiency[13].

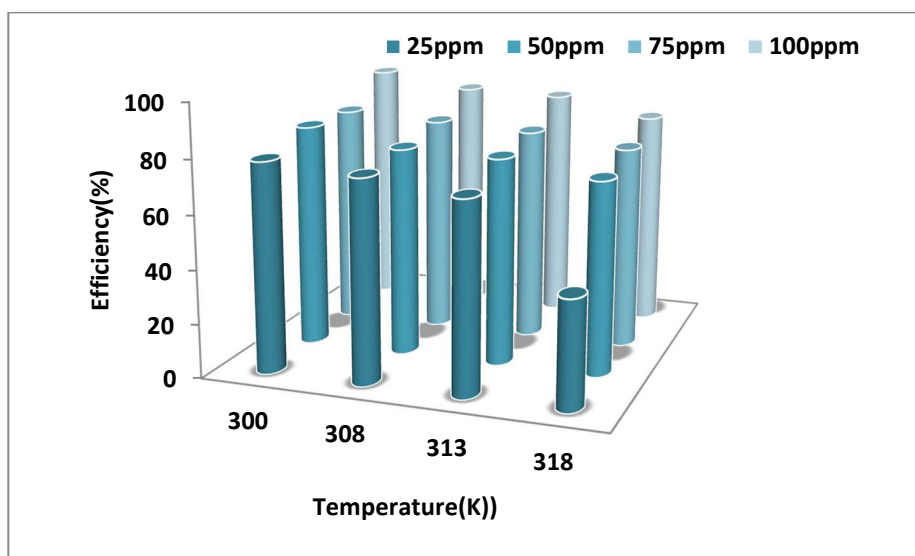


Fig 3.8 Variation of efficiency (IE%) with CMPPC concentration and temperature in 1M HCl

3.2.3 Adsorption Isotherms

The corrosion inhibition of mild steel using CMPPC can be better explained by the adsorption of CMPPC molecules on the metal surface by replacing the water molecules and thus blocking the active sites of corrosion through barrier formation. Several factors do contribute to this process. It can be due to the electrostatic force of interaction between mild steel and the inhibitor or by bond formation activating chemisorption. The orientation of inhibitor molecules affects physisorption while the orientation of the inhibitor and extent of bond

formation affects chemisorptions [14]. To evaluate the nature and strength of adsorption, the surface coverage, θ obtained from EIS as a function of the concentration of the inhibitor is fitted to various isotherms, and from the best fit, the thermodynamic parameters are calculated. In the case of CMPPC, Langmuir adsorption provides the best fitting isotherm and which is evaluated using the equation

$$\frac{C_{inh}}{\theta} = \frac{1}{K_{ads}} + C_{inh} \quad (3.3)$$

and is given in Fig 3.9. Here C_{inh} is the concentration of the inhibitor, and θ is the surface coverage calculated from EIS measurements

$$\theta = \frac{R_{ct} - R_{ct}^*}{R_{ct}} \quad (3.4)$$

where R_{ct} and R_{ct}^* are the charge transfer resistance of the inhibited and uninhibited solutions. The equilibrium constant (K_{ads} ,) for adsorption and desorption, is given by the reciprocal of the Y intercept of the isotherm and free energy of adsorption, ΔG_{ads}^0 , is calculated using the eqn. 2.10 are given in Table 3.5. The calculated values of the regression coefficient (R^2) almost equal to 1 confirm the linearity of the plot between C_{inh}/θ and θ . The decrease in K_{ads} with an increase in temperature shows the weakening of the adsorption process. The negative value of ΔG_{ads}^0 , infers spontaneity of the adsorption process at all temperatures. It is inferred that when it is less than -20kJ/mol the adsorption is physisorption and when it is above -40kJ/mol it is chemisorption. Here the values calculated are between -33kJ/mol and -

25kJ/mol and it proposes spontaneous adsorption of CMPPC on the mild steel surface involving both physisorption and chemisorptions [15]. The decrease in efficiency with an increase in temperature supports preferential physisorption [16]. Vant Hoff equation (2.11) is used to calculate the entropy of adsorption and enthalpy of adsorption. The slope and the intercept of a plot of $\ln K_{ads}$ against $1/T$ give $-\Delta H_{ads}^0/R$ and $\frac{\Delta S_{ads}^0}{R} + \ln \frac{1}{55.5}$. The results obtained are given in Table 3.5. The negative values of ΔH_{ads}^0 indicate the exothermic nature of the adsorption process. Whenever a process is exothermic there occur both chemisorption and physisorption and when it is endothermic the chance for physisorption is minimum [17]. The negative value of ΔS_{ads}^0 further validates the exothermic nature of adsorption.

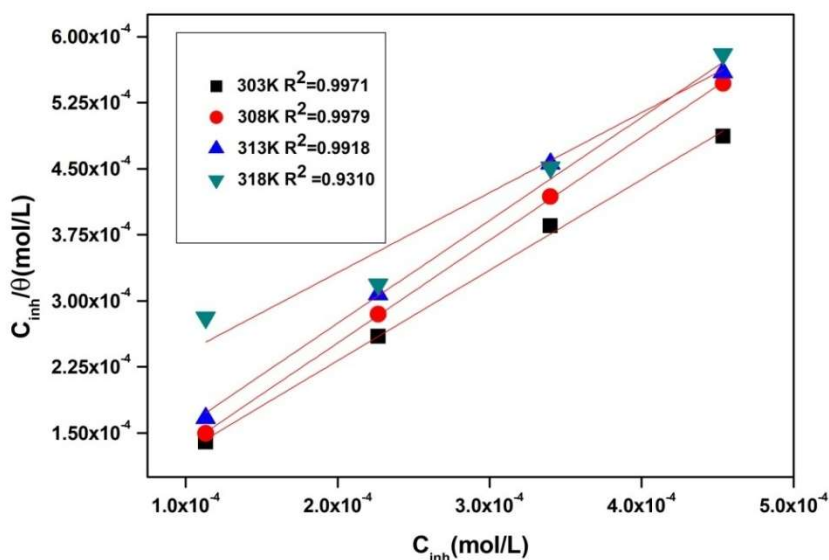


Fig 3.9 Langmuir isotherms of CMPPC obtained by using surface coverage values calculated from the Nyquist plots in 1M HCl

Table 3.5 Adsorption parameters calculated for CMPPC from Langmuir isotherm and Van't Hoff equation

Acid	Parameter	303K	308K	313K	318K	ΔH_{ads}^0 kJ/mol	ΔS_{ads}^0 J/molK
	$K_{\text{ads}} (M^{-1})$	37726	53711	24525	6649		
HCl	ΔG_{ads}^0 (kJ/mol)	-36.30	-38.17	-36.15	-33.89	-95.12	-189.2

3.2.4 Kinetic parameters

The activation parameters such as activation energy (E_a), enthalpy of activation (ΔH_a) and the entropy of activation (ΔS_a) for corrosion inhibition are determined using the Arrhenius eqn.2.12 and the transition state eqn. 2.13. Arrhenius plot of $1/T$ vs $\ln(CR)$ gives a straight line with $-E_a/R$ as the slope. The transition state plot of $\ln(CR/T)$ vs $1/T$ gives a straight line with $-\Delta H_a/R$ as the slope and $\ln(R/Nh) + \Delta S_a/R$ as the intercept. CR values obtained from EIS studies are plots are given as Fig 3.10. The calculated values are given in Table 3.6. The E_a , H_a , and S_a values in the presence of CMPPC are greater than for the blank solution. Adsorption of CMPPC prevents mass and charge transfer and the acid molecules should overcome the high energy barrier to cause corrosion as evident from the higher value of E_a . The positive values of enthalpy of activation imply that metal dissolution is preferably an endothermic process. The increase in ΔH in the presence of CMPPC is caused by the slowing down of metal dissolution [18]. With the addition of the inhibitor the entropy of

activation increases due to the replacement of water molecules on the electrode surface by organic molecule in the aqueous phase.

Table 3.6 Activation parameters for CMPPC in 1M HCl

C_{inh}	$E_a(\text{kJ/mol})$	$\Delta H_a(\text{kJ/mol})$	$\Delta S_a(\text{J/mol K})$
Blank	13.59	12.90	244.22
25ppm	60.90	58.34	380.99
50ppm	52.63	50.06	350.96
75ppm	49.21	46.64	339.29
100ppm	50.73	48.17	342.71

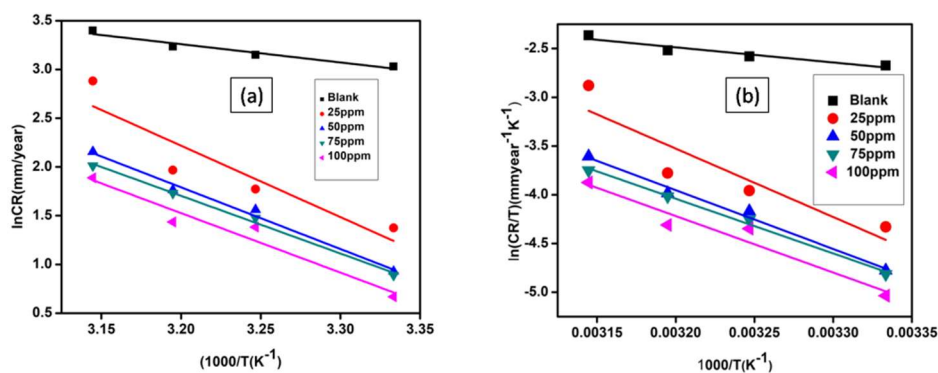


Fig 3.10 (a) Arrhenius and (b) Transition state plot for CMPPC in 1M HCl

3.2.5 Quantum Chemical Calculations

The optimized geometry, ESP map and the FMOs of CMPPC obtained by Gaussian calculations are given in Fig 3.11. The high value of E_{HOMO} indicates the capacity of CMPPC to be adsorbed on the metal surface by donating lone pair of electrons of the oxygen atom and the delocalised π electrons of the phenyl group to the metal. The lower

ΔE value shows its greater corrosion inhibition property[19]. The number of electrons transferred (ΔN) calculated using eqn.2.19. Transfer of electrons between the inhibitor molecule and the metal continues until their chemical potential becomes equal[20]. Comparatively greater values of ΔN represent the greater electron donating capacity of CMPPC. The other parameters such as ionisation enthalpy (IE), related to the energy of frontier orbital as the negative value of E_{HOMO} , and electron affinity (EA), related to the energy of the frontier orbital as the negative value of E_{LUMO} , the hardness (η) and the electronegativity (χ) calculated using equations 2.16 and 2.17 are given in Table 3.7. The corrosion inhibition property of CMPPC can be related to these global parameters in a way that the chemical hardness describes the resistance towards polarisation of the electron cloud and a softer molecule thus will have a smaller ΔE value and better inhibition efficiency.

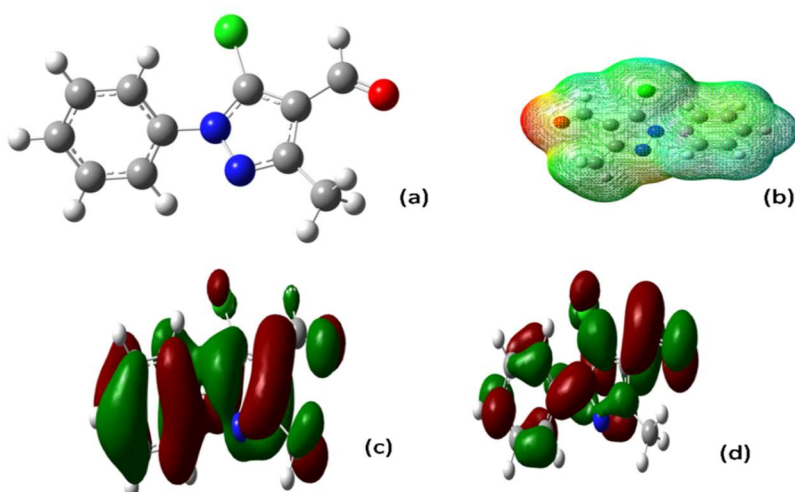


Fig 3.11 a) Optimized geometry, (b) ESP map, (c) HOMO and (d) LUMO of CMPPC

Table 3.7The calculated quantum chemical parameters for CMPPC

Total Energy(a.u)	E_{HOMO} (eV)	E_{LUMO} (eV)	ΔE (eV)	$\mu(D)$	I	A	χ	η	ΔN
-1069.52	-6.53	-1.71	4.82	4.5114	6.53	1.71	4.12	2.41	0.595

3.2.6 Material studio simulations

Various outputs obtained by material studio simulations such as total energy of the metal inhibitor complex, adsorption energy, rigid adsorption energy, deformation energy, and $\frac{dE_{ads}}{dni}$ are given in Table 3.8. Rigid adsorption and deformation energies are the energy released by the unrelaxed and relaxed inhibitor molecule on the metal surface [21]. The other parameters calculated are, the interaction energy (E_i) and binding energy (E_b) between the inhibitor and the mild steel surface is given by the equations

$$E_i = E_{Total} - (E_{surface} + E_{inhibitor}) \quad (3.5)$$

$$E_b = -E_i \quad (3.6)$$

The total energy of the metal adsorbate complex is obtained by adding the energies of the inhibitor molecule and adsorption energy. Fig 3.15 shows the mode of adsorption of CMPPC on (100), (110) and (111) planes of iron. The maximum negative values of adsorption energy and the highest positive values of the binding energy of Fe (111) plane indicate that the inhibitor molecule has a preference for this plane for adsorption[22].

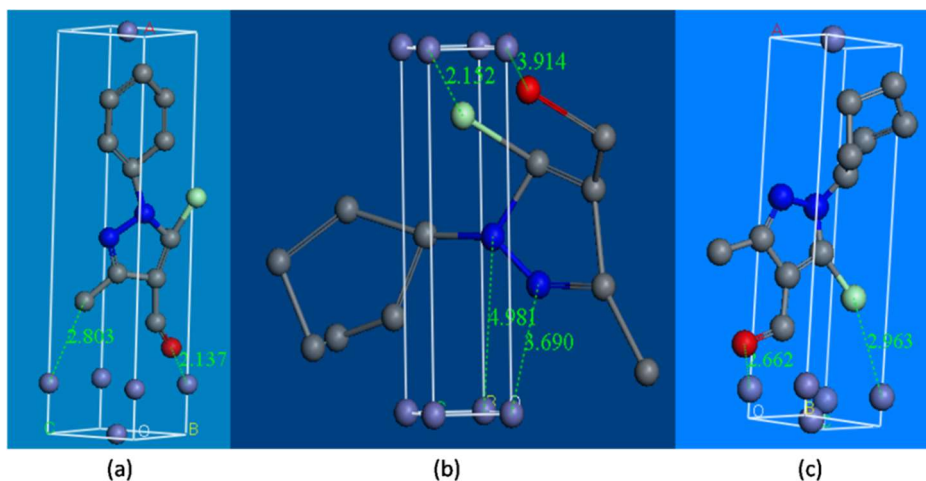


Fig 3.12 Adsorption modes of CMPPC on Fe (100), (110) and (111) planes obtained from Material studio simulation

Table 3.8 Energy parameters calculated by the Material studio Simulation.

Parameters	Fe(100)	Fe(110)	Fe(111)
Total Energy (kcal/mol)	2475	3738	337
Adsorption energy(kcal/mol)	-96789	-61884	-98927
Rigid adsorption energy(kcal/mol)	1716	24249	217
Deformation energy(kcal/mol)	-98505	-86133	-99144
3D atomistic $\frac{dE_{ads}}{dNi}$	-96789	-61884	-98927
$E_{interaction}$ (kcal/mol)	-96756	-61851	-98970
$E_{binding}$ (kcal/mol)	96756	61851	98970

3.2.7 Surface Analysis

SEM images are taken to evaluate the changes in the morphology of mild steel specimen after immersing in the corrosive medium with 100ppm CMPPC and in the blank for 24 hours. Fig 3.13(a) is the SEM

image of mild steel immersed in 1M HCl and it could be observed that the surface is completely damaged whereas Fig3.13 (b), the SEM image of mild steel samples immersed in the inhibited solution clearly shows that the damage is much reduced. This happens to the formation of a protective layer of CMPPC on the metal surface.

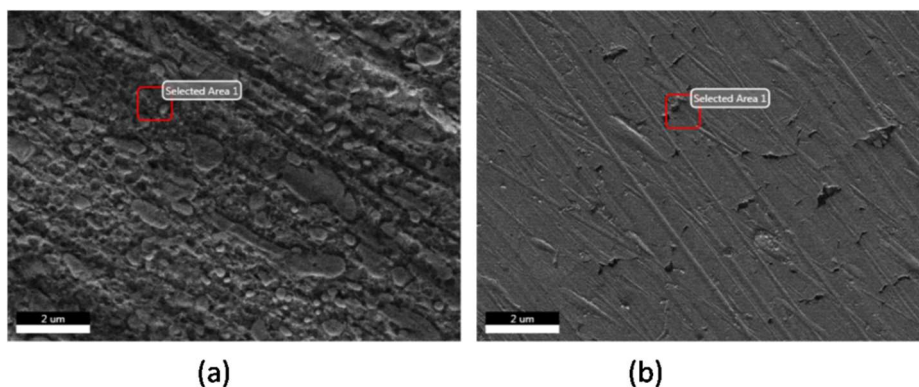


Fig 3.13. SEM images of (a) mild steel immersed in 1 M HCl (b) mild steel immersed in 1 M HCl containing 100ppm CMPPC

3.2.8 Proposed inhibition mechanism

Usually, the presence of polar groups or heteroatoms like nitrogen, oxygen, and sulphur determines the corrosion inhibition properties of organic molecules. The efficiency of adsorption depends on the electron density and polarizability of the group. They are generally adsorbed on the metal surface through unshared pair of electrons of the heteroatoms [23]. The other factors affecting the inhibitory action are molecular size, the heat of hydrogenation, charge density on the adsorption site, etc[24].CMPPC being an aldehyde, the anchoring group is $-CHO$ and the other groups like phenyl, pyrazole ring and methyl group supports the adsorption. ESP map of CMPPC (Fig

3.14(b)) also confirms the maximum availability of electron density on –CHO group and the benzene ring. The quantum mechanical calculations and molecular dynamics simulation reveal that the CMPPC is adsorbed on the metal surface through nitrogen, oxygen, chlorine, and benzene ring. The infrared spectrum of the scrapped film from the metal surface after immersing in the inhibited solution is also given in Fig3.1. A similar spectrum with less peak intensities proves the presence of the CMPPC adsorbed layer on the metal surface.

3.3 Conclusions

- The maximum efficiency of 94%, 93%, and 88% for 100ppm in 0.5M, 1M HCl, 1.5M shows that CMPPC act as a good inhibitor for mild steel corrosion at 300K.
- As the temperature and acid concentration increases, the efficiency decreases. The potentiodynamic polarization studies shows that CMPPC act as a mixed -type inhibitor.
- Corrosion inhibition is through adsorption and it obeys Langmuir adsorption isotherm model and the calculated ΔG suggests mixed adsorption that is a combination of physisorption and chemisorption.
- The higher E_{HOMO} infers the greater electron- donating capacity of CMPPC. The molecular dynamics simulations show that CMPPC is easily adsorbed on Fe(111) plane

References

1. Umoren, S.A., et al., *A critical review on the recent studies on plant biomaterials as corrosion inhibitors for industrial metals*. Journal of Industrial and Engineering Chemistry, 2019.
2. Mathur, P. and T. Vasudevan, *Reaction rate studies for the corrosion of metals in acids—I, Iron in mineral acids*. Corrosion, 1982. **38**(3): p. 171-178.
3. Mu, G.N., X. Li, and F. Li, *Synergistic inhibition between o-phenanthroline and chloride ion on cold rolled steel corrosion in phosphoric acid*. Materials Chemistry and Physics, 2004. **86**(1): p. 59-68.
4. McCafferty, E. and N. Hackerman, *Kinetics of iron corrosion in concentrated acidic chloride solutions*. Journal of the Electrochemical Society, 1972. **119**(8): p. 999-1009.
5. Verma, C., et al., *2, 4-Diamino-5-(phenylthio)-5 H-chromeno [2, 3-b] pyridine-3-carbonitriles as green and effective corrosion inhibitors: gravimetric, electrochemical, surface morphology and theoretical studies*. RSC Advances, 2016. **6**(59): p. 53933-53948.
6. Ammal, P.R., M. Prajila, and A. Joseph, *Effective inhibition of mild steel corrosion in hydrochloric acid using EBIMOT, a 1, 3, 4-oxadiazole derivative bearing a 2-ethylbenzimidazole moiety: Electro analytical, computational and kinetic studies*. Egyptian Journal of Petroleum, 2017.
7. Gholami, M., et al., *Correlated ab initio and electroanalytical study on inhibition behavior of 2-mercaptobenzothiazole and its thiole-thione tautomerism effect for the corrosion of steel (API 5L X52) in sulphuric acid solution*. Industrial & Engineering Chemistry Research, 2013. **52**(42): p. 14875-14889.
8. Gopi, D., et al., *Experimental and theoretical investigations on the inhibition of mild steel corrosion in the ground water medium using newly synthesised bipodal and tripodal imidazole derivatives*. Materials Chemistry and Physics, 2014. **147**(3): p. 572-582.
9. Anupama, K., et al., *Adsorption and electrochemical studies of Pimenta dioica leaf extracts as corrosion inhibitor for mild steel in*

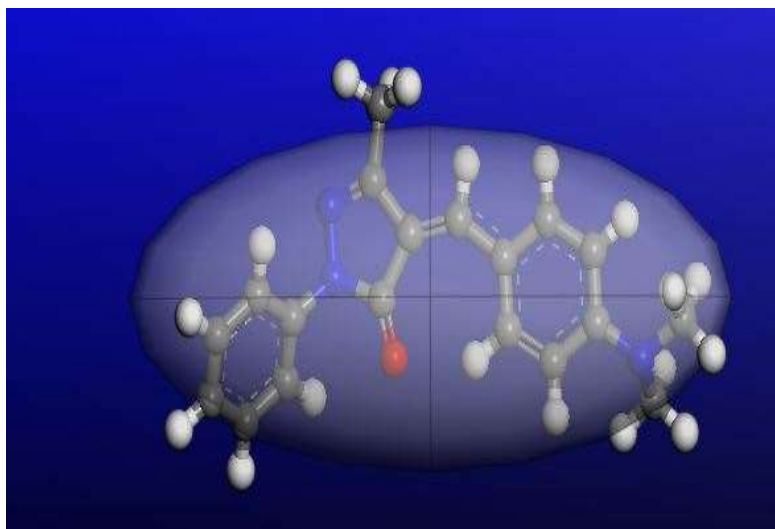
- hydrochloric acid*. Materials Chemistry and Physics, 2015. **167**: p. 28-41.
10. Elshakre, M.E., et al., *On the role of the electronic states of corrosion inhibitors: Quantum chemical-electrochemical correlation study on urea derivatives*. Corrosion Science, 2017. **124**: p. 121-130.
 11. Prabhu, R., et al., *Inhibition effects of some Schiff's bases on the corrosion of mild steel in hydrochloric acid solution*. Corrosion Science, 2008. **50**(12): p. 3356-3362.
 12. Srimathi, M., R. Rajalakshmi, and S. Subhashini, *Polyvinyl alcohol-sulphanilic acid water soluble composite as corrosion inhibitor for mild steel in hydrochloric acid medium*. Arabian Journal of Chemistry, 2014. **7**(5): p. 647-656.
 13. Mishra, A., et al., *Synthesis, characterization and corrosion inhibition studies of N-phenyl-benzamides on the acidic corrosion of mild steel: Experimental and computational studies*. Journal of Molecular Liquids, 2018. **251**: p. 317-332.
 14. Revie, R.W., *Uhlig's corrosion handbook*. Vol. 57. 2011: John Wiley & Sons.
 15. Döner, A., et al., *Experimental and theoretical studies of thiazoles as corrosion inhibitors for mild steel in sulphuric acid solution*. Corrosion Science, 2011. **53**(9): p. 2902-2913.
 16. Ebenso, E. and E. Oguzie, *Corrosion inhibition of mild steel in acidic media by some organic dyes*. Materials Letters, 2005. **59**(17): p. 2163-2165.
 17. Kumari, P.P., P. Shetty, and S.A. Rao, *Electrochemical measurements for the corrosion inhibition of mild steel in 1 M hydrochloric acid by using an aromatic hydrazide derivative*. Arabian Journal of Chemistry, 2017. **10**(5): p. 653-663.
 18. Geethanjali, R. and S. Subhashini, *Thermodynamic characterization of metal dissolution and adsorption of polyvinyl alcohol-grafted poly (Acrylamide-Vinyl Sulfonate) on mild steel in hydrochloric acid*. Portugaliae Electrochimica Acta, 2015. **33**(1): p. 35-48.
 19. Joseph, A. and R. Mohan, *Electroanalytical and computational studies on the corrosion inhibition behavior of ethyl (2-*

- methylbenzimidazolyl) acetate (EMBA) on mild steel in hydrochloric acid*. Research on Chemical Intermediates, 2015. **41**(7): p. 4795-4823.
20. John, S. and A. Joseph, *Theoretical and electrochemical studies on the effect of substitution on 1, 2, 4-triazole towards mild steel corrosion inhibition in hydrochloric acid*. 2012.
 21. Khaled, K. and A. El-Maghraby, *Experimental, Monte Carlo and molecular dynamics simulations to investigate corrosion inhibition of mild steel in hydrochloric acid solutions*. Arabian Journal of Chemistry, 2014. **7**(3): p. 319-326.
 22. Khaled, K., S.A. Fadl-Allah, and B. Hammouti, *Some benzotriazole derivatives as corrosion inhibitors for copper in acidic medium: Experimental and quantum chemical molecular dynamics approach*. Materials Chemistry and Physics, 2009. **117**(1): p. 148-155.
 23. Karthik, R., et al., *Corrosion Inhibition and Adsorption Behavior of 4-Amino Acetophenone Pyridine 2-Aldehyde in 1 M Hydrochloric Acid*. Int J Electrochem Sci, 2015. **10**: p. 4666-4681.
 24. Talati, J. and N. Joshi, *Aldehydes as corrosion inhibitors for aluminium-manganese alloys in potassium hydroxide*. Materials and Corrosion, 1978. **29**(7): p. 461-468.

Chapter 4

Inhibition of Mild Steel Corrosion in HCl using Substituted Pyrazole derivatives

This chapter explains the effect of methyl and propyl groups on the corrosion inhibition property of two pyrazolone chalcones. Electrochemical and non-electrochemical methods are used in this study. Calculations of global descriptors, Fukui indices, binding energy of PD and PD1 on Fe(110) plane is also given in this chapter



Contents

4.1. Introduction.....	91
4.2. Results and discussion	91
4.3. Conclusions	122

4.1 Introduction

Pyrazoles are environmentally benign and biocompatible compounds with antimicrobial, antiviral, anti-inflammatory, antitumor, and anticorrosive properties[1-4]. Studies show that chalcones are potential molecules for therapeutic applications. They act as antifungal, anticancer, anti-inflammatory, etc in the biological field [5]are proved as effective corrosion inhibitors for mild steel in acidic media[6-9]. Agreement between theoretical and experimental data affirms this property of chalcones. This chapter explains the theoretical calculations of two synthesised pyrazolone chalcones of comparable structures and their corrosion inhibition parameters analysed using gravimetric and electrochemical studies.

4.2. Results and Discussion

4.2.1 Synthesis and characterisation of the Inhibitors

The inhibitors **PD** (Fig 2.5) and **PD1** (Fig 2.6)are characterised by UV, IR and NMR spectroscopy. The IR(KBr) (Fig 4.1) peaks ν cm^{-1} ; 2902-2916(-CH stretching), 1680-1582(enone stretching), 3040(=CH stretching). NMR (^1H) details of the inhibitors-PD δ (ppm); (2.1 3H- CH_3 , 2.85 (6H $\text{N}(\text{CH}_3)_2$), 8.5(1H =CH), (6.6-8 9H(M) aromatic rings), PD1 δ (ppm) 0.94(3H CH_3), 1.73-2.43(5H C_2H_5), 2.85(6H $\text{N}(\text{CH}_3)_2$), 8.5(1H =CH), 6.6-8(9H aromatic rings).The UV-visible spectrum of PD and PD1 taken in chloroform (Fig 4.2)gives two bands at 446nm corresponds to $n-\pi^*$ transition and around 252nm and 248nm corresponds to $\pi-\pi^*$ transitions which are characteristic of chalcones [10].The NMR spectra is given in Fig 4.3.

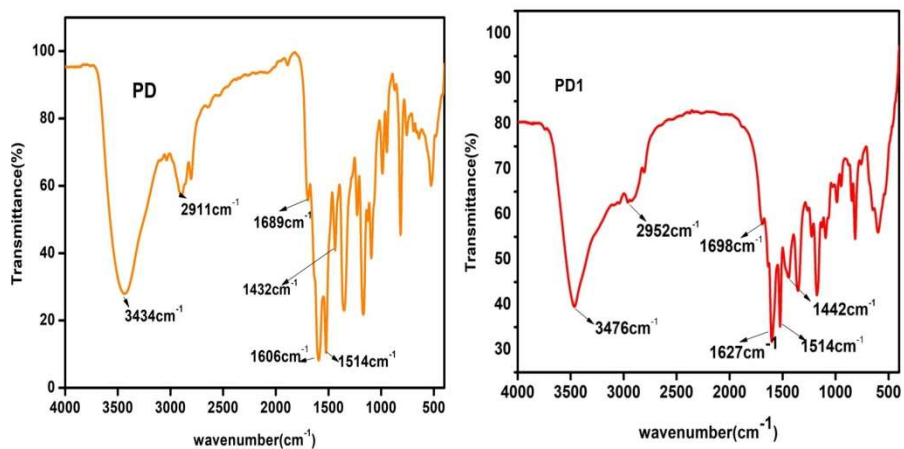


Fig 4.1 IR spectra of PD and PD1

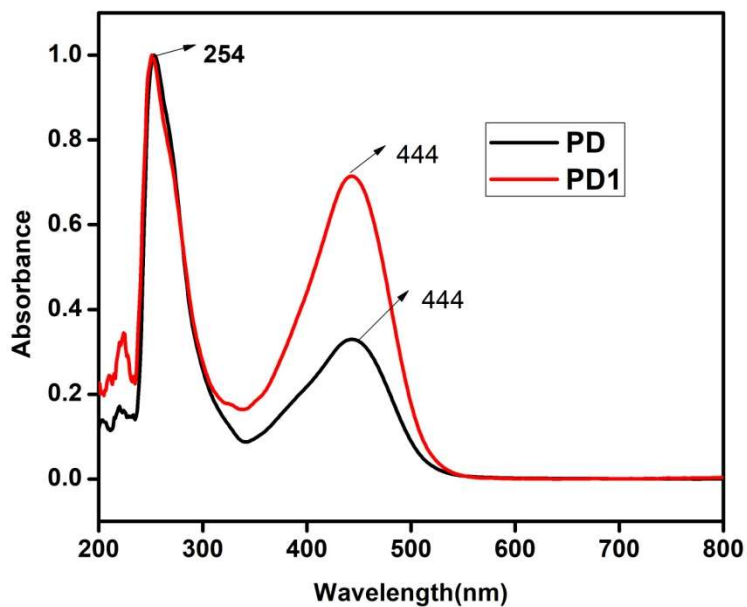


Fig 4.2 UV-Visible spectra of PD and PD1

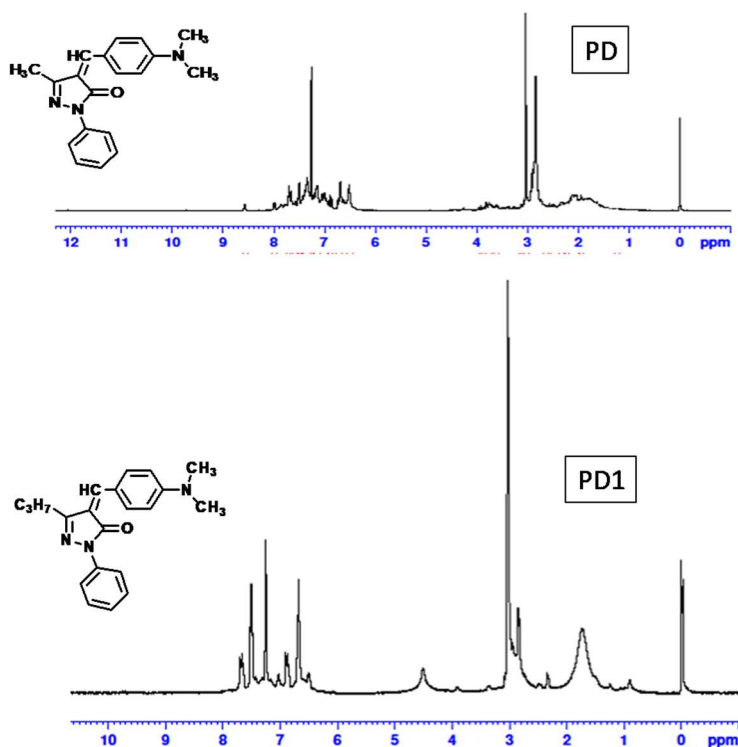


Fig 4.3 ^1H NMR spectra of PD and PD1

4.2.2 Corrosion studies

4.2.2.1 Weight loss analysis

Preliminary analysis of the inhibition properties of PD and PD1 is done using weight loss tests. Table 4.1 gives the results of gravimetric estimations for mild steel corrosion in 1M HCl. The weight loss of mild steel in acidic solution is due to oxidation of Fe at the anode and reduction of hydrogen at the cathode. The weight loss and thus the rate of corrosion is very much decreased in the presence of PD and PD1 because of the quasi substitution of water molecules by PD and PD1

donating the free electrons on the aromatic ring and nitrogen atom to the vacant d orbital of the metal. The increase in efficiency with the increase in concentration of the inhibitor assures the adsorption of the inhibitor molecules on the metal surface reducing corrosion by increasing the surface resistance. The inverse relationship of corrosion rate and efficiency is given in Fig 4.4. A decrease in corrosion rate is observed with an increase in exposure time is due to the development of a protective layer on the metal surface.

Table 4.1 Variation CR and IE% with immersion time for mild steel in 1M HCl in presence of PD and PD1 at room temperature

Time (h)	C _{inh} (ppm)	PD		PD1	
		CR (mgcm ⁻² h ⁻¹)	%IE	CR (mgcm ⁻² h ⁻¹)	%IE
24	Blank	10.40	-----	10.40	-----
	50	0.1574	98.48	0.0937	99.09
	100	0.1145	98.89	0.0914	99.12
	150	0.1018	99.12	0.0798	99.23
	200	0.0879	99.15	0.0775	99.25
72	Blank	2.62	----	2.62	-----
	50	0.1840	92.98	0.3665	94.60
	100	0.1280	95.11	0.1338	95.70
	150	0.0960	95.95	0.0941	96.40
	200	0.0937	96.51	0.0901	96.56

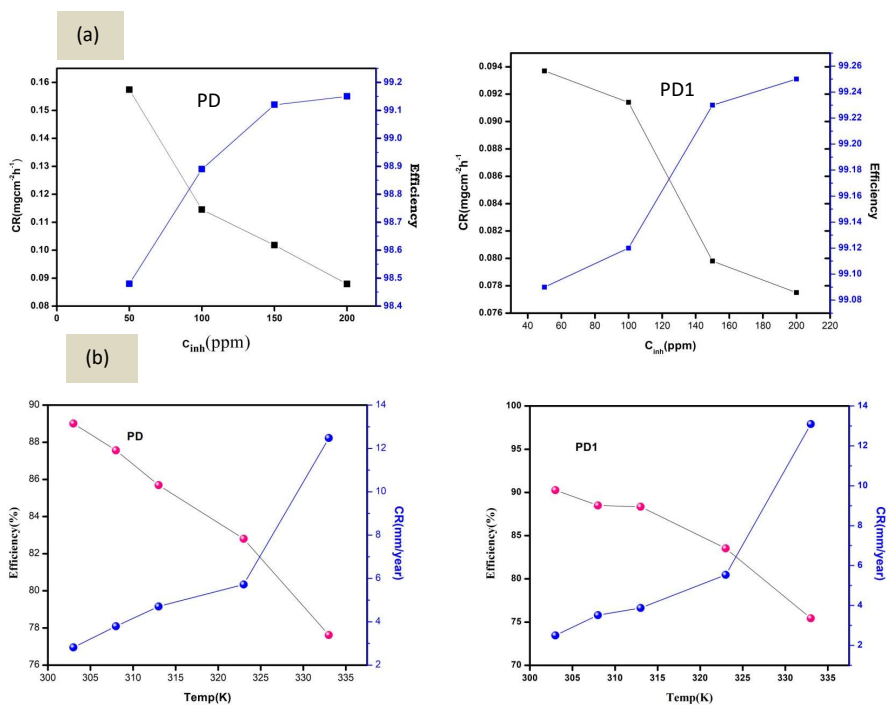


Fig 4.4 (a) Plot of an inverse relationship between CR and %IE for various concentrations of PD and PD1 (b) plot of the effect of temperature on CR and %IE for 200ppm of PD and PD1

4.2.2.2 Electrochemical Analysis

The EIS spectra of PD and PD1 in 0.5M and 1M HCl with varying concentration of the inhibitors and at different temperatures are analysed. The data are given in Table 4.2 and Table 4.3. The entire EIS spectra are recorded at the open circuit potential and OCP is recorded for three minutes. EIS is a powerful technique for analysing the mechanism of electrode corrosion. The corroding system is modelled to an equivalent electrical circuit and when the corrosion is charge transfer controlled the appealing electrical circuit is Randles circuit which includes electrolyte resistance (R_s), polarisation resistance (R_{ct}),

and double-layer capacitance (C_{dl}) given in Fig1.10. The metal solution interface acts as a double layer due to the presence of metal ions and the ions from the electrolyte, perturbs the current flow and thus acts as a capacitor. The addition of inhibitor increases the thickness of the double layer and resists the current flow more effectively. The inverse relationship between C_{dl} and thickness of the double layer can be represented as

$$C_{dl} = \frac{\epsilon\epsilon_0}{d} \quad (4.1)$$

Fig 4.5 and Fig 4.6 explain the variation in charge transfer resistance (R_{ct}) with increases in the inhibitor concentration and temperature. It is clear that as the concentration of the inhibitor increases from 50ppm to 200ppm the charge transfer resistance increases impeding the current flow and thus reducing the corrosion rate. The imperfections of the semicircles are due to frequency dispersion due to factors such as roughness, inhomogeneity of the metal surface, grain boundaries, etc.

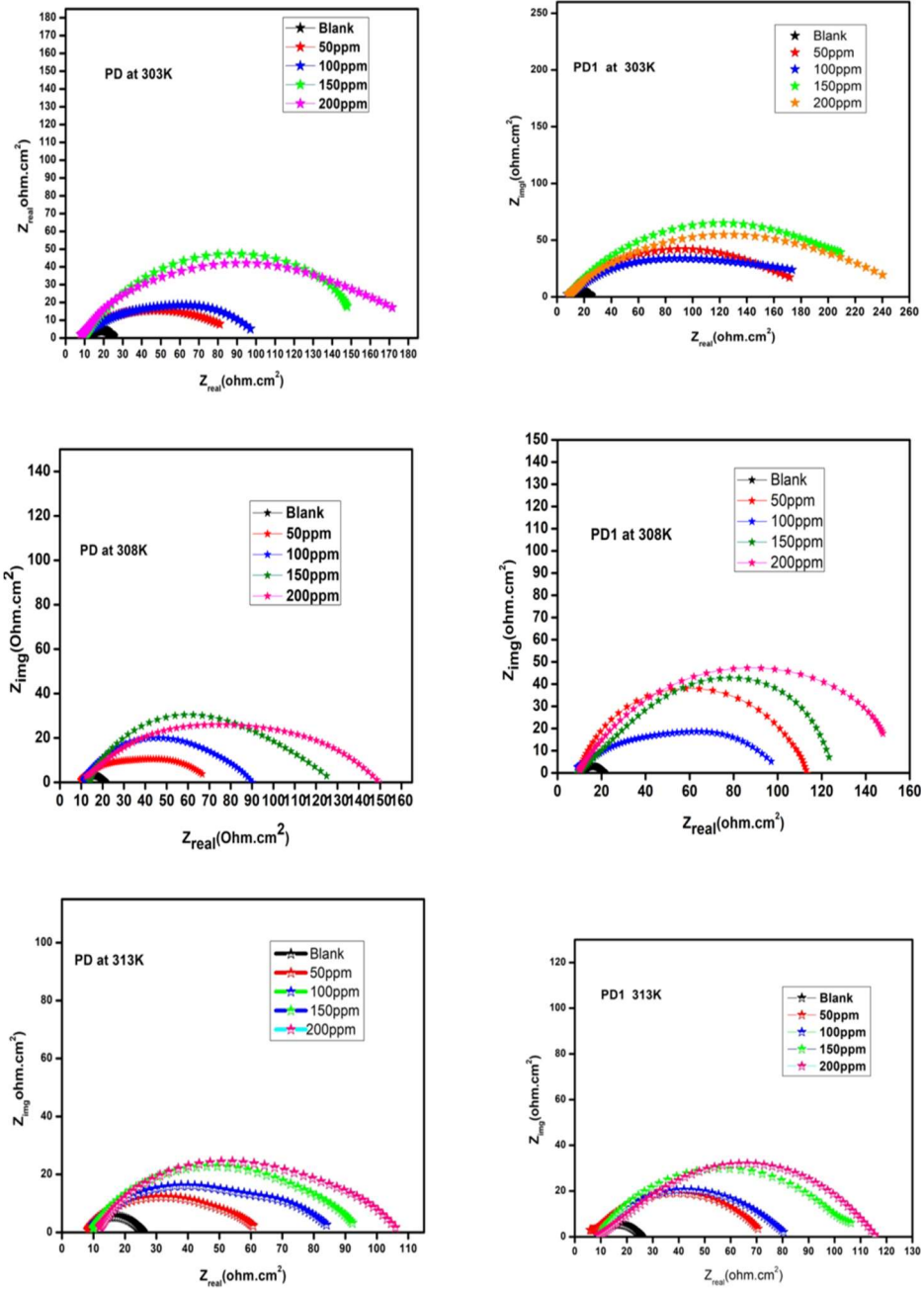


Fig 4.5 Nyquist plot for various concentrations of PD and PD1 in 0.5M HCl at 303K, 308K and 313K

Table 4.2 EIS parameters obtained for mild steel corrosion inhibition in the absence and presence of PD and PD1 in 0.5M HCl at 303K, 308K, and 313K

Temp	PD					PD 1			
	C _{inh} (ppm)	R _{ct} (Ωcm^2)	C _{dl} ($\mu\text{F}/\text{cm}^2$)	I _{corr} (mA/cm ²)	IE%	R _{ct} (Ωcm^2)	C _{dl} ($\mu\text{F}/\text{cm}^2$)	I _{corr} (mA/cm ²)	IE%
303K	Blank	14.22	1514	1.835	-----	14.22	1514		
	50	87.42	697.1	0.2984	83.73	162.5	554.2	0.1605	91.24
	100	94.07	663.9	0.2773	84.88	218.1	363.5	0.1196	93.48
	150	152.6	384.6	0.1709	90.68	239.3	312.5	0.1090	94.05
	200	183.4	309.4	0.1422	92.24	256.8	161.0	0.1016	94.46
308K	Blank	10.44	1668	2.499	----	10.44	1668	2.499	----
	50	69.37	1150	0.3761	84.95	86.94	880.7	0.3001	87.99
	100	91.00	639.4	0.2867	88.52	98.73	560.0	0.2642	89.42
	150	116.0	600.9	0.2249	91.00	103.0	666.8	0.2533	89.86
	200	137.9	192.0	0.1890	92.42	139.9	169.4	0.1865	92.53
313K	Blank	17.36	1427	1.503	----	17.36	1427	1.503	-----
	50	55.84	1045	0.4697	68.91	69.17	570.3	0.3771	74.90
	100	81.14	759	0.3215	78.60	71.80	501.5	0.3633	75.82
	150	85.32	615.8	0.3058	79.65	100.5	514.9	0.2569	82.72
	200	96.45	583.9	0.2705	82.00	107.5	355.1	0.2427	83.96

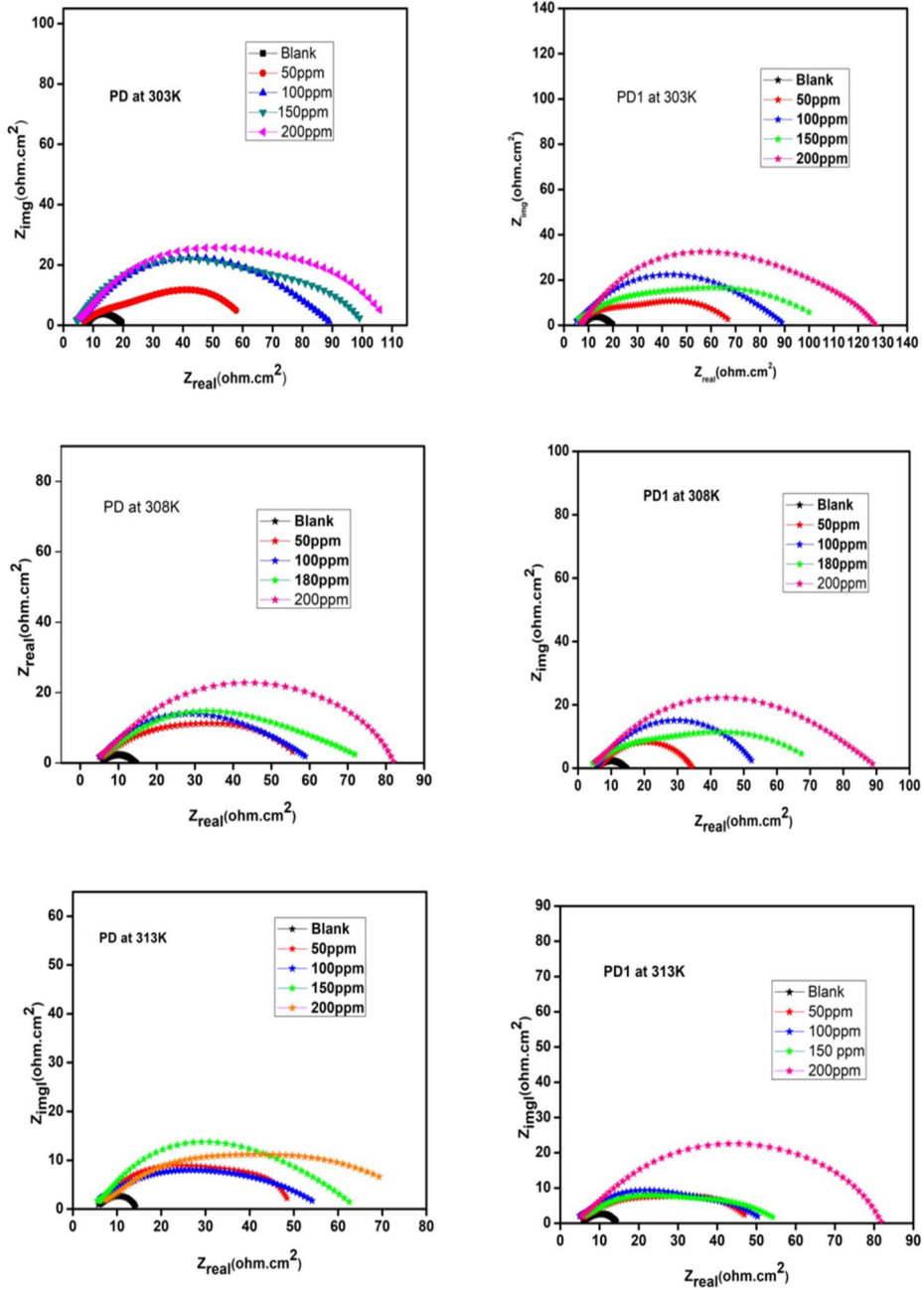


Fig 4.6 Nyquist plot for various concentrations of PD and PD1 in 1M HCl at 303K, 308K and 313K

Table 4.3 EIS parameters obtained for mild steel corrosion inhibition in the absence and presence of PD and PD1 in 1M HCl at 303K, 308K, and 313K

Temp (K)	C _{inh} (ppm)	PD				PD 1			
		R _{ct} (Ωcm ²)	C _{dl} (μF/cm ²)	I _{corr} (mA/cm ²)	IE%	R _{ct} (Ωcm ²)	C _{dl} (μF/cm ²)	I _{corr} (mA/cm ²)	IE%
303	Blank	11.79	1230	2.213	----	11.79	1230	2.213	-----
	50	60.20	379.0	0.4333	80.41	68.19	310.4	0.3826	82.71
	100	70.83	304.9	0.3683	83.34	78.77	307.3	0.3312	85.03
	150	98.54	204.3	0.2647	88.03	100.3	208.2	0.2445	88.24
	200	107.3	180.4	0.2431	89.01	121.0	153.3		90.25
308	Blank	9.91	1882	2.634	----	9.91	1882	2.634	-----
	50	49.15	732.3	0.5308	79.83	56.88	655.1	0.4586	82.57
	100	55.13	689.4	0.4730	82.02	60.53	497.8	0.4310	83.62
	150	73.08	402.2	0.3570	86.43	70.42	402.2	0.3704	85.92
	200	79.68	389.9	0.3274	87.56	86.10	374.5	0.303	88.49
313	Blank	9.18	2144	2.839	---	9.18	2144	2.839	---
	50	47.81	1338	0.545	80.79	47.95	1312	0.545	80.85
	100	59.35	1336	0.439	84.51	51.14	817.1	0.510	82.04
	150	63.39	652.4	0.4115	85.50	55.01	641.1	0.473	83.31
	200	64.23	651.2	0.406	85.69	78.77	330.1	0.334	88.34

4.2.2.3 Potentiodynamic polarisation studies

The collated data of the polarisation studies and the polarisation curves in 0.5M HCl, and 1M HCl are given in Table 4.4, Table 4.5, Fig 4.7, and Fig 4.8. The change of corrosion potential (E_{corr}) does not follow any specific pattern but for most of the inhibited solutions, the E_{corr} is shifted to a more positive value compared to E_{corr} of blank. The difference between E_{corr} of the blank and the inhibited solutions are less than 85mV, points out the mixed type performance of PD and PD1. The positive shift of E_{corr} in the inhibited solutions indicates the influence of PD and PD1 on the anodic conversion of metallic iron to Fe^{2+} than cathodic hydrogen evolution. The inhibition efficiency calculated from the corrosion current density as given in eqn. 2.9 infers that as the concentration of the inhibitor increases the inhibition efficiency increases at all temperatures. The inhibitors block the active sites of corrosion on the metal surface and thus reduce the corrosion rate. Parameters such as current density (I_{corr}), the Tafel constants are affected by the addition of the inhibitor due to the modification of cathodic hydrogen evolution and anodic iron oxidation.

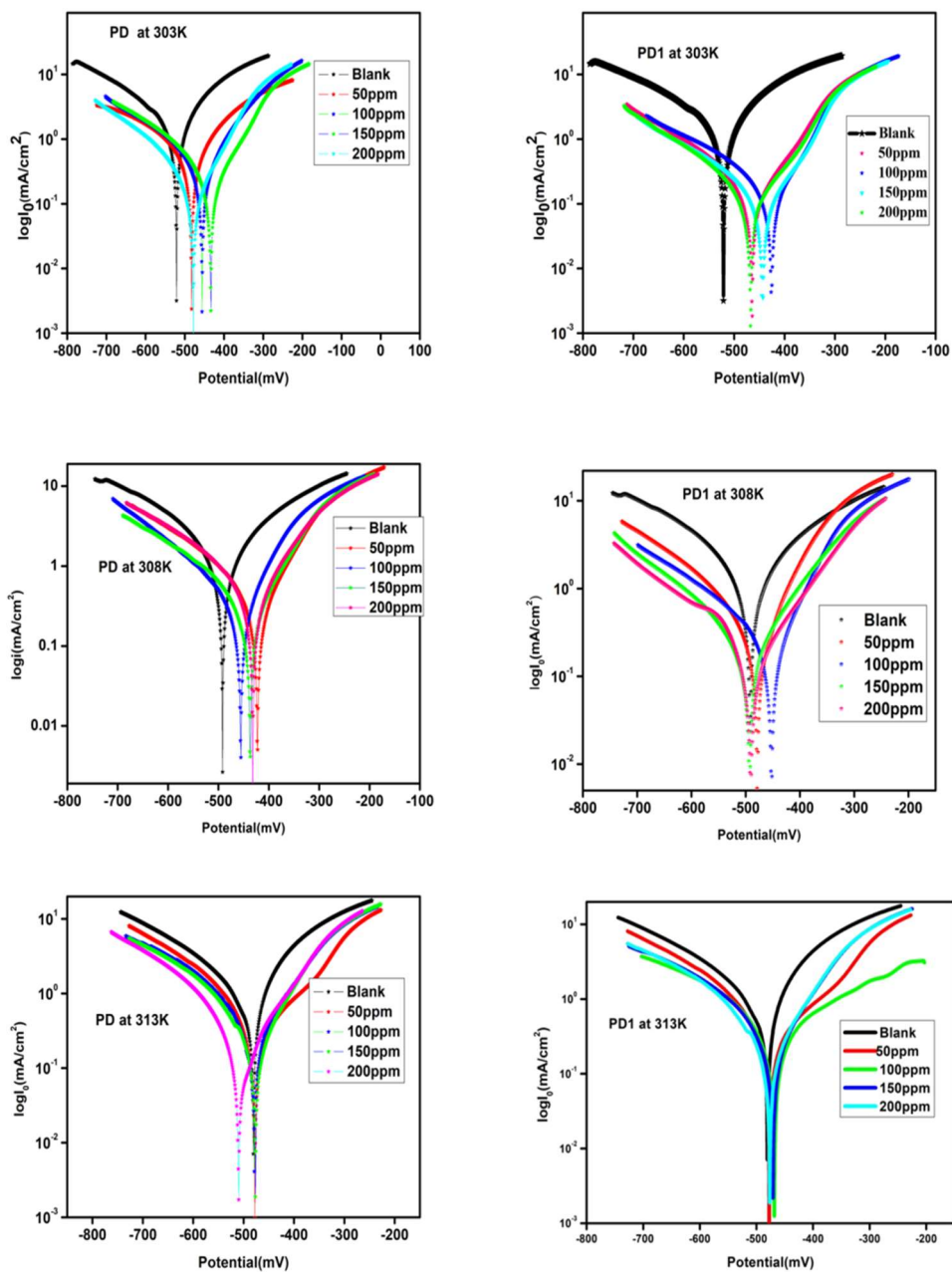


Fig 4.7 The PDP plots for various concentrations of PD and PD1 in 0.5M HCl at 303K, 308K and 313K

Table 4.4 Electrochemical parameters from PDP studies for mild steel corrosion inhibition by PD and PD1 in 0.5M HCl at 303K, 308K, 313K

Temp (K)	C _{inh} (ppm)	PD					PD1				
		-E _{corr} (mV)	β_a (mV)	$-\beta_c$ (mV)	I _{corr} (mA/cm ²)	IE%	-E _{corr} (mV)	β_a (mV)	$-\beta_c$ (mV)	I _{corr} (mA/cm ²)	IE%
303	Blank	490	191	211	1.1922	----	490	191	211	1.1922	
	50	484	105	135	0.3250	72.39	466	102	139	0.1342	88.74
	100	454	88	111	0.2017	83.08	424	94	189	0.1598	86.59
	150	433	97	107	0.1514	87.30	445	99	125	0.0818	93.13
	200	478	96	108	0.1216	89.80	468	127	112	0.0856	92.81
308	Blank	494	193	186	1.2526	-----	494	193	185	1.2526	-----
	50	422	122	207	0.4640	62.95	478	84	117	0.2097	83.25
	100	454	103	191	0.3558	71.51	451	91	197	0.2431	80.59
	150	437	99	137	0.2205	82.39	492	107	128	0.1490	88.10
	200	431	84	96	0.2148	82.85	492	118	99	0.1253	89.99
313	Blank	479	123	224	1.690	-----	479	123	224	1.69	-----
	50	475	127	96	0.2181	87.09	466	95	126	0.2739	83.79
	100	479	108	119	0.2464	85.42	469	86	166	0.2318	86.28
	150	475	89	111	0.1738	89.71	471	91	107	0.1951	87.86
	200	509	113	95	0.1469	91.0	483	111	119	0.2253	86.66

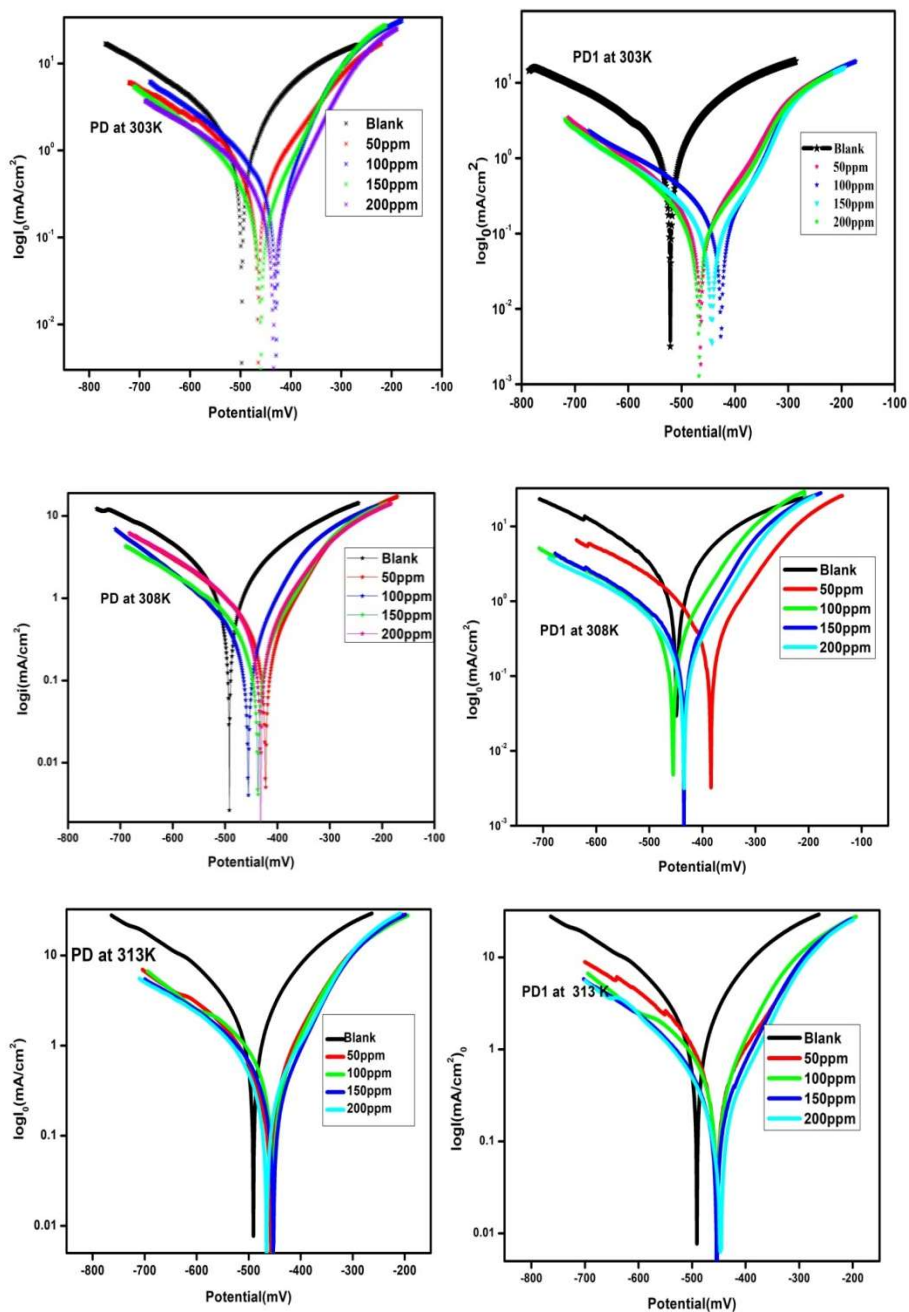


Fig 4.8 The PDP plots for various concentrations of PD and PD1 in 1M HCl at 303K, 308K and 313K

Table 4.5 Electrochemical parameters from PDP studies for mild steel corrosion inhibition by PD and PD1 in 1M HCl at 303K, 308K, and 313K

Temp (K)	C_{inh} (ppm)	PD					PD1				
		$-E_{corr}$ (mV)	β_a (mV)	$-\beta_c$ (mV)	I_{corr} (mA/cm ²)	IE%	$-E_{corr}$ (mV)	β_a (mV)	$-\beta_c$ (mV)	I_{corr} (mA/cm ²)	IE%
303	Blank	490	116	143	1.522	-----	490	116	143	1.522	-----
	50	467	116	116	0.331	78.22	448	121	241	0.545	64.20
	100	429	84	162	0.307	79.81	438	99	205	0.374	75.42
	150	460	90	107	0.182	88.04	448	91	126	0.178	88.28
	200	434	92	132	0.164	89.37	429	83	111	0.129	91.52
308	Blank	450	156	192	1.906	-----	450	122	156	1.966	-----
	50	453	98	179	0.452	76.25	455	128	132	0.530	72.99
	100	483	100	130	0.483	74.61	446	104	111	0.491	75.00
	150	425	90	196	0.502	73.66	456	113	160	0.344	82.48
	200	443	81	107	0.203	89.32	447	91	121	0.189	90.34
313	Blank	491	143	168	2.080	---	491	143	168	2.086	----
	50	456	107	167	0.462	77.77	487	107	168	0.462	77.83
	100	451	101	153	0.445	78.60	452	101	154	0.445	78.66
	150	453	100	149	0.337	83.79	453	101	149	0.337	83.84
	200	464	102	122	0.286	86.24	464	102	122	0.286	86.28

4.2.2.4 Effect of temperature

In order to analyse the effect of temperature on the inhibition efficiency, electrochemical studies at 323K and 333K for 200ppm of PD and PD1 are also carried out in 1M HCl and the data is given in Table 4.7. Both EIS and PDP studies show that inhibition efficiency registers a reverse trend with the temperature. The pronounced hike in the corrosion rate from 2.818 mm/y at 303K to 12.48 mm/y for PD and 2.499 mm/y at 303K to 13.09 mm/y at 333K for PD1 is observed in 1M HCl. It could be seen from Fig.4.9 a and b that as the temperature increases the R_{ct} decreases for both PD and PD1 and inhibition capacity decreases. As per the PDP data for PD1 the current density increases from 0.1097mA/cm² to 0.5120mA/cm² and 0.1468 mA/cm² to 0.5745mA/cm² for PD in 1M HCl at 333K. For a given temperature there is a continuous adsorption-desorption process from the metal surface takes place and equilibrium is attained. With the increase in temperature the equilibrium shifts to desorption leading to increased corrosion rate and decreased efficiency. The phenomenon of inhibition can be assigned as physisorption as the rise in temperature decreases efficiency. For chemisorbed molecules, higher temperature strengthens the interaction, and the efficiency increases[17].

Table 4.6 EIS data of PD and PD1 at 323K and 333K in 1M HCl

Temp (K)	C _{inh} (ppm)	R _{ct} (Ω cm ²)	C _{dl} (μ F/cm ²)	I _{corr} (mA/cm ²)	IE%
323	Blank	9.00	954.1	2.843	----
	200 PD	52.85	306.7	0.493	82.80
	200PD1	54.64	312.2	0.477	83.52
333	Blank	5.42	784.1	4.80	----
	200PD	24.22	654.7	1.07	77.62
	200PD1	23.09	646.5	1.13	75.44

Table 4.7 PDP data of PD and PD1 at 323K and 333K in 1M HCl

Temp (K)	C _{inh} (ppm)	-E _{corr} (mV)	β _a (mV)	$-\beta$ _c (mV)	I _{corr} (mA/cm ²)	IE%
323	Blank	455	108	112	1.2846	-----
	200PD	361	82	100	0.3044	76.30
	200PD1	397	83	99	0.2992	76.70
333	Blank	481	109	111	1.7253	----
	200PD	451	98	99	0.5745	65.67
	200PD1	481	96	144	0.5120	70.32

4.2.2.5 Bode and Phase angle plots

The Bode phase angle and magnitude plots for 200ppm PD and PD1 at various temperatures are given in Fig 4.9 c and d, e and f. The Bode plot explains how the system varies with changes in frequency. At low and high frequencies, the phase shift approaches to zero but at intermediate frequencies, the current lags behind voltage and impedance have an out of phase component which is regulated by the capacitance at the interface.

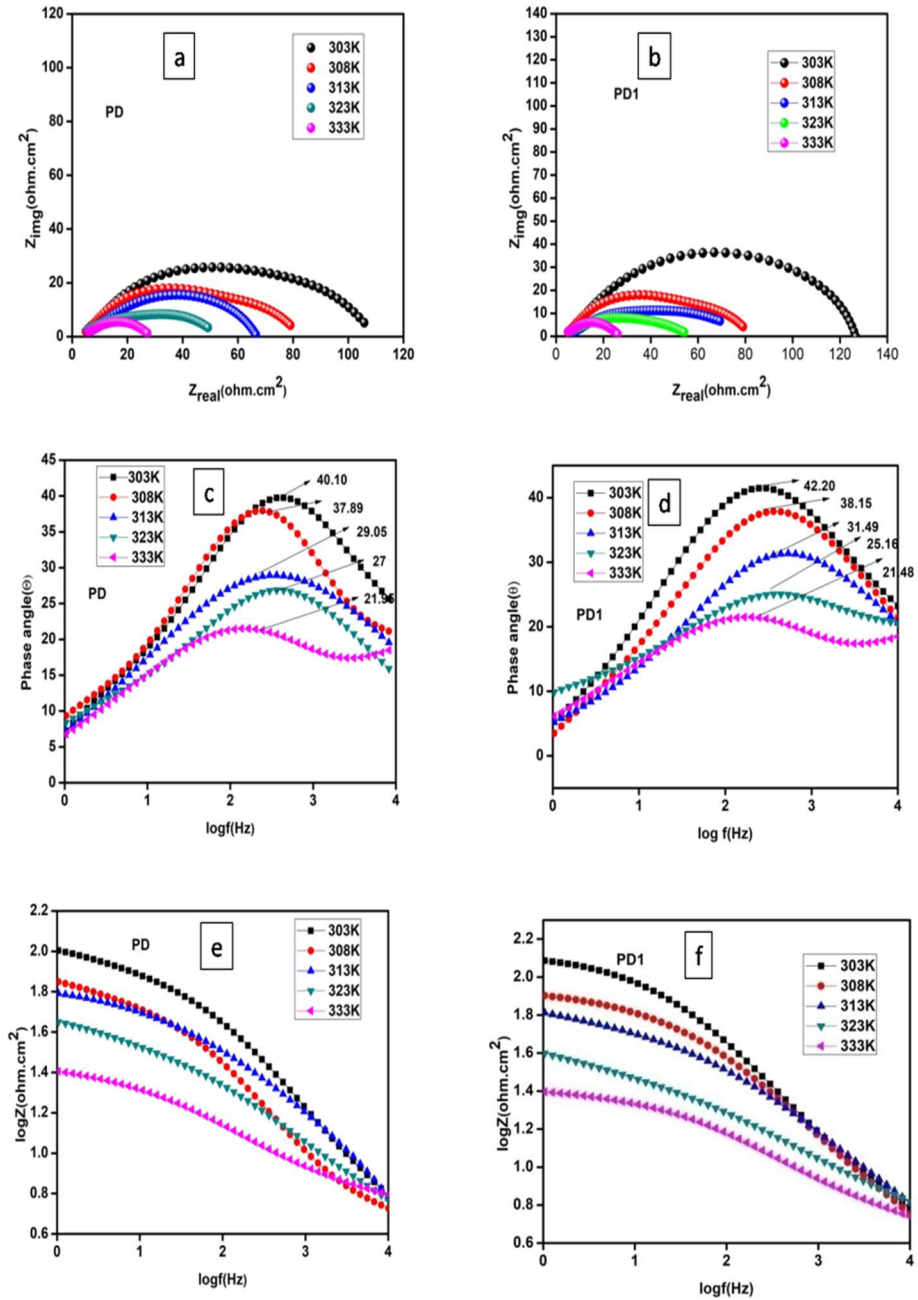


Fig 4.9 The Nyquist, Bode phase angle and magnitude plot for 200ppm of PD and PD1 at different temperatures

For a pure capacitor, the phase angle shift is 90° . Fig 4.9 reveals the phase angle shift is maximum at 303K (40.10 and 42.20) whereas with temperature rise the phase angle shift decreases and reaches a minimum (21.95 and 21.45) at 333K for PD and PD1. This indicates the diminished capacitance behaviour of the inhibitor at high temperatures. In the phase angle plot, there is only one time constant with one maximum at intermediate frequencies which confirms the charge transfer controlled process for corrosion inhibition[18, 19]. The Bode magnitude plot reveals the increased polarisation resistance (R_p) at lower temperature and which affirms the better protection efficiency at lower temperatures. The temperature rise can cause desorption of physically adsorbed molecules, whereas the most effective inhibitors are those which can adsorb chemically by the process of transferring charges between them. Chemisorption is slower than physisorption.

4.2.2.6 Effect of side- chain length on corrosion inhibition

The efficacy of an organic molecule for corrosion inhibition depends on an anchoring group rather than hetero atoms on the anchoring group. Factors such as molecular weight, molecular structure, molecular configuration, the nature of the substituent, the molecular area can also adequately affect inhibition efficacy. The inhibition capacity of the molecule is influenced electronically and sterically by electron releasing groups. Electronically they contribute positively by enhancing the electron density and make the molecule more nucleophilic centres leading to pronounced interaction with metal

atoms. Sterically they affect negatively towards inhibition efficiency. The presence of bulky group makes it difficult for proper orientation on the metal surface[20]. The pyrazolone chalcones PD and PD1 differ in the alkyl group attached to the 3rd position of the pyrazole ring. Alkyl groups being electron releasing groups contribute positively towards corrosion inhibition [21]. It is assumed that below optimum concentration the molecule arranges flat on the metal surface and the dominating interaction is between the metal surface and the inhibitor. The optimum inhibitor concentration at which the molecule arranges vertically on the metal surface is prominent in its inhibitory action. These types of arrangements decrease the wettability of metal surfaces with an increase in hydrophobic carbon chains and enhance corrosion inhibition. Comparison of the inhibition efficiency of PD and PD1 (Fig 4.10) reveals that the PD1 acts as a better inhibitor, though both provide high inhibition efficiency towards mild steel corrosion. This explicitly explains that methyl and the propyl group facilitate the electron- donating capacity of the inhibitor and the proper orientation of the bulky propyl group ensures better protection to mild steel from acidic media [22]. The theoretical calculations, ESP mapping also proves the increased electron density at the pyrazole and the benzene ring with the introduction of the propyl group.

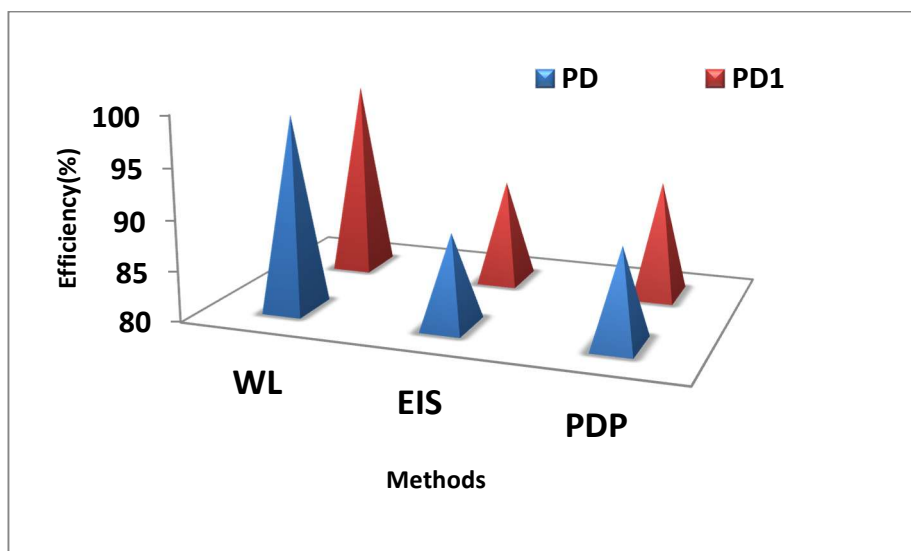


Fig 4.10 Comparison of efficiency of 200ppm of PD and PD1 by different methods in 1M HCl

4.2.3 Adsorption Isotherms

Mixed inhibitors usually protect metals either by chemical or physical adsorption or by film formation. Charge on the metal surface can be defined by the difference between ZCP (Zero charge potential) and E_{corr} . If the difference ($E_{\text{corr}} - \text{ZCP}$) is positive, then the metal is positively charged [23]. The water molecules adsorbed on the metal surface is replaced by inhibitor molecules by physisorption. The strength of adsorption is deduced from the isotherm fitting studies. The usual practice of considering the best-fit isotherm from among different isotherms such as Langmuir, Tempkin, Frumkin, etc is carried out in this study, and the best-fit isotherm given by Langmuir adsorption isotherm model and is represented by eqn.3.3. K_{ads} , the equilibrium constant of adsorption calculated from the isotherm as reciprocal of the Y- intercept. Fig 4.11 gives the isotherm in HCl. The

decrease in K_{ads} with an increase in temperature is attributed to the predominant desorption process. The spontaneity of adsorption is checked by the free energy of adsorption (ΔG_0), which is given by eqn. 2.10. The calculated values are given in Table 4.8. The negative values of the free energy of adsorption indicate the spontaneity of adsorption process. Generally, when values are below -20 kJ/mol the preferred adsorption is physisorption and when the value is above -40 kJ/mol chemisorption is preferred. In the case of PD and PD1 the ΔG_0 values are in between -20 kJ/mol and -40 kJ/mol validating the combined physisorption and chemisorption effects [24]. In accordance with the EIS and PDP values that the decrease in efficiency with a rise in temperature assures predominant physisorption [25]. The entropy of adsorption and enthalpy of adsorption is calculated using Van't Hoff eqn. 2.11. The negative values of enthalpy of adsorption (ΔH^0_{ads}) prove the exothermic nature of adsorption including both physisorption and chemisorption. The change in ΔS^0_{ads} from negative (PD) to positive values may be ascribed to the more ordered arrangement of inhibitor molecules on the metal surface [26].

Table 4.8 The adsorption parameters calculated using Langmuir adsorption isotherm and Van't Hoff equation

Inhibitor	Parameter	303K	308K	313K	ΔH^0_{ads} kJ/mol	ΔS^0_{ads} J/molK
	K_{ads} (M^{-1})	31796	33288	7230		
PD	ΔG^0_{ads} (kJ/mol)	-31.79	-30.69	-30.47	-19.03	-36.96
	K_{ads} (M^{-1})	39447	57339	34558		
PD1	ΔG^0_{ads} (kJ/mol)	-37.37	-37.88	-38.38	-6.695	101.09

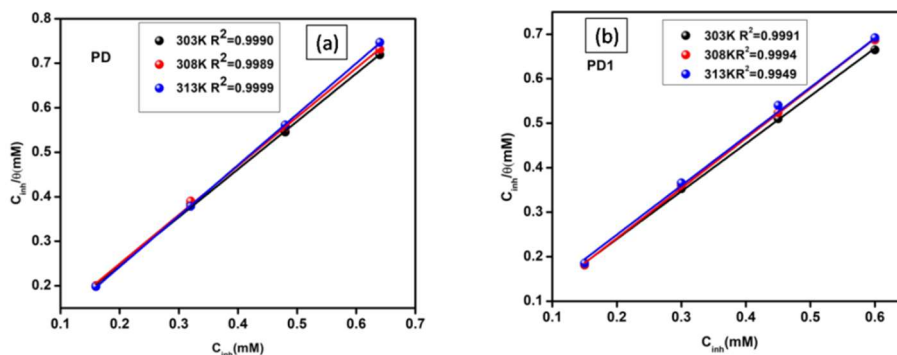


Fig 4.11 Langmuir adsorption isotherm for (a) PD and (b) PD1 in 1M HCl

4.2.4 Kinetic parameters

Activation parameters of the corrosion process are calculated using the Arrhenius eqn.2.12 and transition state eqn.2.13. Fig 4.12 is the plots obtained for PD and PD1 in HCl. The slope of the straight-line graph obtained by plotting $1/T$ against $\ln CR$ gives $-E_a/R$. The hike in E_a (Table 4.9) value of the inhibited solution is associated with an increase in the adsorption of inhibitor molecules which creates an increased energy barrier for corrosion to take place. The slope of the straight-line graph plotting $\ln(CR/T)$ vs $1/T$ gives $-\Delta H_a/R$ and intercept $\ln(R/Nh) + \Delta S_a/R$ where ΔH_a and ΔS_a are the enthalpies of activation and entropy of activation. The closeness of H_a values and E_a values in the inhibited solution emphasise the increase of the energy barrier without a change in the dissolution mechanism. Higher E_a values of the inhibited solution compared to blank proposes physisorption. The positive value of ΔH_a describes the endothermic nature of metal dissolution. The less negative value of ΔS_a of inhibited solution supports the formation of an activated complex in the rate-determining step. The increase in disorder is attributed to the conversion of reactants to activated complex[24].

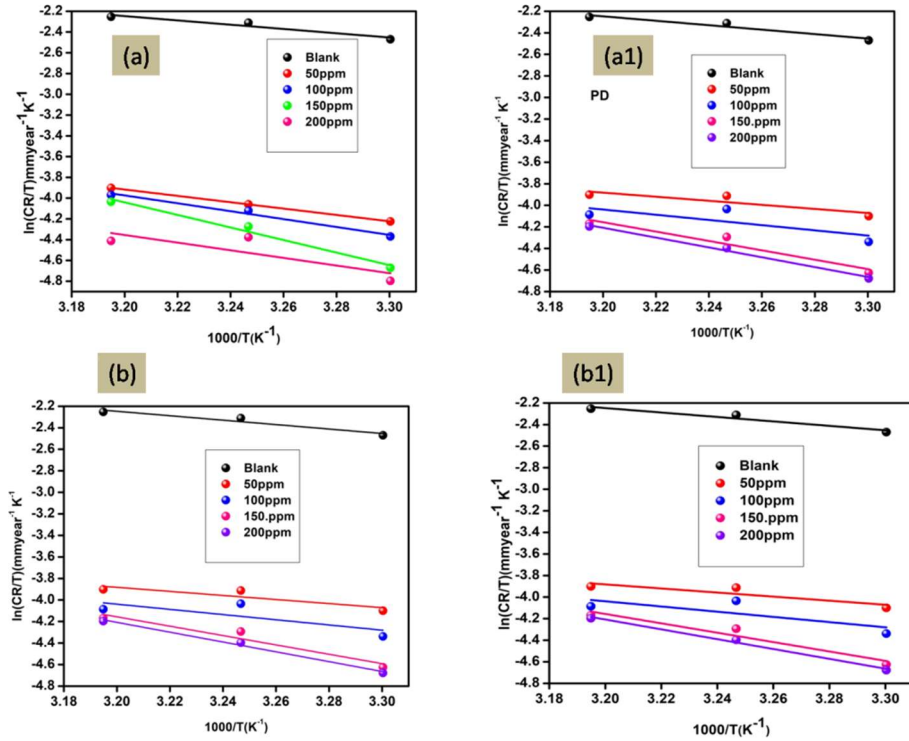


Fig 4.12 Arrhenius (a) and (b) and Transition state (a1) and (b1) for PD and PD1 in 1M HCl

Table 4.9 Kinetic parameters calculated using Arrhenius equation and Transition state plot

	C_{inh} (ppm)	CR (mm/y)			Activation parameters		
		303K	308K	313K	E_a (kJ/mol)	ΔH_a (kJ/mol)	ΔS_a (J/mol K)
PD	Blank	25.64	30.53	32.90	19.69	17.13	-161.37
	50	5.02	6.15	6.32	18.24	15.68	-148.71
	100	4.26	5.48	5.19	18.80	20.07	-129.37
	150	3.06	4.13	4.77	34.86	36.15	-70.31
	200	2.81	3.79	4.70	40.48	37.92	-135.91
PD1	50	4.43	5.31	6.30	27.99	25.43	-179.61
	100	3.83	4.99	5.91	34.18	25.63	-166.89
	150	2.99	4.29	5.48	52.81	50.25	-116.41
	200	2.49	3.51	3.83	33.14	30.57	-111.17

4.2.5 Theoretical calculations

Theoretical calculations done with the help of Gaussian 09 package using B3LYP/6-311G (d, p) level is given in Table 4.10. The optimised geometries of inhibitor molecules are given in Fig 4.13. The electrons are donated from the HOMO and accepted to the LUMO. Therefore the high energy of HOMO, low energy of LUMO, and low ΔE ($E_{LUMO} - E_{HOMO}$) enhances the corrosion inhibition property of organic inhibitor molecules.

Table 4.10 Global parameters obtained for PD and PD1 by geometry optimisation using B3LYP 6-311G (d, p) basis set

Parameter	PD	PD1
Total Energy(a.u)	-975.15	-1053.82
$E_{HOMO}(eV)$	-5.76	-5.51
$E_{LUMO}(eV)$	-2.59	-2.37
$\Delta E(eV)$	3.17	3.14
Hardness $\eta = \frac{\Delta E}{2}$	1.59	1.57
Dipole moment, $\mu(D)$	5.58	8.80
$IE = -E_{HOMO}$	5.76	5.51
$EA = -E_{LUMO}$	2.59	2.37
$\chi = \frac{IE + EA}{2}$	4.18	3.94
$\Delta N = \frac{(\chi_{Fe} - \chi_{inh})\chi}{2(\eta_{Fe} + \eta_{inh})}$	0.89	0.97
$\phi = \frac{\chi_{inh}^2}{4\eta_{inh}}$	2.560	2.478

The inhibitor PD1 with high energy HOMO and low energy LUMO act as better inhibitors whereas low ΔE is obtained for PD. According to the DFT theory electronegativity (χ) of a system with total energy E and N electrons is defined as the first derivative of total energy with

respect to the number of electrons which is equal to the negative of the chemical potential[11].

$$\chi = -\mu = -\left(\frac{\delta E}{\delta N}\right)_{v(r)} \quad (4.2)$$

and defines hardness(η) is the second derivative of E with respect to N.

$$\eta = \left(\frac{\delta^2 E}{\delta N^2}\right)_{v(r)} \quad (4.3)$$

The approximate values of electronegativity(negative of chemical potential) and hardness is given by

$$\chi = -\mu = \frac{(IE + EA)}{2} \quad (4.4)$$

$$\eta = \frac{IE - EA}{2} \quad (4.5)$$

where IE ($-E_{\text{HOMO}}$) and EA ($-E_{\text{LUMO}}$) are the ionisation enthalpy and electron affinity as per Koopman's theorem. When the metal and the inhibitor are brought together the electrons will flow from the inhibitor with low χ to that with metal with high χ value until the chemical potential of the systems is equal[12]. Smaller values of IE of PD1 assure the easy interaction of PD1 with metal causing more corrosion protection than PD. The molecule with higher ΔN is able to donate more electrons to the metal and thus act as a better corrosion inhibitor. PD1 with the fraction of electrons transferred (ΔN) is more could be a good inhibitor. A critical observation of the calculated theoretical value reveals almost the same value for the global parameters with a slightly efficient value for PD1. Fig 4.14(a) gives the electrostatic potential energy (ESP) map of PD and PD1 taken from Gaussian checkpoint files. As per the ESP mapping, regions of higher electrostatic potential

will be blue colour and where the electron density will be minimum whereas regions of lower electrostatic potential will be red colour and where the electron density will be maximum. The ESP map of PD and PD1 points out the pyrazole ring with a carbonyl oxygen atom and the benzene ring attached to the pyrazole are with more electron density. The shift of the methyl group to propyl group in PD1 has improved the electron density of the pyrazole, benzene ring, and the double bond linked to aldehyde. The optimised geometry of the molecules (Fig4.13) show that the lone pair of electron on N of p-dimethyl amino benzaldehyde has undergone delocalisation. HOMO (Fig 4.14.(b)) of PD and PD1 are spread over the aromatic rings, pyrazole ring, and on the heteroatoms, and these regions are electron donating sites whereas the LUMO is not spread over to the benzene ring attached to pyrazole ring and they remain as nucleophilic centres. This is in good agreement with the ESP map.

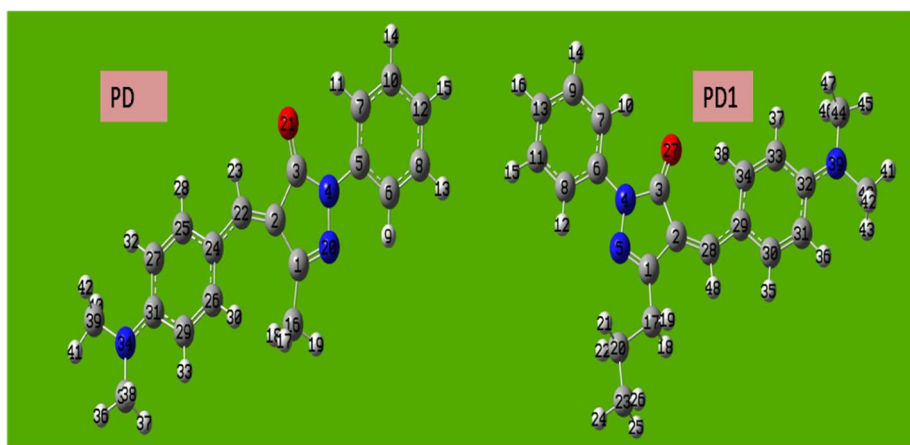


Fig 4.13 Optimised geometry of PD and PD1 obtained by DFT calculations using 6-311G(d, p) basis set

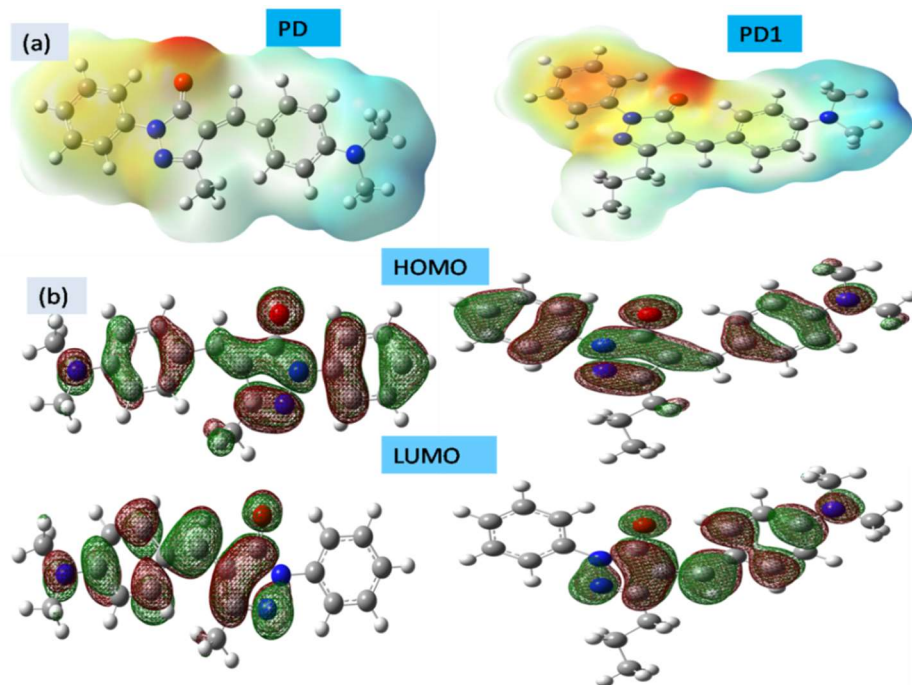


Fig 4.14.a) Electrostatic potential (ESP) map of PD and PD1 on isosurface (b) HOMO and LUMO of PD and PD1

4.2.5.1 Fukui Indices

Fig 4.15 shows the Fukui indices calculated with the help of UCA_FUKUI software which works on the theory of finite difference approximations making use of the NPA (Natural Population Atomic charges) obtained from NBO analysis from Gaussian output files of the inhibitor [13]. The atom with maximum f^- is electron rich centre and act as donors of electrons to the metal and those with higher f^+ are acceptors of electrons. The graph clearly explains that C24, C16, O21 of PD and C34, O27 of PD1 with higher f^- are nucleophilic centres and C3, C6, C27 of PD and C28, C3 of PD1 are electrophilic centres. It could also be observed that the change of methyl to propyl group in

PD1 has increased the nucleophilic nature of the pyrazole ring and the benzene ring attached to it.

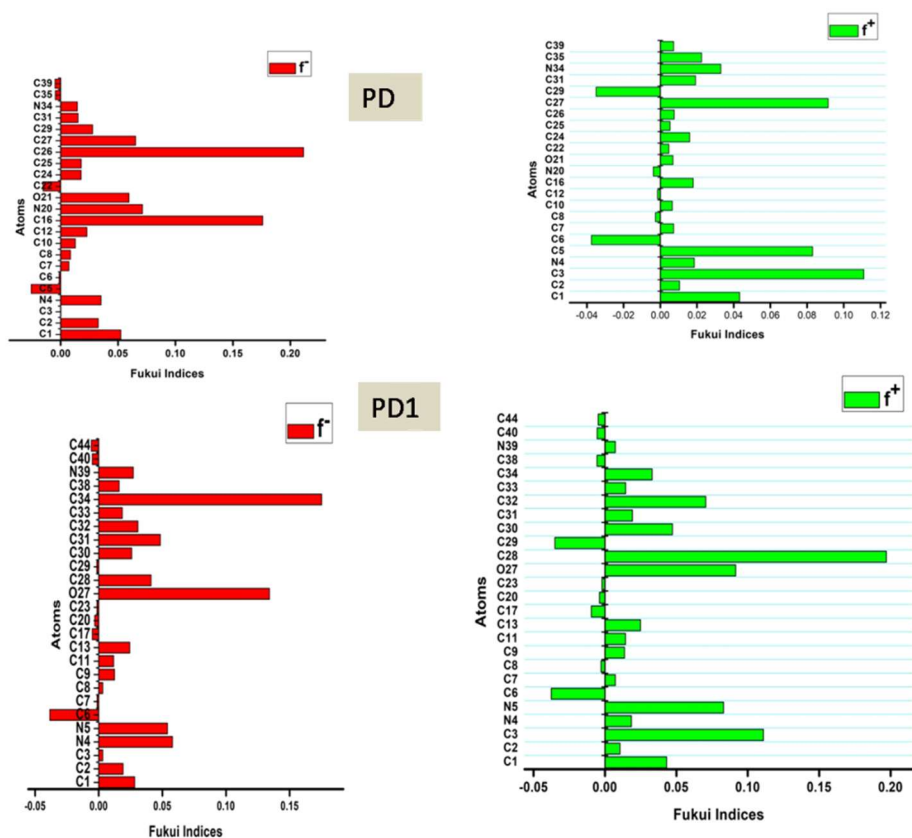


Fig 4.15 Fukui indices of PD and PD1 obtained from NBO analysis

4.2.6 Material studio calculations

Various parameters such as adsorption energy, rigid adsorption energy, deformation energy, dE_{ads}/dN_i are obtained from the adsorption locator calculations of material studio. The rigid adsorption energy is the energy released when the molecule is unrelaxed and the deformation energy is the energy released when the molecule is

relaxed on the metal surface. Adsorption energy is given as the sum of rigid adsorption energy and deformation energy, the energy of interaction (E_i) and binding energy (E_b) is [14] given in Table 4.11. The higher negative values of adsorption energy and energy of interaction and the higher positive value of binding energy prove PD1 as the better inhibitor which is in conformation with the experimental data[15, 16]. Fig 4.16 shows the mode of adsorption of PD and PD1 on Fe (110) plane.

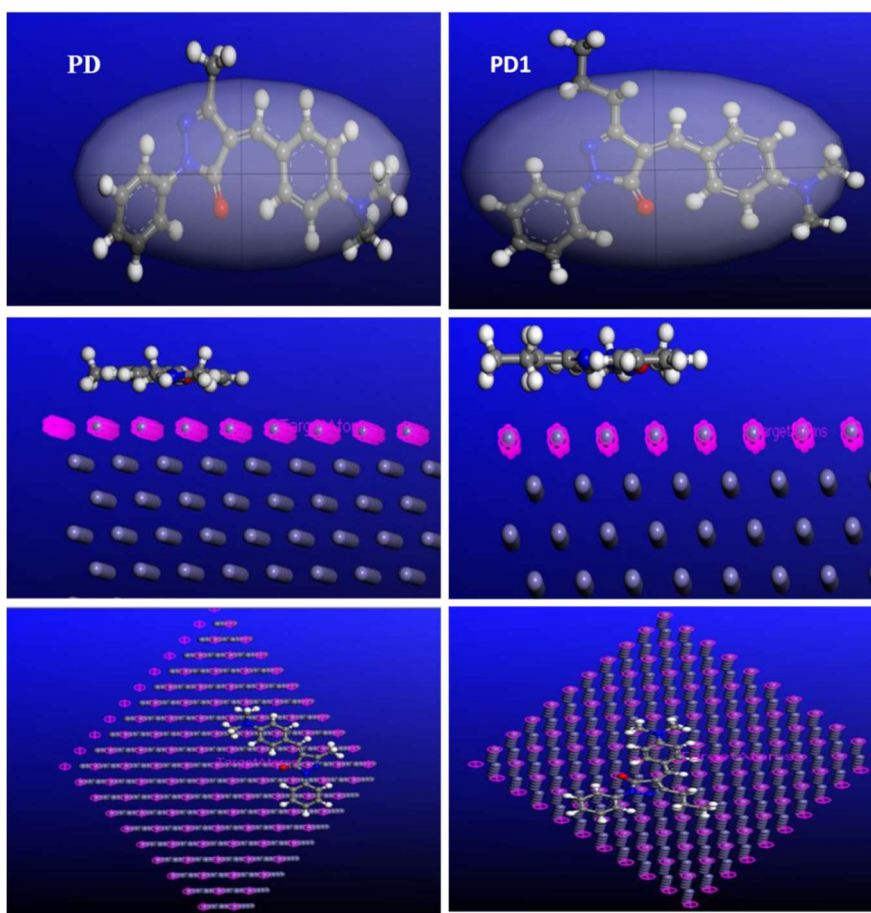


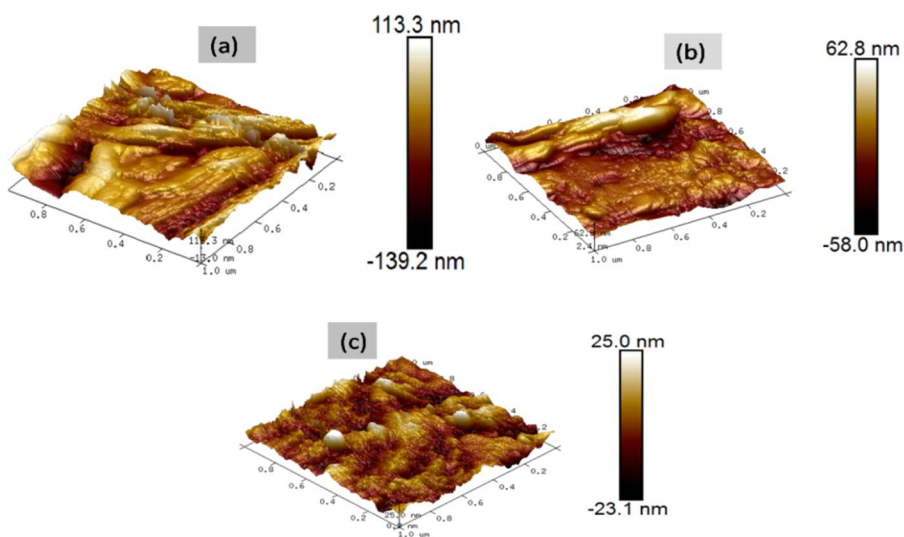
Fig4.16 Adsorption mode of PD ad PD1 obtained by Material Studio simulations

Table 4.11 Energy parameters obtained by Material studio calculations

Inhibitor	PD	PD1
Total Energy(kcal/mol)	-224.50	-254.45
Adsorption Energy(kcal/mol)	-262.86	-286.60
Rigid adsorption energy (kcal/mol)	-220.52	-246.29
Deformation Energy (kcal/mol)	-42.34	-40.39
$E_{\text{interaction}}$ (kcal/mol)	-186.14	-216.09
E_{binding} (kcal/mol)	186.14	216.09

4.2.7 AFM Analysis

The surface analysis of blank, PD, and PD1 using AFM analyser is given in Fig4.17. The average roughness (Ra) for the blank is 25.5nm, PD1 is 4.87nm 11.2nm for PD. The root mean square roughness (Rq) is 33.4 nm for blank, 6.36nm for PD1, and it is 14.8nm for PD. As the metal corrosion is less the roughness also will be less [27]. Therefore, we can conclude that both PD and PD1 give high surface coverage to mild steel specimens in acidic solutions.

**Fig 4.17** AFM images of (a) blank (b) PD and (c) PD1

4.3 Conclusions

1. Pyrazolone chalcones PD and PD1 are efficient inhibitors for MS corrosion in HCl
2. Inhibition efficiency increases with the concentration of the inhibitor but shows a reverse trend with temperature.
3. Both PD and PD1 are mixed-type inhibitors that exert inhibition through pronounced physisorption of inhibitor molecules.
4. The adsorption of the inhibitor is influenced by structure and geometry as evidenced from computational studies
5. The introduction of propyl group provides greater inhibition capacity to PD1.
6. The AFM image shows that the surface roughness of mild steel specimen is decreased by the presence of the inhibitors.

References

1. Dandia, A., et al., *Ultrasound-assisted synthesis of pyrazolo [3, 4-b] pyridines as potential corrosion inhibitors for mild steel in 1.0 M HCl*. ACS Sustainable Chemistry & Engineering, 2013. **1**(10): p. 1303-1310.
2. Cao, K., W. Li, and L. Yu, *Investigation of 1-Phenyl-3-Methyl-5-Pyrazolone as a corrosion inhibitor for mild steel in 1M hydrochloric acid*. Int. J. Electrochem. Sci, 2012. **7**: p. 806-818.
3. Hameed, R.A., et al., *Pyrazole derivatives as corrosion inhibitor for C-steel in hydrochloric acid medium*. J. Mater. Environ. Sci, 2012. **3**(2): p. 294-305.
4. Abdel-Wahab, B.F., R.E. Khidre, and A.A. Farahat, *Pyrazole-3 (4)-carbaldehyde: synthesis, reactions and biological activity*. Arkivoc: Online Journal of Organic Chemistry, 2011.
5. Siddiqui, Z.N., et al., *Thermal solvent-free synthesis of novel pyrazolyl chalcones and pyrazolines as potential antimicrobial agents*. Bioorganic & medicinal chemistry letters, 2011. **21**(10): p. 2860-2865.
6. Fouda, A., M. Elmorsi, and A. Elmekawy, *Eco-friendly chalcones derivatives as corrosion inhibitors for carbon steel in hydrochloric acid solution*. African Journal of Pure and Applied Chemistry, 2013. **7**(10): p. 337-349.
7. Priyadharshini, R.S. and P.M. Sirajudeen, *Corrosion Inhibition Studies on Mild Steel in Acidic Media with 2-Hydroxy-4-methoxy Chalcone*. Chemical Science, 2016. **5**(2): p. 447-457.
8. Fouda, A., et al., *Chalcone derivatives as corrosion inhibitors for carbon steel in 1 M HCl solutions*. Int. J. Electrochem. Sci, 2014. **9**: p. 7038-7058.
9. Lgaz, H., et al., *Insights into corrosion inhibition behavior of three chalcone derivatives for mild steel in hydrochloric acid solution*. Journal of Molecular Liquids, 2017. **238**: p. 71-83.
10. Xue, Y., et al., *An ab initio simulation of the UV/Visible spectra of substituted chalcones*. Central European Journal of Chemistry, 2010. **8**(4): p. 928-936.

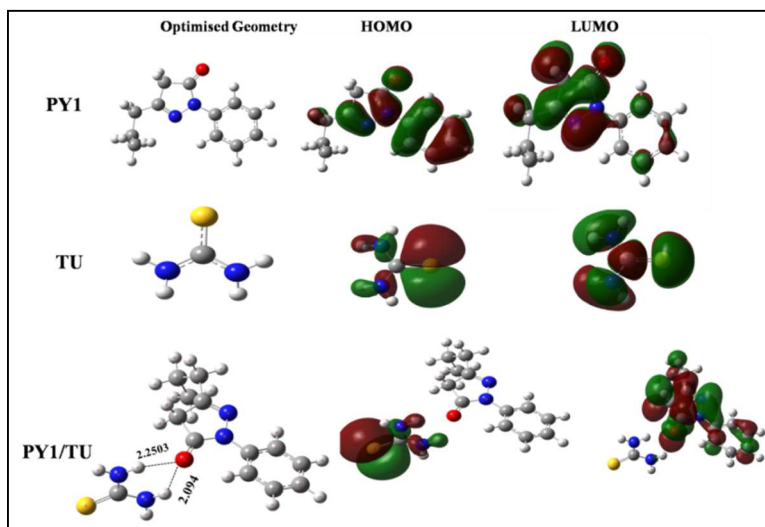
11. Guo, L., et al., *Theoretical evaluation of the corrosion inhibition performance of 1, 3-thiazole and its amino derivatives*. Arabian Journal of Chemistry, 2017. **10**(1): p. 121-130.
12. John, S. and A. Joseph, *Theoretical and electrochemical studies on the effect of substitution on 1, 2, 4-triazole towards mild steel corrosion inhibition in hydrochloric acid*. 2012.
13. Sánchez-Márquez, J., et al., *Introducing "UCA-FUKUI" software: reactivity-index calculations*. Journal of molecular modeling, 2014. **20**(11): p. 2492.
14. Tang, Y., et al., *Experimental and molecular dynamics studies on corrosion inhibition of mild steel by 2-amino-5-phenyl-1, 3, 4-thiadiazole*. Corrosion Science, 2010. **52**(1): p. 242-249.
15. Thomas, A., P.R. Ammal, and A. Joseph, *A comprehensive study of mild steel corrosion in the aggressive acidic environment using CMPPC, a substituted pyrazole derivative*. Chemical Papers, 2020: p. 1-13.
16. John, S., K.M. Ali, and A. Joseph, *Electrochemical, surface analytical and quantum chemical studies on Schiff bases of 4-amino-4H-1, 2, 4-triazole-3, 5-dimethanol (ATD) in corrosion protection of aluminium in 1N HNO₃*. Bulletin of Materials Science, 2011. **34**(6): p. 1245-1256.
17. Srimathi, M., R. Rajalakshmi, and S. Subhashini, *Polyvinyl alcohol-sulphanilic acid water soluble composite as corrosion inhibitor for mild steel in hydrochloric acid medium*. Arabian Journal of Chemistry, 2014. **7**(5): p. 647-656.
18. Chaouiki, A., et al., *Assessing the impact of electron-donating-substituted chalcones on inhibition of mild steel corrosion in HCl solution: Experimental results and molecular-level insights*. Colloids and Surfaces A: Physicochemical and Engineering Aspects, 2020. **588**: p. 124366.
19. Singh, A., et al., *Effect of electron donating functional groups on corrosion inhibition of mild steel in hydrochloric acid: Experimental and quantum chemical study*. Journal of the Taiwan Institute of Chemical Engineers, 2018. **82**: p. 233-251.

20. Elayyachy, M., et al., *New bipyrazole derivatives as corrosion inhibitors for steel in hydrochloric acid solutions*. Materials chemistry and physics, 2005. **93**(2-3): p. 281-285.
21. Cao, S., et al., *Task-specific ionic liquids as corrosion inhibitors on carbon steel in 0.5 M HCl solution: an experimental and theoretical study*. Corrosion Science, 2019. **153**: p. 301-313.
22. De Damborenea, J., J. Bastidas, and A. Vazquez, *Adsorption and inhibitive properties of four primary aliphatic amines on mild steel in 2 M hydrochloric acid*. Electrochimica acta, 1997. **42**(3): p. 455-459.
23. Revie, R.W., *Uhlig's corrosion handbook*. Vol. 51. 2011: John Wiley & Sons.
24. Ammal, P.R., M. Prajila, and A. Joseph, *Physicochemical studies on the inhibitive properties of a 1, 2, 4-triazole Schiff's base, HMATD, on the corrosion of mild steel in hydrochloric acid*. Egyptian Journal of Petroleum, 2018. **27**(3): p. 307-317.
25. Chakravarthy, M. and K. Mohana, *Adsorption and corrosion inhibition characteristics of some nicotinamide derivatives on mild steel in hydrochloric acid solution*. International Scholarly Research Notices, 2014. **2014**.
26. Kumari, P.P., P. Shetty, and S.A. Rao, *Electrochemical measurements for the corrosion inhibition of mild steel in 1 M hydrochloric acid by using an aromatic hydrazide derivative*. Arabian Journal of Chemistry, 2017. **10**(5): p. 653-663.
27. Aslam, R., et al., *Sugar based N, N'-didodecyl-N, N' digluconamideethylenediamine gemini surfactant as corrosion inhibitor for mild steel in 3.5% NaCl solution-effect of synergistic KI additive*. Scientific reports, 2018. **8**(1): p. 1-20.

Chapter 5

Extended protection of mild steel in HCl at elevated temperatures using the synergistic interaction of Pyrazolone and Thiourea

This chapter discusses the combined effect of various concentrations of PY1 and thiourea in the inhibition of mild steel corrosion in 1M HCl. The results show co-adsorption of the inhibitor molecules on the metal surface enhancing the protection capacity at moderate temperatures.



Contents

5.1. Introduction	129
5.2. Results and discussion	129
5.3. Conclusions	145

5.1 Introduction

Corrosion cannot be prevented but the process could be delayed by employing suitable strategies. The use of inorganic/ organic inhibitors is one such attempt. The use of organic inhibitors is more popular than inorganic ions due to various reasons in aqueous acidic solutions. These solutions are commonly used for acid pickling descaling, industrial cleaning, and petrochemical processes. Synergism is a relatively new attempt where the combined effect of different molecules are tried in mitigating metal corrosion is of great interest now[1]. Several studies have been reported on the synergistic interaction of organic molecules with inorganic cations, anions, surfactants, etc [2-11]. Few reports on the synergistic behaviour among organic molecules are seen in the literature [12-15]. The present study focuses on the synergistic interaction of a substituted pyrazolone (PY1) with thiourea (TU) in 1M HCl at different temperatures.

5.2 Results and Discussion

5.2.1 Synthesis and characterisation of the inhibitor

The inhibitor 3-propyl -1-phenyl-1H-pyrazolyl-5(4H)-one (**PY1**) is prepared by the scheme discussed in chapter 2 (Scheme 2.1)[16]. The characterisation of the compound is done using UV-Visible, IR and ^1H and ^{13}C NMR spectrum. ^1H NMR CDCl_3 ; δ ppm; 1.002(CH_3 of propyl group), 1.3(CH_2 propyl group), 1.4 (CH_2 propyl group), 2.3(CH_2 of pyrazole ring), 7.4-8.6(benzene ring). ^{13}C NMR; δ ppm(13.79 1C CH_3), 20.02(1C CH_2), 41.75(1C CH_2 of pyrazole ring), 159.92(1C attached to the pyrazole ring), 172.59(1C $\text{C}=\text{O}$)140.4(1C $\text{C}-\text{N}$), 110-120(2C, 2C, 1C of benzene ring). Fig 5.1 and Fig 5.2 shows the UV-visible, IR and NMR spectra of the compound. Pure thiourea (**TU**) is purchased from Sigma Aldrich.

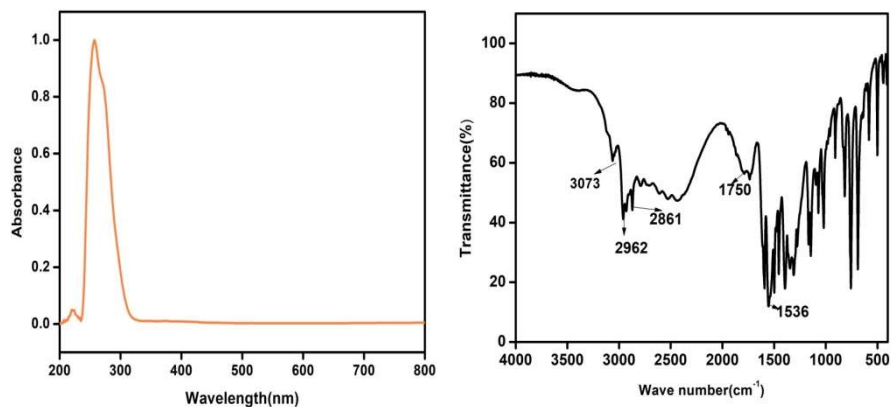


Fig 5.1 UV-Visible and IR spectra of PY1

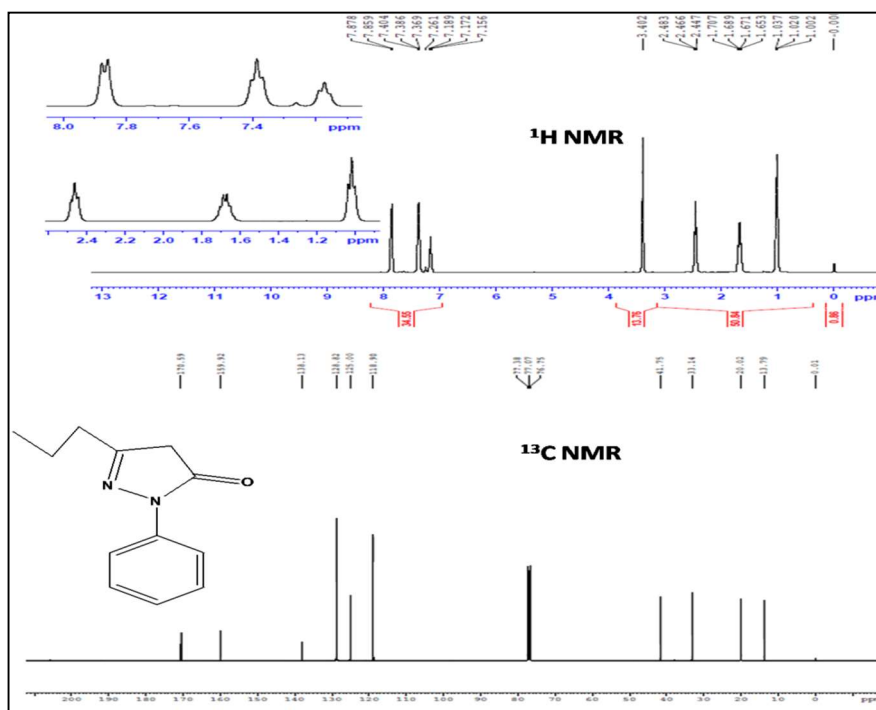


Fig 5.2 ^1H and ^{13}C NMR spectrum of PY1

5.2.2 Corrosion Analysis

5.2.2.1 Weight loss studies

Weight loss analysis of mild steel samples in 1M HCl with varying concentrations of PY1 and a combination of PY1 with 50 ppm of thiourea (TU) is carried out at room temperature for 48 hours. The results are given in Table 5.1. The weight loss is much decreased with the addition of inhibitors inferring that both PY1 and TU act as corrosion inhibitors in HCl media. The inhibitors reduce the weight loss by adsorbing on the metal surface leading to a greater surface coverage[17]. A comparison of the inhibition efficiency of PY1 and a combination of PY1 and TU (Fig 5.3) shows that the inhibition efficiency of PY1 is enhanced to a greater extent by the addition of TU for all concentrations of PY1. Therefore it is inferred that PY1/TU combination act as a synergistic pair in corrosion mitigation of mild steel in HCl.

Table 5.1 Weight loss parameters of mild steel dipped in 1M HCl for 48 h in presence of PY1 and PY1/TU pair

C_{inh} (ppm)	PY1			PY1+50ppm TU		
	Wt.Loss (mg)	CR (mg/cm ² h)	%IE	Wt.Loss (mg)	CR (mg/cm ² h)	%IE
Blank	1248	7.2222	----	1248	7.2222	-----
50TU	79.8	0.4618	93.60	79.8	0.4618	93.60
50	689.6	3.990	44.75	108.9	0.6302	91.27
100	337.7	1.954	72.94	81.1	0.4693	93.50
150	144.5	0.8362	86.01	44.2	0.2557	96.45
200	73.8	0.4270	94.08	29.0	0.1678	97.67

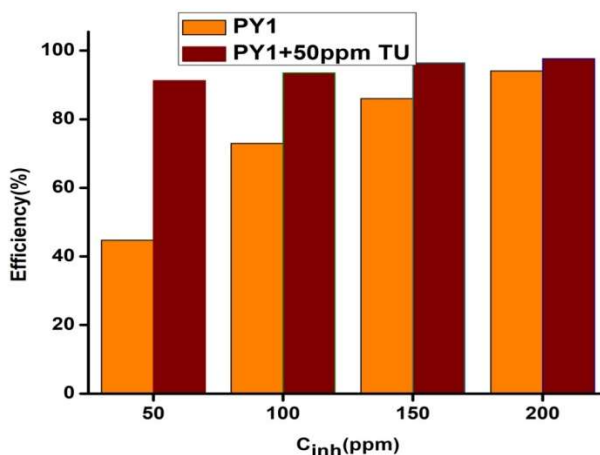


Fig 5.3 A comparison of inhibition efficiencies of PY1 with PY1/TU pair.

5.2.2.2 EIS analysis

EIS provides a convenient method for analysing the metal surface coated with organic molecules. The EIS analysis of PY1 and a combination of PY1 with 50 ppm of TU is done in 1M HCl at four different temperatures. The inhibition efficiency calculated using eqn.2.8 and the other parameters obtained from the circle fit of Nyquist plot considering the metal electrode-electrolyte interface to an equivalent Randles circuit is given in Table 5.2 and Table 5.3. The Nyquist plots for varying concentrations of PY1 with TU are depicted in Fig 5.4. The inset of Fig 5.4 gives the corresponding blank and PY1 alone at the given temperature. The figure clearly describes the increased charge resistance (diameter of the semicircle) of the pair PY1 and TU at all temperatures. The increase in the charge transfer resistance (R_{ct}) and efficiency is attributed to an increase in the thickness of the double layer by the replacement of water molecules on the metal surface by the inhibitor molecules[18]. The double layer capacitance shows a reverse trend to R_{ct} because of an increase in the

thickness of the electrical double layer and decreases in the local dielectric constant due to substitution of high dielectric water molecules by low dielectric inhibitor molecules[19]. The electrode-electrolyte interface act as a differential capacitor due to organic molecules of large volume on the solution side compared to free electrons on the metal surface[20]. Comparison of the inhibition efficiency of PY1 with PY1/TU pair proves the synergistic interaction of the pair enhancing the efficiency from 84.33% to 92.36% at room temperature and 58.31% to 83.41% at 318K (Table5.2 and Table5.3).

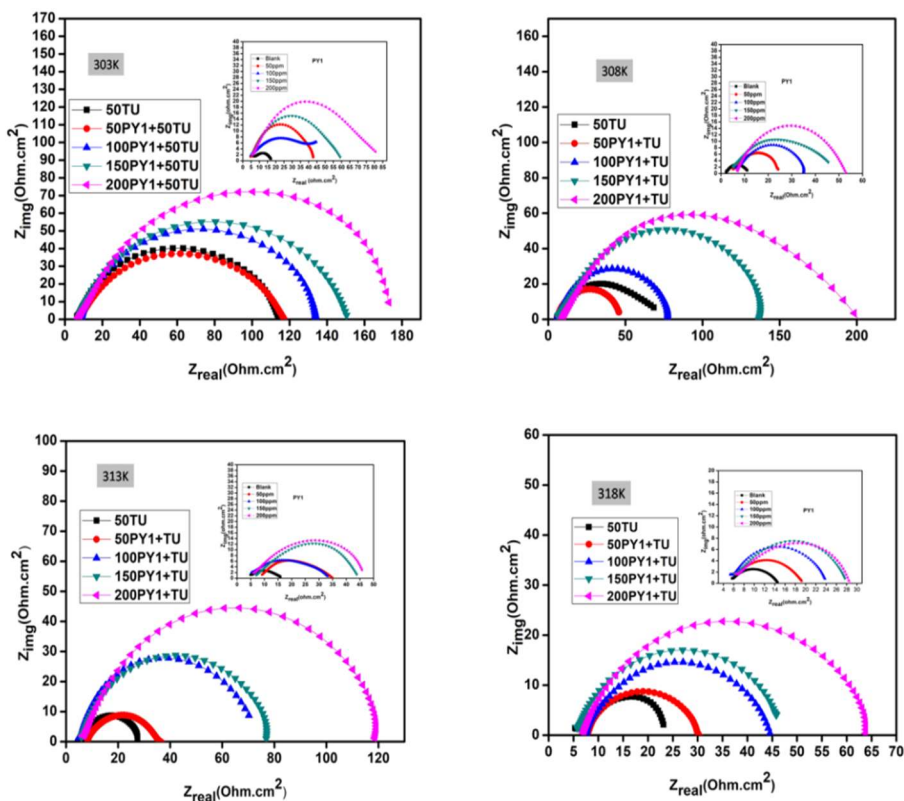


Fig 5.4 Nyquist plots for varying concentration of PY1 (inset) and PY1/TU pair at 303K, 308K, 313K, 318K

Table 5.2 Impedance data obtained for PY1, TU and PY1/TU combinations at 303K and 308K in 1M HCl

Temp (K)	C _{inh} PY1 (ppm)	C _{inh} TU (ppm)	R _{ct} (Ωcm^2)	C _{dl} ($\mu\text{F}/\text{cm}^2$)	I _{corr} (mA/cm^2)	CR (mm/y)	IE%
303	Blank		13.32	3891	1.95	22.70	-----
	0	50	108.70	144.7	0.2400	2.78	87.74
	50	0	39.66	664.0	0.6578	7.62	66.41
	50	50	108.3	229.4	0.2409	2.79	87.70
	100	0	51.50	527.9	0.5026	5.82	74.43
	100	50	127.0	113.6	0.2054	2.38	89.51
	150	0	55.72	471.3	0.4682	4.64	76.09
	150	50	144.4	179.7	0.1807	2.09	90.77
	200	0	78.63	372.7	0.3317	3.84	84.33
	200	50	174.5	126.1	0.1495	1.73	92.36
308	Blank		12.72	3421	2.051	23.77	-----
	0	50	65.89	498.5	0.3959	4.58	80.69
	50	0	26.77	1786	0.9745	11.29	52.48
	50	50	45.78	236.0	0.5698	6.60	55.47
	100	0	31.36	660.5	0.8440	9.78	58.84
	100	50	73.60	148.6	0.3543	4.10	82.71
	150	0	42.72	341.8	0.6106	7.43	70.22
	150	50	136.8	134.6	0.0907	2.21	90.70
	200	0	58.19	453.5	0.5568	6.54	73.60
	200	50	194.3	425.0	0.0134	1.55	93.45

Table 5.3 Impedance data obtained for PY1, TU, and PY1/TU combinations at 313K and 318K in 1M HCl

Temp (K)	C _{inh} PY1 (ppm)	C _{inh} TU (ppm)	R _{ct} (Ωcm^2)	C _{dl} ($\mu\text{F}/\text{cm}^2$)	I _{corr} (mA/cm^2)	CR (mm/y)	IE%
313	Blank		10.07	2267	2.59	30.02	-----
	0	50	22.56	282.4	1.15	13.40	55.36
	50	0	20.77	640.6	1.25	14.56	51.51
	50	50	28.80	628.5	0.9131	10.05	65.03
	100	0	30.91	660.5	0.8440	7.82	67.42
	100	50	68.78	153.8	0.4396	7.31	85.35
	150	0	38.15	912.0	0.6838	7.92	73.60
	150	50	73.62	148.6	0.3543	4.10	86.32
	200	0	46.28	882.6	0.5637	7.01	78.24
	200	50	115.8	119.8	0.2253	2.61	91.30
318	Blank		9.67	2536	2.697	31.26	----
	0	50	20.19	539.6	1.292	14.98	52.10
	50	0	15.25	968.7	1.711	19.83	36.59
	50	50	23.00	356.3	1.134	13.15	57.95
	100	0	19.89	495.2	1.312	15.20	51.38
	100	50	37.71	268.6	0.6918	8.01	74.35
	150	0	23.12	502.1	1.128	13.08	58.17
	150	50	42.61	148.1	0.6122	7.09	77.30
	200	0	23.20	543.6	1.124	13.03	58.31
	200	50	58.32	194.3	0.4473	5.184	83.41

5.2.2.3 Potentiodynamic polarisation studies

The corrosion current density (i_{corr}) obtained by Tafel extrapolation of the linear portions of polarisation curves at higher overvoltage (>50-70mV to E_{corr}) is a direct measurement of corrosion rate (CR) by the following equation.

$$CR(\text{mpy}) = \frac{0.13I_{\text{corr}}E_{\text{wt}}}{d} \quad (5.1)$$

where mpy is the unit of CR in milli inches per year, E_{wt} is the equivalent weight in gram and d is the density in g/cm^3 of the corroding species [21]. In PDP, the polarisation characteristic of the metal is measured as a current response to the applied potential. The polarisation curves obtained by altering the E_{corr} 250mV anodically and cathodically are given in Fig 5.5. The graph clearly explains that the current density decreased much for the PY1/TU pair compared to PY1 indicating the better corrosion inhibition capacity of it. The IE% calculated using eqn. 2.9 is given in Table 5.4 and Table 5.5. The E_{corr} of PY1 is shifted to a more positive value compared to the blank whereas for the PY1/TU pair the shift is towards more negative values. For PY1 /TU pair the body of the polarisation curve is completely shifted from the PY1 curves. The pronounced change in the cathodic polarisation curve validates the influence of the PY1/TU pair on the cathodic hydrogen evolution than the anodic metal dissolution. This is in accordance with the previous reports on the inhibition property of thiourea indicating how a small quantity of TU affects the inhibition mechanism of PY1 [22-24]. The anodic polarisation curves remain almost parallel shows that metal dissolution is not affected by the addition of TU to PY1[25]. However, both PY1 and PY1/TU pair deviate in E_{corr} by $< 85\text{mV}$ pointing out the mixed behaviour of inhibitor molecules.

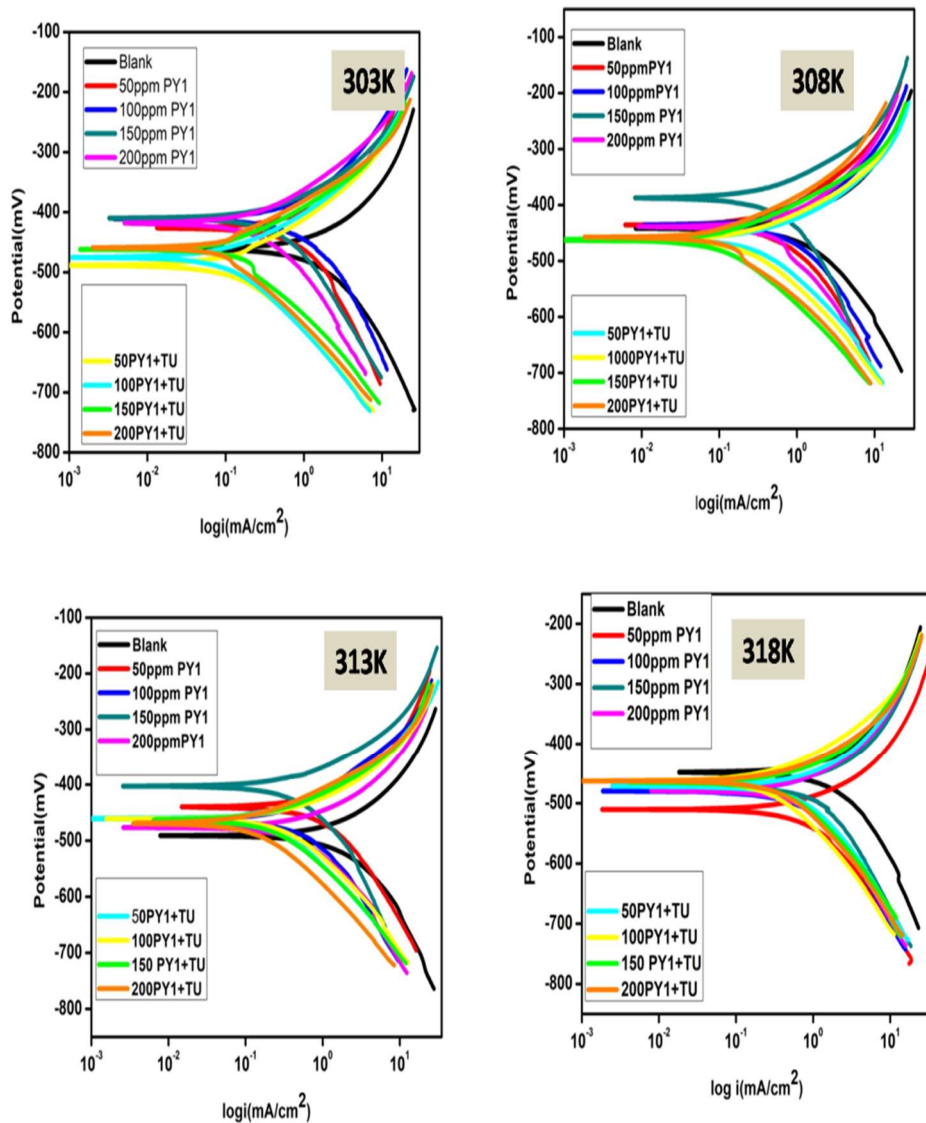


Fig 5.5 The PDP curves for the blank, PY and PY1/TU pair at different temperatures

Table 5.4 The efficiency and the other polarisation parameters obtained from PDP plots of PY1 and PY1/TU pair at 303K and 308K

Temp (K)	C _{inh} ppm	-E _{corr} (mV)	β_a (mV)	$-\beta_c$ (mV)	I _{corr} (mA/cm ²)	CR (mm/y)	IE (%)
303	Blank	462	86	103	0.9687	21.54	----
	50	426	88	138	0.3897	11.70	59.77
	100	412	81	80	0.3440	10.03	64.48
	150	410	75	119	0.3075	10.26	68.25
	200	418	83	112	0.2069	9.764	78.41
	50TU	469	76	111	0.2393	2.773	75.29
	50+50	463	83	99	0.1660	10.14	82.86
	100+50	459	82	137	0.1141	10.93	88.22
	150+50	488	83	99	0.1085	7.424	88.79
	200+50	476	65	93	0.0780	5.591	91.94
308	Blank	443	141	185	1.2274	32.88	
	50	436	73	102	0.6377	13.20	48.03
	100	440	79	141	0.4848	11.42	60.50
	150	437	86	101	0.4119	12.05	66.44
	200	387	67	91	0.3045	12.47	75.19
	50TU	482	90	151	0.3955	20.57	67.77
	50+50	463	83	154	0.2967	14.18	75.58
	100+50	463	76	133	0.2512	13.54	79.53
	150+50	464	81	141	0.1478	13.41	87.95
	200+50	458	74	119	0.1195	6.32	90.26

Table 5.5 The efficiency and the other polarisation parameters obtained from PDP plots of PY1 and PY1/TU pair at 303K and 308K

Temp (K)	C _{inh} ppm	-E _{corr} (mV)	β_a (mV)	$-\beta_c$ (mV)	I _{corr} (mA/cm ²)	CR (mm/y)	IE (%)
313	Blank	491	142	168	1.6697	35.13	-----
	50	439	73	103	0.7476	14.13	55.25
	100	419	60	75	0.6419	11.20	61.55
	150	463	77	81	0.5274	13.84	68.41
	200	405	59	83	0.4185	14.07	74.83
	50TU	481	141	162	0.6569	18.67	60.65
	50+50	464	96	163	0.5291	18.75	68.31
	100+50	461	88	156	0.3002	16.81	82.02
	150+50	462	68	121	0.2703	13.83	83.81
	200+50	467	72	126	0.1383	10.73	91.71
318	Blank	447	135	180	1.8046	32.05	----
	50	472	92	165	0.9729	19.39	46.08
	100	513	96	173	0.9464	24.60	47.55
	150	481	91	129	0.6400	15.76	64.53
	200	479	74	113	0.4899	16.64	72.85
	50TU	481	141	162	0.6569	18.86	63.59
	50+50	473	74	127	0.5405	14.57	70.04
	100+50	463	86	161	0.4888	17.94	72.91
	150+50	468	76	121	0.4000	14.10	77.83
	200+50	465	75	120	0.2545	12.69	88.99

5.2.3 Effect of temperature

With the rise in temperature the inhibition efficiency (%IE) of PY1 decreased considerably to 30.85% at room temperature whereas the decrease in efficiency of the PY1/TU pair is only 9.6% at 318K (Fig 5.6). This indicates that even at moderate temperatures PY1/TU pair acts as an efficient inhibitor. Fig 5.7(a) depicts the R_{ct} values of 200 ppm/50 ppm TU pair at different temperatures. As the temperature increases R_{ct} and %IE decreases. The decrease in %IE could be

explained by changes such as desorption, etching, and fragmentation of the inhibitor molecules[26]. The Bode phase angle plots given in Fig 5.7 (b) shows a single time constant approving the charge transfer controlled dissolution mechanism of metal specimen. The phase angle shift of PY1 from 37.60° is increased to 52.93° for PY1/TU pair explains the improved capacitance behaviour of it. As per the PDP data (Table 5.4 and Table 5.5), the inhibition efficiency is decreased and the corrosion rate is increased with the rise in temperatures which signifies the preferential physisorption mode of adsorption of inhibitor molecules on a metallic surface.

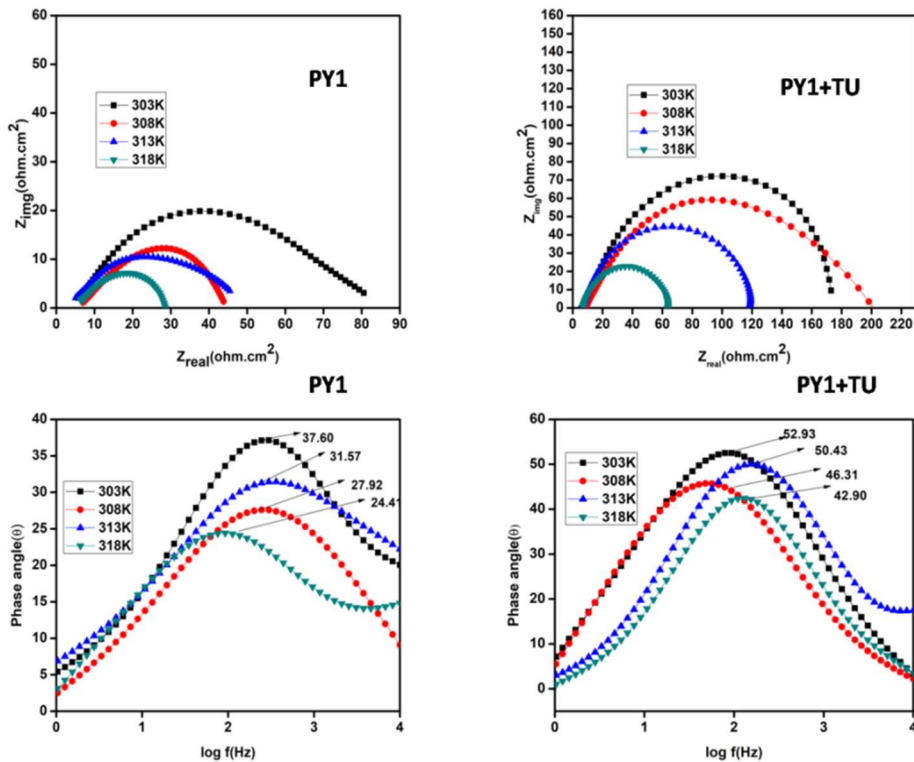


Fig 5.6 The Nyquist and the Bode phase angle plot for 200ppm of PY1 and 200 ppm of PY1/TU pair at different temperatures.

5.2.4 Synergistic interaction of TU and PY1

The existence of the synergism phenomenon between PY1 and TU is evaluated from the synergism parameter calculated using eqn.1.12[27, 28]. The S values are calculated from the data obtained from EIS and PDP are given in Table 5.6. When S is less than one prevails antagonistic interaction which is due to competitive adsorption between the inhibitor molecules, while S greater than one indicates synergistic interaction due to cooperative adsorption of the inhibitor molecules[29]. In this case, the calculated S values are greater than one and specify synergistic interaction of PY1 and TU in mitigating the metallic corrosion.

Table 5.6 Comparison of IE% and synergism parameters obtained at different temperatures

Temp	C _{inh} (ppm)	EIS		S	PDP		
		PY1 (%IE)	PY1/TU (%IE)		PY1 (%IE)	PY1/TU (%IE)	S
303K	50	66.41	87.70	1.76	59.77	82.86	1.52
	100	74.43	89.51	1.81	64.48	88.22	1.59
	150	76.09	90.77	1.81	78.41	88.79	1.62
	200	84.33	92.36	1.87	75.29	91.94	1.67
	50	52.48	55.47	2.42	48.03	75.58	1.46
308K	100	58.84	82.71	1.69	60.50	79.53	1.70
	150	70.22	90.70	1.67	66.44	87.95	1.53
	200	73.60	93.45	1.64	75.14	90.26	1.59
313K	50	51.51	65.03	1.65	55.25	68.31	1.70
	100	67.42	85.35	1.83	61.55	82.02	1.49
	150	73.60	86.30	1.49	68.41	83.81	1.54
	200	78.24	91.30	1.47	74.83	91.71	1.48
318K	50	36.59	57.95	1.53	46.08	70.04	1.57
	100	51.38	74.35	1.39	47.55	72.91	1.53
	150	58.17	77.30	1.43	64.53	77.83	1.65
	200	58.31	83.41	1.33	72.85	88.99	1.53

5.2.5 Adsorption study

To evaluate the strength and nature of adsorption, various isotherms are plotted and the best fitting Langmuir isotherm is drawn taking inhibitor concentration (C_{inh}) in ppm along the X- axis and C_{inh}/θ along the Y- axis as per the equation (1.11) is given in Fig 5.7. The equilibrium constant of adsorption (K_{ads}) is obtained as the reciprocal of the Y- intercept is given in Table 5.7. The maximum value of K_{ads} is obtained for the PY1/TU pair at room temperature implies strong adsorption at this temperature. The free energy of adsorption (ΔG^0) is calculated using the following equation

$$\Delta G_0 = -2.303RT \log(1000K_{ads}) \quad (5.2)$$

where 1000 is the concentration of water in g/dm^3 . The negative values of ΔG^0 assure the spontaneity of the adsorption process. The calculated values are below $-20kJ/mol$ suggests physisorption as the mode of adsorption.

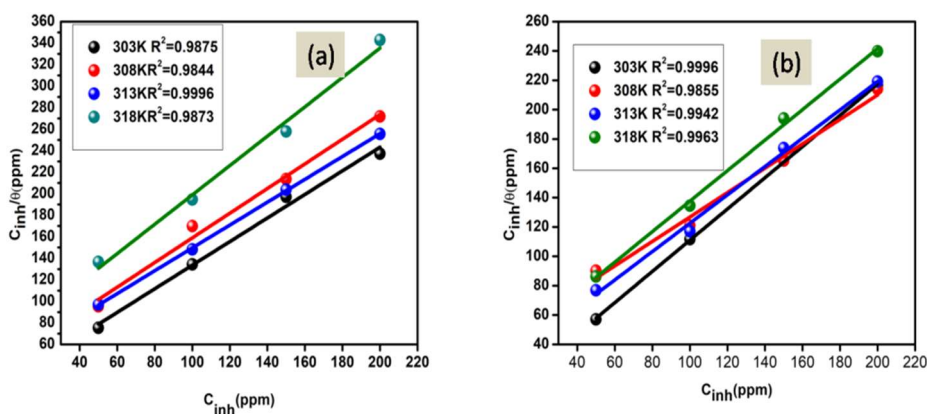


Fig 5.7 Langmuir adsorption isotherms for PY1 and PY1/TU pair at different temperatures

Table 5.7 The thermodynamic parameters obtained from Langmuir adsorption isotherm

Temp	PY1		PY1/TU	
	K_{ads}	$\Delta G_0(\text{kJ/mol})$	K_{ads}	$\Delta G_0(\text{kJ/mol})$
303K	0.0418	-9.40	0.2173	-13.55
308K	0.0225	-7.97	0.0229	-8.02
313K	0.0230	-9.50	0.0385	-9.50
318K	0.0160	-8.96	0.0297	-8.96

5.2.6 Quantum mechanical calculation

The effectiveness of an organic molecule to act as an inhibitor depends on its electronic structure. Therefore quantum chemical calculations remain as a powerful tool for understanding the inhibition mechanism[30]. According to Fukui's frontier molecular orbital theory, the reactivity of a molecule is much related to the energies of HOMO and LUMO. The global parameters for PY1, TU, and PY1/TU are calculated with B3LYP functional with 6-311G (d, p) as the basis set and the values are given in Table 5.8. The low ΔE value of PY1/TU supports better inhibition efficiency for the pair.

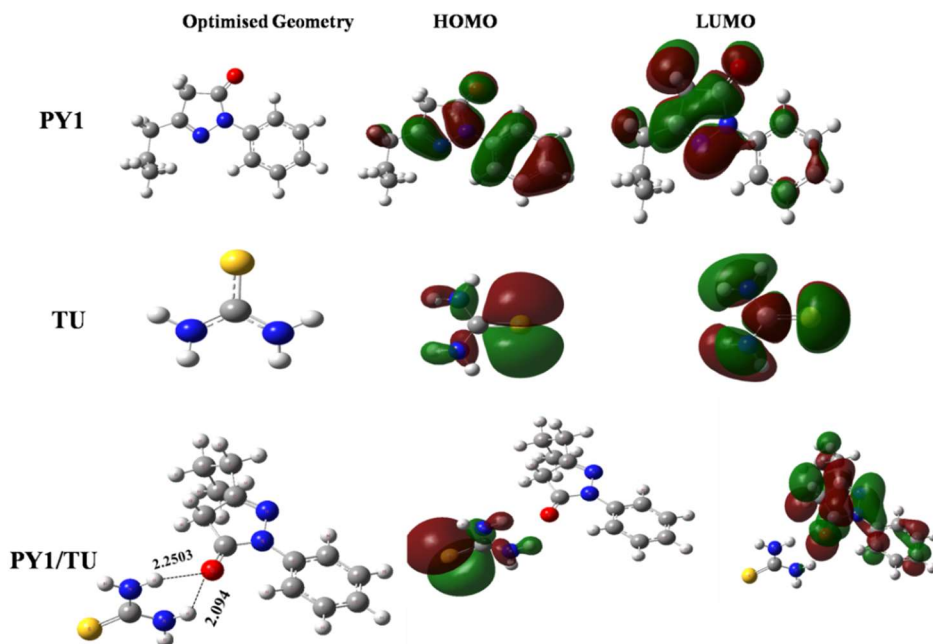


Fig 5.8 The optimised geometries, HOMOs and, LUMOs of PY1, TU, PY1/TU pair

Table 5.8 The global descriptors obtained for PY1, TU, PY1/TU pair by Gaussian calculations

Parameter	PY1	TU	PY1/TU
Total Energy(eV)	-17703	-14920	-32624
E_{HOMO} (eV)	-6.70	- 5.39	-5.91
E_{LUMO} (eV)	-1.21	-0.18	-0.65
ΔE (eV)	5.49	5.39	5.26
Hardness $\eta = \frac{\Delta E}{2}$	2.74	2.69	2.63
Dipolmoment, μ (D)	3.61	5.01	7.98
$IE = -E_{\text{HOMO}}$	6.70	5.39	5.91
$EA = -E_{\text{LUMO}}$	1.21	0.18	0.65
$\chi = \frac{IE + EA}{2}$	3.95	2.78	3.28
$\Delta N = \frac{(\chi_{\text{Fe}} - \chi_{\text{inh}}\chi)}{2(\eta_{\text{Fe}} + \eta_{\text{inh}})}$	0.55	0.76	0.70

5.2.7 Material studio treatment

The mechanism of corrosion inhibition by organic molecules is mainly by the adsorption of inhibitor molecules on the metallic surface. Usually, adsorption is an exothermic reaction. The material studio works on Monte Carlo simulations defines the total energy as the sum of adsorbate components, rigid adsorption, and deformation energy[31]. The interaction energy is defined as the energy released when one mol of adsorbate is adsorbed on the metal surface. It is calculated as

$$E_{int} = E_{total} - (E_{adsorbate} + E_{inhibitor}) \quad (5.3)$$

Binding energy is regarded as the negative of interaction energy. If its value is more positive the binding is stronger and hence the adsorption. The calculated values are given in Table 5.9. Fig 5.8 show the adsorption pattern of PY1 on the Fe (110) plane, in the presence of water molecules and PY1 with thiourea molecules. A flat orientation is seen in all the cases.

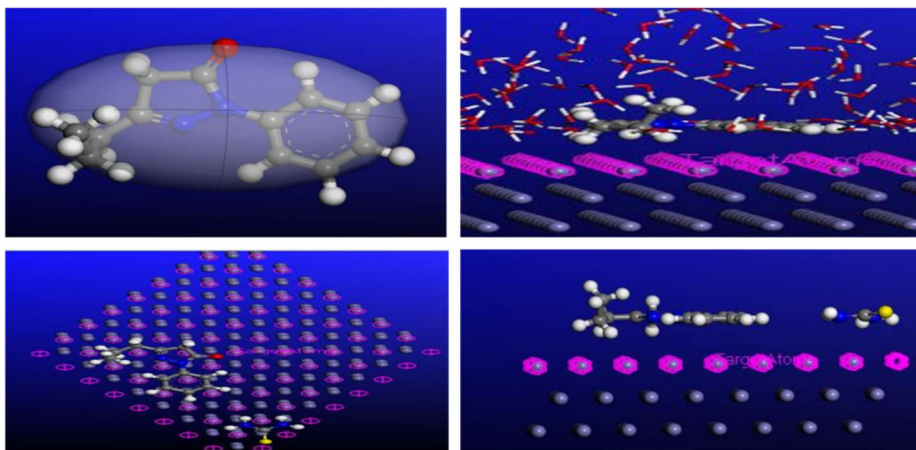


Fig 5.9 Adsorption mode of PY1 on Fe (110) plane

Table 5.9 Energy parameters calculated for PY1/TU pair by material studio calculations

System	E_{Total} (kcal/mol)	E_{ads} (kcal/mol)	E_i (kcal/mol)	E_b (kcal/mol)
PY1+TU	-209.89	-180.81	-238.97	238.97

5.2.7 AFM Analysis

The three dimensional and two dimensional AFM images of the mild steel immersed in 1M HCl containing PY1 and with PY1/TU pair is shown in Fig 5.10. The average roughness (R_a) of the blank is 25.5nm and that of the inhibited one is 18.6nm. The presence of the inhibitor has decreased the surface roughness indicating the inhibition ability of the PY1/TU pair.

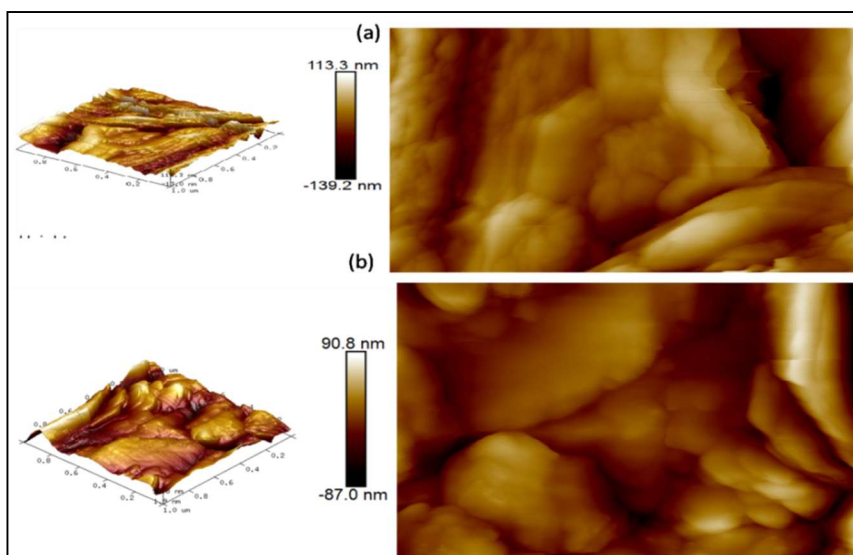


Fig 5.10 AFM images of blank and mild steel dipped in 1M HCl containing (a) PY1 and (b) PY1/TU pair

5.3 Conclusions

- 200 ppm of 3-propyl -1-phenyl-1H-pyrazolyl-5(4H)-one (PY1) gives an inhibition efficiency of 83.4% in 1M HCl at room temperature and 58.31% at 318K.
- The inhibition capacity is enhanced to 92.36% at room temperature and 83.4% at 318K by the addition of 50 ppm of thiourea (TU)
- A synergistic interaction is seen between PY1 and TU and which reduces the corrosion rate through co-adsorption of the molecules.
- The PDP studies show that PY1/TU pair act as a mixed-type inhibitor with a substantial preference for the cathodic reaction.
- With the rise in temperature, the inhibition efficiency decreases and the adsorption studies reveal that the major mode of adsorption is physisorption.
- Though the inhibition efficiency decreases with a rise in temperature the effect of adding TU is more prominent at higher temperatures.
- The theoretical calculations also support the experimental observations giving low ΔE values for the PY1/TU pair compared to PY1 and TU alone.

References

1. Shainy, K., et al., *Synergistic interaction of 2-amino 4-methyl benzothiazole (AMBT) and benzotriazole (BTZ) offers excellent protection to mild steel exposed in acid atmosphere at elevated temperatures: Electrochemical, computational and surface studies*. Egyptian Journal of Petroleum, 2019. **28**(1): p. 35-45.
2. Eduok, U., et al., *Corrosion inhibition and adsorption behaviour of Cocos nucifera L. coir dust for mild steel in 1 M HCl: synergistic effect of iodide ions*. International Journal of Advanced Scientific and Technical Research, 2012. **1**: p. 338-60.
3. Bouhlal, F., et al., *Combination effect of hydro-alcoholic extract of spent coffee grounds (HECG) and potassium Iodide (KI) on the C38 steel corrosion inhibition in 1M HCl medium: Experimental design by response surface methodology*. Chemical Data Collections, 2020. **29**: p. 100499.
4. Umoren, S.A., et al., *A critical review on the recent studies on plant biomaterials as corrosion inhibitors for industrial metals*. Journal of Industrial and Engineering Chemistry, 2019. **76**: p. 91-115.
5. Verma, C., et al., *An overview on plant extracts as environmental sustainable and green corrosion inhibitors for metals and alloys in aggressive corrosive media*. Journal of molecular liquids, 2018. **266**: p. 577-590.
6. Umoren, S.A. and M.M. Solomon, *Synergistic corrosion inhibition effect of metal cations and mixtures of organic compounds: a review*. Journal of environmental chemical engineering, 2017. **5**(1): p. 246-273.
7. Akbarzadeh, S., et al., *A detailed investigation of the chloride-induced corrosion of mild steel in the presence of combined green organic molecules of Primrose flower and zinc cations*. Journal of Molecular Liquids, 2020. **297**: p. 111862.
8. Qian, B., et al., *Synergistic effect of polyaspartic acid and iodide ion on corrosion inhibition of mild steel in H₂SO₄*. Corrosion Science, 2013. **75**: p. 184-192.

9. Musa, A.Y., et al., *Synergistic effect of potassium iodide with phthalazone on the corrosion inhibition of mild steel in 1.0 M HCl*. Corrosion Science, 2011. **53**(11): p. 3672-3677.
10. Han, P., et al., *Synergistic effect of mixing cationic and nonionic surfactants on corrosion inhibition of mild steel in HCl: experimental and theoretical investigations*. Journal of colloid and interface science, 2018. **516**: p. 398-406.
11. Mobin, M., R. Aslam, and J. Aslam, *Synergistic effect of cationic gemini surfactants and butanol on the corrosion inhibition performance of mild steel in acid solution*. Materials Chemistry and Physics, 2019. **223**: p. 623-633.
12. Žerjav, G. and I. Milošev, *Protection of copper against corrosion in simulated urban rain by the combined action of benzotriazole, 2-mercaptobenzimidazole and stearic acid*. Corrosion Science, 2015. **98**: p. 180-191.
13. Ramya, K., R. Mohan, and A. Joseph, *Interaction of benzimidazoles and benzotriazole: its corrosion protection properties on mild steel in hydrochloric acid*. Journal of materials engineering and performance, 2014. **23**(11): p. 4089-4101.
14. Loto, R.T. and O. Tobilola, *Corrosion inhibition properties of the synergistic effect of 4-hydroxy-3-methoxybenzaldehyde and hexadecyltrimethylammoniumbromide on mild steel in dilute acid solutions*. Journal of King Saud University-Engineering Sciences, 2018. **30**(4): p. 384-390.
15. Qiang, Y., et al., *Synergistic effect of tartaric acid with 2, 6-diaminopyridine on the corrosion inhibition of mild steel in 0.5 M HCl*. Scientific reports, 2016. **6**: p. 33305.
16. Bule, S.S., M. Kumbhare, and P. Dighe, *Synthesis and in-vitro biological evaluation of a novel series of 4-(substituted)-5-methyl-2-phenyl-1, 2-dihydro-3H-pyrazol-3-one as antioxidant*. Journal of Chemical, Biological and Physical Sciences (JCBPS), 2013. **3**(3): p. 1996.
17. Prajila, M., A. Thomas, and A. Joseph, *Development of Passive Film and Enhancement of Corrosion Protection of Mild Steel Exposed in Hydrochloric Acid due to the Adsorption of Water Dispersed 4-[(E)-(3, 4-Dihydroxybenzylidene) amino]-6-Methyl-3-Mercapto-1, 2, 4-*

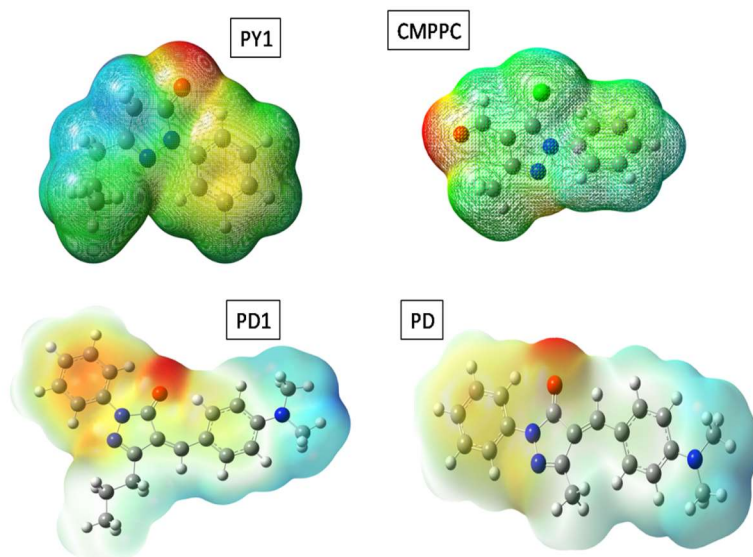
- Triazin-5 (4H)-one (DHMMT)*. Journal of Bio-and Tribo-Corrosion, 2017. **3**(2): p. 16.
18. Anupama, K. and J. Abraham, *Electroanalytical studies on the corrosion inhibition behavior of guava (Psidium guajava) leaves extract on mild steel in hydrochloric acid*. Research on Chemical Intermediates, 2013. **39**(9): p. 4067-4080.
 19. Mahdavian, M. and S. Ashhari, *Corrosion inhibition performance of 2-mercaptobenzimidazole and 2-mercaptobenzoxazole compounds for protection of mild steel in hydrochloric acid solution*. Electrochimica Acta, 2010. **55**(5): p. 1720-1724.
 20. Shainy, K., et al., *Surface interaction and corrosion inhibition of mild steel in hydrochloric acid using pyoverdine, an eco-friendly biomolecule*. Journal of Bio-and Tribo-Corrosion, 2016. **2**(3): p. 20.
 21. Stern, M. and A.L. Geary, *Electrochemical polarization: I. A theoretical analysis of the shape of polarization curves*. Journal of the electrochemical society, 1957. **104**(1): p. 56.
 22. Loto, C., R. Loto, and A. Popoola, *Corrosion inhibition of thiourea and thiadiazole derivatives: a review*. Journal of Materials and Environmental Science, 2012. **3**(5): p. 885-894.
 23. Singh, I., *Inhibition of steel corrosion by thiourea derivatives*. Corrosion, 1993. **49**(6): p. 473-478.
 24. Elshakre, M.E., et al., *On the role of the electronic states of corrosion inhibitors: Quantum chemical-electrochemical correlation study on urea derivatives*. Corrosion Science, 2017. **124**: p. 121-130.
 25. Zhang, W., et al., *Highly effective inhibition of mild steel corrosion in HCl solution by using pyrido [1, 2-a] benzimidazoles*. New Journal of Chemistry, 2019. **43**(1): p. 413-426.
 26. Ammal, P.R., M. Prajila, and A. Joseph, *Effect of substitution and temperature on the corrosion inhibition properties of benzimidazole bearing 1, 3, 4-oxadiazoles for mild steel in sulphuric acid: physicochemical and theoretical studies*. Journal of environmental chemical engineering, 2018. **6**(1): p. 1072-1085.
 27. Umoren, S., Y. Li, and F. Wang, *Synergistic effect of iodide ion and polyacrylic acid on corrosion inhibition of iron in H₂SO₄*

- investigated by electrochemical techniques*. Corrosion Science, 2010. **52**(7): p. 2422-2429.
28. Jeyaprabha, C., S. Sathiyarayanan, and G. Venkatachari, *Co-adsorption effect of polyaniline and halide ions on the corrosion of iron in 0.5 M H₂SO₄ solutions*. Journal of Electroanalytical Chemistry, 2005. **583**(2): p. 232-240.
 29. Larabi, L., et al., *Synergistic influence of poly (4-vinylpyridine) and potassium iodide on inhibition of corrosion of mild steel in 1M HCl*. Journal of Applied Electrochemistry, 2004. **34**(8): p. 833-839.
 30. Ramya, K., R. Mohan, and A. Joseph, *Adsorption and electrochemical studies on the synergistic interaction of alkyl benzimidazoles and ethylene thiourea pair on mild steel in hydrochloric acid*. Journal of the Taiwan Institute of Chemical Engineers, 2014. **45**(6): p. 3021-3032.
 31. Verma, C., et al., *Molecular dynamics and Monte Carlo simulations as powerful tools for study of interfacial adsorption behavior of corrosion inhibitors in aqueous phase: a review*. Journal of Molecular Liquids, 2018. **260**: p. 99-120.

Chapter 6

Protection of Mild steel in H₂SO₄ using CMPPC, PY1, PD and PD1-A comparative study

The inhibition properties of four pyrazole derivatives CMPPC, PD, PD1 and PY1 in 0.5M H₂SO₄ is discussed in this chapter. The effect of temperature and inhibitor concentrations on inhibition capacity is evaluated here. SEM images of mild steel specimens dipped in blank and inhibited solutions are given here.



Contents

6.1. Introduction.....	151
6.2. Results and discussion	151
6.3. Conclusions	170

6.1 Introduction

In the acid pickling and cleaning process of metals, the use of mineral acids such as H_2SO_4 and HCl is very essential. But this environment causes corrosion of metals. Therefore, the use of corrosion inhibitors is inevitable in this process. H_2SO_4 is one of the cheap and readily available acids used in this field. The efficiency of H_2SO_4 highly depends on temperature. The use of H_2SO_4 in the acidification of the oil well is minimum due to the formation of insoluble sulphate sludges [1]. A good number of organic compounds containing lone pairs of electrons act as efficient inhibitors against acidic corrosion [2-4]. This chapter demonstrates the corrosion inhibition property of a few pyrazolone derivatives such as CMPPC, PY1, PD, and PD1 towards mild steel 0.5M H_2SO_4 .

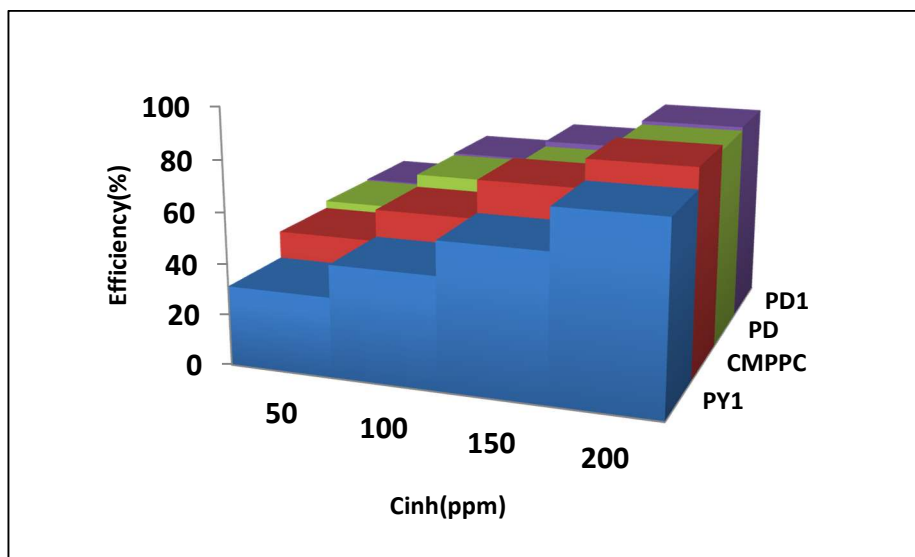
6.2 Result and discussion

6.2.1 Weight loss studies

Weight loss studies of all the four inhibitors are carried out in 0.5M H_2SO_4 for different periods. The result obtained is shown in Table 6.1. The anodic reaction of metal dissolution, the cathodic reaction of hydrogen evolution, and the dissolution of corrosion products lead to weight loss [5]. Fig 6.1 clearly shows that as the concentration of the inhibitor increases the efficiency also increases. The increase in efficiency with an increase in the concentration of the inhibitor is due to the formation of a surface complex utilising the low lying vacant d orbitals of the metal as the acceptor and free electrons of the inhibitor as the donor [6]. The efficiency for 200 ppm of inhibitor follows the order $\text{CMPPC} > \text{PD1} > \text{PD} > \text{PY1}$.

Table 6.1 Weight loss parameters calculated for mild steel in the absence and presence of CMPPC, PY1 PD and PD1 in 0.5M H₂SO₄

Time (h)	C _{inh} (ppm)	CMPPC		PY1		PD		PD1	
		CR (mg cm ⁻² h ⁻¹)	%IE	CR (mg cm ⁻² h ⁻¹)	%IE	CR (mg cm ⁻² h ⁻¹)	%IE	CR (mg cm ⁻² h ⁻¹)	%IE
24	Blank	16.03	----	16.03	-----	11.21	-----	11.21	---
	50	9.250	42.26	10.97	31.49	6.13	45.29	6.08	45.74
	100	7.225	54.92	9.020	44.12	4.48	60.03	4.39	60.80
	150	4.770	70.20	8.950	57.30	3.71	66.85	3.47	69.02
	200	2.973	81.41	4.512	73.26	3.11	79.23	2.16	80.68
48	Blank	7.170	-----	8.63	-----	7.08	----	7.08	---
	50	3.138	56.20	5.45	17.17	6.57	35.30	5.51	45.80
	100	2.591	63.77	3.51	34.87	5.09	49.93	4.93	51.56
	150	1.649	77.00	2.30	57.60	4.53	55.40	4.15	59.14
	200	1.035	85.57	1.32	75.74	4.10	59.66	3.91	61.52

**Fig 6.1** Comparison of inhibition efficiencies of PY1, CMPPC, PD and PD1 by weight loss studies

6.2.2 Electroanalytical studies

6.2.2.1 EIS measurements

Electrochemical impedance measurement (EIS) is a useful tool in analysing the electrode processes. EIS analysis is done after dipping the metallic species in acidic (0.5M H₂SO₄) solution with and without the inhibitor for an hour and after attaining a steady-state potential. The Nyquist plots obtained are depressed semicircles with its centre lying below the real axis[7]. Fig 6.2 and Fig 6.3 gives the Nyquist plot for different compounds with varying inhibitor concentrations. The semi-circular shape for all the compounds indicates that the corrosion in H₂SO₄ is mainly a charge transfer controlled process[8]. Though the R_{ct} (Table 6.2 and Table 6.3) is increased with an increase in the concentration of the inhibitor the shape of the semicircle remains the same and this suggests that the addition of inhibitor does not alter the mechanism of corrosion. The solution resistance R_s (the real axis impedance at high frequencies) is high in 0.5M H₂SO₄ compared to HCl. This could be due to the poor conductivity of the electrolyte compared to the metal or metal surface covered with a film causing high resistance.

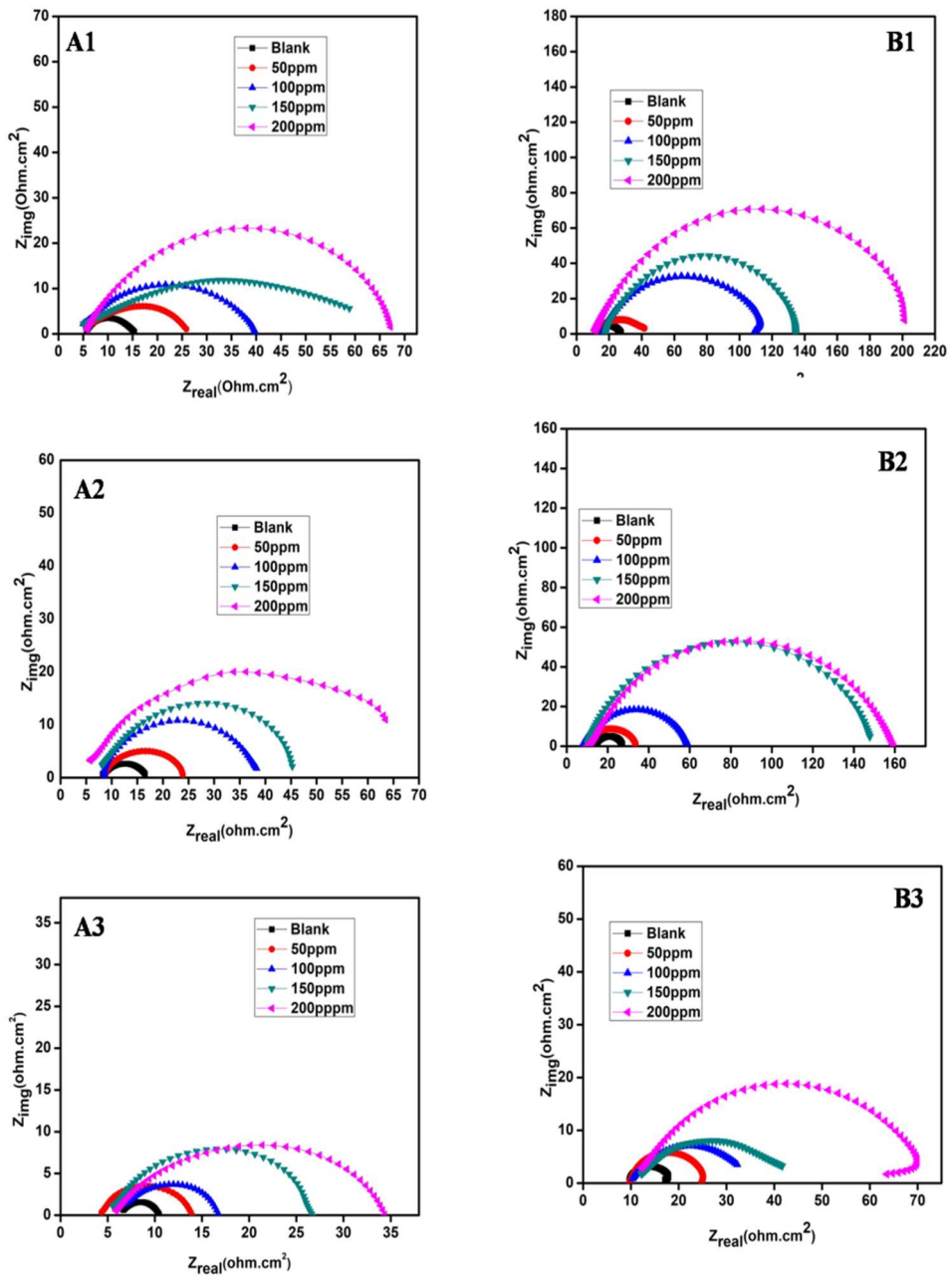


Fig 6.2 Nyquist plots for the inhibition by PY1 and CMPPC in 0.5M H₂SO₄ A1&B1 at 303K, A2&B2 at 308K and A3&B3 at 313K

Table 6.2 EIS parameters for mild steel with and without PY1 and CMPPC in 0.5M H₂SO₄ at different temperatures

Temp (K)	PY1					CMPPC			
	C _{inh} (ppm)	R _{ct} (Ωcm ²)	C _{dl} (μF/cm ²)	I _{corr} (mA/cm ²)	IE%	R _{ct} (Ω.cm ²)	C _{dl} (μF/cm ²)	I _{corr} (mA/cm ²)	IE%
303	Blank	10.21	940.4	2.55	----	14.33	805.9	1.82	----
	50	22.29	644.4	1.17	54.19	33.84	932.1	0.77	57.65
	100	36.39	394.9	0.71	71.94	102.3	217.7	0.25	85.99
	150	64.04	222.0	0.40	84.05	118.9	143.9	0.22	87.94
	200	69.70	215.1	0.37	85.35	199.8	80.10	0.15	92.82
308	Blank	9.21	1293	2.83	----	13.63	354.1	1.91	----
	50	15.87	1103	2.37	41.96	23.48	238.6	1.11	41.95
	100	30.34	590.8	1.19	69.64	45.01	155.6	0.58	69.71
	150	39.49	162.2	0.66	76.67	139.6	84.81	0.19	90.23
	200	62.78	127.2	0.41	85.30	150.3	89.24	0.17	90.93
313	Blank	4.33	2787	6.01	--	8.94	816	2.91	--
	50	9.76	716.8	2.67	55.63	16.01	728.4	1.61	44.15
	100	11.21	479.0	2.37	61.37	25.74	628.2	1.01	65.26
	150	21.78	629.3	1.19	80.11	34.44	571.6	0.75	74.04
	200	28.40	667.4	0.90	85.00	60.41	149.0	0.41	85.20

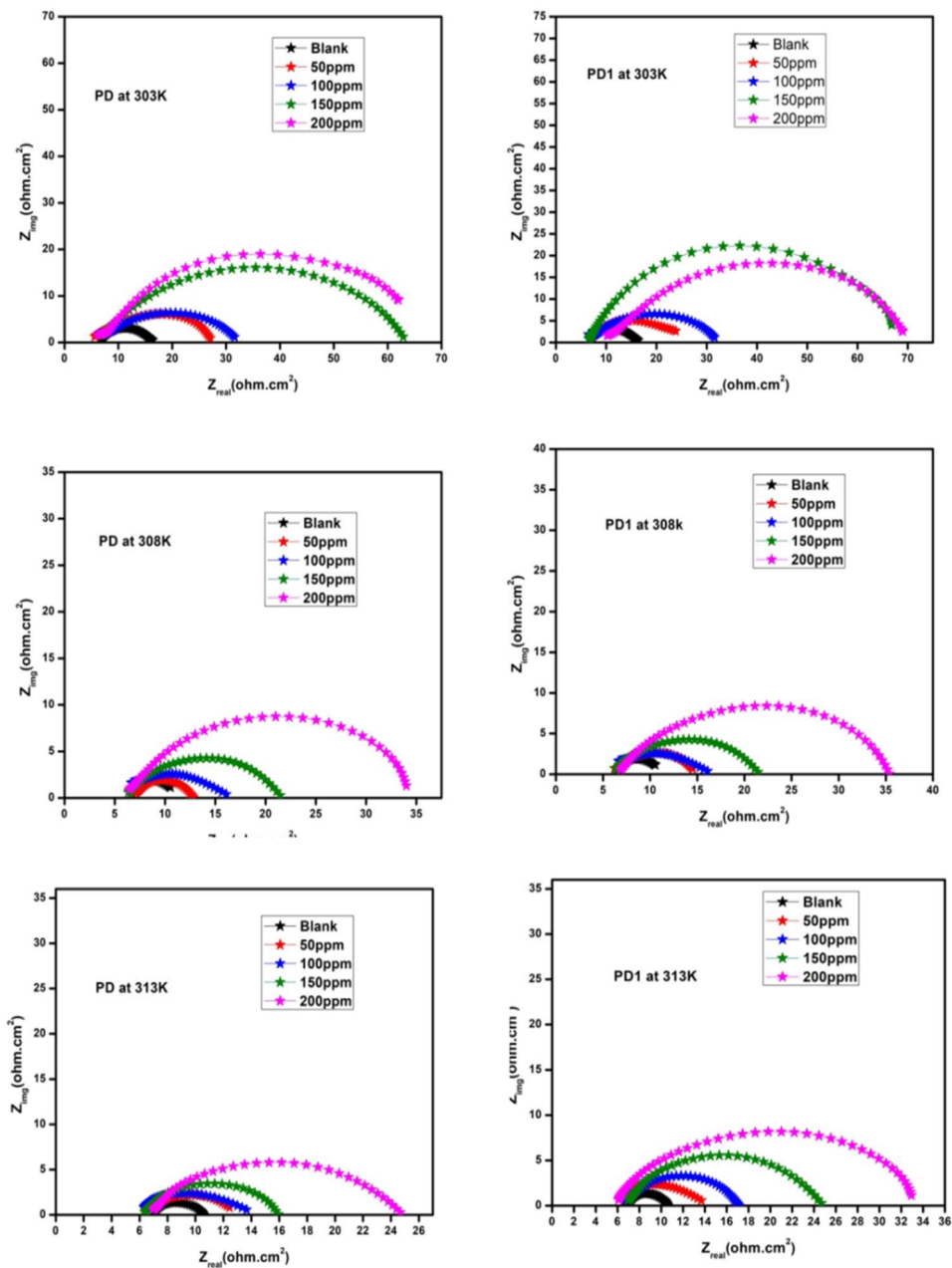


Fig 6.3 Nyquist plots for various concentrations of PD and PD1 in 0.5M H₂SO₄ at 303K, 308K, and 313K

Table 6.3 EIS parameters for the corrosion inhibition mild steel in the absence and presence of PD and PD1 in 0.5M H₂SO₄ at 303K, 308K, and 313K

Temp (K)	C _{inh} (ppm)	PD				PD 1			
		R _{ct} (Ω.cm ²)	C _{dl} (μF/cm ²)	I _{corr} (mA/cm ²)	IE%	R _{ct} (Ω cm ²)	C _{dl} (μF/cm ²)	I _{corr} (mA/cm ²)	IE%
303	Blank	9.28	829	2.538	-----	9.28	829	2.538	-----
	50	23.33	742	1.120	55.93	21.57	764	1.256	52.34
	100	28.47	617	0.916	67.65	27.82	644	0.937	63.04
	150	57.92	417	0.450	82.25	56.25	530	0.452	83.62
	200	63.00	231	0.041	85.38	64.57	401	0.04	85.73
308	Blank	4.475	1049	5.545	-----	4.475	1049	5.545	-----
	50	6.362	966	4.100	28.45	9.751	817	2.832	54.10
	100	11.37	709	2.243	60.64	11.72	674	2.222	61.81
	150	13.07	771	1.996	65.76	18.41	838	1.417	75.69
	200	29.25	529	0.891	84.70	28.88	667	0.903	84.50
313	Blank	3.596	1416	7.254	-----	3.596	1416	7.254	-----
	50	6.735	1011	3.873	46.60	10.68	798	2.443	66.32
	100	8.350	914	3.121	56.93	11.37	476	2.294	68.37
	150	9.760	716	2.673	63.15	15.61	671	1.670	76.96
	200	18.17	853	1.436	80.20	23.28	827	0.922	84.32

6.2.2.2 PDP Analysis

The polarisation analysis gives insight into the action of the inhibitor on the anodic and cathodic events. The polarisation studies of all the four compounds are done by altering the E_{corr} between $\pm 250\text{mV}$ and the polarisation curve obtained are given in Fig 6.4 and Fig 6.5. The important parameters obtained are given in Table 6.4 and Table 6.5. The shift of E_{corr} to a more positive value points out retardation of anodic reaction and to a more negative value indicates retardation of cathodic reaction. Though a regular trend is not observed in this case the E_{corr} value is not shifted more than 85mV indicating a mixed type behaviour of the inhibitors[9]. As the concentration of the inhibitor increases the current density decreases for these compounds. The efficiency calculated using eqn. 2.9 shows that the maximum efficiency is given by CMPPC. The temperature has a negative effect on the protection capacity of the inhibitors suggesting the physisorption mechanism as the major root of adsorption of these inhibitors.

Table 6.4. EIS parameters for the corrosion inhibition mild steel in the absence and presence of PY1 and CMPPC in 0.5M H₂SO₄ at 303K, 308K, and 313K

Temp (K)	PY1				CMPPC			
	-E _{corr} (mV)	CR (mm/y)	I _{corr} (mA/cm ²)	IE%	-E _{corr} (mV)	CR (mm/y)	I _{corr} (mA/cm ²)	IE%
303	476	27.99	1.610		505	20.57	1.2120	-----
	457	13.32	0.848	47.32	504	16.37	0.5152	57.49
	467	12.22	0.617	61.67	461	12.69	0.3488	71.22
	492	9.213	0.336	79.13	455	6.83	0.1722	85.79
	485	8.182	0.286	82.23	454	5.89	0.0901	92.56
308	466	37.41	1.999	-----	499	20.99	1.322	
	458	16.55	0.931	53.42	499	14.95	0.7003	47.62
	466	11.38	0.504	74.78	497	6.73	0.1924	72.52
	467	10.65	0.484	75.78	491	6.70	0.1116	91.58
	476	8.74	0.315	84.24	501	5.93	0.1125	91.49
318	437	40.91	2.017	-----	507	32.27	1.9477	----
	459	40.71	1.118	44.57	500	31.08	1.1343	41.76
	439	12.24	0.649	67.82	496	13.84	0.6352	67.38
	426	10.97	0.487	75.85	492	7.88	0.3232	83.40
	496	9.37	0.314	84.44	470	3.78	0.1875	90.37

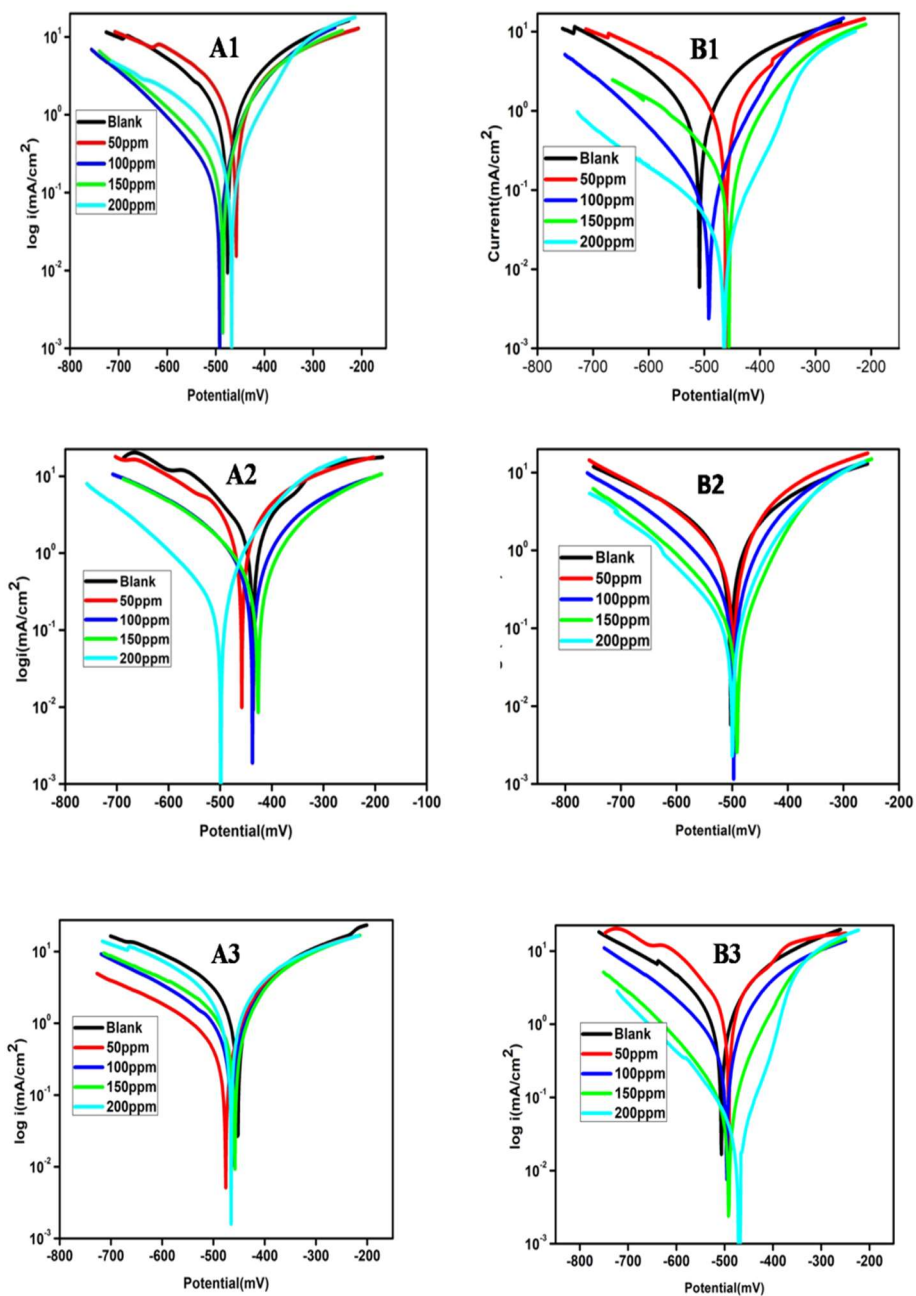


Fig 6.4 The PDP plots for various concentrations of PY1 and CMPPC in 0.5M H_2SO_4 at 303K, 308K and 313K

Table 6.5 Electrochemical parameters from PDP studies for mild steel corrosion inhibition by PD and PD1 in 0.5M H₂SO₄ at 303K, 308K, and 313K

Temp(K)	PD						PD1					
	C _{inh} (ppm)	-E _{corr} (mV)	β _a (mV)	-β _c (mV)	I _{corr} (mA/cm ²)	IE%	-E _{corr} (mV)	β _a (mV)	-β _c (mV)	I _{corr} (mA/cm ²)	IE%	
303	Blank	457	147	193	1.244	----	457	147	193	1.244	----	
	50	478	91	129	0.594	52.25	463	83	115	0.663	46.70	
	100	454	91	136	0.579	53.45	413	60	92	0.408	67.20	
	150	458	98	152	0.432	65.27	444	81	226	0.304	75.56	
	200	440	79	147	0.269	78.37	439	72	126	0.252	79.74	
308	Blank	467	155	180	2.499	----	467	155	180	2.499	----	
	50	445	120	129	1.358	45.65	389	97	100	1.327	46.89	
	100	440	102	164	1.061	57.54	464	84	101	0.795	68.18	
	150	447	100	130	0.943	62.26	420	74	153	0.612	75.51	
	200	434	82	184	0.482	80.71	424	73	161	0.499	80.03	
313	Blank	436	222	235	3.079	-----	436	222	235	3.079	----	
	50	453	123	158	1.532	53.27	461	148	242	1.291	58.07	
	100	454	101	106	1.141	62.94	450	90	142	0.944	69.34	
	150	441	84	116	0.832	72.97	451	76	102	0.881	71.38	
	200	453	75	120	0.732	76.22	451	84	173	0.558	81.87	

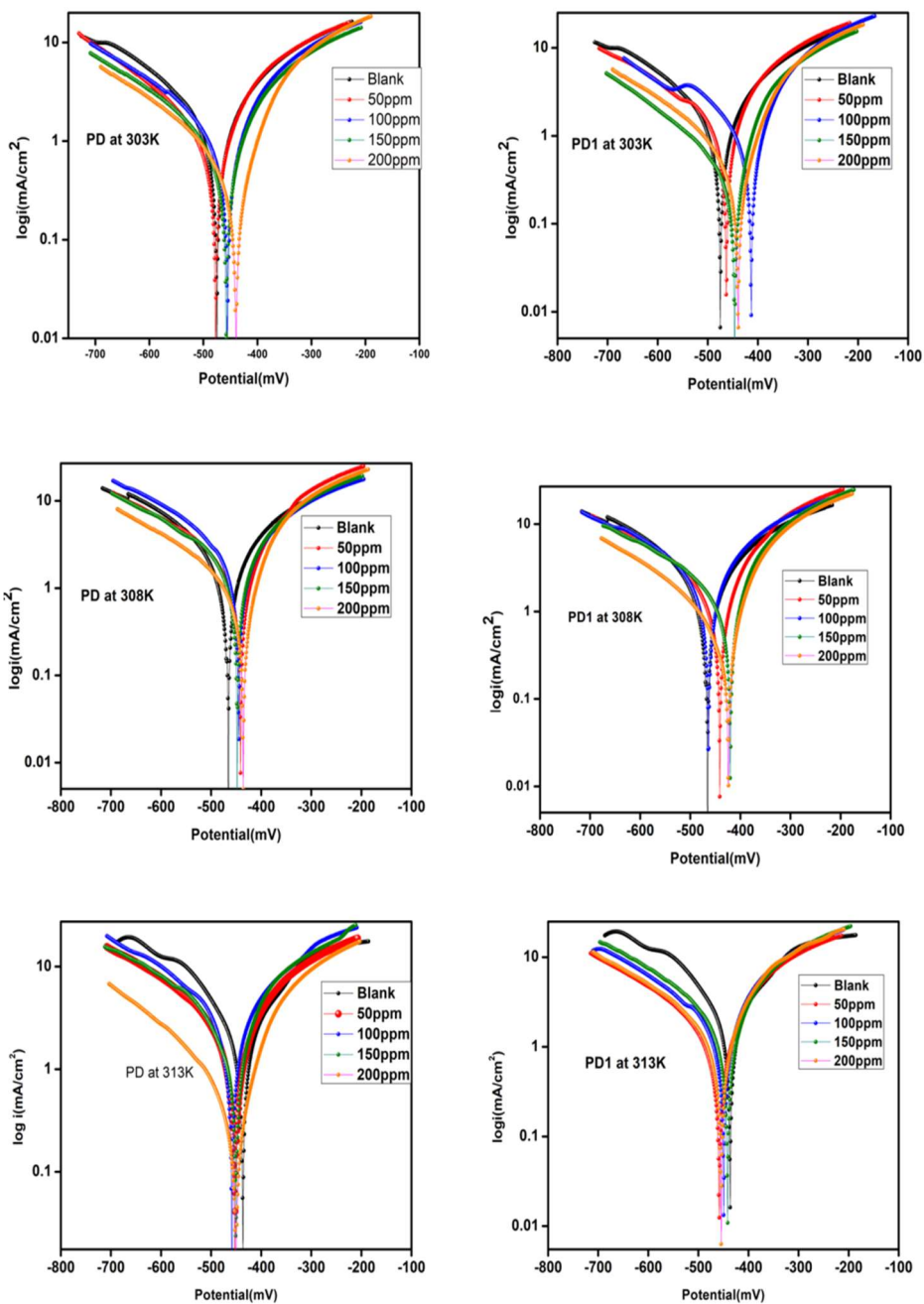


Fig 6.5 The PDP plots for various concentrations of PD and PD1 in 0.5M H₂SO₄ at 303K, 308K, and 313K

6.2.3 Adsorption Studies

Adsorption of organic compounds is believed to be a substitution reaction where water molecules are replaced by organic inhibitor molecules. The adsorption could be by the electrostatic force of interaction between the metal and the inhibitor or by a stronger interaction by sharing the electrons leading to chemisorption. Langmuir adsorption isotherm is found to be the best fitting one and is plotted by taking surface coverage (θ) along the X-axis and C/θ along the Y-axis (Fig 6.6). Here C is the inhibitor concentration in (mM) and θ is %IE/100. The strength of adsorption is measured in terms of the equilibrium constant of adsorption (K_{ads}) obtained as the reciprocal of the Y -intercept of the isotherm is given in Table 6.6. The maximum value is given by CMPPC followed by PD1, PD, and PY1 at room temperature. As the temperature increases, the K_{ads} decrease indicating the prominent desorption of molecules due to an increase in their energy while adsorbing onto the metal surface. The negative values of ΔG_0 assure the spontaneity of adsorption and the calculated values are between -20kJ/mol and -40kJ/mol validating the mixed adsorption process.[10]

Table 6.6 Adsorption parameters for the inhibitors obtained from Langmuir adsorption isotherm

Inhibitor	K_{ads} (M^{-1})			ΔG_{ads}^0 (kJ/mol)		
	303K	308K	313K	303K	308K	313K
PY1	5621	2886	2559	-31.87	-31.19	-30.38
CMPPC	9895	8217	5986	-32.05	-30.42	-25.45
PD	2889	2794	2191	-38.34	-38.34	-37.65
PD1	4979	4792	4673	-36.78	-38.34	-37.65

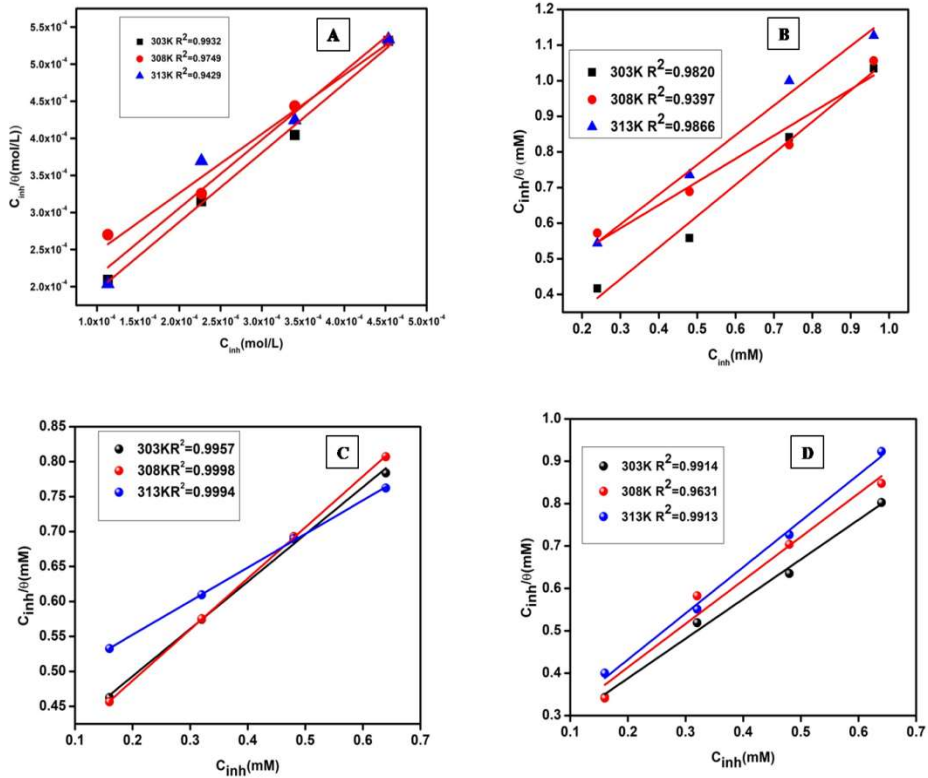


Fig 6.6 Langmuir adsorption isotherms of (A) CMPPC, (B) PY1, (C) PD, and (D) PD1

6.2.4 Effect of temperature on the rate of reaction

While the adsorption studies suggest the spontaneity of corrosion reaction the kinetics throw light into the rate of reaction. Both Arrhenius eqn.2.12 and transition state eqn.2.13 are utilised in calculating the energy of activation (E_a), entropy of activation (ΔS_a), and enthalpy of activation (ΔH_a), and the corresponding plots are given as Fig 6.7 and Fig 6.8. The E_a values of inhibited solutions (Table 6.7) are greater than the uninhibited solutions. The higher E_a value represents the higher energy barrier for the acid molecules to cross to

collide with the metal surface to cause corrosion damage [11]. It is also consistent with the fact that adsorption of inhibitor takes place on the active adsorption sites on the metal surface with the lowest energy. The increase in E_a value also suggests that the preferable mode of adsorption of the inhibitors is physisorption. The positive values of ΔH_a ensure the endothermic nature of metal dissolution. The higher value of ΔH_a in the inhibited solution shows deceleration of metal dissolution in the presence of the inhibitor. The difference between E_a and ΔH_a is almost the same and equals to RT .

$$\Delta H_a = \Delta E_a - RT$$

It is reported that such corrosion reactions involve gas evolution (hydrogen gas) leading to a decrease in total volume [12]. The increase in entropy of activation (ΔS_a) indicates the more disorder in the activated complex formed by the replacement of water molecules by inhibitor molecules [13]. The negative values of ΔS_a shows a more ordered arrangement of inhibitor molecules in the activated complex due to association.

Table 6.7 Kinetic parameters obtained for the inhibitors using Arrhenius and Transition state equations

	C _{inh} (ppm)	CR (mm/y)			Activation parameters		
		303K	308K	313K	E _a (kJ/mol)	ΔH _a (kJ/mol)	ΔS _a (J/mol K)
PY1	Blank	18.21	32.52	69.75	10.58	10.32	119.58
	50	13.56	19.05	30.98	65.07	62.51	171.25
	100	4.86	9.96	26.97	135.00	132.41	204.65
	150	4.77	7.65	13.88	91.68	89.12	161.23
	200	4.33	4.81	10.47	69.32	71.75	179.40
C	Blank	21.10	22.18	33.80	36.99	34.43	-106.5
M	50	8.93	12.88	18.67	58.09	55.53	-43.56
P	100	2.95	6.71	11.75	108.91	106.35	115.29
P	150	2.54	2.16	8.77	96.94	94.38	72.00
C	200	1.51	2.01	4.86	91.74	135.47	203.86
PD	Blank	29.41	64.26	84.08	82.99	80.47	49.34
	50	12.98	47.52	44.89	92.26	95.84	94.40
	100	10.62	26.59	36.17	97.40	94.32	86.69
	150	5.22	23.13	30.98	103.0	138.3	226.90
	200	4.79	10.47	16.64	86.43	95.75	84.40
PD1	50	14.66	32.82	28.31	98.42	49.73	-57.30
	100	10.87	25.75	26.43	96.88	67.84	-17.01
	150	5.24	16.42	19.36	140.91	100.89	-103.01
	200	4.68	10.23	10.69	98.31	62.87	-23.70

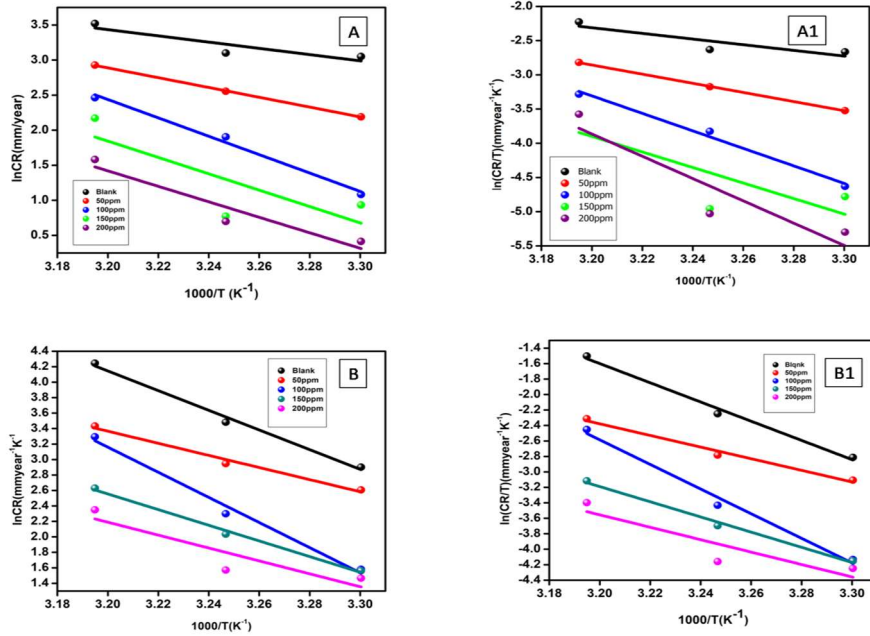


Fig 6.7 Arrhenius and transition state plots of (a) and (a1) CMPPC (b) and (b1) PY1

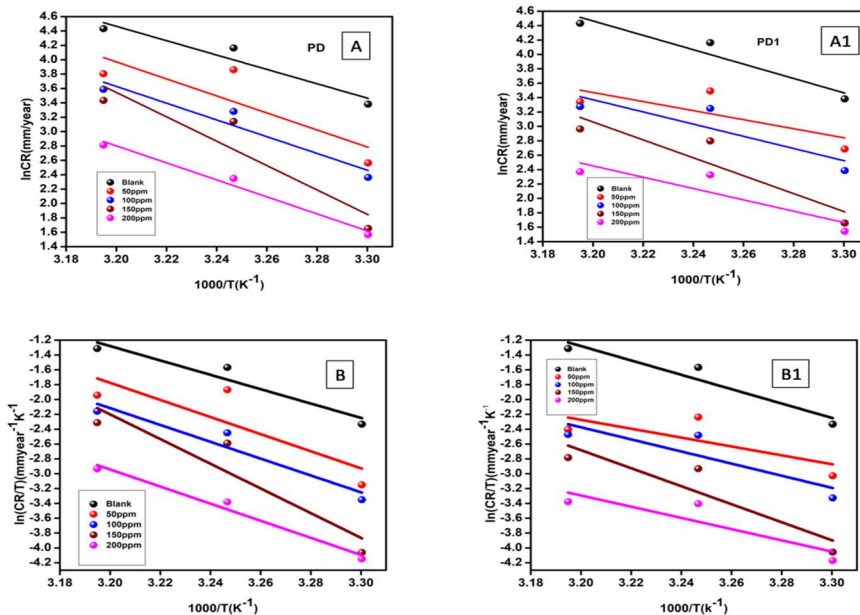


Fig 6.8 Arrhenius and transition state plots of (a) and (a1) PD (b) and (b1) PD1

6.2.5 Surface Analysis

Surface analysis of the polished metal, blank and the inhibited solutions are done with the help of SEM. The perusal of Fig 6.9 clearly shows that the surface is damaged by the acid molecules. But the presence of the inhibitor is seen on the metal surface indicating the adsorption of the inhibitor molecules.

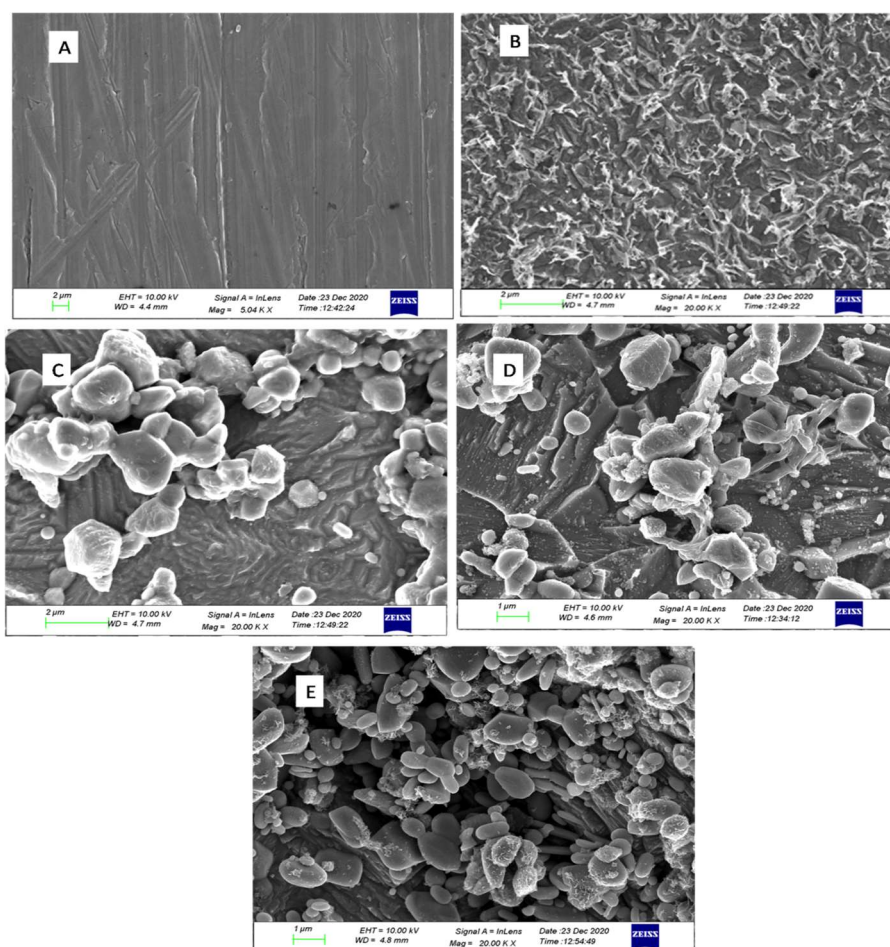


Fig 6.9 SEM images of (A) polished metal surface (B) mild steel dipped 0.5M H₂SO₄ (C) in the presence of CMPPC (D) PD and (E) PY1

6.2.6 Mechanism of inhibition

The inhibition mechanism of organic compound is primarily by adsorption on the metal surface which is free of the oxide film in the acidic solution. The inhibitors which are adsorbed on the metal surface can control the corrosion reaction in several ways. Therefore, it is difficult to assign a particular mechanism for corrosion inhibition by organic molecules. Action of one particular inhibitor can vary with the nature of the metal, the concentration of the inhibitor, the pH of the medium, the nature of the anions in the electrolyte, the secondary products formed, etc. The efficiency of inhibitors with the same functional group will be different depending on the structure of the molecule, the other groups attached, and the length of the hydrocarbon chain[14]. Therefore, comparison of inhibition efficiency has less relevance in this context because they have different functional groups though they all are pyrazolone derivatives. The study shows that they all behave as mixed-type inhibitors against mild steel corrosion and the rise in temperature decrease the efficiency of the systems. The maximum efficiency is given by CMPPC, an aldehyde. Aldehydes are found to be very effective corrosion inhibitors in acidic solutions[14, 15]. PD and PD1 differ only in their alkyl side chain. The results show that the increase in alkyl chain length enhances the protection efficiency. PY1 is the precursor of PD1 is also found to be an efficient inhibitor in mitigating acidic corrosion of mild steel. The ESP map of the inhibitors is given in Fig 6.10. The maximum electron density is seen on the oxygen and the aromatic ring attached to the pyrazole ring.

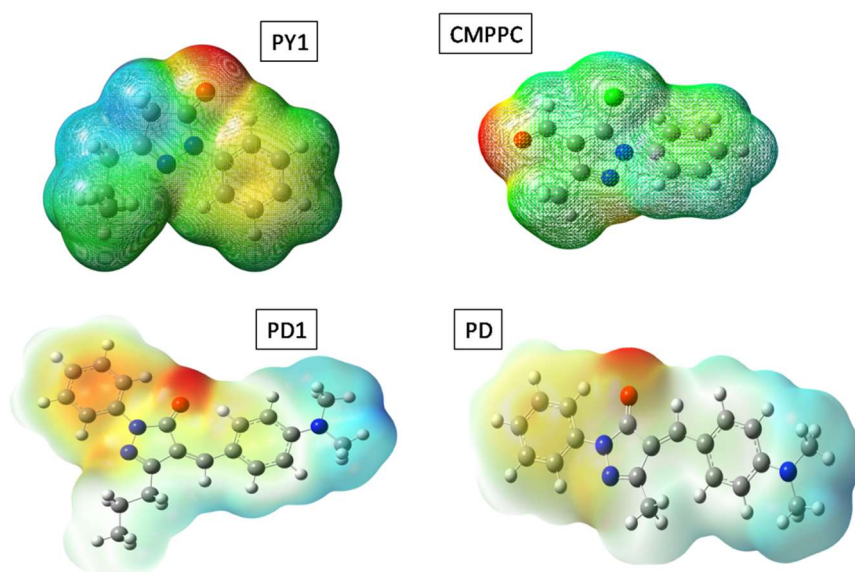


Fig 6.10 ESP map of the inhibitors

6.3 Conclusions

- The corrosion inhibition efficiency of CMPPC, PY1, PD, and PD1 towards mild steel is studied by electrochemical and non-electrochemical methods in 0.5 M H₂SO₄
- These inhibitors are found to have a mixed type behaviour and the process is a charge transfer controlled one.
- They obey the Langmuir adsorption isotherm pattern and the adsorption involves both physisorption and chemisorption.
- The order of efficiency is found to be CMPPC>PD1>PD>PY1.

References

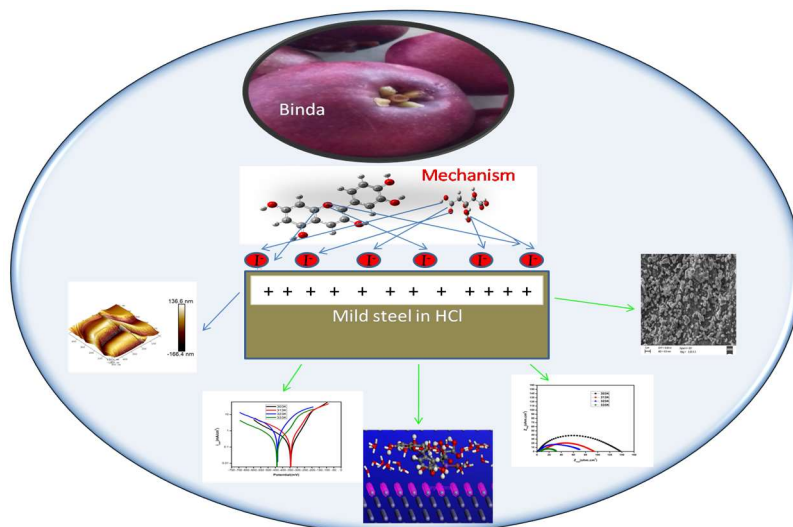
1. Umoren, S.A., et al., *A critical review on the recent studies on plant biomaterials as corrosion inhibitors for industrial metals*. Journal of Industrial and Engineering Chemistry, 2019. **76**: p. 91-115.
2. Hmamou, D.B., et al., *Investigation of corrosion inhibition of carbon steel in 0.5 M H₂SO₄ by new bipyrazole derivative using experimental and theoretical approaches*. Journal of environmental chemical engineering, 2015. **3**(3): p. 2031-2041.
3. Hasanov, R., et al., *Experimental and theoretical calculations on corrosion inhibition of steel in 1 M H₂SO₄ by crown type polyethers*. Corrosion science, 2010. **52**(3): p. 984-990.
4. Ammal, P.R., M. Prajila, and A. Joseph, *Effect of substitution and temperature on the corrosion inhibition properties of benzimidazole bearing 1, 3, 4-oxadiazoles for mild steel in sulphuric acid: physicochemical and theoretical studies*. Journal of environmental chemical engineering, 2018. **6**(1): p. 1072-1085.
5. Ammal P, R., et al., *Protection of mild steel in hydrochloric acid using methyl benzimidazole substituted 1, 3, 4-oxadiazole: computational, electroanalytical, thermodynamic and kinetic studies*. Journal of Adhesion Science and Technology, 2019. **33**(20): p. 2227-2249.
6. Prajila, M. and A. Joseph, *Inhibition of mild steel corrosion in hydrochloric using three different 1, 2, 4-triazole Schiff's bases: a comparative study of electrochemical, theoretical and spectroscopic results*. Journal of Molecular Liquids, 2017. **241**: p. 1-8.
7. John, S. and A. Joseph, *Effective inhibition of mild steel corrosion in 1 M hydrochloric acid using substituted triazines: an experimental and theoretical study*. RSC advances, 2012. **2**(26): p. 9944-9951.
8. Aslam, R., et al., *Sugar based N, N'-didodecyl-N, N' digluconamide ethylenediamine gemini surfactant as corrosion inhibitor for mild steel in 3.5% NaCl solution-effect of synergistic KI additive*. Scientific reports, 2018. **8**(1): p. 1-20.
9. Joseph, A. and R. Mohan, *Electroanalytical and computational studies on the corrosion inhibition behavior of ethyl (2-methylbenzimidazolyl) acetate (EMBA) on mild steel in hydrochloric*

- acid*. Research on Chemical Intermediates, 2015. **41**(7): p. 4795-4823.
10. Shainy, K., et al., *Surface interaction and corrosion inhibition of mild steel in hydrochloric acid using pyoverdine, an eco-friendly biomolecule*. Journal of Bio-and Tribo-Corrosion, 2016. **2**(3): p. 20.
 11. Ammal, P.R., M. Prajila, and A. Joseph, *Physicochemical studies on the inhibitive properties of a 1, 2, 4-triazole Schiff's base, HMATD, on the corrosion of mild steel in hydrochloric acid*. Egyptian Journal of Petroleum, 2018. **27**(3): p. 307-317.
 12. Hegazy, M., et al., *Corrosion inhibition performance of a novel cationic surfactant for protection of carbon steel pipeline in acidic media*. Int. J. Electrochem. Sci, 2018. **13**: p. 6824-6842.
 13. Thomas, A., P.R. Ammal, and A. Joseph, *A comprehensive study of mild steel corrosion in the aggressive acidic environment using CMPPC, a substituted pyrazole derivative*. Chemical Papers, 2020: p. 1-13.
 14. Nathan, C.C., *Corrosion inhibitors*. C. C. Nathan, Editor, published 1973 by NACE, 260, 1973.
 15. Hugel, G. *Corrosion Inhibitors—Study of their Activity Mechanism*. in *1st European Symposium on Corrosion Inhibitors*. Ferrara, Italy: University of Ferrara. 1960.

Chapter 7

Corrosion Inhibition of mild steel in HCl using fruit rind extract of *Garcinia Indica* (Binda)

The characterisation of cyanidin anthocyanins is carried out by UV-Visible spectroscopy. The inhibition capacities of 1% to 4% aqueous extract in different concentrations of HCl and at different temperatures are included in this chapter. The influence iodide on the inhibition capacities of GIW are also discussed in this chapter



Contents

7.1. Introduction.....	173
7.2. Results and discussion	173
7.3. Conclusions	211

7.1 Introduction

In recent years the use of natural products as corrosion inhibitors is more promising in green chemistry perspective due to availability, biodegradability, pollution free and renewable nature [1-5]. Studies show that the corrosion inhibition efficacy of natural products is enhanced by the synergistic interaction between constituent molecules. Various parts of the plants such as flowers, leaves, fruits, etc are proved to be efficient and eco-friendly corrosion inhibitors [6-10]. *Garcinia Indica* is a tropical indigenous tree found in the Western Ghats. The fruit is known by various names such as Binda, Kokkum, Panarpuli, Kattambi etc and in English language it is named as wild mangosteen or red mango. It is a fruit of nutritional value as well as antiglycation, anti-inflammatory, anticancer, antiulcer and antioxidant properties [11-13]. The fruit rind which is having deep purple colour is used as a culinary item and as a natural dye and food colouring agent. The present chapter discusses the corrosion inhibition property of aqueous extract of fruit rind of *Garcinia Indica* (GIW), and the effect of KI on the inhibition capacity of the fruit rind extract. The 10% stock solution is diluted to get 1% to 4% acidic solutions of GIW. Pure KI is purchased from Fischer Scientific.

7.2 Results and Discussion

7.2.1 Chemical composition of the extract

The chief constituents of the fruit rind extract are garcinol, a polyisoprenylated benzophenone a yellow pigment, o-hydroxy citric acid, its lactone, and 2 anthocyanins, as cyanidin-3-sambubioside and cyanidin-3-glucoside (Fig 7.1)[12]. The difference in the structure of cyanidin glucoside and cyanidin sambubioside lies in the carbohydrate

unit which is glucose in cyanidin glucoside and, in sambubioside, a disaccharide of glucose [12]. In addition to these, the fruit rind extract contains smaller quantities of malic acid and tartaric acid. The approximate composition of the fruit rind is given in Table 7.1[14]. The aqueous extract of the fruit mainly contains anthocyanins and hydroxy citric acid. The UV spectrum of the GIW extract (Fig 7.2a) shows a broad peak around 500nm -520nm which is the characteristic peak for cyanidin anthocyanins at low pH[15, 16] where it remains as oxonium ion (Fig 7.2c inset). The UV spectrum of the Fe ions in the presence and absence of the GIW extract shows a decrease in intensity of the peak around 320nm (Fig 7.2b) due to the formation of a protective barrier of the constituent anthocyanins on the iron surface[17]. Fig.7.2c is the complete spectrum of mild steel specimens in 1M HCl containing 4% GIW extract. The peak at 226nm corresponds to π - π^* transitions and peak at 273nm is due to n- π^* absorption. The KBr -IR spectrum of the dried GIW is given in Fig7.2d. Presence of OH group (3440cm^{-1}), C-H stretching (2935cm^{-1}), C=O (1730cm^{-1}), aromatic rings (1613cm^{-1} and 1419cm^{-1}), C-O (1211cm^{-1}), C-O-C stretching (1082cm^{-1}) indicates the presence of cyanidins and hydroxy citric acid.

Table 7.1 An approximate composition of Garcinia Indica Fruit Rind

Sl.No.	Chemical constituent	%
1	Protein	1.92
2	Crude fibre	14.28
3	Total ash	2.57
4	Tannins	2.85
5	Pectin	5.71
6	Starch	1
7	Crude fat	10.0
8	Pigment	2.4
9	Ascorbic acid	0.64
10	Hydroxy citric acid	22.80

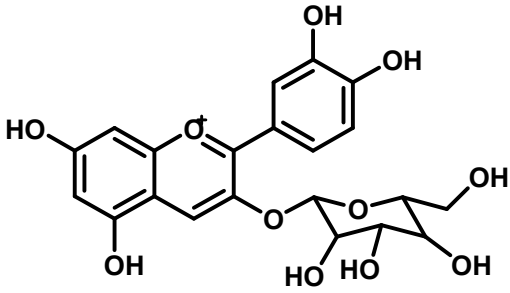
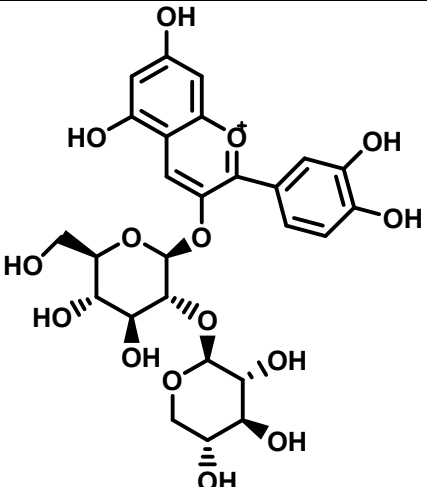
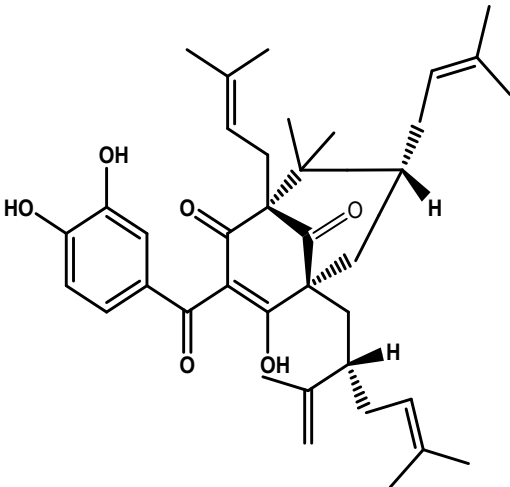
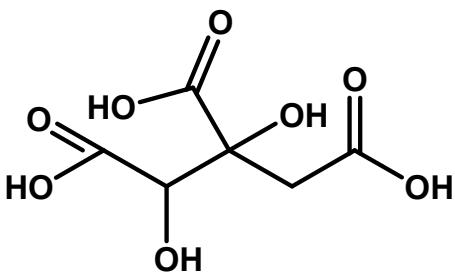
Cyanidin3-glucoside	Cyanidin 3-sambubioside
 <p>The structure shows a cyanidin aglycone core consisting of two phenolic rings connected by a double bond. The left ring has hydroxyl groups at the 3, 4, and 5 positions. The right ring has hydroxyl groups at the 2 and 3 positions. A glucose molecule is attached to the 3-position of the right ring via an oxygen atom.</p>	 <p>The structure shows a cyanidin aglycone core similar to cyanidin 3-glucoside. However, the glucose molecule at the 3-position is linked to a second glucose molecule at its 6-position, forming a disaccharide (sambubioside) moiety.</p>
Garcinol	O-Hydroxy Citric Acid
 <p>The structure is a complex polycyclic molecule. It features a central ring system with multiple methyl groups, a hydroxyl group, and several prenyl side chains. One side chain is a 3,4-dihydroxyphenyl group.</p>	 <p>The structure is a linear molecule consisting of a central carbon atom bonded to a hydroxyl group and three carboxymethyl groups. One of the carboxyl groups is further substituted with a hydroxyl group, making it a hydroxycarboxylic acid.</p>

Fig 7.1 Structures of chief constituents of GIW extract

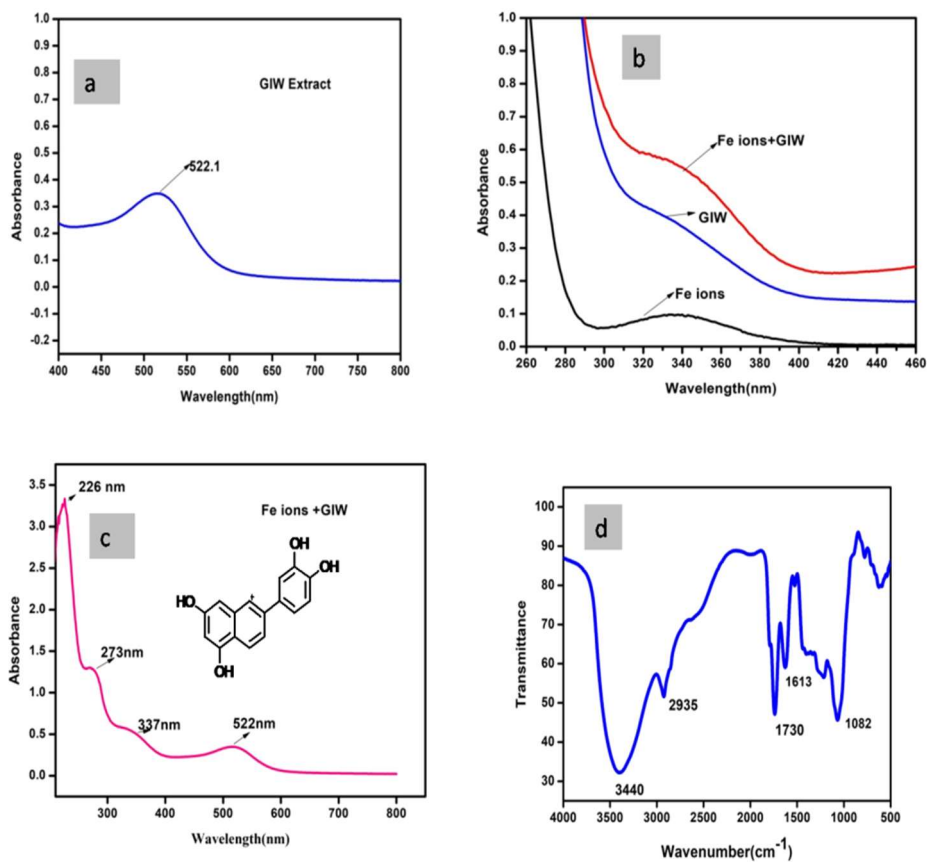


Fig7.2. UV-visible and IR spectra of GIW extract

7.2.2 Corrosion studies

7.2.2.1 Gravimetric Studies

7.2.2.1.1 Effect of immersion time

The result of the gravimetric analysis is given in Table 7.2. The pH of the solution is measured before and after adding the extract and found that the pH is almost unaltered by the addition of the inhibitor. The evaluation of the result shows that as volume percentage of the inhibitor increases the rate of corrosion decreases and inhibition

efficiency increases. This could be explained as blocking of active sites of corrosion on the metallic surface by the major chemical constituent of GIW extract through adsorption. Even after dipping for 96h, the inhibition capacity of 4% GIW extract remained 93.94% assuring the effectiveness of the extract in corrosion mitigation. Generally, a small decrease in efficiency and corrosion rate with the increase in immersion time is attributed to processes such as metal dissolution and slow desorption of a few adsorbed inhibitor molecules from the metal surface. A plot of inhibition efficiency versus GIW concentration (Fig7.3.) shows that the maximum efficiency is given by a volume of 4%.

Table 7.2 weight loss parameters for mild steel in 1M HCl containing GIW extract

Time	24h		48h		72 h		96h		
	C_{inh} (v/V%)	CR (mg/ cm ² .h)	%IE	CR (mg/ cm ² .h)	%IE	CR (mg/ cm ² .h)	%IE	CR (mg/ cm ² .h)	%IE
Blank	16.16	----	9.82	---	9.3402	-----	6.669	-----	
1	0.8194	94.98	0.6521	93.36	0.5671	93.22	0.4571	93.14	
2	0.5347	96.69	0.5214	94.69	0.5054	94.5	0.4253	93.60	
3	0.430	97.33	0.4913	94.99	0.4205	94.77	0.4050	93.92	
4	0.4050	97.28	0.3472	96.46	0.4012	95.6	0.3980	93.94	

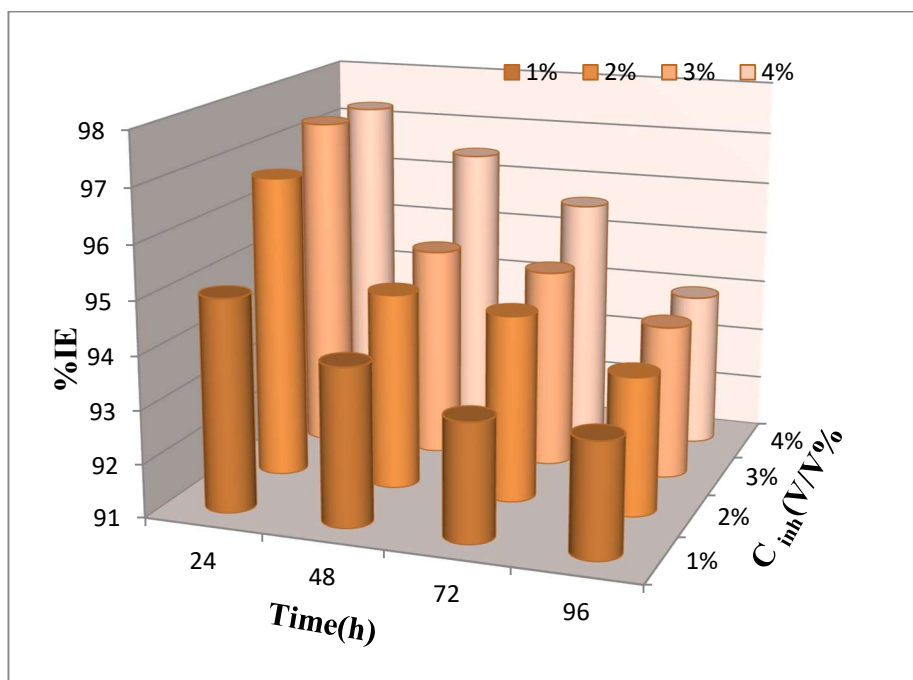


Fig 7.3. Effect of time on the inhibition efficiencies of GIW extract by weight loss method

7.2.2.2 Analysis of EIS data

Electrochemical impedance spectra measure the impedance offered by the electrochemical system which has elements like resistance, capacitance etc. The electrical equivalent circuit for explaining the electrochemical behaviour of a metal in acidic solution is Randles circuit (Fig1.10). The output of EIS analysis is the Nyquist plot where the real part of the impedance is taken along the X-axis and imaginary part along the Y-axis. Charge transfer resistance is obtained as the difference between real axis impedance at the start and finish frequencies. From the values of the charge transfer resistance of the inhibited (R_{ct}^*) and the blank solution (R_{ct}), the efficiency (IE%) is

calculated using the eqn.2.8. At the metal solution interface, the ions from the metal, acid and the inhibitor create an ionic layer with properties of an electrical double layer which cause a barrier to the current flow measured as double-layer capacitance (C_{dl}) which is calculated by eqn. 2.7. The addition of inhibitors increases the thickness of the double layer and thereby reducing the current flow which is necessary for corrosion and thus facilitates the corrosion inhibition[18].

Table 7.3 EIS data obtained for 0.5M and 1.5M HCl in the absence and presence of GIW extract at room temperature

Acid Conc. (mol/L)	0.5			1.5		
C_{inh} (v/V%)	R_{ct} ($\Omega.cm^2$)	C_{dl} ($\mu F/cm^2$)	%IE	R_{ct} ($\Omega.cm^2$)	C_{dl} ($\mu F/cm^2$)	%IE
Blank	22.06	2425	----	14.39		----
1	100.5	754.9	78.04	37.64	506.8	61.76
2	136.8	741.4	83.87	49.04	492.5	70.65
3	176.7	456.6	87.45	53.48	481.0	73.09
4	323.8	188.2	93.18	56.24	478.1	74.41

7.2.2.2.1 Effect of Acid concentration

The R_{ct} and C_{dl} values obtained for 0.5M, 1M, 1.5M HCl for various GIW concentrations are given in Table7.3 and Table7.4. The corresponding Nyquist plots are given in Fig7.4 and Fig7.5. All the Nyquist plot has a single capacitive loop and the radius of the capacitive loops decreases with an increase in concentration of acid for blanks and inhibited solutions containing various GIW concentrations.

The R_{ct} of 4% solution in 0.5M HCl is 323.8, which is reduced to 56.24 in 1.5M HCl. It is proved that with the increase in the concentration of the acid the energy barrier for corrosion decreases and the formation of the activated complex becomes easy leading to higher corrosion rate[19]. The imperfectness of the semicircles is due to frequency dispersion.

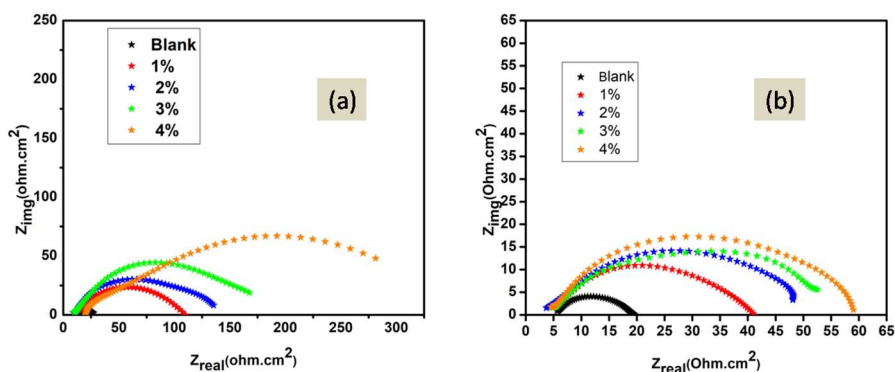


Fig 7.4 Nyquist plots of various concentrations of GIW extract in 0.5M and 1.5M HCl

7.2.2.2.2 Effect of GIW concentration

Nyquist plots of Fig7.5 gives the charge transfer resistance offered in the presence of GIW extract at 303, 308 and 313 K in 1M HCl. As the volume percentage of GIW increases the impedance also increases at all temperatures. This is due to the increase in the thickness of the electrical double layer on the metal electrolyte interface due to the adsorption of a large number of constituent molecules of the fruit rind causing difficulty to mass and charge transfer process which is essential for corrosion. Charge transfer resistance (ohmcm^2), double layer capacitance ($\mu\text{F}/\text{cm}^2$), corrosion current density (mA/cm^2) and corrosion rate (mm/y) obtained from the EIS measurements are given

in Table 7.4. The perusal of this table shows that as the R_{ct} increases C_{dl} decreases at all temperatures. As the concentration of the inhibitor increases the value R_{ct} increases from blank (15.18 to 120.7) to the inhibited 4% solution due to adsorption of the inhibitor molecules on the metal surface. The decrease in the double layer capacitance from 1046 to 177 from the blank to the inhibited solution is due to the increase in the thickness of the double layer.

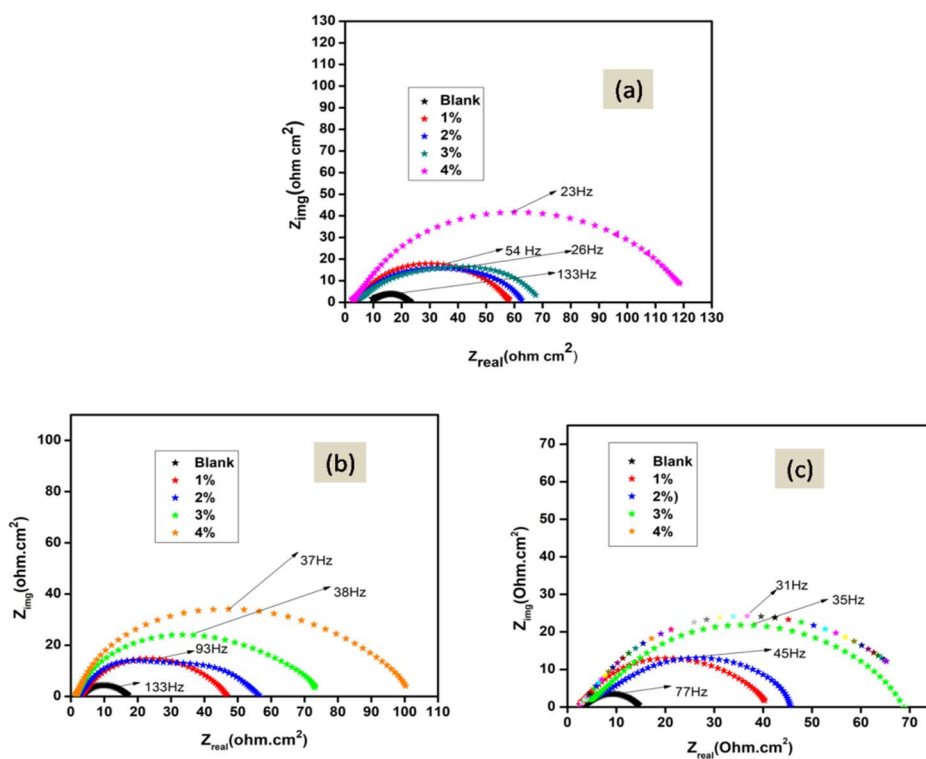


Fig 7.5 Nyquist plots for various concentrations of GIW extract at (a) 303K, (b) 308K, (c) 313K

7.2.2.2.3 Effect of temperature

To understand the effect of temperature EIS studies of 4% GIW extract are done from 303K to 333K and is given in Fig7.6. The diameter of the Nyquist plot is minimum at 333K and maximum at room temperature (303K). For a 4% solution at room temperature the R_{ct} is 120.7 where as it decreases to 34.19 at 333K. This indicates that with an increase in temperature the impedance decreases and the rate of corrosion increases. This is because with a rise in temperature the rate of desorption of inhibitor molecules increases [20]. The values given in Table 7.4 show that even at moderate temperature GIW acts as an efficient inhibitor.

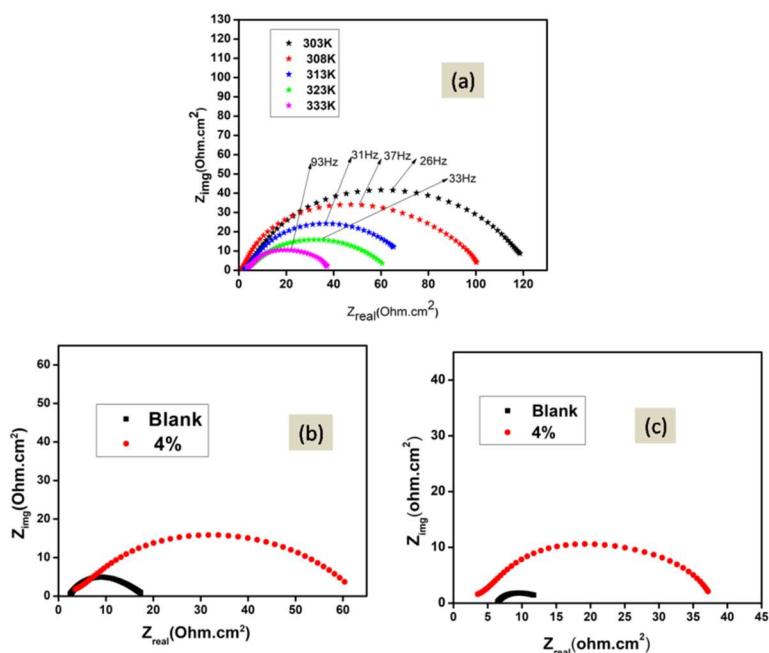


Fig 7.6 The EIS spectra of 4% GIW (a)different temperatures (b)at 323K and (c)333K in 1M HCl

Table 7.4 EIS parameters for GIW extract in 1M HCl at different temperatures

Temp (K)	C _{inh} (v/V%)	R _{ct} (Ω.cm ²)	C _{dl} (μF/cm ²)	I _{corr} (mA/cm ²)	CR (mm/y)	IE%
303	Blank	15.18	1046	1.719	19.92	-----
	1	61.12	336.1	0.4268	4.947	75.16
	2	67.21	271.4	0.4055	4.499	77.41
	3	72.86	229.7	0.3580	4.150	79.16
	4	120.7	177.0	0.2161	2.505	87.42
308	Blank	14.20	1079	1.837	21.29	-----
	1	44.41	455.1	0.5887	6.823	68.02
	2	55.02	307.8	0.4741	5.495	74.19
	3	74.06	300.6	0.3522	4.082	80.82
	4	101.6	196.8	0.2568	2.976	86.02
313	Blank	11.90	1113	2.192	25.41	-----
	1	38.97	483.2	0.6694	7.758	69.46
	2	42.59	321.6	0.6125	7.099	72.05
	3	66.08	308.3	0.3948	4.573	81.99
	4	74.60	251.3	0.3497	4.291	84.04
323	Blank	9.902	1085	2.635	30.53	-----
	4	61.68	304.7	0.4271	4.583	83.94
333	Blank	6.65	1571	3.922	45.45	-----
	4	34.19	358.8	0.763	8.843	80.54

7.2.2.2.4 Bode Plots

The Bode plot is drawn by taking log of the frequency versus phase angle shift and is given in Fig7.7 (a) and (b). Since the electrode-electrolyte interface act as an imperfect capacitor the phase angle deviates from 90°. The phase angles at intermediate frequencies for 4% inhibitor solution is 54.14° and the deviation is maximum for the blank solution (14.82°) reveals the reduced capacitive response and greater corrosion of mild steel in HCl. The Bode plots broaden as the percentage volume of inhibitor increases indicating the adsorption of inhibitor on the metal surface. The increase in temperature does not

affect the shape of the plot but the shift in phase angle is more pronounced at elevated temperatures. (For 303K phase angle is 54.14° and for 333K it is 37.17°) [21].

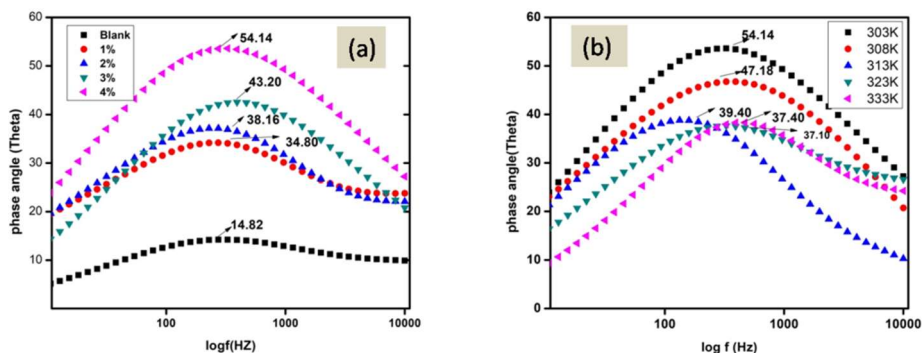


Fig 7.7 (a) Bode plot for GIW at 303K in 1M HCl (b) at different temperatures for 4% GIW extract

7.2.2.3. Polarisation studies

In potentiodynamic polarisation technique, the polarisation characteristic of a sample is studied as current response with applied potential. Potential which are positive of E_{corr} values give rise to anodic current and which are negative of E_{corr} give cathodic current. In order to calculate Tafel constants, I_{corr} , and E_{corr} the linear portions of the polarisation curve (stern diagram) are extrapolated until they intersect as straight lines. Several analytical parameters obtained from the polarisation studies are given in Table 7.5 and Table 7.6. E_{corr} value of the solutions does not follow a definite pattern. But the difference between the E_{corr} of the blank and the inhibited solution is less than 85mV affirms the mixed type behaviour of GIW extract affecting both the anodic ionisation of metal and cathodic hydrogen evolution. The E_{corr} values are shifted to less negative values for the inhibited solution

implies the pronounced effect on the anodic reaction by the inhibitor[22]. The corrosion current density is decreased from 1.4053mA/cm^2 for blank to 0.1455mA/cm^2 for 4% GIW extract at room temperature (Fig7.8). The Tafel plots given in Fig.7.8d for 4% solution at various temperatures also show that I_{corr} values increase from 0.1455mA/cm^2 at 303K to 0.5479mA/cm^2 at 333K. This could be attributed due to desorption of constituent molecules from the metal surface due increase in temperature/energy. The efficiency calculated using the corrosion current density values (eqn.2.9) is in close agreement with EIS results[23].

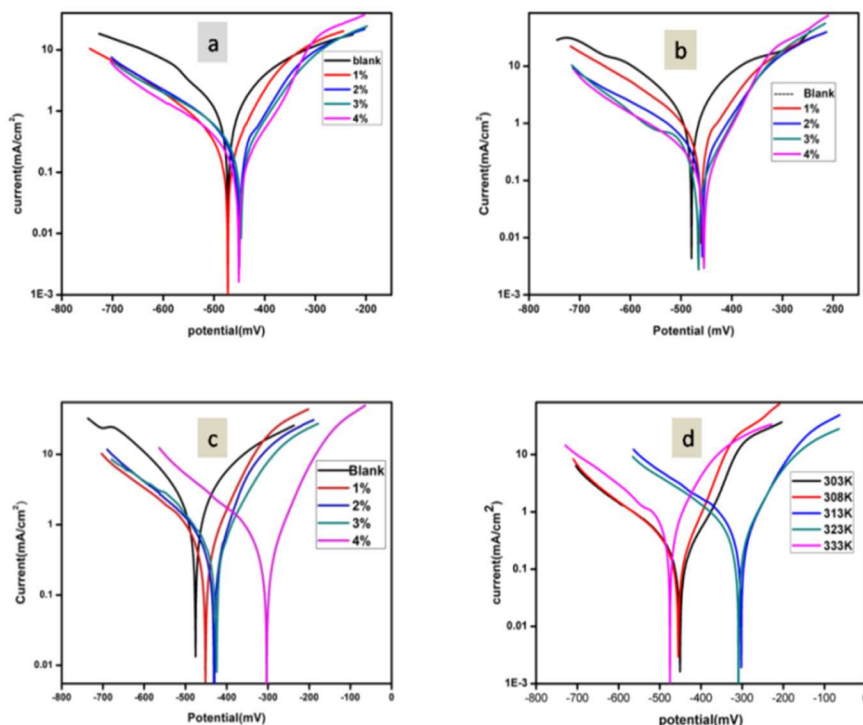


Fig 7.8 Tafel plots for GIW extract in 1M HCl at (a)303K (b) 308K (c)313K and(d) 4% GIW at various temperatures

Table 7.5 PDP parameters obtained for GIW for 0.5M, 1.5M HCl at room temperature

Acid Conc. (mol/L)	0.5			1.5		
C_{inh} (v/V%)	$-E_{corr}$ (mV)	I_{corr} (mA/cm ²)	%IE	$-E_{corr}$ (mV)	I_{corr} (mA/cm ²)	%IE
Blank	488	1.2125	-----	449	1.5806	-----
1	459	0.2521	79.92	453	0.5186	67.18
2	457	0.0902	92.56	441	0.4527	71.35
3	447	0.0806	93.30	496	0.4496	71.55
4	453	0.0783	93.58	514	0.4113	76.99

Table 7.6 Polarisation parameters for GIW extract at different temperatures in 1M HCl

Temp (K)	C_{inh} (v/V%)	$-E_{corr}$ (mV)	β_a (mV)	$-\beta_c$ (mV)	I_{corr} (mA/cm ²)	IE% (%)
303	Blank	472	169	182	1.4053	-----
	1	460	88	148	0.3194	77.27
	2	449	90	153	0.2793	80.12
	3	446	86	126	0.2233	84.11
	4	451	85	113	0.1455	89.4
308	Blank	475	123	137	1.2554	----
	1	461	104	162	0.5197	58.60
	2	458	97	183	0.4249	66.12
	3	465	82	153	0.2167	82.73
	4	455	72	145	0.1924	84.67
313	Blank	474	202	202	1.4989	-----
	1	452	87	128	0.4348	70.99
	2	432	76	140	0.4147	72.33
	3	427	85	121	0.3748	74.99
	4	302	78	203	0.3291	78.04
323	Blank	424	102	107	2.0016	-----
	4	303	104	204	0.4759	76.22
333	Blank	468	106	115	2.1629	-----
	4	474	83	170	0.5479	74.66

7.2.3 Influence of KI on the inhibition property of GIW extract

7.2.3.1 Gravimetric analysis

The effect of adding various concentrations of KI (50ppm-200ppm) to different concentrations of GIW extract in 1MHCl for 24 hours at room temperature is studied using weight loss analysis and the results are given in Table 7.7. It could be noted that the addition of KI to GIW extract increases efficiency and reduce the corrosion rate to a varying degree. In general, as the concentration of KI increases from 50-200 ppm the efficiency increases. Therefore 200ppm of KI is taken for electrochemical analysis to verify the extend of synergistic interactions.

Table 7.7 Weight loss data of mild steel in 1M HCl with GIW/KI pair for 24hours

C_{inh} (v/V%)	50ppm KI		100ppm KI		200ppm KI	
	CR (mg/cm ² .h)	%IE	CR (mg/cm ² .h)	%IE	CR (mg/cm ² .h)	%IE
Blank	14.70	----				
1	0.7361	90.96	0.7511	90.77	0.6817	91.63
2	0.5567	94.23	0.5423	94.38	0.4537	95.30
3	0.4560	95.61	0.4594	95.58	0.4074	96.08
4	0.5104	95.09	0.4756	95.42	0.4181	95.97

7.2.3.2 EIS Analysis

Fig 7.9 gives Nyquist plot for GIW and 200ppm of KI at various temperatures. All plots have only one capacitive loop indicating that the corrosion of mild steel in the blank and the inhibited solution is controlled by the charge transfer process [24]. The diameter of the semicircle increases with an increase in the concentration of the inhibitor shows that the charge transfer process becomes difficult with the addition of KI assuring the synergistic interaction. Comparison of the Nyquist plot of GIW (Fig7.5) and GIW with KI (Fig7.9) indicated that the diameter and its depressed nature increases for the synergistic pair. The depression of the semicircles is usually attributed to surface roughness, impurities, grain boundaries, etc. known as frequency dispersion[25]. In such cases, CPE (constant phase element) is introduced instead of double-layer capacitance (C_{dl}) [26]. The impedance by the CPE is given as

$$Z_{CPE} = \frac{1}{Y_0 (j\omega)^n} \quad (7.1)$$

$$C_{dl} = Y_0 (\omega)^{n-1} \quad (7.2)$$

where Y_0 is the numerical value of CPE, j is the imaginary number and ω is the angular frequency given as $2\pi f_{max}$ where f_{max} is the frequency at which the y (imaginary) component of impedance spectrum has the maximum value, n is the inhomogeneity constant, and can have values between 0 and 1. When $n=1$ represents an ideal capacitor, $n=0$ pure resistance, and when $n=-1$ represents a inductor. The parameters obtained are given in Table7.8. Contrary to the usual observation it is

seen that the addition of KI increases both charge transfer resistance and double layer capacitance (C_{dl}). At 303K the C_{dl} for 4% GIW is 177.0 μ F and for 4% GIW/KI system is 400.2 μ F, at 313K the values are 251.3 μ F and 268.4 μ F at 323K the values are 304.7 μ F and 660.4 μ F and at 333K the values are 358.3 μ F and 1113 μ F (Table7.4). The increase in C_{dl} shows better barrier to the charge transfer causing reduction in corrosion. Eqn.7.2 reveals that the decrease in 'n' causes increase of C_{dl} . A comparison of the n values guarantees an increase in the C_{dl} of the mixture of GIW and KI (Table7.10). This behaviour could also be explained with the help of eqn.7.3.

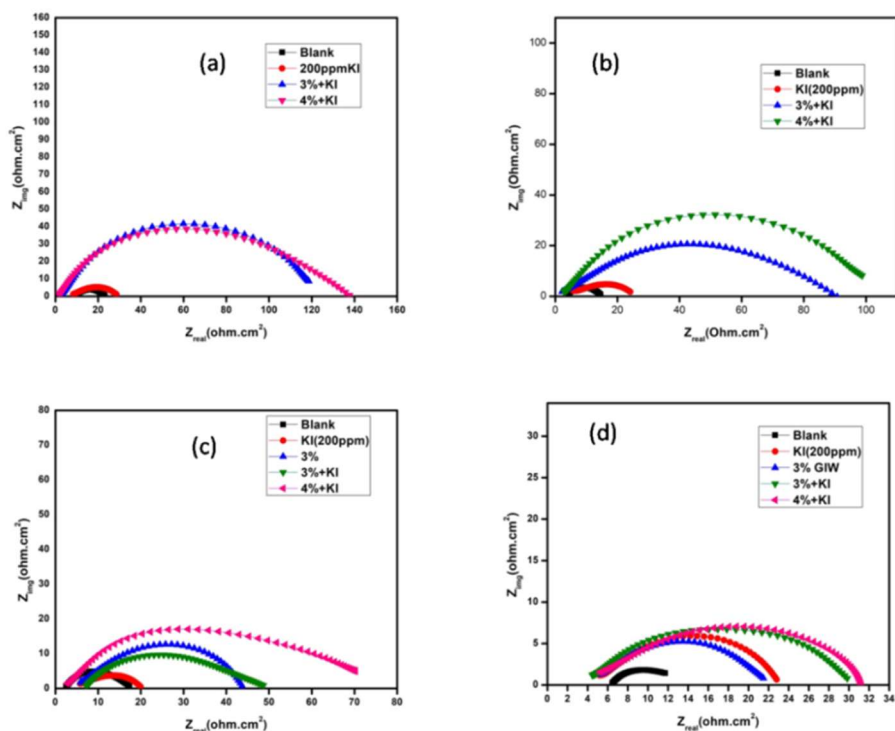


Fig 7.9 The Nyquist plot obtained for GIW & KI synergistic pair at (a) 303K, (b) 313K, (c) 323K and (d) 333K

$$C_{dl} = \frac{1}{\omega(R_{ct})} \quad (7.3)$$

where $\omega = 2\pi f$, f is the frequency at which the imaginary part of the impedance spectrum has the maximum value. The perusal of the Nyquist plots reveals that though R_{ct} of the synergistic pair increases the f_{max} of the synergistic pair is low compared to GIW extract alone. As f_{max} is lower for a solution containing GIW and KI than the solutions with GIW alone, therefore the C_{dl} increases for the synergistic pair [24, 27].

Table 7.8 EIS data of mild steel dipped in 1M HCl with and without GIW/KI pair at different temperatures

Temp	C_{inh}	R_{ct} ($\Omega.cm^2$)	C_{dl} ($\mu F/cm^2$)	I_{corr} (mA/cm^2)	CR (mm/y)	IE%
303K	Blank	15.18	1046	1.719	19.92	---
	KI(200ppm)	22.47	1797	1.616	13.46	32.40
	3%GIW+KI	111.3	663.4	0.2344	2.717	85.06
	4%GIW+KI	138.7	400.2	0.1088	2.180	89.05
313K	Blank	11.90	977.4	2.192	25.41	----
	KI(200ppm)	22.69	2161	1.922	22.28	47.55
	3%GIW+KI	90.43	740.4	0.3497	4.053	87.12
	4%GIW+KI	101.3	268.4	0.2575	2.985	88.25
323K	Blank	9.902	1085	2.635	30.53	---
	KI(200ppm)	15.86	1918	1.645	19.06	37.56
	3% GIW	38.98	403	0.6675	7.731	74.59
	3%GIW+KI	43.20	1312	0.6039	6.999	77.07
	4%GIW+KI	74.60	660.4	0.3497	4.053	86.72
333K	Blank	6.65	1571	3.922	45.45	---
	KI(200ppm)	18.30	651.8	1.403	16.26	63.66
	3% GIW	17.72	839.9	1.472	17.06	62.47
	3%GIW+KI	27.12	1297	0.9619	11.15	75.47
	4%GIW+KI	28.19	1113	0.9254	10.73	76.41

7.2.3.3 Potentiodynamic polarisation studies

The values of corrosion current density (i_{corr}), and Tafel constants (β_a and β_c) obtained by Tafel extrapolation of the current potential curve to the corrosion potential (E_{corr}) are given in Table 7.9. The extrapolation of the polarisation curve to obtain the Tafel constants is often difficult due to the nonlinearity of the polarisation curves under actual experimental conditions. The disparity in the anodic curve is attributed to the formation of passive film by corrosion products.

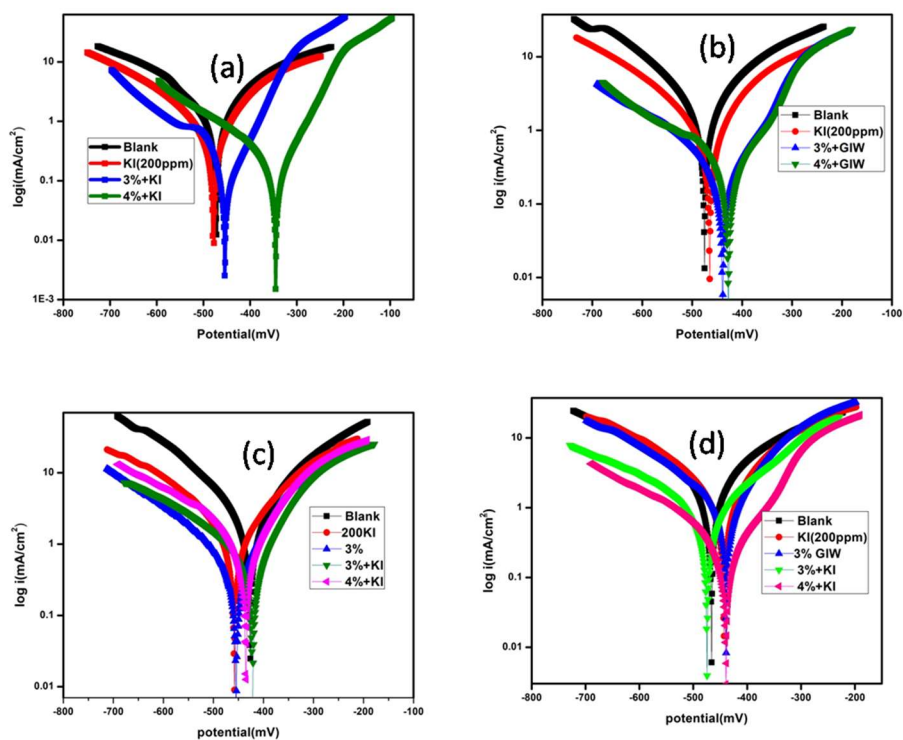


Fig 7.10 The PDP plots for GIW/KI pairs at (a) 303K, (b)313K, (c)323K and (d) 333K

Table 7.9 PDP data of mild steel dipped in 1M HCl with and without GIW/KI pair at different temperatures

Temp(K)	C _{inh}	-E _{corr} (mV)	β _a (mV)	-β _c (mV)	I _{corr} (mA/cm ²)	IE%
303	Blank	473	169	182	1.4053	----
	KI(200ppm)	448	118	190	1.0373	26.18
	3%GIW+KI	455	74	149	0.1578	88.77
	4%GIW+KI	345	74	116	0.1360	90.32
313	Blank	474	202	201	1.4989	---
	KI(200ppm)	463	80	101	0.8938	40.36
	3%GIW+KI	439	82	84	0.2027	86.47
	4%GIW+KI	428	81	85	0.1527	89.83
323	Blank	424	102	107	2.0016	----
	KI(200ppm)	443	93	115	1.0802	46.03
	3% GIW	455	74	97	0.3738	81.32
	3%GIW+KI	420	62	92	0.3391	83.05
	4%GIW+KI	346	76	108	0.3590	82.06
333	Blank	468	106	115	2.1629	---
	KI(200ppm)	460	95	92	0.7696	64.43
	3% GIW	440	91	128	0.7394	66.74
	3%GIW+KI	459	88	77	0.6636	69.31
	4%GIW+KI	436	108	145	0.4011	81.45

The shortening of the linear part of the cathodic polarisation curve is due to the development of concentration polarisation by slow diffusion of oxidising species in the static electrolyte [28]. However, from Fig7.10 it could be observed that there are considerable linear portions for both anodic and cathodic curves. The E_{corr} of the inhibited solutions is shifted to less negative value compared to the blank solution and especially of the synergistic pairs (Fig7.10). Yet the shift in E_{corr} values of the inhibited solutions is less than ±85mV approving the mixed

type behaviour of GIW/KI pair affecting both the anodic metal dissolution than the cathodic hydrogen evolution [29]. Corrosion current densities decrease with an increase in the concentration of the inhibitor indicating the inhibitory action of the GIW/KI pair. The addition of inhibitor reduces both anodic and cathodic current densities and act as a mixed type inhibitor [30].

7.2.3.4 Synergism between GIW and KI

The synergistic inhibitory action of organic compounds with KI is quite common especially with positively charged species. Larger size and ease of polarizability make iodide ion the best choice for synergistic action among the halide ions. The combined effect of the constituent molecules makes GIW extract an efficient inhibitor for mild steel in acidic medium. Further, the addition of iodide ion to these compounds enhances the efficiency of the system. The pre adsorbed iodide ions on the metal attract constituent compounds specially the positively charged cyanidin molecules from the solution and form a better protective covering on the metal surface. The ESP map of the components is shown in Fig 7.11. The blue regions are with maximum electrostatic potential and electrophilic centres. It could be observed that the cyanidin molecule is ready for an interaction with a nucleophile such as iodide ions. The weight loss studies, electrochemical impedance analysis, and the potentiodynamic polarisation studies show that the inhibition efficiency and surface coverage (θ) is enhanced by the addition of KI to GIW extract. The extent of the synergism can be evaluated by calculating the synergism parameter (S), given by the eqn.1.12 [28]. Table 7.10 gives the synergism parameter calculated for electrochemical studies. The values

S greater than one assumes cooperative adsorption of the molecules less than one indicates competitive interaction between the molecules[31, 32]. The iodide ion improves the inhibition property by a co-adsorption mechanism. If it is competitive adsorption the iodide ion and the organic molecule take different sites for adsorption and when it is cooperative adsorption the organic molecules will be adsorbed on a layer of iodide ions which are already adsorbed on the metal surface. In some cases both can occur together. The synergism parameters calculated are greater than one supports the cooperative adsorption of GIW/KI pair. The mild steel surface is believed to be positively charged in acidic solution and the approach of positively charged organic species is enhanced by the iodide ion acting as plug point for organic molecule [29].

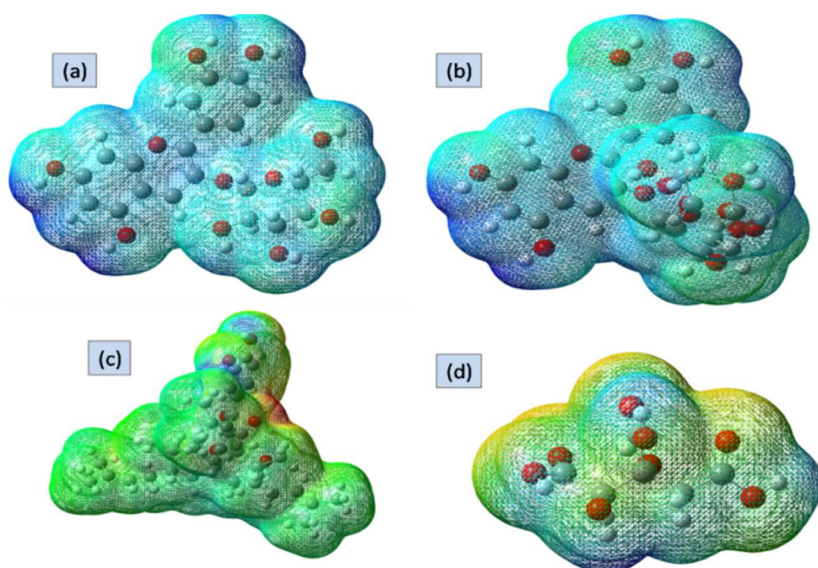


Fig 7.11 ESP map of the constituent molecules depicting the electron density of the molecules (a)cyanidin glucoside, (b)cyanidin sambubioside, (c) garcinol (d)ortho hydroxyl citric acid

Table 7.10 The values of CPE constant and synergism parameters(S) for GI/KI pair at different temperatures

Temp (K)	C _{inh.} (v/V%)	EIS		GIW +KI	N	PDP		Synergism parameter	PDP
		GIW	n			GIW	GIW +KI		
303	3	79.16	0.43	85.06	0.61	84.11	88.77	1.29	1.24
	4	87.42	0.77	89.05	0.60	89.78	90.32	1.34	1.27
313	3	81.99	0.73	87.12	0.55	74.99	86.47	1.33	1.33
	4	83.11	0.77	88.25	0.72	78.04	88.63	1.33	1.32
323	3	74.59	0.74	77.07	0.63	81.32	83.05	1.44	1.52
	4	83.94	0.61	86.72	0.52	76.22	82.06	1.40	1.49
333	3	62.47	0.68	75.47	0.59	66.66	69.31	1.65	1.89
	4	80.54	0.70	76.41	0.60	74.66	81.45	1.88	1.69

7.2.4 Adsorption Studies

Adsorption is a process of separation of molecules from one phase and accumulation of these molecules on another surface. Corrosion inhibition through adsorption is believed to be a quasi-substitution between molecules from the solution phase to a metal surface and water molecules from the metal surface to the solution phase. The inhibition property of natural products is by monolayer or multilayer adsorption of constituent organic molecules on the metal surface. In order to know the nature of adsorption and the interaction of the constituent molecules, adsorption isotherms like Langmuir, Temkin, Frumkin and Freundlich isotherms are drawn. Both GIW and KI obeys Langmuir adsorption model (Fig7.12). By its very nature, Langmuir isotherm suggests equal surface energy to all the active sites and assumes the formation of a monolayer of the adsorbed molecules on a homogeneous surface without the interaction of individual molecules

of GIW extract [33]. The negative values of free energy of adsorption, ΔG_0 confirms the spontaneity of adsorption of molecules and less negative values of free energy (-12kJ/mol) suggests physisorption of the constituent molecules through electrostatic force of attraction between the positively charged metal surface and electron-rich aromatic rings or by back donation of electrons from the metal surface to the molecules and free -OH groups of cyanidin molecules (Table7.11). The negative value of enthalpy of adsorption proves the exothermic nature of adsorption and validates physisorption of molecules on the surface. Due to the confinement of adsorbed molecules on the mild steel surface entropy of adsorption decreases.

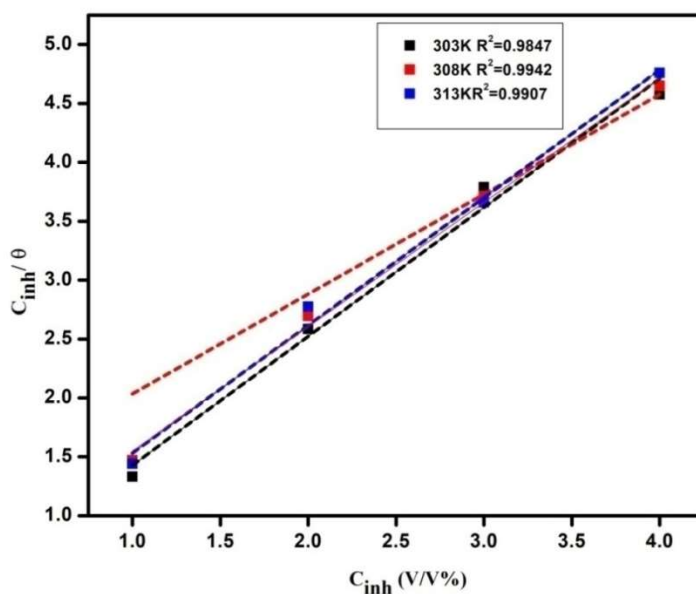


Fig 7.12. Langmuir adsorption isotherm for GIW extract at different temperatures in 1M HCl

Table 7.11 Thermodynamic parameters of adsorption of GIW extract on mild steel surface in 1M HCl

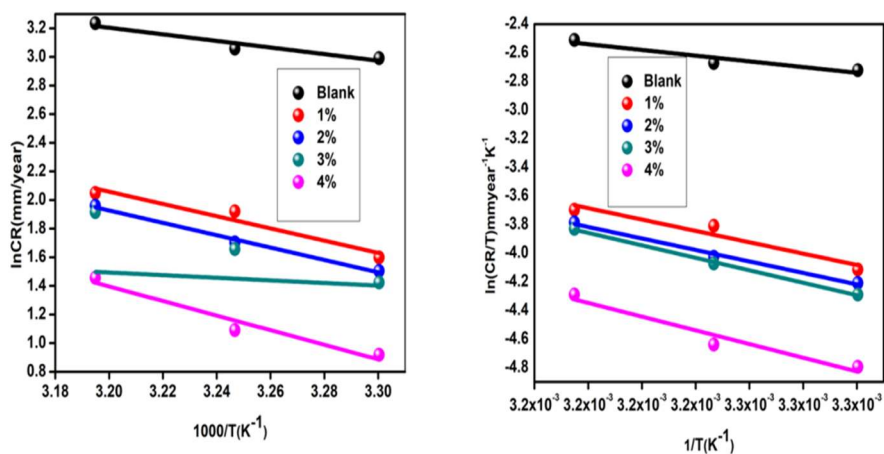
Temp	Slope	R ²	K _{ads}	ΔG ₀ (kJ/mol)	ΔH ⁰ _{ads}	ΔS ⁰ _{ads}
303K	1.09	0.9847	2.9940	-12.880		
308K	1.08	0.9942	2.0283	-12.095	-31.62	-63.33
313K	1.08	0.9908	2.2300	-12.538		

7.2.5 Kinetics of corrosion inhibition

The activation parameters for corrosion inhibition (Table 7.12) are studied using the Arrhenius equation by plotting $\ln(\text{CR})$ vs $1000/T$ and transition state equation. The higher value of activation energy (E_a) for the inhibited solution than the uninhibited solution affirms the adsorption of constituent molecules on the mild steel surface that leads to a higher energy barrier for acid molecules to cause corrosion in inhibited solutions. E_a values greater than 20kJ/mol assure surface process (physisorption) for corrosion inhibition. The entropy of activation and enthalpy of activation are calculated from the plot of $\ln(\text{CR}/T)$ vs $1/T$ (Fig 7.13). The positive value of enthalpy of activation (ΔH_a) describes the endothermic nature of metal dissolution. The difference between E_a and ΔH_a is equalled to 2.56kJ/mol and 2.64kJ/mol for GIW/KI pair which is closer to RT and it suggests the unimolecular mechanism for mild steel dissolution. The more positive values of entropy of activation (ΔS_a) in the inhibited solution assume the formation of an activated complex in the rate-determining step and more disorder when the reactant is converted to activated complex and this trend is absent for the GIW/KI pair.

Table 7.12 Kinetic parameters of corrosion inhibition by GIW and GIW/KI pair extract

	Arrhenius plot (1000/T Vs logCR)		Transition state plot (ln(CR/T) Vs 1/T)	
	Ea(kJ/mol)	ΔH_a (kJ/mol)	ΔS_a (kJ/molK)	Ea- ΔH_a (kJ/mol)
Blank	19.14	16.58	255.57	2.56
1%	35.55	32.99	298.56	2.56
2%	35.93	33.37	298.68	2.56
3%	38.80	36.24	307.53	2.56
4%	42.35	39.72	314.80	2.63
3%+KI	46.74	44.10	-92.70	2.64
4%+KI	38.79	36.15	-152.81	2.64

**Fig 7.13** Arrhenius and transition state plot of GIW

7.2.6 Calculation of global descriptors

The various global parameters obtained from geometry optimisation of cyanidin glucoside, cyanidin sambubioside, garcinol, and hydroxy citric acid are given in Table 7.13. The high energy of HOMO validates the tendency to donate electrons and low energy of LUMO agrees the capacity to receive electrons. Here the highest energy HOMO is that of garcinol and the lowest energy LUMO is that of cyanidin glucoside and cyanidin sambubioside. The low energy of LUMO of anthocyanin derivatives describes its inhibition property through the back donation of electrons from the metal surface. Lower ΔE assumes better activity and better inhibition efficiency. Cyanidin sambubioside and glucoside with the lowest ΔE will act as an efficient inhibitor. According to HSAB theory, hard acids combine with hard bases and soft acids combines with soft bases. Iron in acid solution is considered to be soft. Softness (the reciprocal of hardness ($1/\eta$)) is minimum for hydroxy citric acid and can have potential ability to combine with the metal. Two different explanations are given for dipole moment (μ) value. One group suggests better efficiency for compounds with high dipole moment due to increased dipole-dipole interactions. A few suggest lower values of dipole moment for increased efficiency by an accumulation of molecules on the metal surface. The lower dipole moment value of cyanidin glucoside ensures its capacity to be adsorbed on the metal surface. The molecule with higher electron affinity (EA) tends to be efficient inhibitors by accepting electrons from the metal surface[34]. Cyanidin glucoside and sambubioside having a higher electron affinity can be adsorbed on the metal.

According to Lukovit's study the fraction of electron transferred ΔN , from the inhibitor increases its inhibition efficiency and negative values of ΔN is characteristic of the electron-accepting tendency of inhibitor molecules from the metal through back donation. The general idea of the global electrophilicity index (ϕ) is that higher the value greater is its capacity to accept electrons. The higher ϕ values of anthocyanin derivatives show that they accept electrons from the iron surface[35]. The optimised geometries, HOMO and LUMO of anthocyanin derivative, hydroxy citric acid and garcinol are given in Fig7.14 and Fig7.15

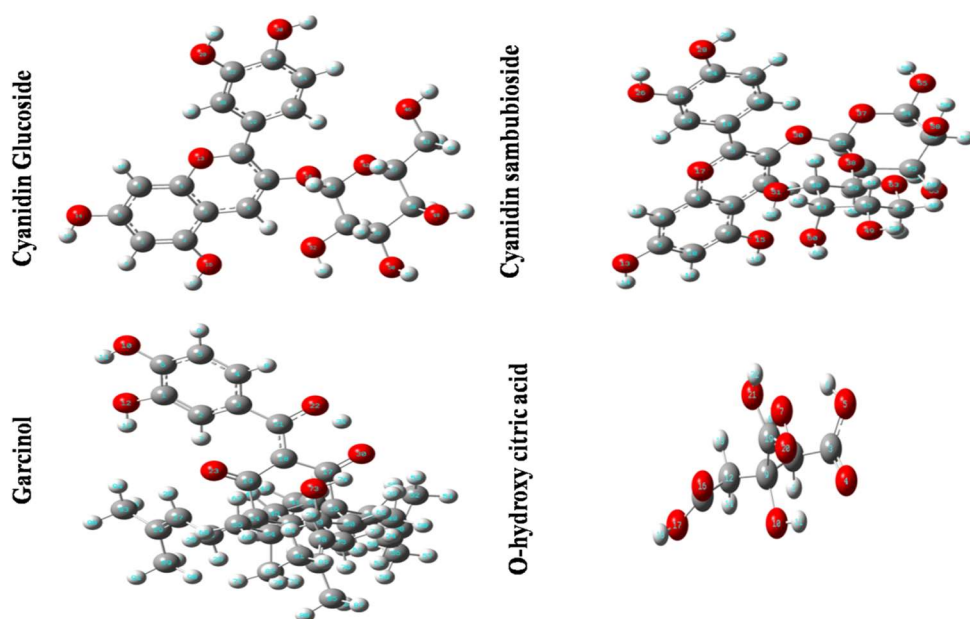


Fig 7.14 Optimised geometries of major constituent molecules

Table 7.13 Global parameters of the chief constituent molecules obtained using B3LYP/6-31G (d, p)

Parameter	Cyanidin Glucoside	Cyanidin Sambubioside	Garcinol	Hydroxy Citric acid
Total Energy (a.u)	-1640.17	-2097.11	-1930.7	-830.8
$E_{\text{HOMO}}(\text{eV})$	-9.10	-8.81	-6.06	-8.07
$E_{\text{LUMO}}(\text{eV})$	-6.27	-6.03	-2.10	-1.61
$\Delta E(\text{eV})$	2.83	2.78	3.96	6.46
Hardness $\eta = \frac{\Delta E}{2}$	1.41	1.39	1.98	3.23
Dipole moment, $\mu(\text{D})$	3.10	5.13	6.40	2.85
$IE = -E_{\text{HOMO}}$	9.10	8.81	6.06	8.07
$EA = -E_{\text{LUMO}}$	6.27	6.03	2.10	1.61
$\chi = \frac{IE + EA}{2}$	7.68	7.42	4.08	4.84
$\Delta N = \frac{(\chi_{\text{Fe}} - \chi_{\text{inh}})\chi}{2(\eta_{\text{Fe}} + \eta_{\text{inh}})}$	-0.24	-0.15	0.73	0.33
$\phi = \frac{\chi_{\text{inh}}^2}{4\eta_{\text{inh}}}$	10.45	9.90	2.10	1.81

7.2.7 Condensed Fukui functions

The specific sites of electron donation and acceptance are obtained from condensed Fukui indices. Higher values of f^+ indicate the greater capacity of those sites for receiving charges and higher values of f^- assures the greater capability of those sites to donate charges and thus we can predict the sites of adsorption on the metal surface[36]. The calculated values of few atoms are given in Table7.13. In the case of cyanidin glucoside C9 and O28, of cyanidin sambubioside C2 and C10, of garcinol C18 and C37, of hydroxy citric acid C15 and O4 are with maximum f^+ and f^- (Table7.14). Those sites with higher f^+ receive electrons from the metal atom by back donation whereas sites with maximum f^- donate electrons and form bonds with the metal surface.

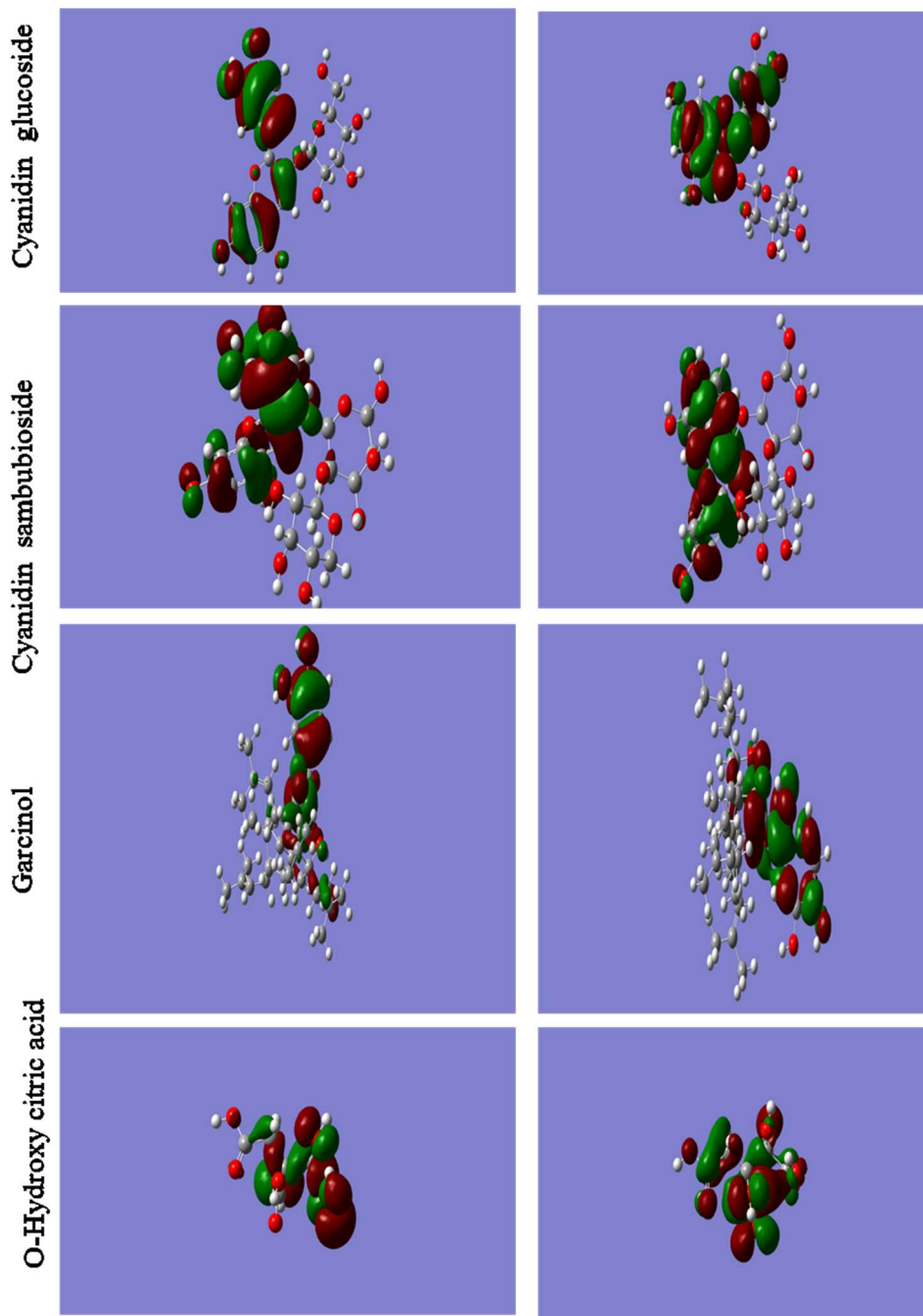


Fig 7.15 HOMO and LUMO of constituent molecules

Table 7.14 Condensed Fukui functions of a few atoms of constituent molecules

Hydroxy citric acid			Cyanidin glucoside			Garcinol			Cyanidin sambubioside		
At oms	f_k^+	f_k^-	At oms	f_k^+	f_k^-	At oms	f_k^+	f_k^-	At oms	f_k^+	f_k^-
C1	0.079	0.074	C1	0.141	0.109	C3	0.037	0.029	C1	0.002	0.014
C3	0.033	0.036	C3	0.079	0.095	C4	0.053	0.117	C2	0.147	0.045
O4	0.026	0.196	C5	0.062	0.071	C5	0.067	0.058	C3	0.054	0.064
O5	0.040	0.127	C9	0.175	0.021	O10	0.070	0.063	C5	0.045	0.013
O7	0.032	0.059	O13	0.066	0.013	O12	0.038	0.040	C8	0.062	0.069
O9	0.120	0.122	O14	0.065	0.072	C14	-0.03	0.027	C10	0.131	0.1007
O10	0.018	0.164	O16	0.052	0.051	C16	0.010	-0.04	O13	0.059	0.072
C12	0.451	0.082	O18	0.022	0.023	C17	-0.01	0.049	O15	0.046	0.047
C15	0.701	0.037	C19	0.021	0.072	C18	0.074	0.112	O17	0.062	0.007
O16	0.235	0.069	C24	0.077	0.102	C21	-0.02	0.086	C18	-0.001	0.017
O17	0.132	0.080	C26	0.004	0.014	O22	0.026	0.101	C19	0.083	0.047
O19	0.124	0.045	O28	0.044	0.112	O23	0.031	0.043	C20	0.104	0.081
O20	0.053	0.081	O30	0.064	0.097	C24	0.022	-0.03	C21	-0.001	0.006
O21	0.015	0.070	C38	0.039	0.029	O73	0.015	-0.01	C22	0.077	0.082
			C43	0.057	0.061	C75	0.004	0.009	C24	0.005	0.013

7.2.8 Monte Carlo simulations

A deeper understanding of the adsorption pattern of the molecules can be obtained by Monte Carlo simulations. The simulations are done using the Biovia Material studio 2017 software. Fe (110) plane is selected for the studies. Cyanidin, the core moiety of cyanidin glucoside and cyanidin sambubioside, and o-hydroxy citric acid are selected for the studies. In the first model cyanidin (CY) and o-hydroxy citric acid (OHC) are separately adsorbed on Fe (110) plane after optimisation of the molecules using forcite Module. The adsorption studies are done using the adsorption locator Module. Fig7.16 and Fig7.17 give the different adsorption pattern of CY and OHC on Fe (110) plane. Both CY and OHC are not flat on the metal

surface. o-hydroxy citric acid is vertically arranged with its free acidic group pointing towards the metal and acts as a nucleophilic centre, where as cyanidin's benzene ring which is attached to ring with oxygen as the heteroatom is closer to the iron surface. The second model considered is in which cyanidin and o-hydroxy citric acid are adsorbed together on the same Fe (110) plane. In the third model CY and OHC and iodide ions are adsorbed together on the metal surface. In the fourth model CY, OHC, two KI and thirty H₂O molecules are adsorbed together on the metal surface to mimic the most probable situation. In all these cases the orientation of the molecules are different and the energy of interaction is calculated to know the favourable adsorption of these molecules on the metal surface. The energy of interaction (E_i) is calculated as

$$E_i = E_{total} - (E_{Fe(110)} + E_{adsorbate}) \quad (7.4)$$

where E_{total} is the sum of adsorbate energy and adsorption energy [37]. In the present case, the energy of the substrate Fe(110) is taken as zero [38]. Higher negative values of adsorption energy and energy of interaction indicate strong adsorption on the metallic surface. Binding energy is the negative of interaction energy should be more positive for an efficient adsorption process. The values obtained and calculated (Table 7.15) reveals that the binding energy of the system increases when it adsorbs cyanidin, ortho hydroxy citric acid, KI, and water molecules. The higher positive binding energy value of CY than OHC assures the better adsorption capacity of cyanidin compared to citric acid [39].

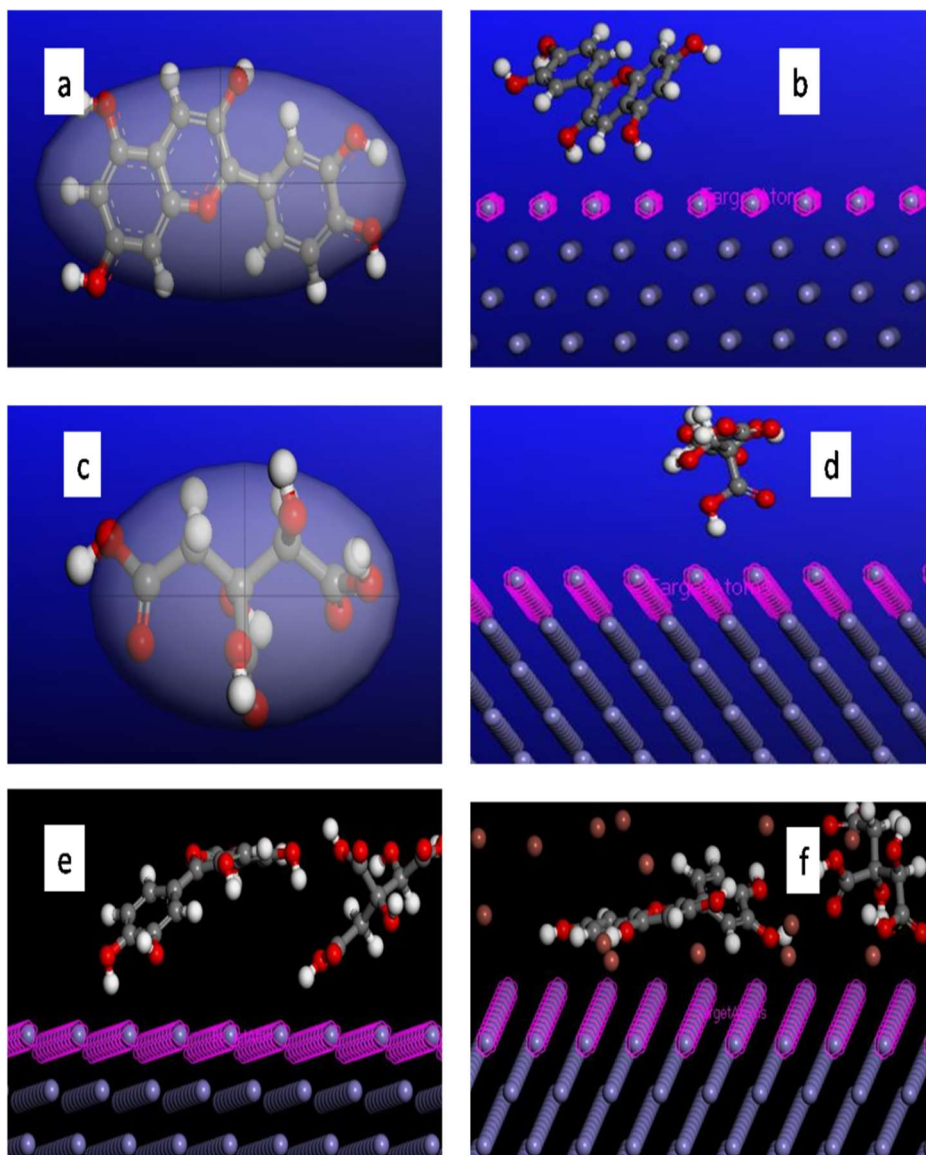
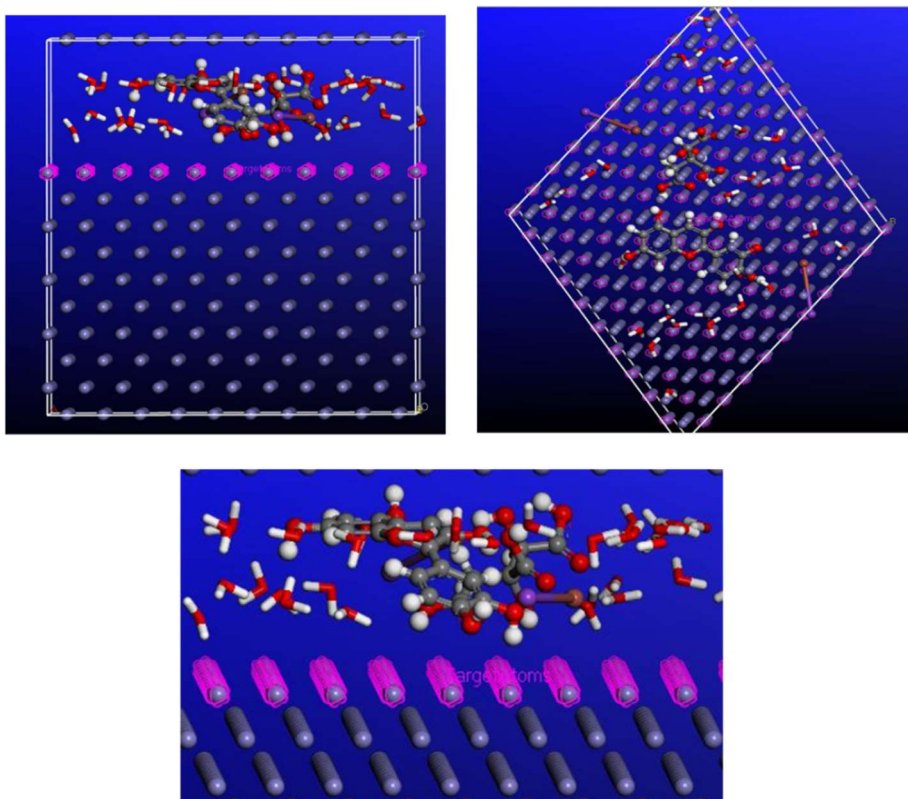


Fig 7.16 (a) CY (b) adsorption mode of CY on Fe(110) (c) OHC (d) the adsorption mode of OHC on Fe(110) plane (e) combined adsorption of CY and OHC (f) combined adsorption of CY, OHC and iodide ions

Table 7.15 The energy parameters obtained by material Studio calculations

System	E_{inh} (Kcal/mol)	E_{Total} (Kcal/mol)	E_{ads} (Kcal/mol)	E_i (Kcal/mol)	E_b (Kcal/mol)
CY	32.77	-178.84	-211.61	-146.06	146.06
OHC	2.49	-123.79	-115.31	-121.29	121.29
CY+OHC	35.26	-304.86	-308.04	-261.60	261.60
CY+OHC+2KI+3 0 H ₂ O	75.51	-895.49	-971.01	-819.98	819.98

**Fig 7.17** The combined adsorption mode of CY.OHC, 2KI and 30 H₂O molecules on Fe (110) surface

7.2.9 Surface Analysis

7.2.9.1 AFM studies

Fig 7.18 is the AFM images of metal samples dipped in blank and in the inhibited solution. The surface topology of samples is studied using this image. The average roughness (Ra) corresponding to the blank is 25.5nm and the root mean square roughness (Rq) is 33.4nm. For the sample dipped in HCl containing GIW extract the Ra value is 16.8nm and the Rq value is 21.9nm. This indicates the formation of a compact protective film on the metal surface. The average roughness of the metal sample dipped in GIW/KI pair is increased to 39.0nm from 6.03nm for the steel sample dipped in acid containing GIW.

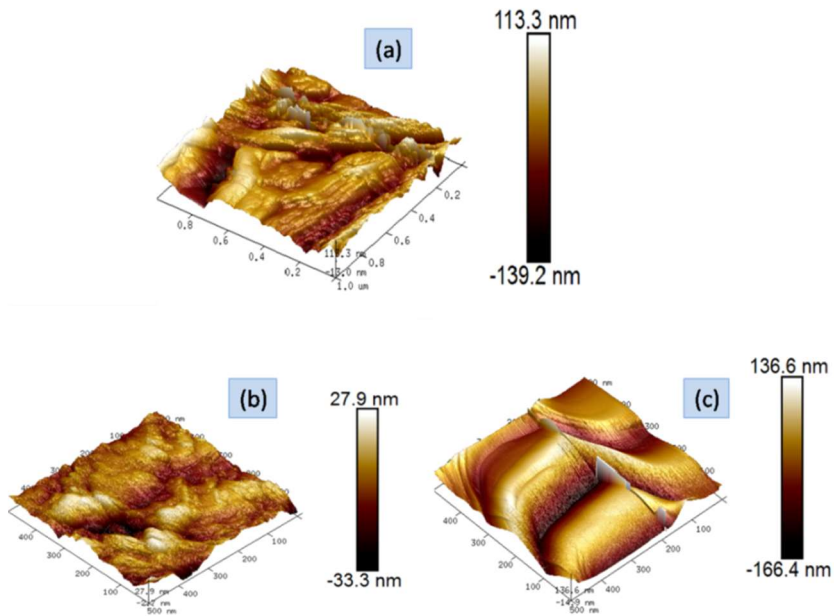


Fig 7.18 AFM images of the mild steel sample dipped in (a) 1M HCl, (b) HCl containing GIW, (c) HCl containing GIW/KI pair

The increase in roughness is due to the presence of iodide ions which hinders the free movement of the AFM tip [40]. This is in agreement with the EIS value affirming depressed nature of the semicircles of Nyquist plot of GIW/KI pair.

7.2.9.2 SEM Analysis

The SEM images of the mild steel specimens dipped in the blank (1M HCl) and the inhibited solution is also given in Fig 7.19. The surface is seriously damaged by HCl. Fig 7.19(b) and (c) represents, the SEM images of the inhibited solution exhibits a protective layer on the metal surface ensuring corrosion inhibition.

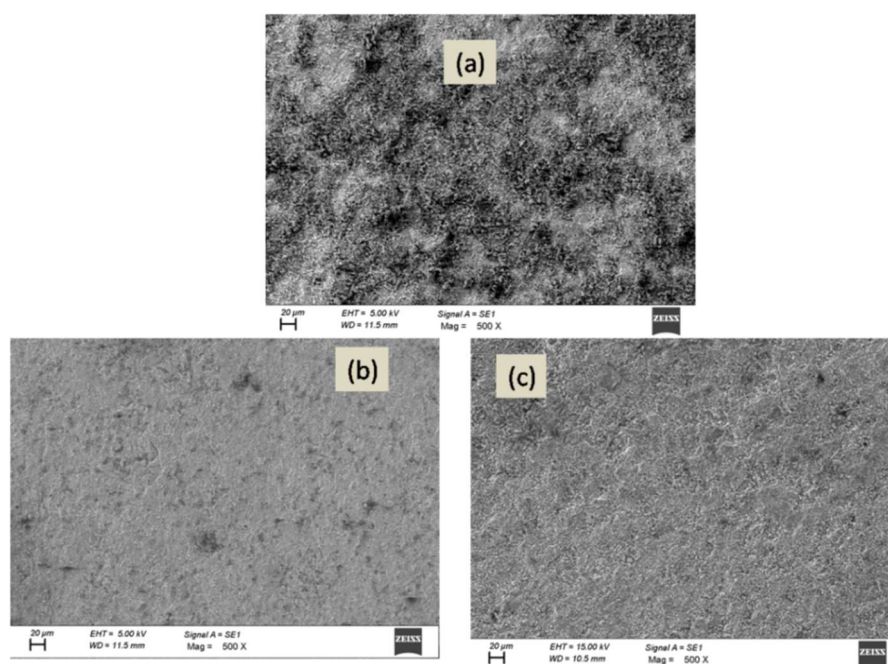
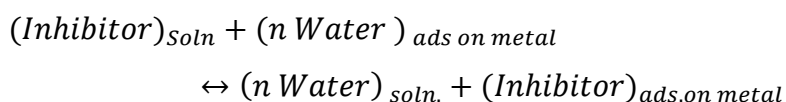


Fig 7.19 The SEM images of the mild steel samples dipped in (a) 1M HCl, (b) HCl with GIW, and (c) HCl with GIW and KI

7.2.10 Mechanism of inhibition

The effective molecules of GIW extract which offer protection to mild steel are water-soluble cyanidins and orthohydroxy citric acid. The process of inhibition by organic molecules is through the formation of a protective film on the metal surface by replacing the water molecules on the metal surface by inhibitor molecules.



The type of adsorption depends on the charge of the metal surface as well as the chemical structure of the active inhibitor components. The charge on the metal surface is given as the difference between E_{corr} (corrosion potential) and ZCP (zero charge potential) and when it is negative the metal surface is negatively charged and attract positively charged molecules and when it is positive metal surface prefer negatively charged molecules. Usually, the Fe in HCl is found to be positively charged and the chloride ions can be pre-adsorbed on the mild steel surface[41].

The inhibition mechanism by GIW extract can be explained in three different ways.

1. By the electrostatic interaction between the positively charged molecules such as cyanidin anthocyanins and the negatively charged chloride ions.

2. The adsorption can be by sharing of lone pair of electrons of oxygen atoms of cyanidin molecules and o- hydroxy citric acid and pi electrons of aromatic rings of cyanidin to the vacant d orbitals of metal atom. It is found that as the number of –OH group increases the inhibition efficiency of anthocyanins increases[34]. The use of hydroxy citric acid as an inhibitor is recommended because of the presence of acidic group [42].
3. From the theoretical calculations, it can be attributed to the back bonding of cyanidin with metal-centered d orbitals. From the theoretical calculations, it is seen that cyanidins can act as efficient inhibitors by accepting electrons from the metal surface too, for cyanidins in acid remain as oxonium ion. Adsorption and kinetics studies explain the preferable physisorption of constituent molecules in the metal surface.
4. The mechanism of inhibition by GIW/KI could be explained as follows. The chemisorbed iodide ions can act as a bridge between organic molecules and the metal surface. Most often the cation type organic molecules act synergistically with KI. The synergism can be due to interaction between the molecules of inhibitor formulations or by an interaction between the ions of the aqueous phase and one of the inhibitor molecules. The mechanism of iodide adsorption is believed to be adsorption of the iodide ion on the positively charged metal surface followed by taking up of positively charged organic molecules from the double layer by these iodide ions [43]. Another possibility is the adsorption of ion-

pair formed between iodide and the inhibitor. Reported studies show that pigments/dyes are efficient inhibitors especially as synergistic pair with halide ions[44]. Therefore it could be concluded that the cyanidin molecules which are positively charged in the acidic solution and the o-citric acid which are protonated in the acidic solution are adsorbed from the double layer on to the iodide ion layer and this ion pair increases the thickness of the double layer, and the charge transfer resistance and surface coverage. Another possible mechanism is that the iodide ions stabilises the adsorbed film of the constituent molecules.

7.3 Conclusions

1. Garcinia Indica fruit rind extract (GIW) is used as a corrosion inhibitor for mild steel in HCl medium. The extract contains compounds with oxygen heteroatom and aromatic rings such as cyanidin anthocyanins, hydroxy citric acid and garcinol.
2. GIW acts as an efficient inhibitor for mild steel corrosion in HCl at different temperatures and acid concentrations. An efficiency of 93.18% in 0.5M HCl, 87.42%, in 1M HCl and 74.41% for 1.5M HCl at room temperature. The efficiency at 333K is found to be 80.54%.
3. GIW/KI pair acts as a synergistic pair improving the protection capacity of GIW in acidic medium. The efficiency increases to 90.32% in 1M HCl at room temperature.

4. Potentiodynamic studies show GIW act as a mixed type inhibitor and adsorption process obey Langmuir adsorption.
5. The kinetic and adsorption studies affirm the physisorption of molecules. The physisorption is assumed to be the interaction between the positively charged anthocyanins and preadsorbed chloride ions on the metal surface. In the case of GIW/KI pair the pre adsorbed iodide ion act as a link between metal surface and constituent molecules.
6. Theoretical calculations showed that constituent molecules can be adsorbed on the metal surface by donating electrons of the oxygen atoms or aromatic rings or by engaging in back donation between metal orbitals and the anthocyanin molecules.

References

1. Abiola, O.K. and Y. Tobun, *Cocos nucifera L. water as green corrosion inhibitor for acid corrosion of aluminium in HCl solution*. Chinese Chemical Letters, 2010. **21**(12): p. 1449-1452.
2. Alvarez, P.E., et al., *Rollinia occidentalis extract as green corrosion inhibitor for carbon steel in HCl solution*. Journal of industrial and engineering chemistry, 2018. **58**: p. 92-99.
3. Asadi, N., et al., *Utilizing Lemon Balm extract as an effective green corrosion inhibitor for mild steel in 1M HCl solution: a detailed experimental, molecular dynamics, Monte Carlo and quantum mechanics study*. Journal of the Taiwan Institute of Chemical Engineers, 2019. **95**: p. 252-272.
4. Umoren, S.A., et al., *A critical review on the recent studies on plant biomaterials as corrosion inhibitors for industrial metals*. Journal of Industrial and Engineering Chemistry, 2019.
5. Chigondo, M. and F. Chigondo, *Recent natural corrosion inhibitors for mild steel: an overview*. Journal of Chemistry, 2016. **2016**.
6. Khan, M., et al., *Evaluation of Matricaria aurea Extracts as Effective Anti-Corrosive Agent for Mild Steel in 1.0 M HCl and Isolation of Their Active Ingredients*. Sustainability, 2019. **11**(24): p. 7174.
7. Hassannejad, H. and A. Nouri, *Sunflower seed hull extract as a novel green corrosion inhibitor for mild steel in HCl solution*. Journal of Molecular Liquids, 2018. **254**: p. 377-382.
8. Molina-Ocampo, L., M. Valladares-Cisneros, and J. Gonzalez-Rodriguez, *Using hibiscus sabdariffa as corrosion inhibitor for Al in 0.5 M H₂SO₄*. Int. J. Electrochem. Sci, 2015. **10**: p. 388-403.
9. Yetri, Y. and N. Jamarun, *Inhibitory action of theobroma cacao peels extract on corrosion of mild steel in different media*. RJC, 2016. **9**(4): p. 716-727.
10. Manikandan, C.B., et al., *Corrosion Inhibition of Mild Steel by using Banana Peel Extract*. 2018.
11. Padhye, S., et al., *Emerging role of Garcinol, the antioxidant chalcone from Garcinia indica Choisy and its synthetic analogs*. Journal of hematology & oncology, 2009. **2**(1): p. 38.

12. Swami, S.B., N. Thakor, and S. Patil, *Kokum (Garcinia indica) and its many functional components as related to the human health: a review*. Journal of Food Research and Technology, 2014. **2**(4): p. 130-142.
13. Jagtap, P., K. Bhise, and V. Prakya, *A phytopharmacological review on Garcinia indica*. International Journal Of Herbal Medicine, 2015. **3**(4): p. 02-07.
14. Sampathu, S. and N. Krishnamurthy, *Processing and utilization of Kokam (Garcinia indica)*. Indian Spices, 1982.
15. Elham, G., et al., *Isolation and structure characterization of anthocyanin pigments in black carrot (Daucus carota L.)*. Pakistan journal of biological sciences, 2006. **9**(15): p. 2905-2908.
16. Giusti, M., *Wrolstad 2005. Characterization and measurement of anthocyanins by uv-visible spectroscopy. Unit F1. 2*. Handbook of food analytical chemistry. Wiley, New York, NY: p. 19-31.
17. Odewunmi, N., S. Umoren, and Z. Gasem, *Watermelon waste products as green corrosion inhibitors for mild steel in HCl solution*. Journal of Environmental Chemical Engineering, 2015. **3**(1): p. 286-296.
18. Khaled, K. and S. Abdel-Rehim, *Electrochemical investigation of corrosion and corrosion inhibition of iron in hydrochloric acid solutions*. Arabian Journal of Chemistry, 2011. **4**(4): p. 397-402.
19. Khadom, A.A., et al., *The effect of temperature and acid concentration on corrosion of low carbon steel in hydrochloric acid media*. American Journal of Applied Sciences, 2009. **6**(7): p. 1403-1409.
20. Prajila, M., A. Thomas, and A. Joseph, *Development of Passive Film and Enhancement of Corrosion Protection of Mild Steel Exposed in Hydrochloric Acid due to the Adsorption of Water Dispersed 4-[(E)-(3, 4-Dihydroxybenzylidene) amino]-6-Methyl-3-Mercapto-1, 2, 4-Triazin-5 (4H)-one (DHMMT)*. Journal of Bio-and Tribo-Corrosion, 2017. **3**(2): p. 16.
21. Singh, A., et al., *Effect of electron donating functional groups on corrosion inhibition of mild steel in hydrochloric acid: Experimental and quantum chemical study*. Journal of the Taiwan Institute of Chemical Engineers, 2018. **82**: p. 233-251.

22. Olasunkanmi, L.O., et al., *Some quinoxalin-6-yl derivatives as corrosion inhibitors for mild steel in hydrochloric acid: experimental and theoretical studies*. The Journal of Physical Chemistry C, 2015. **119**(28): p. 16004-16019.
23. Elshakre, M.E., et al., *On the role of the electronic states of corrosion inhibitors: Quantum chemical-electrochemical correlation study on urea derivatives*. Corrosion Science, 2017. **124**: p. 121-130.
24. Qiang, Y., et al., *Synergistic effect of tartaric acid with 2, 6-diaminopyridine on the corrosion inhibition of mild steel in 0.5 M HCl*. Scientific reports, 2016. **6**: p. 33305.
25. Ramya, K. and A. Joseph, *Synergistic effects and hydrogen bonded interaction of alkyl benzimidazoles and thiourea pair on mild steel in hydrochloric acid*. Journal of the Taiwan Institute of Chemical Engineers, 2015. **52**: p. 127-139.
26. Musa, A.Y., et al., *Inhibition of aluminum corrosion by phthalazinone and synergistic effect of halide ion in 1.0 M HCl*. Current Applied Physics, 2012. **12**(1): p. 325-330.
27. Ammal, P.R., M. Prajila, and A. Joseph, *Physicochemical studies on the inhibitive properties of a 1, 2, 4-triazole Schiff's base, HMATD, on the corrosion of mild steel in hydrochloric acid*. Egyptian Journal of Petroleum, 2018. **27**(3): p. 307-317.
28. Umoren, S., Y. Li, and F. Wang, *Synergistic effect of iodide ion and polyacrylic acid on corrosion inhibition of iron in H₂SO₄ investigated by electrochemical techniques*. Corrosion Science, 2010. **52**(7): p. 2422-2429.
29. Musa, A.Y., et al., *Synergistic effect of potassium iodide with phthalazone on the corrosion inhibition of mild steel in 1.0 M HCl*. Corrosion Science, 2011. **53**(11): p. 3672-3677.
30. Mohamad, A.B., et al., *Synergistic of a coumarin derivative with potassium iodide on the corrosion inhibition of aluminum alloy in 1.0 M H₂SO₄*. Metals and materials international, 2014. **20**(3): p. 459-467.
31. Sedik, A., et al., *Synergistic Effect of L-Methionine and KI on Copper Corrosion Inhibition in HNO₃ (1M)*. Sensors & Transducers, 2014. **27**(Special Issue).

32. Ramya, K., R. Mohan, and A. Joseph, *Adsorption and electrochemical studies on the synergistic interaction of alkyl benzimidazoles and ethylene thiourea pair on mild steel in hydrochloric acid*. Journal of the Taiwan Institute of Chemical Engineers, 2014. **45**(6): p. 3021-3032.
33. Rugmini Ammal, P., M. Prajila, and A. Joseph, *Physicochemical studies on the inhibitive properties of a 1, 2, 4-triazole Schiff's base, HMATD, on the corrosion of mild steel in hydrochloric acid*. Egypt. J. Pet, 2017.
34. Hadisaputra, S., et al. *Which anthocyanin is the best corrosion inhibitor?* in *IOP Conference Series: Materials Science and Engineering*. 2019. IOP Publishing.
35. Guo, L., et al., *Theoretical evaluation of the corrosion inhibition performance of 1, 3-thiazole and its amino derivatives*. Arabian Journal of Chemistry, 2017. **10**(1): p. 121-130.
36. Rodríguez-Valdez, L.M., A. Martínez-Villafañe, and D. Glossman-Mitnik, *Computational simulation of the molecular structure and properties of heterocyclic organic compounds with possible corrosion inhibition properties*. Journal of Molecular Structure: THEOCHEM, 2005. **713**(1-3): p. 65-70.
37. Verma, C., et al., *Molecular dynamics and Monte Carlo simulations as powerful tools for study of interfacial adsorption behavior of corrosion inhibitors in aqueous phase: a review*. Journal of Molecular Liquids, 2018. **260**: p. 99-120.
38. John, S., K.M. Ali, and A. Joseph, *Electrochemical, surface analytical and quantum chemical studies on Schiff bases of 4-amino-4H-1, 2, 4-triazole-3, 5-dimethanol (ATD) in corrosion protection of aluminium in 1N HNO₃*. Bulletin of Materials Science, 2011. **34**(6): p. 1245-1256.
39. Tang, Y., et al., *Experimental and molecular dynamics studies on corrosion inhibition of mild steel by 2-amino-5-phenyl-1, 3, 4-thiadiazole*. Corrosion Science, 2010. **52**(1): p. 242-249.
40. Jaseela, P. and A. Joseph, *Development of Flower Like Hierarchical Thiourea Loaded Titania-Poly Vinyl Alcohol Nano Composite Coatings for the Corrosion Protection of Mild Steel in Hydrochloric Acid*. Journal of Inorganic and Organometallic Polymers and Materials, 2018. **28**(4): p. 1468-1482.

41. Dehghani, A., et al., *Electronic/atomic level fundamental theoretical evaluations combined with electrochemical/surface examinations of Tamarindus indica aqueous extract as a new green inhibitor for mild steel in acidic solution (HCl 1 M)*. Journal of the Taiwan Institute of Chemical Engineers, 2019. **102**: p. 349-377.
42. Aquino-Torres, E., et al., *The influence of iodide in corrosion inhibition by organic compounds on carbon steel: Theoretical and experimental studies*. Applied Surface Science, 2020: p. 145928.
43. Oguzie, E., Y. Li, and F. Wang, *Corrosion inhibition and adsorption behavior of methionine on mild steel in sulfuric acid and synergistic effect of iodide ion*. Journal of colloid and interface science, 2007. **310**(1): p. 90-98.
44. Umoren, S. and M. Solomon, *Effect of halide ions on the corrosion inhibition efficiency of different organic species—A review*. Journal of Industrial and Engineering Chemistry, 2015. **21**: p. 81-100.

Chapter 8

Inhibition of mild steel corrosion in HCl using Myristica fruit rind extract

The inhibition property of aqueous (MFV) and ethanolic (MFE) of Myristica fruit rind are evaluated using weight loss, EIS and PDP analysis. The characterisation of the constituent molecules is done using GCMS analysis. Geometry optimisation of the most abundant molecules is also carried out.



Contents

8.1. Introduction.....	219
8.2. Results and discussion	219
8.3. Conclusions	239

8.1 Introduction

Myristica fragrans (nutmeg) is an evergreen tropical tree found in India, Indonesia, South Africa, and Sri Lanka [1, 2]. Nutmeg mace/aryl is a world-known spice. Seed and mace are the most used parts of nutmeg. They exhibit antimicrobial, anti-inflammatory, analgesic, and hepatoprotective properties. They also show antituberculosis and anticancer properties [3-5]. The third important part of nutmeg is its pericarp or the fruit rind which is the outermost part of it and is thick and fleshy. 80-85% by mass of the fresh fruit is the pericarp which has an aromatic smell and which limits the common use of this pericarp despite its medicinal properties. A small amount of pericarp is used for different preparation such as jam, jelly, and pickle. The remaining large amount of rind is wasted. Studies show that the fruit rind is rich in a variety of volatile and non-volatile organic compounds with heteroatoms [6, 7]. In this background, we decided to investigate the corrosion inhibition property of nutmeg fruit rind extract for the protection of commercial iron in HCl.

8.2 Results and Discussion

8.2.1 Chemical composition of the extract

The fruit rind extract contains a large number of volatile and non-volatile compounds. N. Mini Raj et al reported the biochemical constitution of the fruit rinds collected from seventeen farms and summarised the composition as given below.

Table 8.1 Approximate chemical composition of nutmeg fruit rind

Sl.No	Chemical constituent	Composition
1	Moisture	87.1-89.4%
2	Acidity	1.28-1.92%
3	Ascorbic acid	4.5-9.5 mg/100g
4	Calcium pectate	0.21-1.08%
5	Protein	0.21-1.85
6	Phenol	27.8-55mg/100g
7	Starch	0.3-1.22g/100g
8	Tannin	143-750mg/100g
9	Total minerals	2.01-2.50%
10	Total fibre	2.06-3.65%

The chemical constituents of the nutmeg fruit pericarp are analysed by Choo et al[7] and the non-volatile components are determined by K.Sajan Francis et al[6]. In the present study, 10% aqueous and ethanolic extract is used as the stock solution. The aqueous extract is acidic due to the presence of ascorbic acid whereas the ethanolic extract is neutral with the presence of other organic compounds[8]. The IR spectra of ethanolic(MFE) and aqueous extract(MFW) is given in Fig8.1(B). The fingerprint region is the same for both and an increase in intensity and an extra peak around 1740cm^{-1} is shown by MFE.

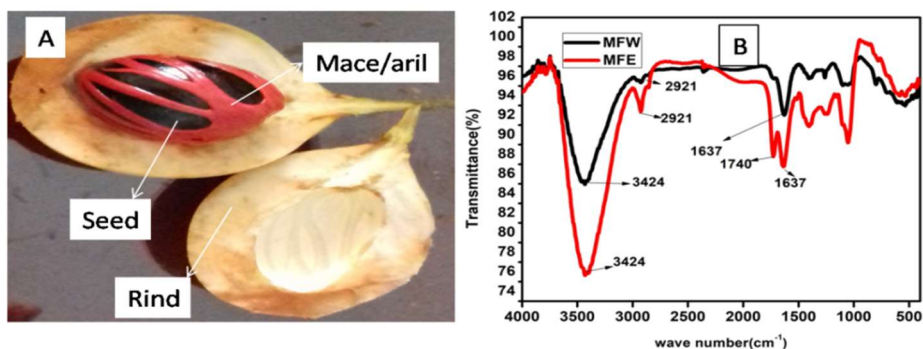


Fig 8.1 (A) the nutmeg fruit (B) IR spectra of MFE and MFW

Two peaks are observed (Fig 8.2(A)) in the UV-Visible spectra of the aqueous (MFW) and the ethanolic (MFE) extract. The peak at 309nm for MFE and 279nm for MFW indicates $n-\pi^*$ transitions and the other peak corresponds to $\pi-\pi^*$ transitions. A red shift is observed for the $n-\pi^*$ transition of MFE pointing out extended conjugation or additional auxochromes [9]. Fig8.2(B) and Fig 8.2(C) show the UV spectra of ascorbic acid taken in water and in alcohol and that of MFW and MFE .MFW shows a peak that corresponds to ascorbic acid whereas MFE has no matching peak with ascorbic acid taken in ethanol. From these observations, it is inferred that aqueous extract contains a greater quantity of ascorbic acid. Studies also show that the ascorbic acid is readily soluble in water (300g/L at 20⁰C) but much less soluble in ethanol (20g/L at 20⁰C) [10].

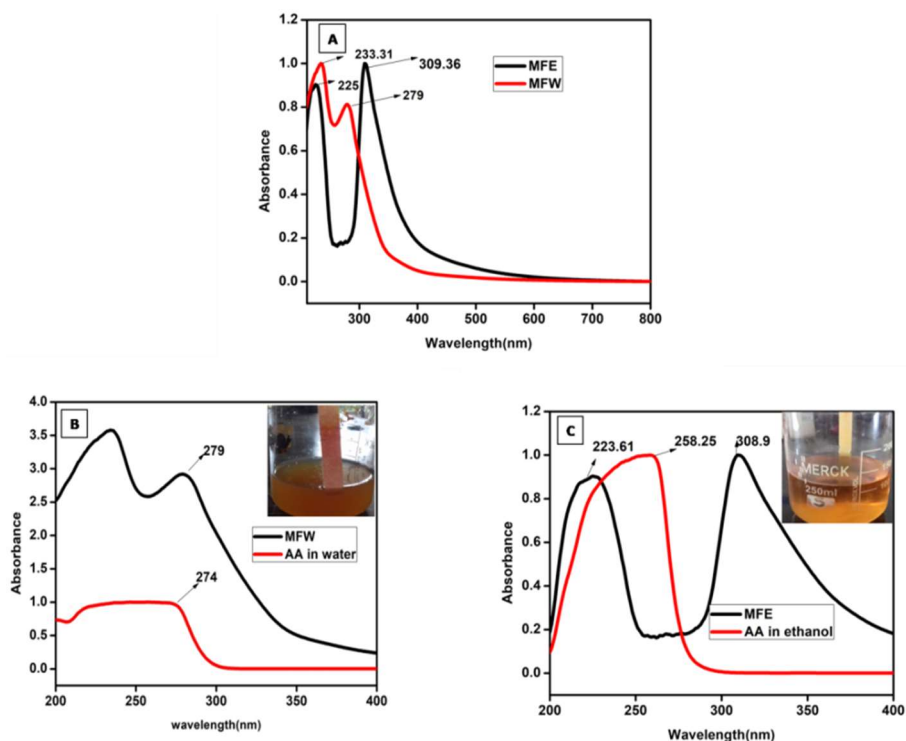


Fig 8.2 UV-Visible spectra of (A) MFW and MFE (B) MFW and ascorbic acid in water (C) MFE and ascorbic acid in ethanol

A better idea about the composition of the fruit rind extract is obtained from the gas chromatographic analysis of the ethanolic extract. The chromatogram (Fig 8.3) shows the presence of seven components and the peak heights indicate the presence of small quantities of these components. The current report matches with the report of Choo et al [7, 8]. All the constituent molecules contain heteroatoms, aromatic rings, and π electrons.

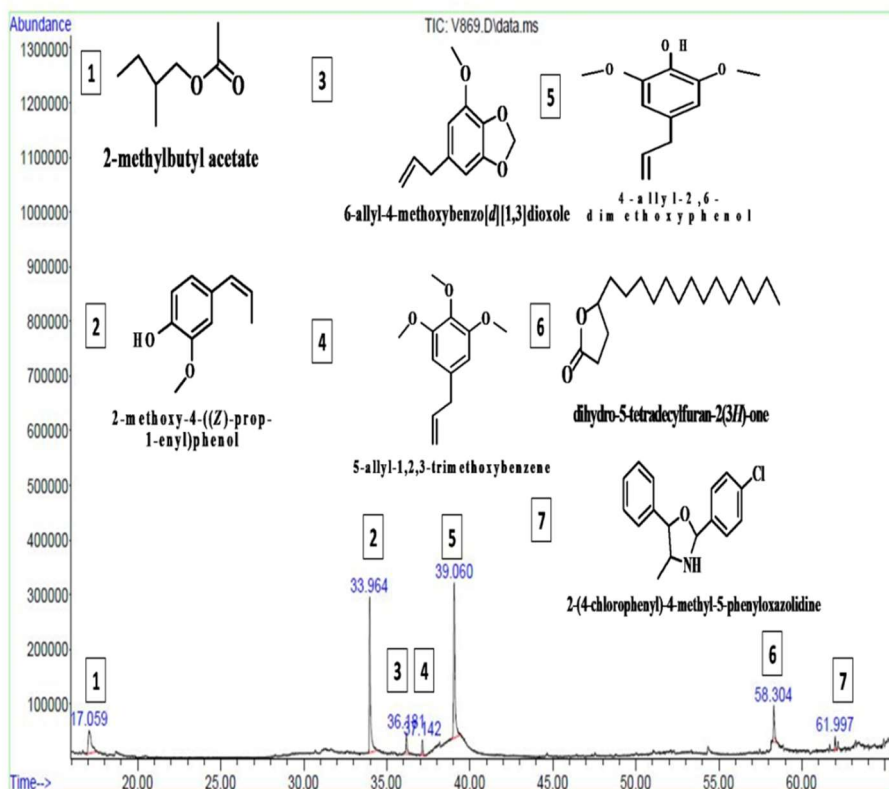


Fig 8.3 The GC- MS chromatogram of ethanolic extract of fruit rind and the constituent molecules present in it

8.2.2 Corrosion Analysis

8.2.2.1 Weight loss Analysis

The weight loss analysis of mild steel coupons in 1M HCl with and without MFE and MFW is carried out at different time intervals. The data is used for the calculation of inhibition efficiency (eqn.2.1) and corrosion rate (eqn.2.2) (Fig8.4) and is given in Table 8.2. Both MFW and MFE give an efficiency above 90% for an exposure of 24 hours whereas with the increase of time duration to 120 hours the inhibition capacity of MFW considerably decreases and MFE sustains the

protection capacity [11]. This could be due to the presence of ethanol-soluble organic compounds along with water-soluble ascorbic acid. The decrease in corrosion rate with time is due to the formation of protective coating which slows down further corrosion [12]. The increase in efficiency with the increase in the concentration of the inhibitor is attributed to the replacement of more water molecules by inhibitor molecules blocking the active sites of corrosion.

Table 8.2 Weight loss parameters of mild steel in 1M HCl with varying concentrations of MFW and MFE at room temperature

Time	24h			48h		72h		120h	
	C_{inh} (v/V%)	CR (mg/cm ² h)	%IE	CR (mg/cm ² h)	%IE	CR (mg/cm ² h)	%IE	CR (mg/cm ² h)	%IE
Blank		13.35	-----	12.35	-----	8.53		4.22	-----
M	1	2.197	83.54	2.464	80.05	2.349	72.56	2.115	49.90
F	2	1.723	87.10	1.349	89.08	1.865	78.13	1.780	57.38
F	3	1.240	90.71	1.170	90.46	1.670	80.41	1.315	68.86
W	4	1.075	91.95	1.053	91.53	0.984	86.45	0.9018	78.64
Blank		10.60	----	9.33	---	7.28		6.32	
M	1	1.532	89.19	0.9699	89.68	0.7452	89.74	0.5509	91.28
M	2	1.1526	91.92	0.7326	92.08	0.5594	92.31	0.3729	93.89
F	3	0.8702	93.90	0.6364	93.23	0.4930	93.23	0.3379	94.65
E	4	0.7800	94.53	0.6083	93.52	0.3622	95.02	0.1217	95.23

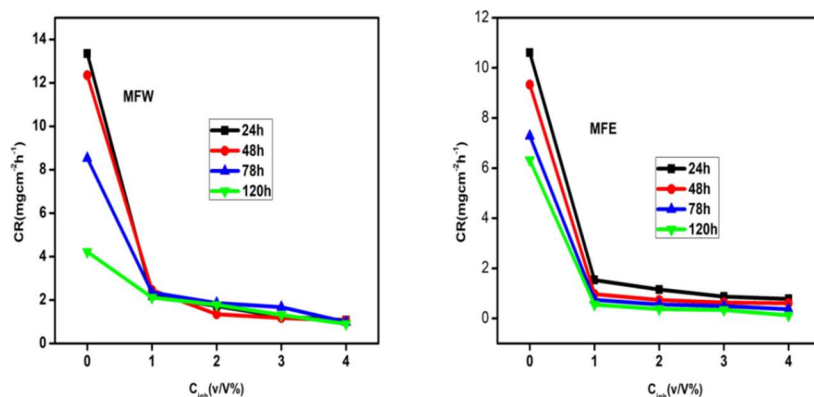


Fig 8.4 The variation of CR with exposure time for MFW and MFE

8.2.2.2 EIS studies

To analyse the kinetics of corrosion and the capacitive behaviour of the inhibitor the impedance spectra are taken in 1M HCl at 303K, 308K, and 313K. The information gathered from the analysis and the efficiency calculated using eqn. 2.8 is given in Table 8.3, and Table 8.4. The Nyquist plots (Fig 8.5) of MFW and MFE shows a single capacitive loop proves the charge transfer controlled process in corrosion inhibition [13, 14]. As the concentration of the inhibitor increases the charge transfer resistance (R_{ct}) increases and offers better protection efficiency. The increase of R_{ct} causes an increase in the thickness of the electrical double layer and thus prevents the flow of electrons and ions thus reduce the rate of corrosion [15]. The 3% MFE solution offers maximum efficiency (%IE) and beyond this optimum concentration, the inhibition efficiency decreases. The temperature rise reduces the inhibition capacity of MFW to a considerable extent while MFE maintains the inhibition capacity above 90% at 313K. The Bode phase angle plot (Fig 8.6 and Fig 8.7) shows a single relaxation constant that confirms the charge transfer controlled process. The Bode magnitude plot (Fig 8.6 and Fig8.7) shows the improved capacitive nature of MFW and MFE with an increase in concentration[16].

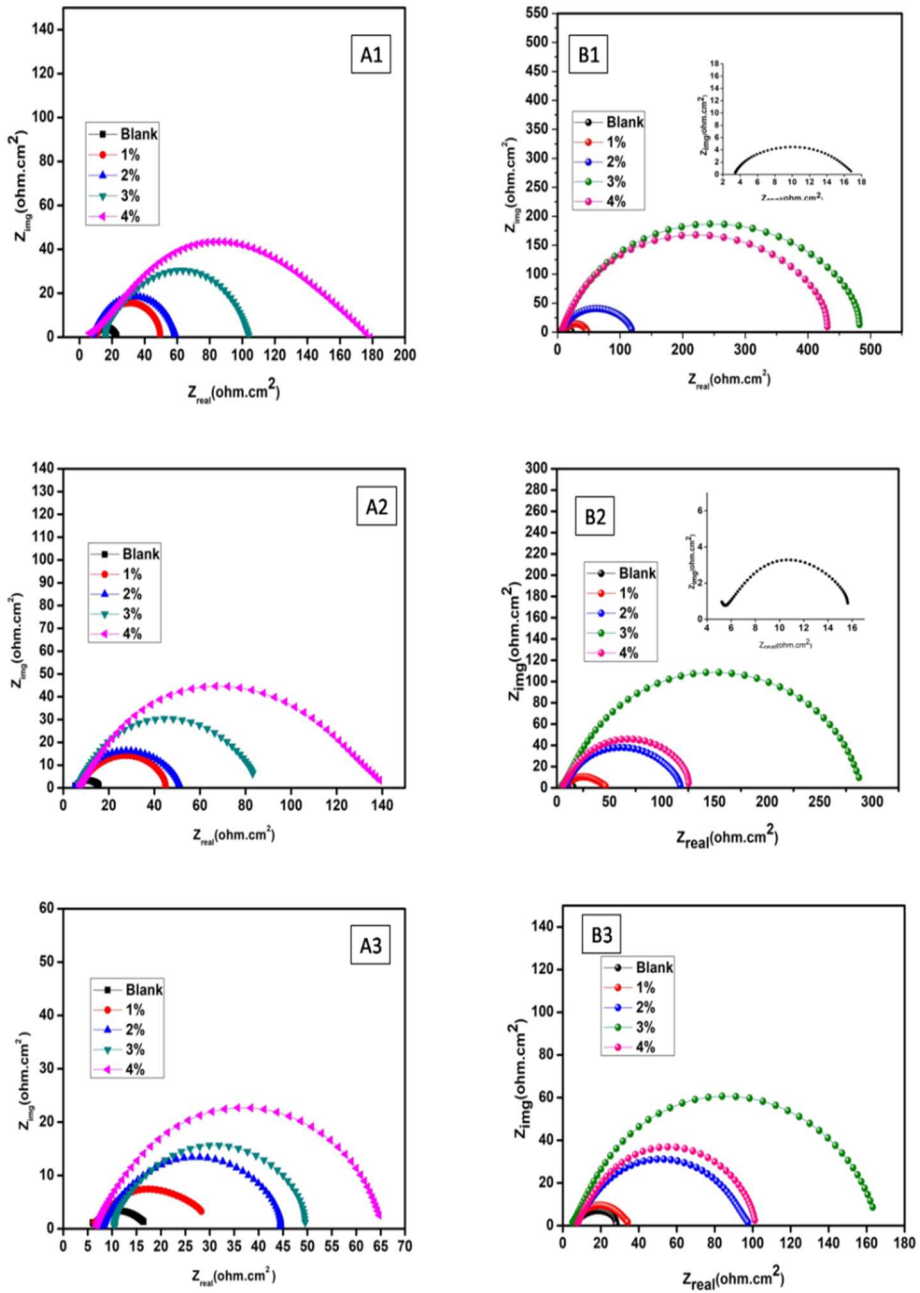


Fig 8.5 Nyquist plots for a varying concentration of MFW and MFE at different temperatures

Table 8.3 EIS parameters of MFW in 1M HCl at different temperatures

Temp	$C_{inh}(v/V\%)$	$R_{ct}(\Omega cm^2)$	$C_{dl}(\mu F/cm^2)$	$I_{corr}(mA/cm^2)$	CR (mm/y)	IE%
303K	Blank	13.67	1564.0	1.908	22.12	-----
	1	40.27	416.2	0.6478	7.50	66.05
	2	52.12	361.4	0.5005	5.51	73.77
	3	89.00	245.3	0.2931	3.39	84.64
	4	173.1	175.0	0.1507	1.74	92.10
308K	Blank	12.45	1552	2.095	22.42	-----
	1	37.91	587.8	0.6881	7.97	67.15
	2	46.31	400.1	0.5587	6.46	73.11
	3	79.92	267.4	0.3264	3.78	84.42
	4	131.2	230.9	0.1945	2.25	90.51
313K	Blank	12.00	2135	2.111	24.46	----
	1	25.25	1361	1.025	11.88	52.47
	2	37.78	572.0	0.6905	8.00	68.23
	3	40.43	391.4	0.452	7.47	70.31
	4	59.17	295.3	0.4422	5.12	79.71

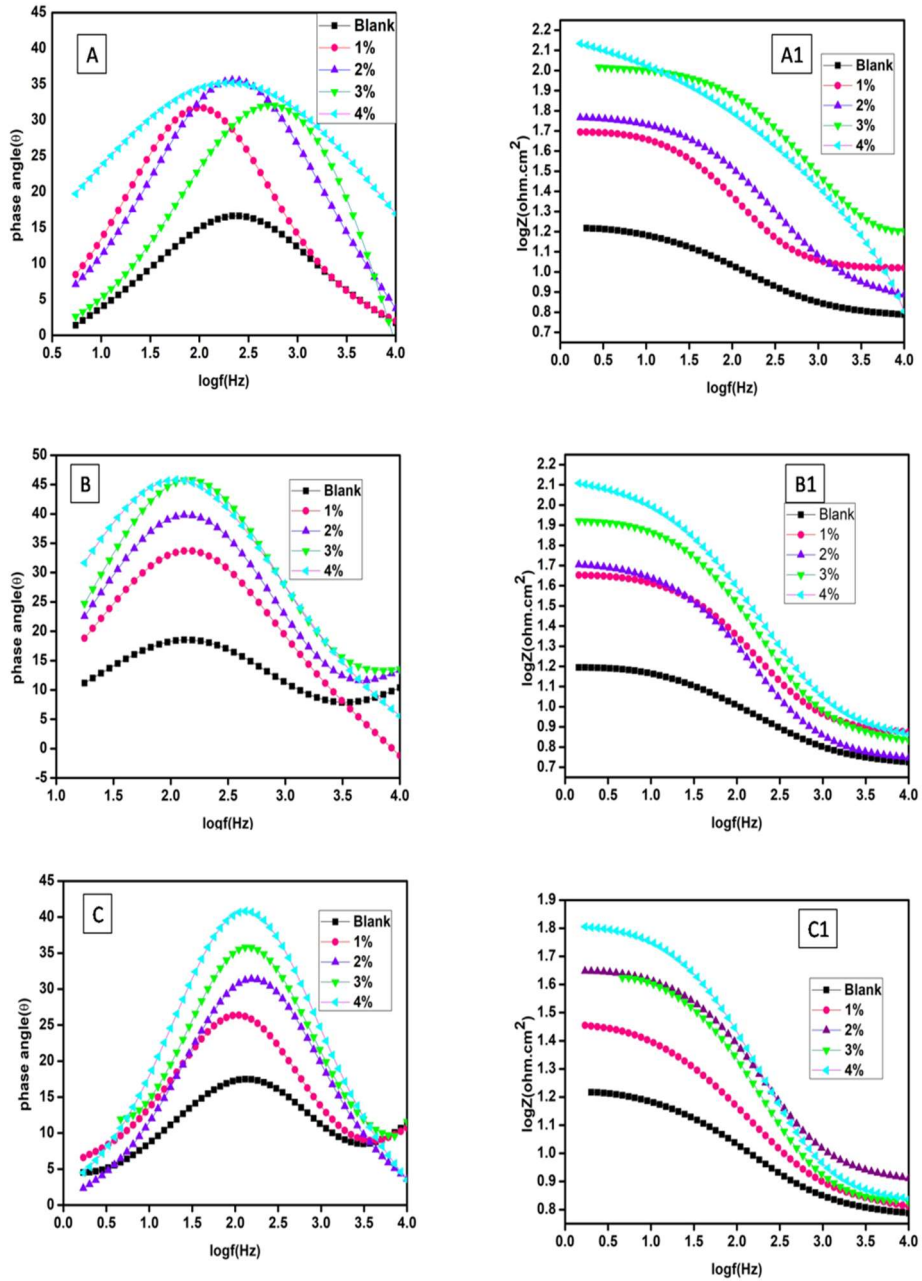


Fig 8.6 The Bode phase angle and Bode magnitude plots for MFW at different temperatures

Table 8.4 EIS parameters of MFE in 1M HCl at different temperatures

Temp	C_{inh} (v/V%)	R_{ct} (Ωcm^2)	C_{dl} ($\mu\text{F}/\text{cm}^2$)	I_{corr} (mA/cm^2)	CR (mm/y)	IE%
303K	Blank	13.67	564.0	1.908	22.12	----
	1	40.29	278.7	0.6475	7.50	75.16
	2	116.3	158.0	0.2243	2.60	88.24
	3	491.0	99.96	0.0531	0.61	97.21
	4	435.7	91.87	0.0598	0.69	96.86
308K	Blank	12.45	3552	2.095	22.42	----
	1	40.87	707.0	0.6383	7.39	69.53
	2	112.3	166.2	0.2323	3.35	88.91
	3	289.6	104.9	0.0900	1.04	95.70
	4	123.9	117.4	0.2105	0.94	89.95
313K	Blank	12.00	2135	2.111	24.46	----
	1%	30.75	380.2	0.8484	9.83	60.97
	2%	92.82	212.3	0.2810	3.25	87.07
	3%	162.4	139.0	0.1606	1.86	92.61
	4%	93.07	164.8	0.2803	3.24	89.95

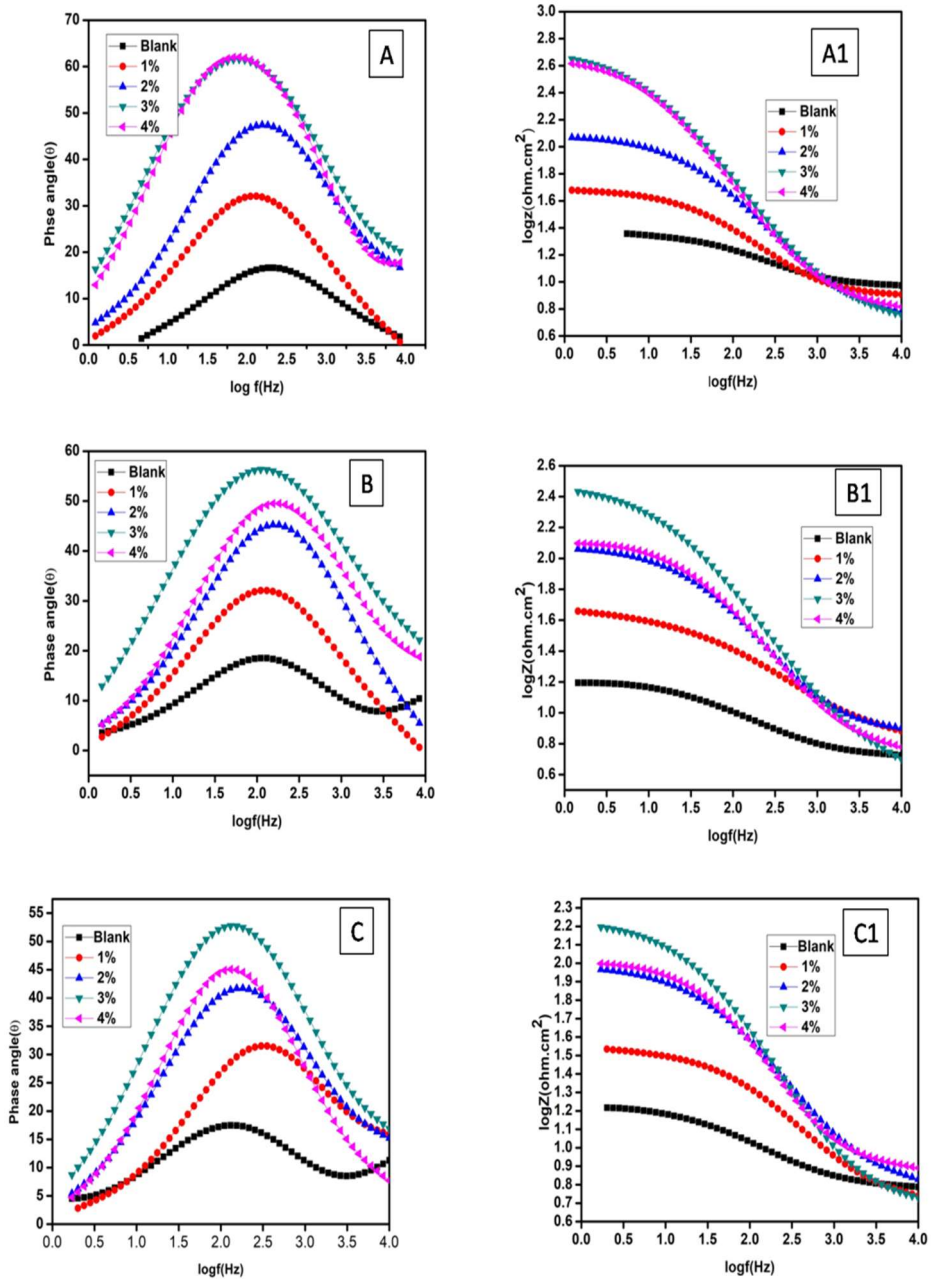


Fig 8.7 The Bode phase angle and Bode magnitude plots for MFE at different temperatures

8.2.2.3 Potentiodynamic polarisation (PDP) studies

The PDP analysis of mild steel coupons in 1M HCl with and without the inhibitor is carried out at 303K, 308K, and 313K. The collated data is given in Table 8.5 and Table 8.6. The polarisation curve is shown in Fig 8.8. No regular trend in the E_{corr} is observed with the addition of the inhibitor. It is altered not more than $\pm 85\text{mV}$ characterising the mixed type inhibition mechanism of MFW and MFE[17]. The cathodic and anodic Tafel constants are affected by the addition of the extract. As the concentration of the inhibitor increases the corrosion current density decreases while the increase in temperature causes an increase in corrosion current density. The efficiency is calculated using eqn. 2.9 [18]

Table 8.5 PDP parameters of MFW in 1M HCl at different temperatures

Temp	C_{inh} (v/V%)	$-E_{\text{corr}}$ (mV)	β_a (mV)	$-\beta_c$ (mV)	I_{corr} (mA/cm ²)	CR (mm/y)	IE%
303K	Blank	466.80	75	217	1.0823	20.21	----
	1	484.12	64	110	0.3115	9.93	71.21
	2	460.50	67	98	0.3007	9.72	72.21
	3	463.98	79	132	0.2076	7.83	80.81
	4	462.9	71	130	0.0862	6.73	92.03
308K	Blank	468.74	183	191	1.8105	38.04	-----
	1	457.89	104	189	0.4704	12.52	74.01
	2	504.17	81	96	0.4026	8.98	77.76
	3	455.56	56	111	0.3451	7.93	80.93
	4	475.91	58	104	0.2001	7.55	88.94
313K	Blank	466.19	216	228	2.0105	43.24	-----
	1	470.48	80	117	0.7280	13.42	63.79
	2	474.33	69	111	0.5329	11.90	73.49
	3	479.31	70	136	0.4057	9.64	79.82
	4	479.61	68	152	0.3961	8.12	80.29

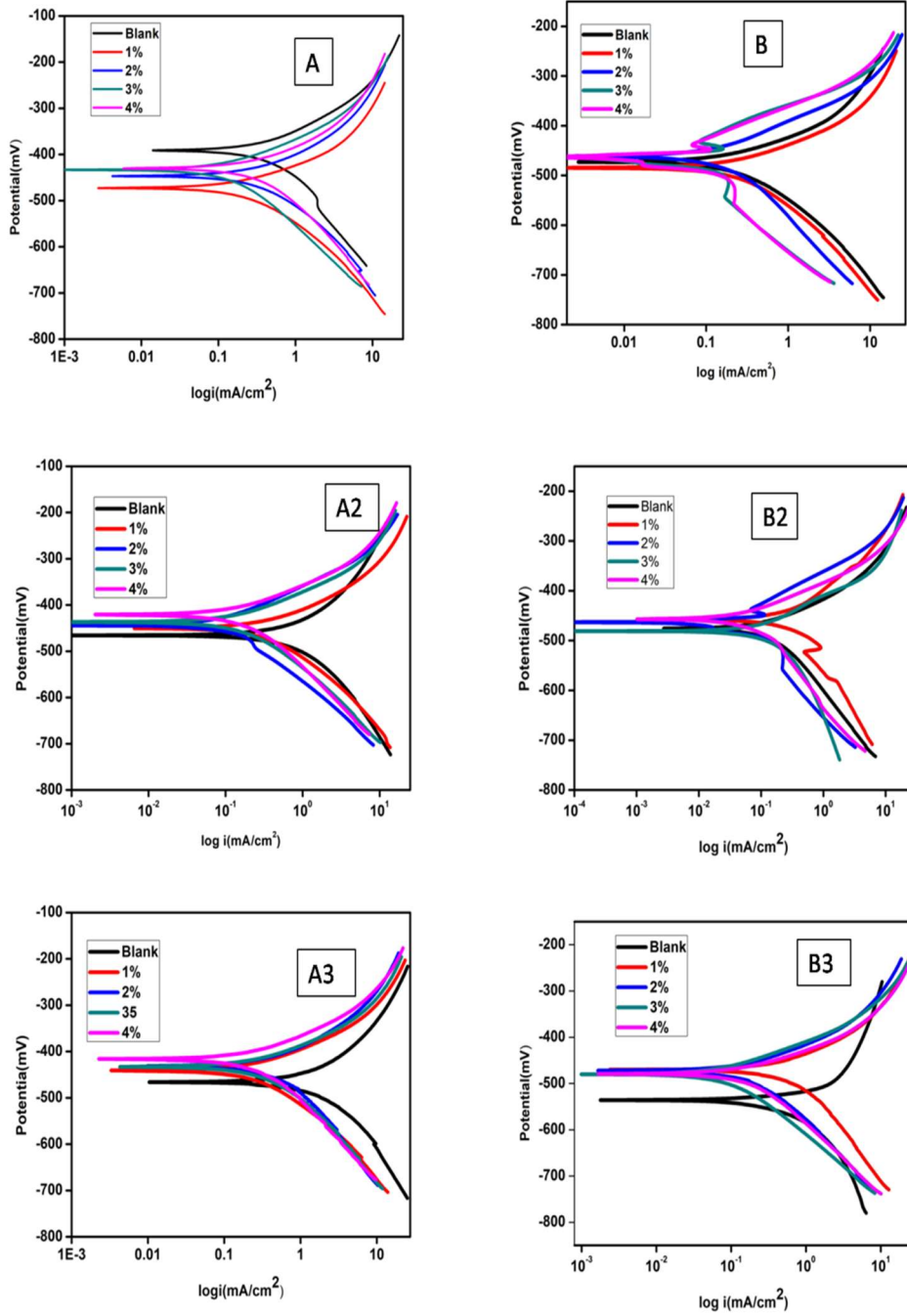


Fig 8.8 The PDP curves for MFW and MFE at different temperatures

Table 8.6 PDP parameters of MFE in 1M HCl at different temperatures

Temp	C _{inh} (v/V%)	-E _{corr} (mV)	β_a (mV)	$-\beta_c$ (mV)	I _{corr} (mA/cm ²)	CR (mm/y)	IE%
303K	Blank	391.52	75	217	1.0823	20.21	-----
	1	445.83	79	12	0.2952	9.76	72.72
	2	432.38	76	108	0.1780	9.03	83.70
	3	433.68	79	147	0.0548	8.98	94.93
	4	466.80	59	81	0.1505	6.69	88.69
308K	Blank	468.74	183	191	1.8105	38.04	-----
	1	443.23	72	90	0.5674	12.67	68.66
	2	450.03	79	116	0.3276	11.64	81.96
	3	440.02	84	85	0.1088	7.18	93.99
	4	420.92	69	99	0.1729	7.05	90.45
313K	Blank	466.19	216	228	2.0105	43.24	-----
	1	396.6	147	200	0.9011	13.33	55.18
	2	431.61	82	109	0.4038	10.00	84.86
	3	433.5	60	81	0.2042	9.97	89.84
	4	414.05	86	175	0.4094	8.34	79.63

8.2.3 Adsorption studies

Adsorption of organic compounds from the acidic electrolyte is considered to be a quasi-substitution of water molecules on the metal surface [19]. Adsorption isotherms are drawn to analyse the nature and strength of adsorption. Langmuir isotherm is found to be the best fitting one for MFW and MFE (Fig 8.9) which is drawn using the eqn.1.11. The equilibrium constant of adsorption (K_{ads}) given by the reciprocal of the Y-intercept and the free energy of adsorption (ΔG_0) calculated eqn.2.10 is given in Table 8.7. The K_{ads} values of MFE are greater than that of MFW indicates the strong adsorption of constituent

molecules on the metal surface. Spontaneous adsorption is concluded from the negative ΔG_0 values and indicates physisorption as the major mode of adsorption[20].

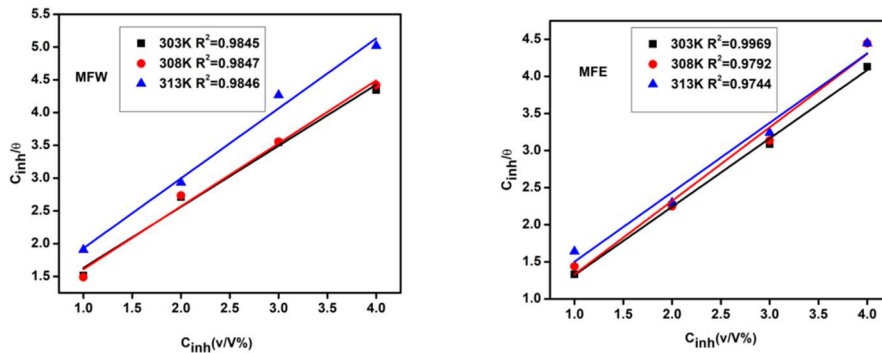


Fig 8.9 The Langmuir adsorption isotherms for MFW and MFE

Table 8.7 The thermodynamic parameters from Langmuir adsorption isotherm

		MFW		MFE	
Temp	K_{ads}	ΔG_0 (kJ/mol)	K_{ads}	ΔG_0 (kJ/mol)	
303K	1.43	-18.30	2.51	-19.72	
308K	1.54	-18.80	2.94	-20.45	
313K	1.33	-18.29	1.76	-19.45	

8.2.4 Effect of temperature and Kinetics of the reaction

Temperature is an important factor that determines the adsorption of inhibitor on the metal surface and inhibition efficiency. Processes such as etching, desorption, and fragmentation of the inhibitor can happen at higher temperatures. The Arrhenius (eqn.2.12) and transition state

plots (eqn.2.13) is used for calculating the activation parameters[21] and are given in Fig 8.10. The increase in activation energy (E_a) (Table 8.8) with an increase in concentration of the inhibitor indicates the adsorption of more and more molecules on the metal surface so that acid molecules have to cross high energy barrier to cause corrosion[12]. The positive value of enthalpy of activation (H_a) shows the endothermic nature of metal dissolution. The positive values of entropy of activation prove more randomness in the formation of the activated complex from reactants[22].

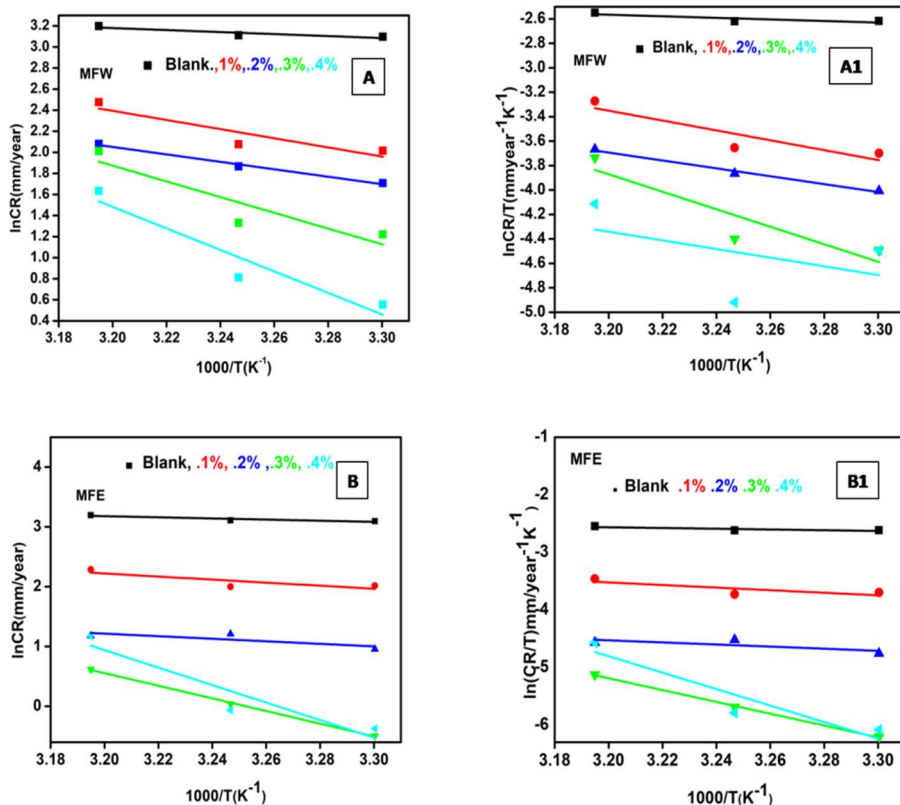


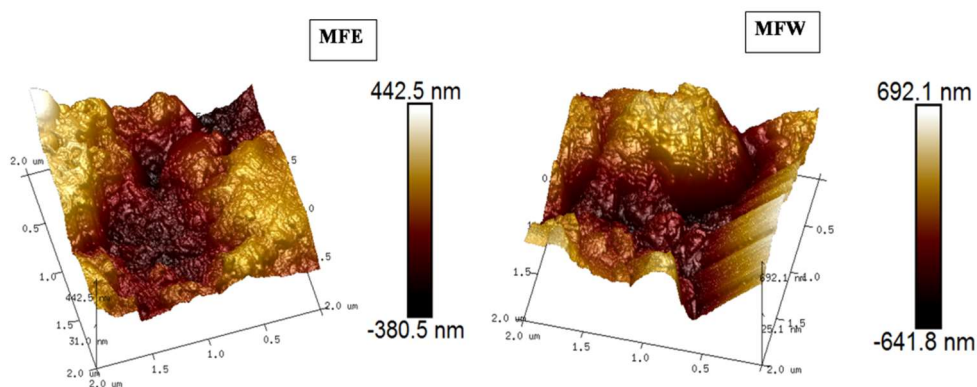
Fig 8.10 The Arrhenius and the Transition state plot for MFW and MFE

Table 8.8 The kinetic parameters of MFW and MFW calculated using Arrhenius and transition state equation

		E_a (kJ/mol)	ΔH_a (kJ/mol)	ΔS_a (kJ/mol. K)	$E_a - \Delta H_a$ (kJ/mol)
M	Blank	7.89	5.33	201.7	2.56
F	1%	36.12	33.55	118.0	2.57
W	2%	29.37	26.81	142.4	2.56
	3%	62.04	59.48	39.36	2.56
	4%	84.85	29.42	139.8	
M	1%	18.64	21.20	-111.23	2.56
F	2%	15.15	17.71	-130.95	2.56
E	3%	85.45	87.87	92.44	2.42
	4%	118.98	121.54	199.21	2.56

8.2.5 Surface Analysis

Surface analysis of mild steel specimens dipped in 1M HCl for 24 hours with MFE and MFW are given in Fig 8.11. The average roughness (R_a) of MFW is 177nm and that of MFE is 108nm indicating the reduction in the surface roughness and corrosion rate.

**Fig 8.11** AFM images of mild steel dipped in 1M HCl containing MFW and MFE

8.2.6 Mechanism of inhibition

Natural products act as efficient corrosion inhibitors through the adsorption of constituent organic molecules with aromatic rings and heteroatoms on the metal surface. Ascorbic acid is found to be one of the chief constituents of both MFW and MFE. Fig 8.12 shows the optimised geometry, HOMO and LUMO of ascorbic acid.

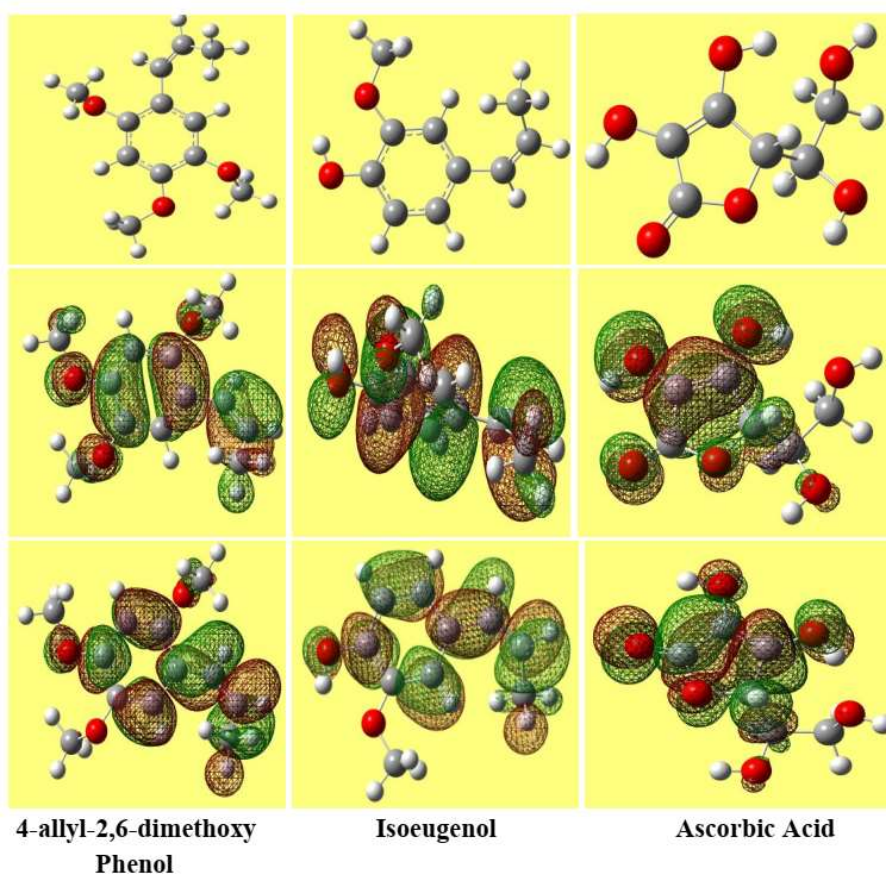


Fig 8.12 The optimised geometry, HOMO and LUMO of most abundant molecules of MF extract

Table 8.9 Global descriptors of the abundant components of Myristica fruit rind extract

Parameter	Ascorbic Acid	Isoeugenol	4-allyl-2,6-dimethoxy Phenol
Total Energy(eV)	18638	14663	18849
E _{HOMO} (eV)	-6.43	-5.66	-5.72
E _{LUMO} (eV)	-1.08	-0.795	-0.730
ΔE(eV)	5.35	4.86	4.99
Hardness $\eta = \frac{\Delta E}{2}$	2.67	2.43	2.49
Dipolmoment,μ(D)	7.05	2.94	1.58
IE=-E _{HOMO}	6.43	5.66	5.72
EA=-E _{LUMO}	1.08	0.795	0.73
$\chi = \frac{IE + EA}{2}$	3.75	3.22	3.22
$\Delta N = \frac{(\chi_{Fe} - \chi_{inh})\chi}{2(\eta_{Fe} + \eta_{inh})}$	0.60	0.77	0.75

The corrosion inhibition property of ascorbic acid is reported in the literature[23, 24]. The UV visible spectra ensure the presence of other water-soluble organic compounds in the aqueous extract. The ethanolic extract contains a variety of organic compounds[8]. The GC MS of the ethanolic extract indicates the presence of compounds such as 2-methyl butylacetate, 6-allyl-4-methoxy benzo[d][1, 3]dioxole, dihydro-5-tetradecylfuran-2[3H]one, 2-methoxy-4((z)-prop1-enyl) phenol (isoeugenol), 4-allyl-2, 6-dimethoxy phenol, 2, (4-chlorophenyl)-4-methyl-5-phenyloxazolidine. Fig 8.12 and table 8.9 gives the optimized geometry, HOMO, LUMO and global descriptors

of the most abundant constituents of *Myristica Fragrans*. The synergistic interaction of all these compounds makes MFE an efficient inhibitor against mild steel corrosion in acidic media.

8.3 Conclusions

- The corrosion inhibition property of aqueous (MFW) and ethanolic (MFE) extract of *Myristica Fragrans* (nutmeg) fruit rind is investigated in 1M HCl at different temperatures
- The characterisation of the constituent molecules is done with the help of UV, IR, and GC-MS
- The aqueous extract is rich in ascorbic acid and is acidic, while ethanolic extract contains a few other organic compounds and is neutral
- The weight loss studies show that the increase in immersion time decreases the corrosion protection capacity of MFW whereas the MFE sustains the efficiency up to 95.23% after immersing for 120 hours.
- The EIS studies indicate the charge transfer controlled process for corrosion inhibition.
- The PDP studies prove the mixed type behaviour of MFW and MFE in corrosion mitigation
- The corrosion protection of MFW and MFE is by adsorption of constituent molecules on the metal surface through physisorption which obeys Langmuir adsorption isotherm

References

1. Raj, N.M., et al., *Fruit rind constituents in nutmeg (Myristica fragrans) morphotypes*. Journal of Plantation Crops, 2016. **44**(3): p. 153-157.
2. Jaiswal, P., et al., *Biological effects of Myristica fragrans*. Annual review of biomedical sciences, 2009. **11**: p. 21-29.
3. Morita, T., et al., *Hepatoprotective effect of myristicin from nutmeg (Myristica fragrans) on lipopolysaccharide/d-galactosamine-induced liver injury*. Journal of Agricultural and Food Chemistry, 2003. **51**(6): p. 1560-1565.
4. Ganeshchandra, S., et al., *Behavioral actions of Myristica fragrans*. Indian Journal of Pharmacology, 2001. **33**(6): p. 417.
5. Nadkarni, K., *Indian materia medica; Dr. KM Nadkarni's Indian Materia Medica: with Ayurvedic, Unani-Tibbi, Siddha, Allopathic, Homeopathic, Naturopathic & Home Remedies, Appendices & Indexes*, 1996. **1**.
6. Francis, K.S., E. Suresh, and M.S. Nair, *Chemical constituents from Myristica fragrans fruit*. Natural Product Research, 2014. **28**(20): p. 1664-1668.
7. Choo, L.C., S.M. Wong, and K.Y. Liew, *Essential oil of nutmeg pericarp*. Journal of the Science of Food and Agriculture, 1999. **79**(13): p. 1954-1957.
8. Jimoh, S.O., O.H. Labo-Popoola, and K.A. Alabi, *Radical Scavenging Capacity and Efficacy of Myristica fragrans (Nutmeg) Metabolites on Cladosporium herbarum of Food Origin*. Microbiology Research Journal International, 2017: p. 1-8.
9. Dehghani, A., et al., *Electronic/atomic level fundamental theoretical evaluations combined with electrochemical/surface examinations of Tamarindus indica aqueous extract as a new green inhibitor for mild steel in acidic solution (HCl 1 M)*. Journal of the Taiwan Institute of Chemical Engineers, 2019. **102**: p. 349-377.
10. Shalmashi, A. and A. Eliassi, *Solubility of L-(+)-ascorbic acid in water, ethanol, methanol, propan-2-ol, acetone, acetonitrile, ethyl*

- acetate, and tetrahydrofuran from (293 to 323) K. Journal of Chemical & Engineering Data, 2008. **53**(6): p. 1332-1334.
11. Prajila, M., A. Thomas, and A. Joseph, *Development of Passive Film and Enhancement of Corrosion Protection of Mild Steel Exposed in Hydrochloric Acid due to the Adsorption of Water Dispersed 4-[(E)-(3, 4-Dihydroxybenzylidene) amino]-6-Methyl-3-Mercapto-1, 2, 4-Triazin-5 (4H)-one (DHMMT)*. Journal of Bio-and Tribo-Corrosion, 2017. **3**(2): p. 16.
 12. Ammal, P.R., M. Prajila, and A. Joseph, *Effect of substitution and temperature on the corrosion inhibition properties of benzimidazole bearing 1, 3, 4-oxadiazoles for mild steel in sulphuric acid: physicochemical and theoretical studies*. Journal of environmental chemical engineering, 2018. **6**(1): p. 1072-1085.
 13. Aquino-Torres, E., et al., *The influence of iodide in corrosion inhibition by organic compounds on carbon steel: Theoretical and experimental studies*. Applied Surface Science, 2020. **514**: p. 145928.
 14. Alvarez, P.E., et al., *Rollinia occidentalis extract as green corrosion inhibitor for carbon steel in HCl solution*. Journal of industrial and engineering chemistry, 2018. **58**: p. 92-99.
 15. Hassannejad, H. and A. Nouri, *Sunflower seed hull extract as a novel green corrosion inhibitor for mild steel in HCl solution*. Journal of Molecular Liquids, 2018. **254**: p. 377-382.
 16. Singh, A., et al., *Effect of electron donating functional groups on corrosion inhibition of mild steel in hydrochloric acid: Experimental and quantum chemical study*. Journal of the Taiwan Institute of Chemical Engineers, 2018. **82**: p. 233-251.
 17. Khan, M., et al., *Evaluation of Matricaria aurea extracts as effective anti-corrosive agent for mild steel in 1.0 M HCl and isolation of their active ingredients*. Sustainability, 2019. **11**(24): p. 7174.
 18. Odewunmi, N., S. Umoren, and Z. Gasem, *Utilization of watermelon rind extract as a green corrosion inhibitor for mild steel in acidic media*. Journal of Industrial and Engineering Chemistry, 2015. **21**: p. 239-247.
 19. Olasunkanmi, L.O., et al., *Some quinoxalin-6-yl derivatives as corrosion inhibitors for mild steel in hydrochloric acid: experimental*

- and theoretical studies*. The Journal of Physical Chemistry C, 2015. **119**(28): p. 16004-16019.
20. Zhang, W., et al., *Highly effective inhibition of mild steel corrosion in HCl solution by using pyrido [1, 2-a] benzimidazoles*. New Journal of Chemistry, 2019. **43**(1): p. 413-426.
 21. Kumari, P.P., P. Shetty, and S.A. Rao, *Electrochemical measurements for the corrosion inhibition of mild steel in 1 M hydrochloric acid by using an aromatic hydrazide derivative*. Arabian Journal of Chemistry, 2017. **10**(5): p. 653-663.
 22. Hegazy, M., et al., *Corrosion inhibition performance of a novel cationic surfactant for protection of carbon steel pipeline in acidic media*. Int. J. Electrochem. Sci, 2018. **13**: p. 6824-6842.
 23. Chidiebere, M.A., et al., *Ascorbic acid as corrosion inhibitor for Q235 mild steel in acidic environments*. Journal of Industrial and Engineering Chemistry, 2015. **26**: p. 182-192.
 24. Ferreira, E., et al., *Evaluation of the inhibitor effect of L-ascorbic acid on the corrosion of mild steel*. Materials Chemistry and Physics, 2004. **83**(1): p. 129-134.

Summary and Future Outlook

Summary and Future Outlook

The focus of this piece of work is to synthesise and analyse the corrosion inhibition properties of natural as well as synthetic organic compounds containing N, S, O heteroatoms, aromatic rings and π electron systems. We have selected a few pyrazole derivatives and two fruit rind extracts for the study. The fruit rind extract contains a large amount of heterocyclic aromatic compounds which can efficiently reduce corrosion rate. We have synthesised four pyrazole derivatives and the characterisation of the compounds is done using UV, IR, and NMR spectroscopy.

The corrosion inhibition property of these molecules towards mild steel corrosion in dilute HCl and H₂SO₄ is carried out using weight loss, EIS (electrochemical impedance spectroscopy), and PDP (potentiodynamic polarisation) techniques. The Nyquist plots for all the inhibitors have a single capacitive loop which indicates the charge transfer controlled process for corrosion inhibition. Therefore the electrical equivalent circuit used is the Randles circuit. The shift of E_{corr} of the inhibited solutions from the blank solutions are less than $\pm 85\text{mV}$ and which affirms the mixed type behaviour of these molecules affecting both anodic reaction of metal dissolution and cathodic reaction of hydrogen evolution. But few of them show more inclination towards the anodic reaction. The effect of temperature, acid concentration, and inhibitor concentrations on the corrosion inhibition property of the inhibitors are done. Maximum efficiency of 93% is obtained for 100ppm CMPPC in 1M HCl at room temperature. The inhibition efficiency of 89.01%, 90.25%, 84.33% for 200ppm of PD, PD1 and PY1 is given in 1M HCl at room temperature. The efficiency is decreased by the increase of temperature and the acid concentrations for all inhibitors. The addition of 50ppm of TU increased the efficiency

Summary and Future Outlook

of PY1 to 92.36% at room temperature and from 58.31% to 83.41% at 318K. Studies carried out in 0.5M H₂SO₄ give maximum efficiency by CMPPC. Several factors such as molecular structure, solubility, anchoring group etc affect the inhibition capacity of the inhibitors. GIW extract contains o- hydroxy citric acid and cyanidin anthocyanins which could be easily adsorbed on the metal surface. An efficiency of 87.42% at 303K and 80.54% at 333K is given by 4% GIW. The addition of 200ppm of KI to GIW increases the efficiency to 89.05% at 303K. The preadsorbed iodide ions act as a link between the metal surface and cyanidin molecules and thus enhance the inhibition capacity. The ethanolic extract of fruit rind of *Myristica Fragrans* (MFE) shows an inhibition efficiency of 96.86% whereas the aqueous extract gives an efficiency of 92.10%. Even at higher temperatures, MFE sustains high efficiency.

All the inhibitors show Langmuir adsorption isotherm as the best fitting isotherm and the values of free energy of adsorption (ΔG_0) indicate the spontaneity of adsorption. The ΔG_0 values are for all the inhibitors are below -40kJ/mol indicating mixed type adsorption involving both physisorption and chemisorptions. The kinetic parameters such as activation energy, enthalpy of activation and entropy of activation show decrease in the rate of metal corrosion by the addition of inhibitor.

Geometry optimisation of all the inhibitor molecules is carried out using Gaussian 09 package taking B3LYP 6311G (d,p) basis set. The global descriptors calculated gave an idea about the inhibition property of the molecules. The Fukui indices calculated using the UCA_ Fukui software explain the nucleophilic and the electrophilic centres of the

inhibitor molecules. The material studio simulations helped in the visualisation of the adsorption pattern of the inhibitor molecules on the metal surface and calculation of its binding energy.

The surface morphology of the blank and the inhibited solutions is observed using SEM and AFM. The roughness of the metal surface is decreased by the adsorption of the inhibitor molecules on the metal surface. SEM images gave an idea of the surface damage caused by the immersion of mild steel samples in an acid medium.

Future Outlook

The analysis of naturally occurring plant products as corrosion inhibitors is a passion of the time because of environmental concerns and the presence of variety of organic compounds. One of the limitations of the work is the identification of the most active components which reduce corrosion rate. Another question that arises is the exact mechanism of the corrosion inhibition by these materials. Extended research is required to know whether the individual molecule is efficient or by the synergistic interactions of different molecules provide protection to metals always. Sustainability and high temperature protection efficiency in strong acid needed attention and further investigation. Testing of industrial applicability of these plant extract is to be considered in the future. Coating of these easily available materials using ecofriendly binder is also a future concern.

LIST OF PUBLICATIONS

1. *A comprehensive study of mild steel corrosion in the aggressive acidic environment using CMPPC, a substituted pyrazole derivative*, **Asha Thomas, P. Rugmini Ammal, Abraham Joseph**, *Chemical Papers* (2020): 1-13. (Springer)
2. *A green approach to corrosion inhibition of mild steel in hydrochloric acid using fruit rind extract of Garcinia indica (Binda)*, **Asha Thomas, M. Prajila, K.M. Shainy, Abraham Joseph**, *Journal of Molecular Liquids* 312 (2020): 113369. (Elsevier)
3. *Development of Passive Film and Enhancement of Corrosion Protection of Mild Steel Exposed in Hydrochloric Acid due to the Adsorption of Water Dispersed 4-[(E)-(3, 4-Dihydroxybenzylidene) amino]-6-Methyl-3-Mercapto-1, 2, 4-Triazin-5(4H)-one(DHMMT)*, **M. Prajila, Asha Thomas, Abraham Joseph**, *Egyptian journal of petroleum* 27.4 (2018): 621-632 (Springer)
4. *Synergistic interaction of 2-amino 4-methyl benzothiazole (AMBT) and benzotriazole (BTZ) offers excellent protection to mild steel exposed in acid atmosphere at elevated temperatures: Electrochemical, computational and surface studies*, **K.M. Shainy, Anupama R. Prasad, Asha Thomas, Abraham Joseph**, *Egyptian Journal of Petroleum*, 28(1), (2019)35-45 (Elsevier)
5. *Inhibition of mild steel corrosion in HCl using aqueous and alcoholic extracts of Crotalaria Pallida – A combination of experimental, simulation and theoretical studies* **A.T.Jeeja Rani, Asha Thomas, Abraham Joseph**, *Journal of Molecular Liquids* 334(2021):116515 (Elsevier)
6. *Extended protection of mild steel in molar HCl using the Garcinia Indica fruit rind extract (GIW) and iodide ions; electrochemical, thermodynamic and kinetic studies* **Asha Thomas, Jeeja Rani A T, and Abraham Joseph**, *Journal of the Indian Chemical Society* (Elsevier) (Accepted)

List of Presentations

1. “The effect of temperature on the Corrosion inhibition properties of 5 -Chloro-3-methyl-1-phenyl-1H-pyrazole-4-carbaldehyde for Mild Steel in HCl” - FCS 2019, Dept of Chemistry, University of Calicut
2. “A comprehensive study of Mild Steel corrosion in aggressive acidic environment using Garcinia Indica (GI) fruit rind extract”- International Seminar, EFCS-2019, Dept. Of Chemistry, Farook College